Declaration

I declare that this thesis has not been submitted as an exercise for a degree at this or any other university and it is entirely my own work, except where otherwise acknowledged. I agree to deposit this thesis in the University's open access institutional repository or allow the Library to do so on my behalf, subject to Irish Copyright Legislation and Trinity College Library conditions of use and acknowledgement.

Paul Cassidy

September 2017

Acknowledgements

I would like to thank my supervisor, Professor Pete Humphries, for giving me the opportunity to carry out this project, and for his support over the course of my PhD. Special thanks to Dr. Lawrence Tam for his supervision, guidance, and encouragement throughout my research. Massive thank you to Dr. Ester-Reina Torres, Dr. Joseph Sherwood, Professor Darryl Overby, and Professor Dan Stamer for all their expertise. Thank you also to Dr. Anna-Sophia Kiang, Dr. Marian Humphries, and Dr. Matthew Campbell for their continued help and advice. Thanks to Dr. Matthew Lawrence, RxGen, St Kitts, for generosity with his time and resources. Thank you to the European Research Council for funding my studies.

I am indebted to my fellow students Jeffrey O'Callaghan and Darragh Crosbie for their constant advice, patience, help, and for making work fun, thanks for everything lads. Thanks to Bennett and Jebb, for your friendship and the countless great memories, you guys are the best. Thanks to Danny, Adrian, and Niamh for all the craic in Island Key, it will be missed! Thanks to Killian, Natalie, Ciara, Ema, Eoin, Áine, Lara, Ruth, Cathy, Cecilia, Mei-ling, Blounty, my DUSAC friends, and all my friends, for all the hijinks, scandal, adventures, holidays, gigs, and pints over the past four years. Finally to parents, and to all my family, I wouldn't be here if it wasn't for all the unconditional love and support you've given me over the years. Thank you.

Summary

Primary open-angle glaucoma (POAG) is one of the leading causes of blindness worldwide, affecting an estimated 44.1 million people, with the number of affected individuals predicted to rise to 79.8 million by 2040, largely due to rapidly increasing aging populations (Tham et al. 2014). POAG is characterised by elevated intraocular pressure (IOP) due to increased resistance to the outflow of aqueous humor (AH) through the conventional outflow pathway, comprising the trabecular meshwork (TM) and Schlemm's canal (SC), through which the majority of AH drainage occurs in humans. This elevated IOP causes damage to and loss of the axons of the optic nerve, with subsequent retinal ganglion cell (RGC) death in the retina, together termed glaucomatous optic neuropathy. As RGC function to transmit visual signals from the retina to the brain, this damage leads to a progressive, irreversible loss of visual field. The most common current treatments for POAG are topically applied medications that aim to reduce IOP through lowering the production rate of AH, or increasing the outflow rate of AH through the unconventional outflow pathway. There is an unmet need for therapies that target the site of increased outflow resistance in POAG, the conventional outflow pathway.

In this thesis, a novel approach to the treatment of POAG was investigated through targeting of the conventional outflow pathway. AH enters SC either via a transcellular route, through large transcellular pores, or a paracellular route, through paracellular pores at tight junction (TJ) mediated cell boundaries. First, potential TJ proteins were identified as therapeutic targets through microarray and western blot analysis of cultured human SC cells, as well as through immune-staining of mouse and primate eyes. The ability to downregulate these selected TJ proteins using siRNA was demonstrated. Next, the effect of downregulation of these TJ proteins was investigated in wildtype mice through injection of siRNA into the anterior chamber. This showed an increase in the outflow of AH from the anterior chamber, as measured by perfusion, and a lowering of IOP, measured by rebound tonometry, through increasing the number of open intercellular pores, visualised by transmission electron microscopy. This demonstrated the viability of this downregulation as a potential novel therapeutic approach to the treatment of POAG. IOP reduction and AH outflow increase was also demonstrated in a mouse model of steroid-induced glaucoma. The same approach was

attempted in wildtype primates, with no effect on AH outflow or IOP detected. Later analysis showed that downregulation of target TJ proteins had been unsuccessful in these animals. Potential improved RNAi delivery mechanisms are discussed.

In addition, the effect of the cytokine interleukin-18 (IL-18) on AH outflow and SC permeability was investigated in the final chapter of this thesis. IL-18 is known to affect vascular permeability and TJ expression, and is upregulated in response to anti-VEGF therapy. Treating cultured human SC cells *in vitro* with recombinant IL-18 resulted in decreased permeability to ions and macromolecules, and upregulation of the TJ protein tricellulin. *In vivo* injection of IL-18 caused a reduction in AH outflow as shown by perfusion, while measurement of AH outflow in knockout mice deficient in active IL-18 showed an increased level of AH outflow as compared to wildtype controls, indicating a potential role for IL-18 in regulation of AH outflow. Analysis of human POAG patient AH, and AH from mouse models of glaucomatous optic neuropathy, showed no increased in IL-18 concentration in AH over controls.

Glossary of abbreviations

AAV	Adeno-associated virus
AH	Aqueous humor
AQP	Aquaporin
ASB10	Ankyrin repeats and suppressor of cytokine signalling box-containing protein-10
ASC	Apoptosis-associated speck-like protein containing a caspase recruitment domain
BBB	Blood-brain barrier
BCF	Brain capillary fraction
C	Conventional outflow facility
CARD	Caspase recruitment domain
CLAN	Cross-linked actin network
C_r	Reference conventional outflow facility at 8 mmHg
DAMP	Damage-associated molecular pattern
DEX	Dexamethasone
ECM	Extracellular matrix
EM	Electron microscopy
ER	Endoplasmic reticulum
FITC	Fluorescein isothiocyanate
GC	Glucocorticoid
GUK	Guanylate kinase
GV	Giant Vacuole
GWAS	Genome-wide association study
HUVEC	Human umbilical vein endothelial cell
iBRB	Inner blood-retinal barrier
IHC	Immunohistochemistry
IL-18	Interleukin-19
IL-18bp	Interleukin-18 binding protein
IL-18R	Interleukin-18 receptor

IOP	Intraocular pressure
JAM3	Junctional adhesion molecule-3
JAMA	Junctional adhesion molecule A
JCT	Juxtacanalicular tissue
LC	Lamina cribrosa
LCM	Laser capture microdissection
MMP	Matrix metalloprotease
MYOC	Myocilin
NF-κB	Nuclear factor kappa-B
NK	Natural Killer
NLR	NOD-like receptor
NLRP3	NACHT, LRR and PYD domain containing protein-3
NO	Nitric oxide
NT	Non-targeting
NTG	Normal tension glaucoma
OHT	Ocular hypertension
ONC	Optic nerve crush
ONH	Optic nerve head
OPTN	Optineurin
PACG	Primary angle-closure glaucoma
PAMP	Pathogen-associated molecular pattern
PDG	Pigment dispersion glaucoma
PDZ	PSD95-DLGA-ZO-1 homology
POAG	Primary open-angle glaucoma
PRR	Pattern recognition receptor
PXG	Pseudo-exfoliative glaucoma
PYD	Pyrin domain
RGC	Retinal ganglion cell
RNAi	RNA interference
ROS	Reactive oxygen species
SC	Schlemm's Canal
SCEC	Schlemm's canal endothelial cell

SEM	Scanning electron microscopy
SH3	SRC homology 3
shRNA	short hairpin RNA
sIOP	Spontaneous IOP
siRNA	Short interfering RNA
T	Targeting
TBK1	TANK-binding kinase -1
TEER	Trans-endothelial electrical resistance
TEM	Transmission electron microscopy
TIGR	Trabecular meshwork induced glucocorticoid response (See MYOC)
TIMP	Tissue inhibitor if matrix metalloprotease
TIR	Toll-IL-1 receptor
TJ	Tight Junction
TJP1	Tight junction protein-1 (ZO-1)
TLR	Toll-like receptor
TM	Trabecular meshwork
VEGF	Vascular endothelial growth factor
ZO-1	Zonula occludens-1

Table of contents

Declaration I

Acknowledgements II

Summary III

Glossary of abbreviations V

Table of contents VIII

Chapter 1: Introduction: On aqueous humor outflow dynamics and glaucoma 1

Anatomy of the eye in brief 1

Aqueous humor flow dynamics 3

Aqueous humor formation 5

Unconventional outflow pathway 6

Conventional outflow pathway 6

Schlemm's canal inner wall pores 9

Isolation of cells of the conventional outflow pathway 10

Generation of outflow resistance in the conventional pathway 11

Features of glaucoma 14

Intraocular pressure and ocular hypertension 14

The optic nerve head 15

Glaucomatous optic neuropathy 15

Types of glaucoma 17

Primary angle-closure glaucoma 17

Primary open-angle glaucoma 18

Normal tension glaucoma 18

Pseudoexfoliative glaucoma 19

Pigment dispersion glaucoma 19

Secondary glaucoma 20

Epidemiology and risk factors of glaucoma 20

Genetics of primary open angle glaucoma 21

Current treatments for primary open-angle glaucoma 22

Pharmacological treatment 23

Surgical intervention 25

Summary 26

Chapter 2: Characterisation and modulation of Schlemm's canal tight junction proteins 27

Introduction 27

Structure and composition of tight junctions 27

Tight junction mediated control of paracellular permeability 29

Tight junctions of Schlemm's canal 32

Aims 33

Results 34

Characterisation of tight junction expression in human SC endothelial cells 34

Validation of tight junction siRNAs 40

Discussion 44

Statement on collaboration 46

Chapter 3: Investigating the therapeutic potential of RNAi mediated downregulation of tight junction proteins in Schlemm's canal 47

Introduction 47

Modulation of tight junction protein expression 47

Pressure dependence of aqueous humor outflow 49

Measuring aqueous humor outflow facility 50

Aims 52

Results 53

Perfusion Systems 53

Effect of siRNA modulation of tight junctions on murine conventional outflow 58

Effect of siRNA modulation of tight junctions on murine intraocular pressure 62

Ultrastructural analysis of Schlemm's Canal after siRNA modulation of selected tight junction components 63

Adaptation of *iPerfusion* system to facilitate primate *in vivo* conventional outflow measurement 66

Analysis of effect of delivery of siRNA targeting tight junction components on protein levels in dissected primate outflow tissues 73

Mouse *in vivo* measurement of spontaneous IOP 73

Discussion 78

Statement on collaboration 83

Chapter 4: Investigation of a murine model of ocular hypertension 84

Introduction 84

Selecting a murine model of ocular hypertension 84

The DBA/2J mouse 85
Induced models of ocular hypertension 86
Models of ocular hypertension with increased outflow resistance in the trabecular meshwork 86
Aims 89
Results 90
Evolution of elevated intraocular pressure in dexamethasone treated mice 90
Potential reasons for high baseline IOP readings 92
Effect of siRNA treatment on intraocular pressure in dexamethasone treated mice 94
Effect of siRNA treatment on outflow facility in dexamethasone treated mice 96
Discussion 99
Statement on collaboration 102
Chapter 5: The effect of IL-18 on Schlemm's canal endothelial permeability and conventional outflow facility 103
Introduction 103
The innate immune system and sterile inflammation 103
The NLRP3 inflammasome 104
Interleukin-18 106
Sterile inflammation and primary open-angle glaucoma 108
Potential relevance of interleukin-18 to outflow facility 108
Aims 109
Results 110
Effect of interleukin-18 on Schlemm's canal endothelial paracellular permeability 110
Effect of interleukin-18 on Schlemm's canal endothelial cell viability 112
Effect of interleukin-18 on Schlemm's canal endothelial cell tight junction expression 113
Effect of interleukin-18 on conventional outflow facility 115
Conventional outflow facility in knockout mice deficient in active interleukin-18 115
Interleukin-18 levels in aqueous humor in a model of axonal damage 118
Interleukin-18 levels in human glaucomatous aqueous humor 120
Discussion 121
Statement on collaboration 123

Conclusion **124**

Materials and Methods **129**

Cell culture **129**

Human tight junction PCR array **129**

Western blotting **130**

Immunohistochemistry **131**

siRNA **132**

Cell viability **132**

Pump based perfusion **133**

iPerfusion **133**

Intracameral injection **134**

Rebound tonometry **135**

Transmission electron microscopy **135**

Primate *in vivo* iPerfusion **136**

Murine spontaneous IOP measurement **136**

Dexamethasone micro-osmotic pump implantation **137**

Trans-endothelial electrical resistance measurement **137**

Cell permeability assay using FITC-dextran **138**

Optic nerve crush **138**

ELISA **139**

References **140**

Appendix **163**

Chapter 1: Introduction: On aqueous humor outflow dynamics and glaucoma

This chapter will provide an outline of the anatomy of the human eye, together with an explanation of the dynamics of aqueous humor outflow and the generation of outflow resistance. The clinical features of glaucoma, its epidemiology, and contributory genetic factors will be discussed, as well as a summary of the currently available treatments for glaucoma, where the need for improved and more targeted therapies is made clear.

Anatomy of the eye in brief

The anatomy of the eye can be divided grossly in to an anterior and posterior chamber, with the iris demarcating the boundary between the two, fig 1.1. The anterior chamber is bounded by the cornea at its anterior aspect, and the iris at its posterior aspect, with the pupil in the middle of the iris allowing the passage of light through to the retina. The region where the iris and cornea meet is referred to as the iridocorneal angle. The anterior chamber is filled with a fluid called aqueous humor (AH), which has a high rate of turnover, providing nutrients to the avascular tissues of the front of the eye, and mechanical support to the eye through maintaining intraocular pressure (IOP). The lens lies behind the iris, held in place by suspensory ligaments, and functions to focus light before it reaches the retina.

The posterior chamber is also fluid filled, but in this case, with vitreous humor, an optically clear gelatinous mass with a low turnover rate. At the rear of the eye lies the retina containing the photoreceptor cells and associated neural cells. The macula is a region located near the centre of the retina in the human eye which contains the photoreceptor cells responsible for high acuity central vision perception. The fovea is a small pit in this region containing large amounts of cone cells, responsible for colour perception. The visual signals generated by the photoreceptor cells of the retina exit the eye towards the visual cortex of the brain though the optic nerve. The retina can be considered a peripheral tissue of the central nervous system, and is formed during embryonic development as an outpocketing of brain neural tissue. As would be expected of central nervous system tissue, the retina possesses a complex arrangement

of different neural cell types which perceive light, and convert this perception to an electrical signal to be carried to the brain, as shown in fig 1.2.

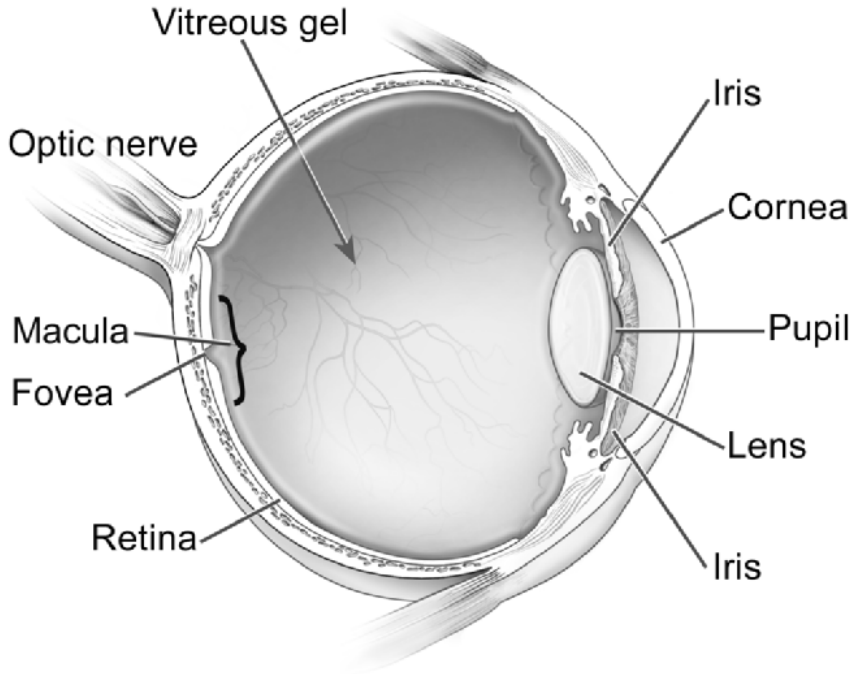

Figure 1.1: The anatomy of the eye.

The major tissues of the whole human eye are shown labeled here, with the anterior chamber to the right of the diagram and the posterior chamber to the left. From the National Eye Institute image bank.

The rod and cone cells of the outer retina perceive light through the interaction of photons with pigments contained within membranous disks of their outer segments, leading to alterations in membrane potential, and the subsequent release of neurotransmitters at the outer plexiform layer, where photoreceptors form synapses with bipolar cells. These bipolar cells act as intermediaries, and pass the signal to the dendritic synapses of the retinal ganglion cells (RGCs) at the inner plexiform layer. The large axon bodies of the RGCs carry the action potential of these signals away from the retina, with the axons converging at the optic nerve head to form the optic nerve itself, with signals subsequently passing to the brain for higher level processing (Purves et al. 2001). This pathway is referred to as a three-neuron chain. Horizontal cells in the retina allow for lateral interactions in the outer plexiform layer, while amacrine cells provide the same function in the inner plexiform layer, amongst other functions.

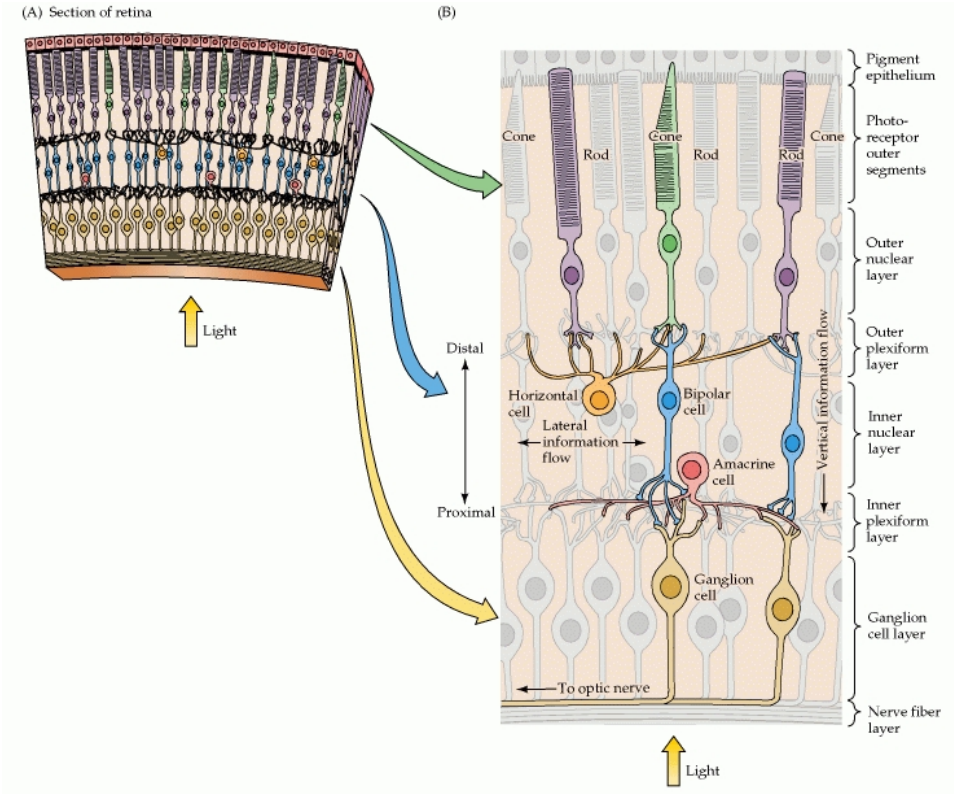

Figure 1.2: The structure of the retina.

(A) Representation of the overall structure of the retina at the posterior of the eye, with the bottom of the diagram representing the anterior direction.

(B) Diagram of the neural circuitry of the retina, showing a three- neuron chain for transmission of visual signals to the brain, from photoreceptor cells, through bipolar cells, to the retinal ganglion cells. (Purves et al. 2001)

Aqueous humor flow dynamics

AH is a clear fluid which provides nutrition to non-vascular anterior chamber tissues, in this manner acting as a replacement to the absent blood supply. As well as nourishing these cells, it removes secreted metabolic byproducts through its high turnover rate, and carries neurotransmitters and growth factors (Goel et al. 2010). AH also functions to maintain the fluid pressure within the eye, IOP, which is a generated through a balance of AH production and its clearance from the anterior chamber, fig 1.3. In glaucoma, changes to the rate of AH clearance, leading to an imbalance between AH formation and clearance rates, cause IOP to become pathologically elevated. It is therefore important to understand the normal flow patterns of AH in the eye before considering the biology of the eye in the glaucomatous state. AH is produced by the cells of the

ciliary epithelium, which line the processes of the ciliary body, and moves forward through the iris into the anterior chamber. In the anterior chamber, temperature differentials between AH near the cooler corneal surface and warmer interior of the eye cause convective flow patterns to arise (Heys & Barocas 2002).

From the anterior chamber, AH can leave the eye via two distinct pathways. The first, known as the unconventional, or uveoscleral outflow pathway, involves the drainage of AH through the ciliary muscle, exiting the eye through the suprachoroidal space and the sclera. The second route, known as the conventional, or trabecular, outflow pathway involves drainage of AH through the trabecular meshwork (TM), into the lumen of a canal, called Schlemm's canal (SC). SC runs around the circumference of the iridocorneal angle, with AH exiting the lumen through collector channels which drain into the episcleral veins.

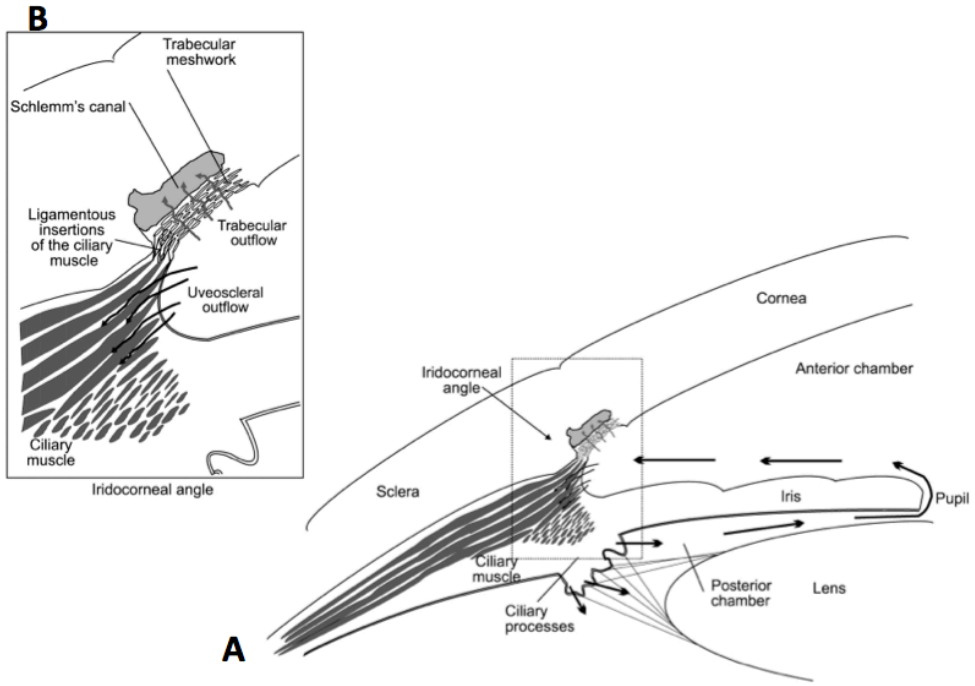

Figure 1.3: Anatomy of the iridocorneal angle and aqueous humor flow pathways.

A. *The structure of the iridocorneal angle and the route taken by aqueous humor, from its formation at the ciliary processes, movement around the iris, entering the anterior chamber through the pupil, and finally moving in to the angle itself.*

B. *Inset. The structure of the two drainage pathways in the angle, with conventional, or trabecular, outflow passing through the trabecular meshwork in to the lumen of Schlemm's canal, and unconventional, or uveoscleral, outflow draining through the interstitial space between fibers of the ciliary muscle,* (Llobet et al. 2003).

Aqueous humor formation

AH is derived from peripheral blood and is secreted by the epithelial cells of the ciliary processes into the AC, representing a blood-aqueous barrier (BAB). AH must pass through several tissue barriers before reaching the interior of the eye, these barriers being the capillary walls, the stroma of the ciliary body, and the epithelial cell layer. Both passive and active processes are involved in the formation of AH, with passive processes leading to the accumulation of AH components in the stroma of the ciliary body, while active secretion is necessary to complete AH formation (Goel et al. 2010).

Passive diffusion allows solutes, in particular lipid soluble molecules, to enter the stroma through across the lipid membranes of capillaries in a concentration dependent manner. Similarly, passive ultrafiltration occurs to move water and water-soluble solutes to the stroma, through fenestrations between the vascular endothelial cells of the capillaries, driven by an osmotic gradient and a differential pressure gradient. This ultrafiltration is size and charge selective, mediated by the fenestrated pores in the capillary endothelium (Civan & Macknight 2004).

Active secretion accounts for 80 – 90 % of AH formation, with this secretion occurring at the non-pigmented epithelial cells of the ciliary processes (Mark 2010). Protein transporters in the cell membranes of these cells mediate selective transcellular movement of water, charged ions, and other molecules. Aquaporins (AQPs) form molecular water channels, allowing bulk flow of water against an osmotic gradient, and AQP1 and AQP4 have been demonstrated to contribute to the formation of AH (Yamaguchi et al. 2006). Other specialized channels actively transport ions including Cl^-, HCO_3^-, and Na^+, as well as biomolecules such as ascorbic acid, and amino acids, across the epithelial layer (Goel et al. 2010). AH turnover occurs at a rate of 1 – 1.5 % of the anterior chamber volume per minute, at an average of 2.4 μL/min in healthy individuals (Brubaker 1997).

Once secreted, AH is composed primarily of water, carrying ions, carbohydrates, amino acids and proteins, and dissolved gases, and is slightly hypertonic as compared to blood plasma. A major difference between plasma and AH composition is the protein concentration, with AH having 200 times less protein, while glucose and urea levels are approximately 80 % of that seen in plasma (Goel et al. 2010).

Unconventional outflow pathway

The existence of the unconventional outflow pathway was inferred through early tracer studies showing the accumulation of tracer molecules in the ciliary body, choroid and sclera following perfusion of these molecules into the anterior chamber. Later studies carried out by Anders Bill in the 1960s introduced radiolabeled tracers into the anterior chamber, which were then shown to accumulate in the same tissues as mentioned above. Bill showed that the tracer accumulated at a constant rate, differing from the diffusion rate of the tracer, leading him to conclude that an AH flow pathway existed out of the anterior chamber through the ciliary muscle and in to the suprachoroidal space (Johnson et al. 2015; Bill 1965).

In the unconventional pathway, AH enters the trabecular meshwork as normal, and from there can move laterally, directly in to the interstitial spaces of the longitudinal bundles of the ciliary muscle, as there is no epithelial barrier blocking access of AH to these spaces (Alm & Nilsson 2009). From the ciliary muscle AH then enters the suprachoroidal space where it can exit the eye by several different pathways, with selective drainage of different AH components occurring through different exit routes. Transcleral drainage can occur through perivascular spaces, accommodating the drainage of larger proteins across the sclera, while smaller molecules and water can exit across the sclera independently of sclera pores through direct diffusion (Jackson et al. 2006; Krohn & Bertelsen 1997). Removal of AH can also occur through osmotic driven forces in the choroid, with drainage though the uveovortex veins (Johnson et al. 2015)

The proportion of AH draining from the anterior chamber via the unconventional outflow pathway exhibits high interspecies variability. In humans, reported values of the amount of outflow occurring through the unconventional pathway vary from 12 – 54 % of total AH outflow, with similar values reported in primates, while in cats, values as low as 3 % are reported (Alm & Nilsson 2009). In certain mice strains, values as high as 80 % of total outflow have been reported (Aihara et al. 2003a).

Conventional outflow pathway

The conventional outflow pathway is located in the iridocorneal angle, adjacent to the unconventional outflow pathway, fig.1.3, within a circumferential groove known as

the scleral sulcus. The TM is located at the inner portion of this sulcus, and is the region of the outflow pathway that AH first reaches, while SC is located past the TM at the interior, fig 1.4.

The TM consists of several layers of structural lamellae, beams of connective tissue composed of collagenous and elastic fibres, covered by TM cells. The beams are attached anteriorly to Descemet's membrane, and extend in a posterior direction where they branch and attach to the scleral spur and ciliary body stroma. The posterior branching of the lamellae gives the TM a triangular shape with a narrow anterior area and wide posterior (Tamm 2014).

The TM can be classified into three main regions, fig 1.4. The inner layer, called the uveal meshwork, consists of up to three layers of TM cell-covered beams originating from the ciliary body at their anterior side. This layer is loosely organized and has large extracellular spaces. The middle layer, the corneoscleral meshwork, is composed of 8 – 15 layers of beams covered in TM cells, which are thicker than uveal beams and originate at the scleral spur (Tamm 2014). The extracellular spaces of the corneoscleral meshwork become progressively narrower as they approach Schlemm's canal (Abu-Hassan et al. 2014). These two layers together form a filtering meshwork that acts to clear debris from the aqueous humor as it drains out of the AC, with the cells in these TM layers displaying high phagocytic activity removing cellular debris from AH as it passes through, to prevent clogging of the meshwork downstream (Llobet et al. 2003; Abu-Hassan et al. 2014). The final layer, the cribriform meshwork, or juxtacanalicular tissue (JCT), is the narrowest of the three layers. The JCT does not possess any beams, and is instead a loose connective tissue composed of 2 – 5 layers of cells surrounded by an extensive fibrillary extracellular matrix (ECM). The JCT has the smallest extracellular spaces in the TM (Tamm 2009). The TM cells of the JCT form elongated processes, attaching to other TM cells, or to the endothelial cells of the SC inner wall, forming a complex 3-dimensional cellular network.

The final barrier to aqueous humor before it leaves the eye via the lumen of SC is the inner endothelial wall of the canal, composed of Schlemm's canal endothelial cells (SCECs). Here AH can take two main routes into the canal lumen, a transcellular route, through large pores in SCECs, and a paracellular, also called intercellular, route between the spaces at cell-cell junctions of the inner wall of Schlemm's canal, fig. 1.4. After AH enters the SC lumen, it is drained through collector channels and returns to peripheral circulation through the episcleral veins. Reports of human conventional

outflow range in value from 40 % to as high as 90 % of total AH outflow, while in mice values are lower, ranging from 20 – 40 % (Braunger et al. 2015a; Lei et al. 2011; Crowston et al. 2004).

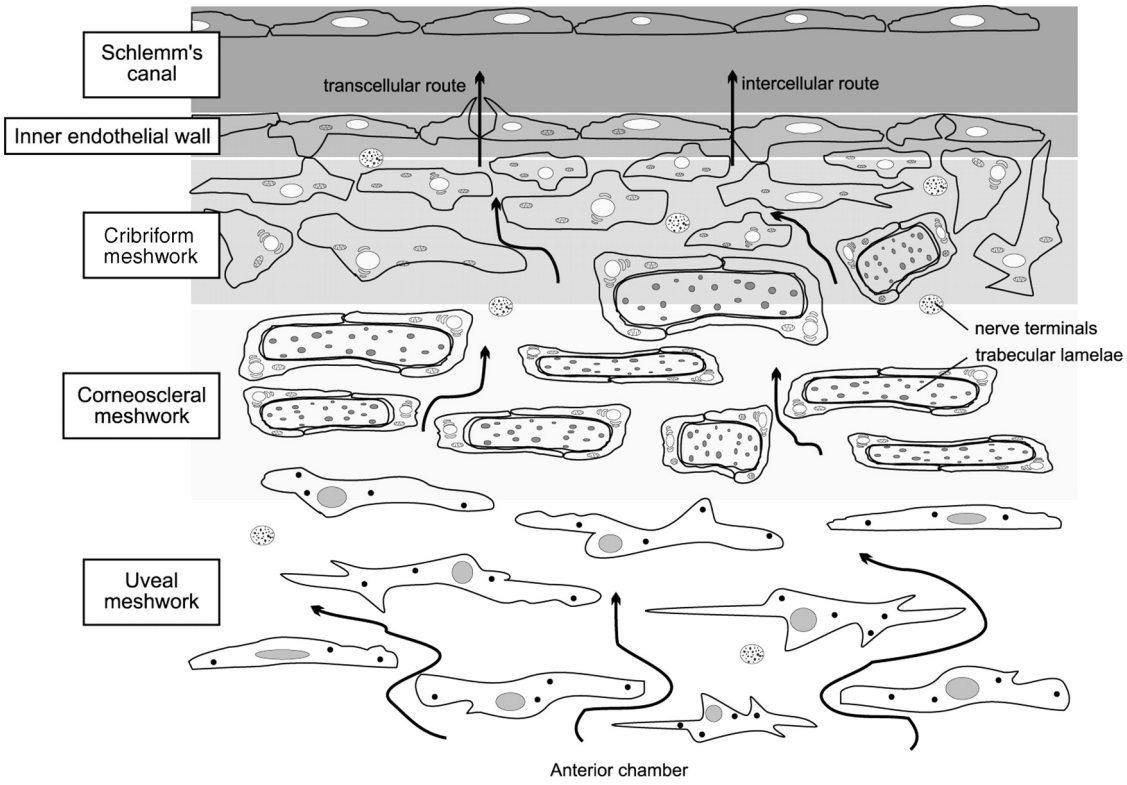

Figure 1.4: The structure of the conventional outflow pathway

Arrows here show the direction of aqueous humor flow through the conventional outflow pathway, beginning at the uveal meshwork, and moving through the corneoscleral meshwork, to the cribriform, or juxtacanalicular, meshwork. From there, flow passes across the inner endothelial wall of Schlemm's canal by either a transcellular or intercellular, also known as paracellular, route, to the canal lumen (Llobet et al. 2003).

Interestingly, outflow of AH through the conventional outflow pathway is highly segmental around the circumference of the iridocorneal angle, as demonstrated by the non-uniform accumulation of perfused tracers (Overby et al. 2009). Studies of differences in ECM gene expression between high and low flow regions of the conventional pathway showed differential expression of different collagen genes between these areas, and enrichment of the proteoglycan versican in low flow regions,

indicating that ECM expression may have a role in segmental outflow (Vranka et al. 2015; Keller et al. 2011).

Schlemm's canal inner wall pores

SCECs form two distinct pore types at the SC inner wall, large intracellular pores contained within Giant vacuoles (GVs), and smaller paracellular pores which form between the cell membranes of adjacent inner wall cells (Ethier et al. 1998). GVs are cellular features that are unique to inner wall SCECs, representing large drainage structures across the inner wall endothelium. These structures take the form of large outpouchings of SCECs into the canal lumen, with the interior cavity of the vacuole being entirely extracellular, and contain large transcellular pores up to 2 μm in size through which AH can pass and reach the SC lumen (Tamm 2014). GVs form in response to the large pressure gradient between the basal and apical sides of SCECs, with the size and density of GVs increasing in proportion to IOP (Pedrigi et al. 2011). GVs are also shown to disappear rapidly when IOP is experimentally lowered to 0 mmHg (Brilakis & Johnson 2001). Inner wall SCECs are connected at their cellular margins by cell-cell junctional complexes called tight junctions (TJs), which restrict paracellular AH flow in a closed state (Ye et al. 1997). Paracellular pores can form as circular dilations of the intercellular space between SCECs, allowing the egress of AH from the JCT to the SC lumen. Paracellular pores also form in response to pressure induced cellular strain, with increased biomechanical strain leading to an increase in paracellular pore density. In contrast to transcellular pores, paracellular pore diameter is not affected by increased strain (Braakman et al. 2014). Along with an increase in pressure drop across the SC inner wall driving the increased formation of both pore types through deformation of the cells, other biomechanical factors influence the extent of pore formation. Factors such as cellular stiffness, contractile state, and attachments to basement membranes or adjacent cells have been demonstrated to influence the formation of both pore types in SCECs (Stamer et al. 2015). While little is known of the direct relationship between opening of paracellular pores and the formation of GVs and transcellular pores, disruption of TJ strands would be expected to reduce cellular stiffness, potentially leading to a greater formation rate of transcellular pores (Braakman et al. 2014; Stamer et al. 2015; Braunger et al. 2015b)

Isolation of cells of the conventional outflow pathway

The two main cell types of the conventional outflow pathway, TM cells and SCECs, have been isolated from donor human eyes, and cultured *in vitro*, allowing further study of their cellular and molecular properties.

The first of these cell types to be isolated were TM cells, isolated through dissection of TM strands and outgrowth of cells from the explant onto a culture plate (Polansky et al. 1981; Polansky et al. 1979). These cells appeared as broad, flat cells, exhibiting cellular branching, and growing in monolayers (Alvarado et al. 1982). TM cells were shown to have several TM specific features, such as expression of a low-density lipoprotein receptor, absence of von Willebrand factor, a vascular endothelial cell marker protein, and high extracellular levels of tissue plasminogen activator (Chang et al. 1991; Snyder et al. 1993). TM cells were also shown to express myocilin in response to treatment with glucocorticoids (Polansky et al. 2000). While this isolation process achieved culture of TM cells, the cellular yield was low, and the process inherently selected for peripheral cells and cells with faster migration rates, giving rise to non-representative populations of TM cells. Improvements came through using a modified protocol intended for isolation of microvascular endothelial cells. This process consisted of the dissection of the TM explants from human donor eyes, and *in vitro* digestion of the ECM surrounding TM cells, creating a suspension of human TM cells. In this manner, TM cellular yield was greatly increased, and a more representative population of TM cells cultured (Stamer et al. 1995). This same ECM digestion process was utilized to isolate TM cells from donor eyes of patients with primary open-angle glaucoma (POAG) (Stamer et al. 2000).

Similarly, human SCECs have been isolated, cultured and characterised. This was achieved through dissection of donor anterior chambers into wedges, and insertion of a gelatin-coated suture into the SC lumen. The sutures were later removed and used to seed adherent SCECs onto culture plates. This resulted in the culture of fusiform cells in linear monolayers, visually distinct from TM cells isolated from the same eye. SCECs were shown to express cell surface markers CD44 and CD54, along with other proteins such as tissue plasminogen activator, and myocilin. Myocilin expression in SCECs however, unlike in TM cells, was not responsive to glucocorticoid treatment, with protein expression levels remaining unchanged (Stamer et al. 1998). Later analysis of these SCECs also showed expression of vascular endothelia cadherin and fibulin-2

as further proteins which differentiate SCECs from TM cells (Perkumas & Stamer 2012). Analysis of SCECs derived from glaucomatous donor eyes showed altered pore formation as compared to cells from healthy eyes, exhibiting significantly reduced paracellular and transcellular pore density when perfused. As these pores are the transport route for AH into the SC lumen, this has clear implications for the increased resistance seen in glaucoma. Glaucomatous SCECs also showed increased cellular stiffness than normal controls, which was postulated to contribute to difficulties in pore formation (Darryl R Overby, Zhou, Vargas-Pinto, Pedrigi, Fuchshofer, Braakman, Gupta, Perkumas, Sherwood, et al. 2014).

Generation of outflow resistance in the conventional pathway

The conventional outflow rate of AH is the primary determining factor in the level of IOP, with resistance to AH outflow giving rise to pressure in the eye. While the exact site of this outflow resistance generation within the conventional pathway is not fully characterised, it is known that is generated within the deeper regions of the pathway, in the area occupied by both the JCT and the inner wall of SC. This must be the case due to the highly porous structure of the uveal and corneoscleral meshworks. Modelling of outflow resistance generation has shown that a single pore of the diameter observed in the outer meshworks could accommodate the total AH outflow of an eye. As such, these regions must have negligible contribution to resistance generation. Tissues downstream of the JCT and SC inner wall, such as the SC lumen and episcleral veins, can also be excluded as having a major role in outflow resistance generation, as similarly their large diameters have been shown by hydrodynamic modelling to have no significant contribution to AH flow resistance (Johnson 2006). Direct measurement of the pressure in the lumen of SC in primates also showed that it was at the same level as episcleral venous pressure, being approximately 8 mmHg below IOP, indicating the pressure drop occurs upstream of this point, which must be at the SC inner wall or JCT (Mäepea & Bill 1989).

The inner wall endothelial cells of SC generate outflow resistance through formation of a confluent vessel wall with cell-cell contacts maintained by TJs. The inner wall endothelium of SC has an unusually high hydraulic conductivity as compared to other endothelial cell layers, having one of the highest hydraulic conductivities in the body (Johnson 2006). Ultrastructural examination of this region provides an

explanation for this level of conductivity, through visualisation of the density of micron scale pores present on the SC inner wall, with up to 1000 pores/mm^2 reported (Ethier et al. 1998). Early SEM studies concluded that the SC inner wall could not provide more than 10 % of total outflow resistance (Svedbergh & Bill 1972). Additionally, AH can also pass between the TJ strands that hold non-pore forming areas of adjacent cell membranes in close contact. Experiments have shown shown accumulation of cationised ferritin accumulates at TJs when perfused in to enucleated human eyes, with a corresponding decrease in outflow facility, the ratio of AH outflow to pressure, (Ethier & Chan 2001). It has also been shown that there are significantly fewer pores at the inner wall of glaucomatous eyes than seen in normal eyes, while areas of high paracellular pore density have been demonstrated to co-localise with high flow segments of the conventional outflow pathway (Johnson et al. 2002; Braakman et al. 2015).

The JCT region would therefore be expected to account for the remainder of AH outflow resistance generation necessary to maintain IOP. This region has extensive, tortuous, sub-micron diameter intercellular AH flow pathways, which, if empty, would not contribute greatly to AH outflow resistance (Ethier et al. 1986). In order for this tissue region to generate the necessary outflow resistance observed *in vivo*, these extracellular spaces would have to be filled with a resistive substance that was not visible in TEM images. Use of alternative tissue preparation techniques for TEM allowed greater preservation of extracellular structures, showing extensive ECM present in the intercellular spaces of the JCT, but with some large open spaces still present (Johnson 2006; Gong et al. 2002). Additionally, matrix metalloproteases (MMPs), which degrade ECM components, have been shown to reduce outflow resistance when perfused in to enucleated eyes , and when secreted in to the AH, further indicating the role of ECM in the JCT in outflow resistance generation (O'Callaghan et al. 2017; Bradley et al. 1998). Despite this, it remains unclear the extent to which the JCT region generates resistance to AH outflow.

While the site of major conventional outflow resistance generation has been mapped to the SC inner wall and JCT regions in multiple studies, current data are unable to confirm whether a single one of these sites is the greatest mediator of outflow resistance. Instead, a synergistic model of outflow resistance generation has been proposed, in which the inner wall of SC and the JCT together are responsible for the bulk of conventional outflow facility generation. Under this model, referred to as the

funneling model of outflow resistance generation, as SC inner wall pores are spatially separated on the inner wall, AH moving from the JCT into these pores must converge, or funnel, from wide areas of the JCT to discrete pores on the inner wall, fig 1.5.

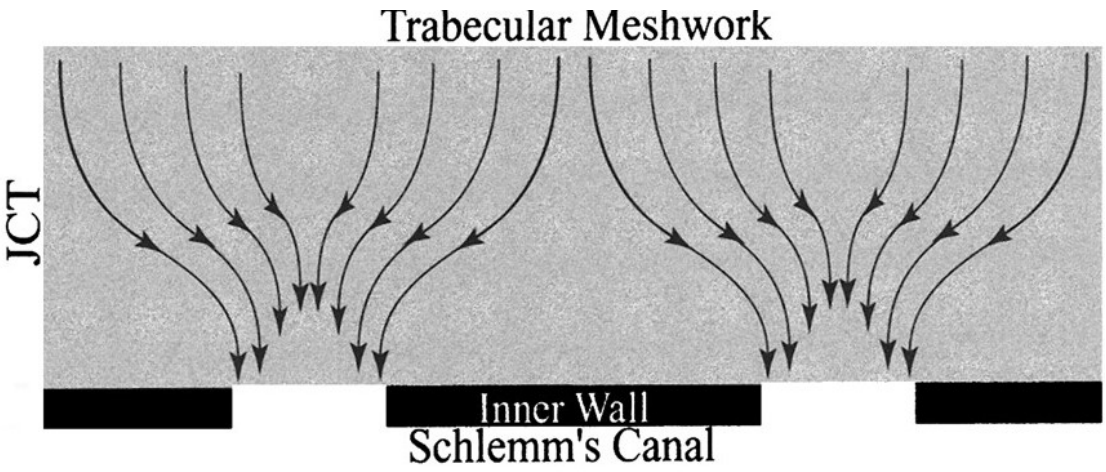

Figure 1.5: The funneling model of outflow resistance generation.

A representation of the convergence, or funneling, of aqueous humor flow, represented by arrows, from the JCT region towards discrete pores on the inner wall of Schlemm's canal. Adapted from Overby et al. 2002.

This non-uniform flow increases the effective length of the AH flow pathway through the JCT, thereby increasing its hydraulic resistance by a factor of 30 when considering pore density alone, or a factor of 15 when considering that the majority of these inner wall pores are contained within giant vacuoles, which have larger diameter basal openings than pores alone (Johnson et al. 1992; Overby et al. 2009). Evidence in support of this model is seen in studies of the 'washout' effect observed in perfusion studies, where outflow resistance progressively decreases over time. This effect can be reversed through lowering of IOP to 0 mmHg, with normal outflow resistance seen after this pressure reduction. This effect is seen to be caused by a separation of the inner wall of SC from the JCT, removing any funneling effect, and decreasing outflow resistance, while lowering of IOP allows the tissues to re-attach, and restores outflow resistance to normal values (Overby et al. 2009; Overby et al. 2002). The level of attachment of the JCT to the SC inner wall may also help explain segmental outflow pattern in the conventional pathway, with flow preferentially reaching regions with separation between the tissues. Treatment of eyes with Rho kinase inhibitors, discussed in more

detail later in this chapter, has been shown to convert segmental outflow patterns to an evenly distributed flow pattern, with a concomitant increase in separation of the inner wall from the JCT (Lu et al. 2008).

Outflow resistance is a dynamic, rather than fixed, property of the conventional outflow pathway. When the anterior chambers of enucleated human eyes are perfused at physiological flow rates until IOP stabilizes, and then subjected to a doubling of inflow rates, IOP is seen to also double immediately, indicating no initial change in outflow resistance. However, over the course of several days of perfusion at this constant high flow rate, IOP is seen to gradually decrease until it reaches the level seen at the original flow rate, showing a clear adaptation of outflow resistance in response to increased pressure. Similarly, doubling of applied perfusion pressure shows an immediate doubling of inflow rate of perfusate, which then subsequently continues increasing further to account for high IOP (Acott et al. 2014).

Features of glaucoma

The term glaucoma encompasses a group of different disorders all sharing similar symptoms and ocular pathology. These diseases are typically characterized by a reduction in the outflow of AH from the anterior chamber, resulting in elevated IOP, a state referred to as ocular hypertension (OHT). Outward pressure in the eye occurring during OHT leads to damage of the neural tissue of the retina and optic nerve head (ONH), due to the elevated pressure exerting an outward force on the ONH, deepening the optic disk, leading to optic nerve atrophy and RGC loss (Noecker 2006). This damage is known as glaucomatous optic neuropathy, and causes progressive loss of visual field.

Intraocular pressure and ocular hypertension

IOP refers to the fluid pressure in the interior of an eye, maintained by AH through the balance of its production rate and clearance rate from the anterior chamber. While the fluid of the posterior chamber, the vitreous humor, is also subject to this same pressure, its low turnover rate means that it has a negligible role in the generation of IOP. This fluid pressure is necessary to maintain the shape and structure of the globe, as well as ensuring constant ocular properties of the cornea through sustaining tautness

of the tissue. Further, IOP also drives the turnover of AH in the anterior chamber, which provides nutrition to non-vascular anterior chamber tissues (Goel et al. 2010). The normal expected IOP in healthy individuals ranges from 10 – 20 mmHg, with an average of around 14 mmHg, while ocular hypertension is regularly defined as being IOP higher than 22 mmHg (Hoehn et al. 2013; Watson et al. 1996; Camras 1996). IOP values exhibit high levels of diurnal variation, with a range of up to 10 mmHg reported (Asrani et al. 2000).

The optic nerve head

The ONH, also known as the optic disk due to its circular appearance in fundus images, is the point at which retinal ganglion cell axons converge and exit the retina towards the brain through pores in a layered connective tissue called the lamina cribrosa (LC). No photoreceptors are present at the surface of the optic nerve head, and as such it is a visual blind spot. The convergence of RGC axons form a shallow depression in the retina referred to as the optic cup, fig. 1.6 (Weinreb & Khaw 2004). Increased outward pressure occurring during OHT is equal in all directions, and elevated IOP increases the pressure gradient at the ONH. As the sclera is perforated at the ONH, it represents a mechanical weaker point than the rest of the posterior chamber, and as such the increased pressure gradient causes the ONH to recede, increasing the depth and width of the optic cup. The ratio of cup width to disk width, and the change in this ratio over time, can be a measure of the progression of glaucoma, as the ONH is pushed posteriorly by elevated IOP, widening and deepening the optic cup. The depth of the optic cup can also be assessed in patients using several different techniques, such as optical coherence tomography or scanning laser polarimetry. The reflectivity of the ONH under examination is also an indicator of glaucomatous state, with healthy eyes having bright reflections, while in glaucoma, reflectivity is reduced in area and intensity due to loss of retinal fibres (Weinreb & Khaw 2004).

Glaucomatous optic neuropathy

The mechanism by which neural damage occurs in glaucoma is not as yet fully understood. Typically, high IOP leads to deformation and stretching of the LC and the axons of RGCs, leading to RGC death, fig. 1.6 (Bellezza et al. 2003; Fechtner &

Weinreb 1994). This could be a direct result of the mechanical deformation of the LC damaging RGC axons in the ONH. While the LC provides a support structure for RGC axons by surrounding the axons as they pass through LC pores, deformation of the LC can widen or distort these pores, reducing the physical support provided and causing axonal damage. The axons are also stretched by the deformation and posterior movement of the ONH, also causing mechanical damage (Fechtner & Weinreb 1994).

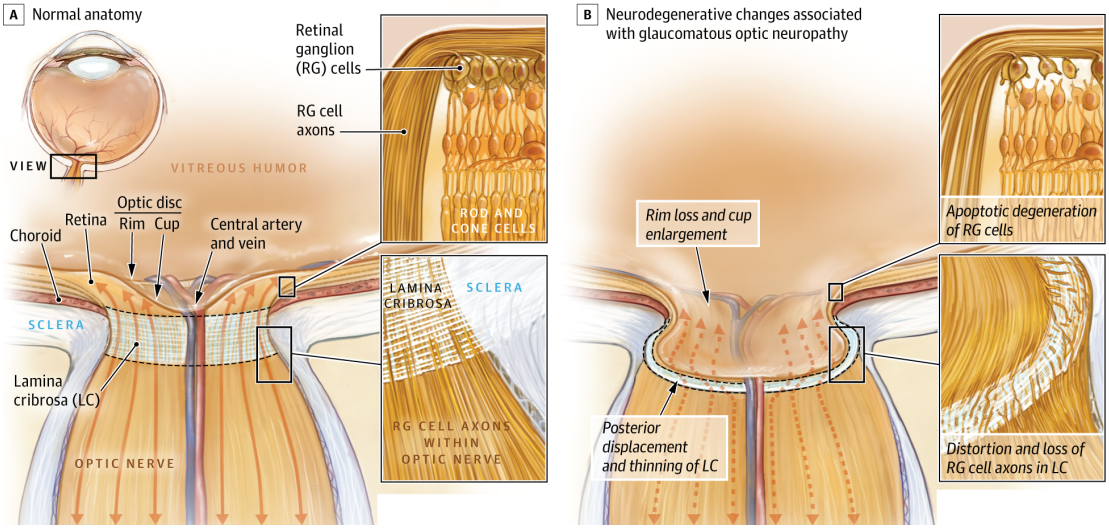

Figure 1.6: Neurodegenerative changes associated with glaucomatous optic neuropathy.

A. Representation of a healthy optic disk, with convergence of RGC axons from the retina forming a shallow depression, leading through the lamina cribrosa, forming the optic nerve which carries visual signals to the brain.

B. Anatomical features of glaucomatous optic neuropathy. The optic cup has been displaced posteriorly, with damage and loss of RGC axons in the lamina cribrosa, and death of RGC cell bodies in the retina. Adapted from Weinreb et al. 2014.

Along with mechanically induced damage, increases in IOP can also have an effect on retrograde transport in the ONH, depriving RGC cell bodies of neurotrophic factors and preventing recycling of cellular components. This has been demonstrated in experimental models of OHT, with transport of radiolabeled neurotrophic factors being shown to be inhibited by elevated IOP (Quigley et al. 2000). This would lead to induction of cell death due to trophic insufficiency.

Factors independent of IOP can also have an effect of glaucomatous optic neuropathy. An example of this is dysregulation of blood flow to the retina causing ischemia induced hypoxic conditions and subsequent RGC death (Harris et al. 1998;

Harris et al. 2005; Flammer & Orgül 1998). Other factors such as immune system dysregulation, impaired glutamate signaling, and oxidative stress have also been proposed as potential contributors to glaucomatous optic neuropathy also (Weinreb & Khaw 2004).

Types of glaucoma

The term glaucoma describes a group of similar disorders, with the two main classes of the disease being primary open-angle glaucoma, (POAG), and primary angle-closure glaucoma, (PACG), while several other less common classes of glaucoma also exist, such as normal tension glaucoma (NTG), pseudo-exfoliative glaucoma (PXG), pigment dispersion glaucoma (PDG), as well as multiple forms of secondary glaucoma resulting from other conditions or states.

Primary angle-closure glaucoma

In PACG, the route of movement of AH towards normal drainage pathways out of the anterior chamber, which are located in the iridocorneal angle, is occluded by the iris, fig. 1.7 (Lee & Higginbotham 2005). The iridocorneal angle is referred to as anatomically closed in cases where greater than 270° of the circumference of the iridocorneal angle is occluded. Angle closure leads to OHT and glaucomatous optic neuropathy as described above. While PACG is regularly asymptomatic until advanced vision loss has occurred, in approximately one third of cases it occurs in an acute disease state, with patients presenting with symptoms such as conjunctival hyperemia, an unreactive pupil, pain, nausea, and significantly raised IOP, usually higher than 30mmHg (Weinreb et al. 2014). The occlusion of the iridocorneal angle can occur by a number of different mechanisms. Resistance to AH flow through the pupil may cause a buildup of pressure behind the iris, leading to the apposition of the iris against the cornea, referred to as an iris bombe, thereby obstructing the flow of fluid out of the AC. This is referred to as a pupillary block and occurs more commonly in eyes with shallow anterior chambers (Wang et al. 2002). A malformation of the iris, known as plateau iris, can also cause PACG in the absence of a pupillary block, causing an apposition of the iris against the corneal endothelium called iris crowding, as is seen commonly in Asian patient populations (He et al. 2006). Other anatomical factors that make contribute to

development of PACG include anteriorly positioned lens, peripheral iris thickness, and iris curvature, all contributing to the proximity of the iris to the corneal endothelium in the iridocorneal angle (Nongpiur et al. 2011).

Primary open-angle glaucoma

In contrast to PACG, in POAG the iridocorneal angle remains open, and the resistance to aqueous humor outflow arises within the outflow tissues themselves, specifically in the conventional outflow pathway, fig. 1.7 (Lee & Higginbotham 2005). While it is known the pathological increased resistance to AH outflow occurs in the conventional outflow pathway, the cellular or molecular basis for the pathogenesis of this increased resistance is not known. Dysregulation of the maintenance of IOP homeostasis in different manners have been suggested as contributors to glaucomatous reduction in AH outflow, including mechanisms as diverse as changes in pore density, increased ECM expression in the TM, changes to the contractility or rigidity of TM or SC cells, changes to cytoskeletal arrangement, disruption of the ability to sense elevated IOP, regulation of segmental outflow, or oxidative damage to cells (Kwon et al. 2009; Stamer & Acott 2012). It is likely that a widely varying combination of these potential contributors to increased outflow resistance occur in different patients.

Normal tension glaucoma

NTG is considered a subtype of POAG, as the iridocorneal angle similarly remains anatomically open (Mousa & Beidoe 2012). In NTG, however, while glaucomatous optic neuropathy and loss of visual field occur as in all other glaucoma types, IOP remains within the range of normal levels. This damage in the absence of OHT is not fully understood, but possibly occurs due to reduced perfusion of the ONH due to lower ocular blood flow levels, or structural abnormalities in the connective tissue supporting the optic nerve leading to a lower IOP threshold for development of optic neuropathy, (Mousa & Beidoe 2012; Mozaffarieh & Flammer 2013; Burgoyne 2011). Abnormally low blood pressure could also be a factor, artificially increasing the pressure gradient between the interior and exterior of the eye at the ONH, or through loss of sufficient ocular perfusion (Mallick et al. 2016).

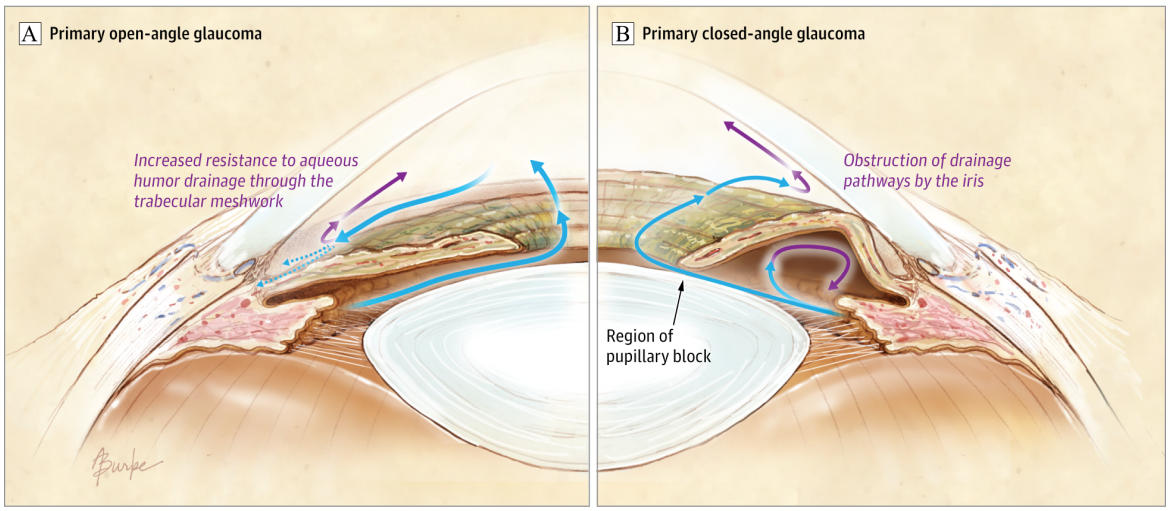

Figure 1.7: Primary open-angle glaucoma and primary angle-closure glaucoma.

A. In POAG, increased resistance to AH outflow occurs within the conventional outflow pathways itself, with the iridocorneal angle remaining open.

B. In PACG, the iris blocks the flow of AH into the iridocorneal angle, preventing its drainage through either the conventional or unconventional outflow pathways. Adapted from Weinreb et al. 2014

Pseudoexfoliative glaucoma

PXG occurs in patients with pseudoexfoliation syndrome, and is again a form of POAG. In this disorder, granular protein deposits occur throughout the body, and accumulate in the anterior chamber, where they become lodged in the conventional outflow pathway. Here, they form a physical block to AH outflow, causing intermittent large elevations in IOP, and IOP fluctuations, leading to glaucoma progression as in other forms of the disease (Lee 2008). The presence of pseudoexfoliation material in the anterior chamber is also associated with degeneration of the iris, lens and cornea, which also may contribute to the disease state (Schlötzer-Schrehardt & Naumann 2006).

Pigment dispersion glaucoma

Representing another form of POAG, PDG manifests in a similar manner to PXG, through clogging of the conventional outflow pathway. In the case of PDG, disturbance of the iris pigment in the anterior chamber causes its release in to AH, and movement

to the iridocorneal angle, where it forms a physical barrier to outflow as in the case of protein deposits in PXG. Pigment dispersion may occur due to friction between the iris and corneal endothelium (Michelessi & Lindsley 2016).

Secondary glaucoma

Several forms of secondary glaucoma exist, where glaucoma is a consequence of a different disease state. Examples of this include inflammatory glaucoma, phacogenic glaucoma, which is induced by cataracts, glaucoma arising as a result of intraocular hemorrhage, neovascular glaucoma, or steroid induced glaucoma.

Epidemiology and risk factors of glaucoma

Glaucoma is one of the leading causes of blindness worldwide, with a global prevalence of 3.05 % for POAG, and 0.50 % for PACG. An estimated 13 % of all blindness in Europe is caused by glaucoma, affecting 6.7 million, and costing on average almost €17000 per patient per year to manage (Poulsen et al. 2005; Tham et al. 2014). While estimates from 2014 state that approximately 64.3 million people worldwide were affected by POAG and PACG, it is predicted that this number will rise by 74% to 111.8 million by 2040, with this increase occurring disproportionately in Africa and Asia, due to larger population numbers, and relatively low current elderly populations, as compared to Europe and North America. Reasons for this projected increase centre largely around the trend towards increasingly aged populations worldwide, with age being one of the largest risk factors associated with glaucoma, the odds ratio for glaucoma being reported as 1.79 for every decade increase in age (Tham et al. 2014). Many other risk factors exist that contribute to the prevalence of glaucoma, such as ethnicity and gender. The effect of ethnicity on the prevalence of POAG is most clearly seen through its increased prevalence amongst those of African descent, 5.4 %, as compared to the global average of 3.05 %, while PACG is more prevalent amongst Asian populations, with a prevalence of 1.2 %, versus 0.5 % globally. Gender also plays a role in the prevalence of POAG, with males being 36 % more likely to have the disease than females. Habitation area also seems to be a factor, as those that live in urban areas are 58 % more likely to have the disease, (Tham et al. 2014). Other baseline factors that can be used to predict the onset of glaucomatous optic neuropathy and vision loss in

patients with high IOP that have yet to develop glaucoma symptoms include large optic cup-to-disk ratio, and level of elevated IOP itself, while patients with thin central corneas have a 3-fold higher risk of developing POAG (Gordon et al. 2002).

Genetics of primary open angle glaucoma

While POAG is a complex, multifactorial disease, twin studies and pedigree analysis have revealed that it is also to some extent heritable. Genetic studies have revealed two different classes of genes related to POAG, those that directly cause POAG, and those that increase the risk for developing the disease likely when found in combination with other alleles or environmental factors.

Myocilin (*MYOC*) was the first gene to be implicated in the direct causation of POAG, through linkage analysis of patients with juvenile onset POAG (Stone 1997). It was later shown to be mutated in 2 – 4 % of POAG patients in a large cohort, with varying mutations present, usually transmitted in an autosomal dominant manner and associated with significantly elevated IOP (Fingert et al. 1999; Fingert 2011). Mutations in *MYOC* associated with juvenile POAG have been shown to cause IOP elevation beyond 40 mmHg, while mutations associated with adult onset disease generally cause IOP elevations to the range of 25 – 40 mmHg (Kwon et al. 2009). The normal function of myocilin is as yet unknown, however, the wild type form is secreted, while mutant forms cannot be secreted and accumulate intracellularly in the TM, (Jacobson et al. 2001). This accumulation has clear potential to cause damage to TM cells, leading to the pathological development of POAG.

Optineurin (*OPTN*) is another causative gene associated with POAG, transmitted autosomal dominantly, again identified by linkage analysis, and shown to be expressed in the TM, ciliary processes, retina, and brain (Rezaie 2002). *OPTN* was also shown to be associated with the NTG subset of the POAG cohort, indicating that unlike *MYOC*, it does not have a role in IOP elevation. While the normal biological function of this protein is not known, its expression in the TM is seen to be induced in organ culture by high IOP, steroid exposure, and exposure to TNFα, indicating a potential protective role in response to stressors (Challa 2009). *OPTN* overexpression also confers resistance to oxidative stress, while similar overexpression of mutant forms of the gene fail to protect cells from oxidative stress induced apoptosis (De Marco et al. 2006). The protein product of *OPTN* interacts with TANK-binding kinase-1 (*TBK1*), another gene

associated with POAG, specifically NTG. *TBK1* copy number variations are seen in patients of African origin with NTG (Fingert 2011). Again, little is known of the protein's function, or role in the development of NTG, but it seems to interact with proteins in the NF- kB signaling pathway.

A further gene identified as being associated with POAG is ankyrin repeats and suppressor of cytokine signaling box-containing protein 10 (*ASB10*), with mutations identified in two different patient cohorts. *ASB10* is expressed in the TM and SC inner wall, as well as the ciliary processes. The role of the protein is not known, but silencing of the gene in TM in organ culture was shown to reduce outflow facility by 50 % (Pasutto et al. 2012).

Genes identified as causative for POAG currently only account for approximately 10% of all POAG cases (Janssen et al. 2013). In addition to pathological Mendelian genes, genome-wide association studies (GWAS) have identified several loci that seem to increase the risk of developing POAG. Notable among these loci are the *caveolin* genes, *CAV1* and *CAV2*, expressed in the retina, TM and SC, and postulated to alter TGF-β signaling (Fingert 2011; Liu & Allingham 2017). Other genes such as *FOXC1, AFAP1, CKDN2B-AS1, TMCO1* and *SIX1* have also been shown by GWAS to be associated with POAG, among many other genes (Abu-Amero et al. 2015; Allingham et al. 2009; Liu & Allingham 2017). Risk alleles thus far identified for POAG have modest odds ratios as compared to those identified for other ocular diseases, indicating that aside from cases of PAG caused directly by mendelian mutations, the disease case is likely brought about by the combined minor effects of a huge number of genetic risk factors, in addition to environmental effects (Fingert 2011).

Current treatments for primary open-angle glaucoma

As elevated IOP is by far the main risk factor for the development and progression of POAG, the current therapeutic approach for POAG focuses mainly on reducing IOP, with the aim of slowing or halting further damage to the retina, with IOP reduction in fact being the only proven means of treating POAG (Weinreb et al. 2014). Several large-scale studies have shown that reduction in ocular hypertension is effective in glaucoma treatment and management, with reduction in IOP delaying or preventing the onset of POAG in patients with elevated IOP and no glaucomatous symptoms, and in reducing progression of the disease in newly diagnosed POAG patients (Kass et al. 2002; Heijl et al. 2002).

Target reduction in IOP is generally 20 – 50 % of pre-treatment level, with level of IOP decrease being further adjusted downwards if vision loss or optic nerve recession progresses (Prum et al. 2016). Reduction in IOP is generally first attempted through the use of topical pressure lowering medications, with surgical intervention being carried out in patients that fail to achieve target IOP reduction.

Pharmacological treatment

Elevated IOP is brought about by a decrease in the clearance of AH from the anterior chamber through the conventional outflow pathway, while outflow rates are affected, inflow of AH remains unchanged, leading to a state of OHT. Pharmacological approaches aim to restore the balance of inflow and outflow rates of AH, through increase either unconventional or conventional outflow of AH or decreasing the rate of production of AH.

Prostaglandin analogues, for example latanoprost, or bimatoprost, are generally the first line of treatment for POAG, representing the most commonly prescribed topical treatment, and additionally having been shown to be the most effective of all IOP reducing topical treatments (Li et al. 2016). Prostaglandin analogues have been shown to significantly increase outflow of AH through the unconventional outflow pathway, and also appear to increase conventional outflow of AH to some extent (Mastropasqua et al. 2014; Toris et al. 2008). While the mechanism by which prostaglandin analogues increase outflow is as yet not fully understood, it has been demonstrated that treatment brings about an increase in MMP expression in the unconventional outflow pathway, and a resultant reduction in ECM protein levels (Gaton et al. 2001; Sagara et al. 1999). This would be expected to reduce the resistance of this pathway to AH outflow, leading to an increased unconventional outflow rate of AH, and concomitant reduction in IOP.

β-adrenergic blockers, for example timolol or levobunolol, represent another class of topical IOP lowering medications, used as a second line approach to the treatment of POAG, when first line medications have failed to achieve adequate reduction in IOP, or in patients contraindicated for the use of prostaglandin analogues. These medications block β1- and β2- adrenergic receptors, which are expressed to a high degree at the non-pigmented ciliary epithelium, the site of AH production (Trope & Clark 1982). These medications cause a reduction in the production rate of AH at this site, likely due to receptor blocking causing an excess of noradrenaline, reducing the blood supply to the

ciliary processes, and thereby decreasing the fluid available for AH production (Brooks & Gillies 1992). β-adrenergic blockers exhibit a significant side effect profile, including ocular irritation, and are contraindicated in patients with asthma and chronic obstructive pulmonary disease (Weinreb et al. 2014).

Carbonic anhydrase inhibitors, acetazolamide for example, also function to decrease the production rate of AH at the ciliary processes, in this case through inhibition of the formation of bicarbonate, thought to be necessary for maintaining sodium concentrations necessary for osmotically driven AH secretion (Goel et al. 2010; Mousa & Beidoe 2012).

Cholinergic medications, such as pilocarpine, function to increase the outflow of AH through both the conventional and unconventional outflow pathways, through inducing contraction of the ciliary muscle. This contraction pulls on the trabecular beams anchored to the ciliary muscle, opening the spaces of the trabecular meshwork, indirectly increasing conventional outflow facility (Mousa & Beidoe 2012).

Rho-kinase inhibitors, for example ripasudil or netarsudil, are an emerging class of IOP lowering drugs for the treatment of POAG. These drugs increase outflow through the conventional outflow pathway by altering multiple sites within the pathway, leading to an increase in high flow regions. While the exact molecular mechanism for this effect is as yet not known, treatment is correlated with an expansion of the TM and JCT, and dilation of the episcleral veins. Greater changes to segmental flow are observed at the episcleral veins than at the SC inner wall, suggesting that the site of action is distal to SC (Ren et al. 2016). No drugs in this class have yet been granted FDA approval, and currently are only available in Japan.

While the pathological increase in AH outflow resistance observed in POAG occurs in the region of the JCT and SC inner wall, the most commonly prescribed IOP lowering medications mainly target the site of AH production, and the unconventional outflow pathway, with only indirect effects on the conventional outflow pathway occurring only. Additionally, prostaglandin analogues, the most prescribed and most effective of all classes of IOP lowering medications, failed to achieve adequate IOP reduction in 25 - 50 % of treated patients (Scherer 2002). The development of conventional outflow targeted therapies, with specific emphasis on therapies targeting the site of glaucomatous reduction in AH outflow, is currently viewed as an essential step in the treatment and management of glaucoma (Stamer 2012).

Surgical intervention

In cases where pharmacological treatment fails to produce the necessary reduction in IOP to slow or stop the progression of POAG, surgical intervention may be required. In some cases, such as severe OHT, surgery may represent a first line therapy (Weinreb et al. 2014). Surgical intervention in the treatment of POAG can be either laser based, or incisional. Laser trabeculoplasty involves the exposure of the TM to laser energy directed through the cornea, with no surgical incisions occurring. The mechanism by which laser trabeculoplasty functions to reduce IOP is not fully understood, but several theories have been proposed. A mechanical theory posits that heat energy from laser exposure causes tissue burns, leading to a contraction of collagen fibres in the TM. This would in turn stretch surrounding tissues, widening the TM and increasing conventional AH outflow. A biological theory proposes that conventional outflow rate increase is a result of ECM remodeling induced by laser induced cytokine release. A further theory states that laser exposure stimulates cell division and subsequent repopulation of the TM (Stein & Challa 2007). In a trial of selective laser trabeculoplasty, 89 % of treated eyes had a reduction in IOP of greater than 5 mmHg (Melamed et al. 2003).

The most common incisional surgery for the treatment of POAG is trabeculectomy, whereby a portion of the conventional outflow pathway is surgical removed, creating a new outflow pathway, with low resistance to AH outflow, to the subconjunctival space (Lee & Higginbotham 2005). While trabeculectomy is effective in lowering IOP, it is not without complications. Scar formation after surgery may block the newly formed outflow pathway, and infection is a significant risk (Weinreb et al. 2014). Other minimally invasive surgical procedures, referred to as non-penetrating surgeries, as they do not penetrate the anterior chamber completely, can be used in the place of trabeculectomy. Examples of non-penetrating surgeries for POAG include deep sclerectomy, where a portion of the deep sclera is removed, viscocanlostomy, where a viscous gel is injected into a portion of the lumen of SC to open the canal and creat a channel from the SC lumen to a scleral reservoir, and canaloplasty, where the entirety of the SC lumen is threaded with a catheter and injected with a viscoelastic gel, while also having a suture loop introduced to hold the canal open. While these non-penetrating procedures have been demonstrated to not lower IOP to the same extent as trabeculectomy, the do however effectively lower IOP, and with less incidence of post-surgical complications than trabeculectomy (Rulli et al. 2013). Surgical devices may

also be implanted into the anterior chamber to allow bulk outflow of AH across the sclera, and trans-trabecular stents may be inserted, bypassing the site of greatest conventional outflow resistance by connecting the outer TM to the lumen of SC (Ahmed et al. 2014; Lee & Higginbotham 2005).

Summary

This introductory chapter has shown the processes through which AH inflow and outflow occurs in healthy eyes, along with the loss of homeostatic IOP in glaucomatous eyes due to aberrant high resistance to AH outflow through the conventional outflow pathway. The resultant anatomical changes, glaucomatous optic neuropathy, and vision loss associated with this increased outflow resistance was explained. Current treatments for POAG were discussed, highlighting the need for novel therapies that target the conventional outflow pathway.

In the following chapters of this thesis, the main objective is to investigate a novel therapeutic approach to the treatment of POAG, by increasing the outflow of AH through the conventional outflow pathway through the targeting of the tight junctions of Schlemm's canal, as well as the investigation of the effect of the cytokine interleukin-18 on Schlemm's canal permeability and conventional outflow facility.

Chapter 2: Characterisation and modulation of Schlemm's canal tight junction proteins

Introduction

As has been discussed in the general introduction of this thesis, all AH leaving the eye via the conventional outflow pathway must pass through the trabecular meshwork and subsequently cross the inner wall endothelium of Schlemm's canal, entering the canal lumen, before returning to peripheral blood circulation through the episcleral veins. As such, it is desirable to characterise the factors that determine the hydraulic conductivity of this pathway.

Endothelial and epithelial cells form monolayers that function to physically separate different biological compartments in organisms, acting as barriers to fluid, ion, and macromolecular flux. In order for these monolayers to function as effective barriers, the plasma membranes of the cells in these monolayers must be maintained in close contact to prevent uncontrolled paracellular movement of biomolecules across the cellular sheet, while also still allowing for selective paracellular diffusion of molecules that are necessary for maintenance of tissue homeostasis. This is achieved through the formation of cell-cell junctional complexes known as tight junctions (TJs) between apposed plasma membranes of adjacent cells.

The focus of this chapter is the characterisation of TJs present between the endothelial cells of SC inner wall, and the validation of their modulation with the intention of increasing paracellular permeability, and therefore elimination of AH from the anterior chamber.

Structure and composition of tight junctions

While investigations into the nature of cell-cell junctions have been carried out since the 19th century, with densely stained regions termed desmosomes observed between cells via light microscopy, it was the development of transmission electron microscopy (TEM) that brought about the ability to distinguish between differing cell-cell junctions. The recognition of TJs, initially called zonula occludens, as a distinct form of junction came with ultrastructural visualization by TEM, showing that TJ complexes were

composed of varying numbers of plasma membrane contact points between cells, forming “a continuous belt-like attachment”, with electron dense regions present in the cytoplasm underlying these contact points, later termed a junctional plaque (Farquhar & Palade 1963).

Subsequent to the identification of TJs by TEM, freeze fracture electron microscopy was utilized to visualize the hydrophobic interior of the plasma membrane phospholipid bilayer of cells joined by TJs. This analysis revealed the presence of complex networks of branching and interlinking transmembrane strands embedded in the cell membrane, which were believed to represent the physical barriers to paracellular diffusion. Further, it was shown that tissues known to form tighter barriers to paracellular transport had more complex junctional strand composition, while those with low resistance to paracellular flow had more simplistic networks composed of fewer junctional strands (Claude & Goodenough 1973).

The first protein component of TJ complexes to be identified was zonula occludens-1 (ZO-1), a 220 kDA intracellular protein localised to the previously identified cytoplasmic junctional plaques (Stevenson et al. 1986). ZO-1 is an adapter protein, with several protein binding domains, that forms a molecular bridge between transmembrane TJ components and the cytoskeleton of cells possessing TJs. Binding to transmembrane proteins occurs at the N-terminal region of the protein, through several different domains, namely, PSD95-DLGA-ZO-1 homology (PDZ), SRC homology 3 (SH3), and guanylate kinase (GUK) domains. The ZO-1 homologues, ZO-2 and ZO-3, which differ from each other in their C-terminal domains, are also localised to the same region of the TJ complex. Many other PDZ domain-containing proteins are also present in the TJ plaque, including MUPP1, MAGI, and PALS1. These proteins in turn can bind to further adapter proteins, for example cingulin or cortactin, which then bind the actin cytoskeleton, or can interact directly with cytoskeletal components themselves (Zihni et al. 2016).

This identification of ZO-1 was later followed by the identification of the transmembrane proteins that formed the cell-cell contacts of TJs, most notably the claudin family of TJ proteins, of which 26 exist in humans, which when expressed in non-TJ forming cells are alone sufficient to bring about the formation of TJ like structures. Also identified was junctional adhesion molecule A (JAMA), as well as the MARVEL domain containing protein family, comprising occludin, tricellulin (also

known as MARVELD2, which is specifically localised to tricellular cell junctions) and MARVELD3 (Zihni et al. 2016; Furuse et al. 1998).

Claudin family proteins have four membrane-spanning regions, forming two extracellular loops, the first of which are typified by the amino acid sequence W-GLW-C-C, while the second extracellular loop of claudin proteins is believed to be responsible for mediating claudin-claudin interactions in TJs, along with a C-terminal PDZ binding domain that interacts with PDZ domain containing proteins such as ZO-1 (Anderson & Van Itallie 2009; Blasig et al. 2006). Claudin proteins form the main components of the transcellular TJ strands observed in early freeze fracture EM images. Different claudin family proteins can from these strands together and bind with claudins on the apposing cell membrane in a homo- or hetero- dimeric fashion, with only specific claudin combinations capable of forming heterodimers, holding the cells in close contact and thereby forming TJs (Furuse et al. 1999).

Tight junction mediated control of paracellular permeability

TJs act as a barrier to paracellular flow, but do not represent absolute barriers to paracellular movement of ions or macromolecules. Rather, TJs act in a size and charge selective manner to form semi-permeable cellular barriers between tissue compartments, with the size and charge selectivity thought to represent two distinct pathways through the TJ complex.

Movement across TJs through the charge selective pathway takes place by the passage of charged ions, and also small, uncharged molecules, through pores in TJs in a diffusion dependent manner. These pores are estimated to be 4-8 Å in diameter, and as such freely allow the diffusion of water, approximately 3 Å, and other small, uncharged molecules, but can restrict the permeability of specific charges of ions across the barrier (Zihni et al. 2016). It has been shown that the claudin composition of a TJ has a role in the charge selectivity of that junction, with specific expression patterns of claudin family proteins correlating with the charge selectivity of the TJ. For example, expression of claudin-2, -10b, or 14 in cell monolayers reduces their permeability to cations, while similarly, claudin -10a and -17 reduce permeability to anions. Interestingly, expression of certain claudin proteins in cells can also have the opposite effect, increasing permeability to certain charged molecules rather than decreasing, for example claudin-7 expression increasing permeability to cations, illustrating that

claudins do not just physically block transport of ions, but rather may be actively involved in selective movement of charged ions across the TJ (Amasheh et al. 2002; Van Itallie et al. 2006; Ben-Yosef et al. 2003; Krug et al. 2012). The charge selectivity of claudins is thought to be controlled by residues in the extracellular loops of the transmembrane proteins, which, besides forming dimers with claudins on apposing cells, also are proposed to form pores composed of β-barrel structures consisting of extracellular regions of both claudins in the dimer (Suzuki et al. 2015). Under this model, the charge of amino acid residues contained within these pores would determine the charge selectivity of the pore. Post-translational modifications of claudins also play a role in the regulation of their charge selectivity, with phosphorylation of claudin-14 leading to an increase in paracellular permeability to negatively charged chloride ions (Yamauchi et al. 2004).

In addition to their role in charge selective paracellular transport, TJs are also known to control the passage of larger macromolecules across TJ mediated barriers in a size selective manner, allowing molecules as large as 60 Å to pass between cells. As these molecules are larger than any open space in the TJ cleft, they cannot passively diffuse across the TJ. While this size selective pathway is not currently fully understood, proposed models suggest that TJ strands could dynamically remodel around macromolecules as they slowly move paracellularly, keeping the TJ in a closed state while the molecule crosses the cell layer (Zihni et al. 2016). What is clear from existing data however, is that, as is the case in charge selectivity, the claudin expression profile of a TJ plays a role in size selective paracellular movement. Claudin-5, an integral claudin of the blood-brain barrier (BBB) and inner blood-retinal barrier (iBRB), appears to regulate the size of macromolecules that can cross these barriers. Mice deficient in claudin-5 shown no alterations to blood vessel development or morphology, but tracer studies show their BBB and iBRB become permeable to molecules up to 800 Da in size (Nitta et al. 2003). Post-translational modification of TJ proteins, particularly claudin family proteins, is an important factor in the regulation of both their activity and subcellular localisation. These modifications occur primarily in the cytoplasmic carboxyl tail of the proteins (Gonzalez-Mariscal et al. 2010). Phosphorylation of claudin-5 promotes its recruitment into TJs in brain endothelial cells, resulting in a reduced BBB permeability, while phosphorylation of claudin-16 prevents its degradation (Ishizaki et al. 2003; Ikari et al. 2008). Phosphorylation of claudin proteins can also act to prevent their integration into TJ complexes, as is the case with the

phosphorylation of the PDZ binding domain of claudin-4 (Tanaka et al. 2005). Similarly, the phosphorylation of claudin-1 can cause it to be localised to the cytoplasm from cell membranes (French et al. 2009). Other forms of post-translation modification, such as palmitoylation or glycosylation also occur in claudin proteins (Gunzel & Yu 2013).

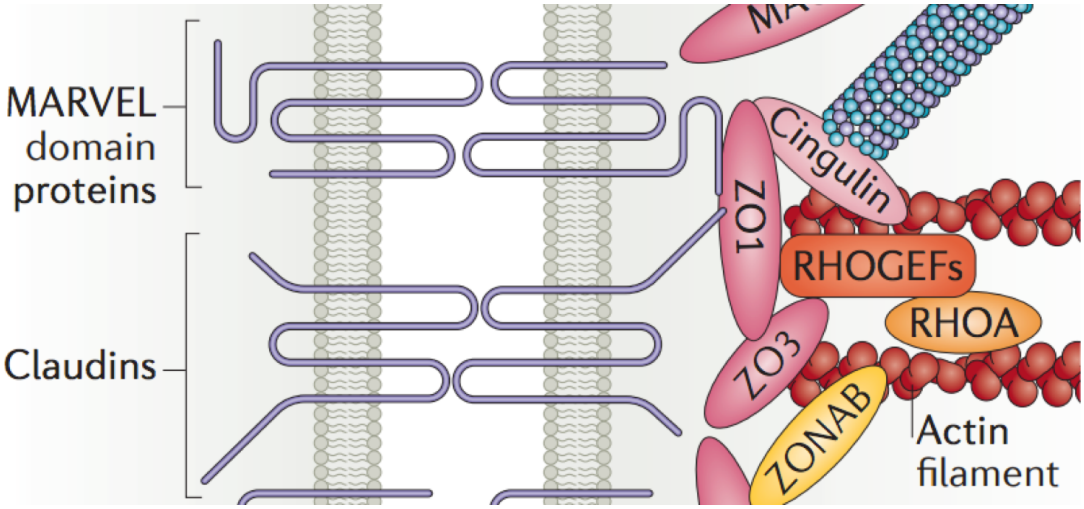

Figure 2.1: Protein components of tight junctions

This figure shows the representative proteins involved in the formation of tight junction plaques, with transmembrane MARVEL-domain containing proteins and Claudin family proteins, and intracellular zonula occludens proteins. Adapted from (Zihni et al. 2016).

The ability of TJs to maintain a sealed cellular monolayer is instrumental in their maintenance of the blood-aqueous barrier (BAB), separating peripheral blood flow from AH at several sites within the eye. The SC inner wall prevents retrograde flow of episcleral venous blood into the AC, as a constant pressure differential acts to maintain unidirectional flow. In the case of hypotony reversing the pressure differential, GVs collapse, acting in the manner of a non-return valve, preventing the retrograde flow of blood through GV pores (Braakman et al. 2016). The BAB is also present at the ciliary epithelium, the site of AH secretion into the AC, where TJs allow for the ultrafiltration of AH from stromal blood, and in the vasculature of the iris, where vascular TJs prevent diffusion of blood and plasma-derived proteins into the iris stroma, and therefore the AC (Freddo 2013).

Tight junctions of Schlemm's canal

The endothelial tight junctions of Schlemm's Canal differ from those seen in other cell types in several ways. Early studies using electron microscopy showed zonula occludens were present at endothelial cell junctions in Schlemm's Canal as is seen in vascular endothelia (Vegge 1967). Subsequent freeze fracture studies showed that Schlemm's Canal endothelial cells TJs were composed of parallel junctional strands with minimal branching which did not form complex bidimensional networks. The lack of branching between TJ strands in SC endothelia leads to the formation of channels between junctional strands that are continuous from the JCT to the SC lumen. These channels were identified as a potential paracellular route for AH outflow into the SC lumen through intercellular clefts in SC inner wall endothelia (Raviola & Raviola 1981; Bhatt et al. 1995). Early tracer studies using cationised ferritin showed staining of cell membranes lining channels between tight junctions in SC inner wall endothelium, showing therefore that these channels represented a paracellular pathway across SC inner wall. Further, these channels were of greater size and number in eyes that were fixed at elevated pressure, (Epstein & Rohen 1991). Additionally, endothelial tight junctions in perfused human donor eyes were shown by freeze fracture to exist in single and double stranded forms at the majority of TJs, with a minority of TJs having three or more junctional strands. The complexity of these junctions was shown to be responsive to applied pressure in the eye, with the number of junctional strands decreasing as perfusion pressure increased, (Ye et al. 1997). The above features are in contrast to TJs of most other ocular endothelia, particularly vascular endothelia, which are composed of complex networks formed of multiple TJ strands, and do not exhibit dynamic regulation in response to pressure, with no changes to TJ strand structure in response to perfusion pressure (Fujimoto 1995; Schneeberger & Karnovsky 1976).

Schlemm's canal endothelium also differs from other ocular endothelia in that it has remarkably high hydraulic conductivity, with Schlemm's canal having a hydraulic conductivity of $4000{-}9000\times10^{-11}$ cm^2 sec/g, significantly higher than other ocular barriers, and possibly one of the highest hydraulic conductivities of all body vessel linings (Johnson 2006). The inner wall endothelium of SC is also permeable to higher molecular weight tracer molecules than other endothelia of the eye, with labelled ferritin (450 kDa) staining the interior of paracellular pores, while the inner blood-retinal barrier (iBRB) excludes molecules as small as 500 Da (Epstein & Rohen 1991;

Campbell et al. 2009). It must be noted that these differences in endothelial permeability cannot be solely apportioned to differences in TJ structure and organization as, in addition to TJ mediated paracellular transport into the SC lumen, SCECs possess giant vacuoles containing large intracellular pores. These intracellular pores have an average pore size of approximately 1 μm in diameter, with pores greater than 3 μm reported (Sit et al. 1997). In the iBRB, ZO-1, occludin and claudin-5 are instrumental in maintaining barrier function, with claudin-5 particularly important in controlling paracellular permeability (Campbell & Humphries 2012; Morita et al. 1999). While the TJ expression profile of SC cells has not been studied extensively, ZO-1 has been seen to be expressed in these cells, and to be upregulated in models of steroid induced glaucoma, with a corresponding decrease in the hydraulic conductivity of the conventional outflow pathway (Underwood et al. 1999). Prior to this study, no claudin family proteins had been identified as being expressed in human Schlemm's canal endothelial cells.

Aims

The aim of this chapter was to characterise the expression profile of TJ components in cultures human SC cells, as well as in murine and primate models, with the intention of selecting potential therapeutic targets to be used to increase the hydraulic conductivity of the conventional outflow pathway by enhancing paracellular permeability. Modulation of the expression of selected TJ components of these cells using siRNA was to be investigated.

Results

Characterisation of tight junction expression in human SC endothelial cells

Characterisation of the tight junction expression profiles was initially approached *in vitro* through the microarray expression analysis of cultured human SC endothelial cell (SCEC) strains and TMC strains obtained from post mortem donor eyes. RNA was extracted from SCEC strains derived from four individual donors and the mean normalised expression ($2^{-\Delta Ct}$) of genes encoding claudin and adhesion junctional proteins was analysed, fig. 2.1. The resulting expression profile identified claudin-11, also known as oligodendrocyte specific protein, as one of the most highly expressed claudin family TJ protein in the cultured SCEC strains. Additionally, the TJ proteins, zonula ocludens-1 (ZO-1), also known as tight junction protein-1 (TJP1), an integral part of TJ complexes, and junctional adhesion molecule-3 (JAM3) were also identified as being expressed at high levels in these cells. Interestingly, the most significantly expressed TJ proteins that form the basis of TJ in vascular endothelial cell layers in human and murine brain and retinal endothelia, claudin-5 and occludin, were only detected at low levels in human SCEC in this array. These data indicate that claudin-11 is the dominant claudin in TJs of cultured SCEC, with ZO-1 being a major TJ associated protein in cultured SCEC. JAM3, while highly expressed, is unlikely to play a large role in endothelial permeability as, while it is a TJ component, it is not essential for TJ formation or maintenance, as is the case with claudin proteins and ZO-1.

RNA expression levels for ZO-1 and CLDN11 from cultured SCEC strains were compared to expression levels from cultured primary TMC strains, to analyse whether TJ formation was exclusive to the endothelial cells of SC, or if the TJ formation also occurred in the TM, fig. 2.2. This revealed that there was 2.52 fold higher expression of claudin-11 in SCECs as compared to TMCs, whereas no significant difference in expression levels of ZO-1 was detected between SCECs and TMCs. As members of the claudin family of proteins form the most integral structural component of TJs, this indicated that the cells of the TM were not likely to form functional TJs, and therefore would not be considered as a potential target for RNAi mediated increase of paracellular permeability.

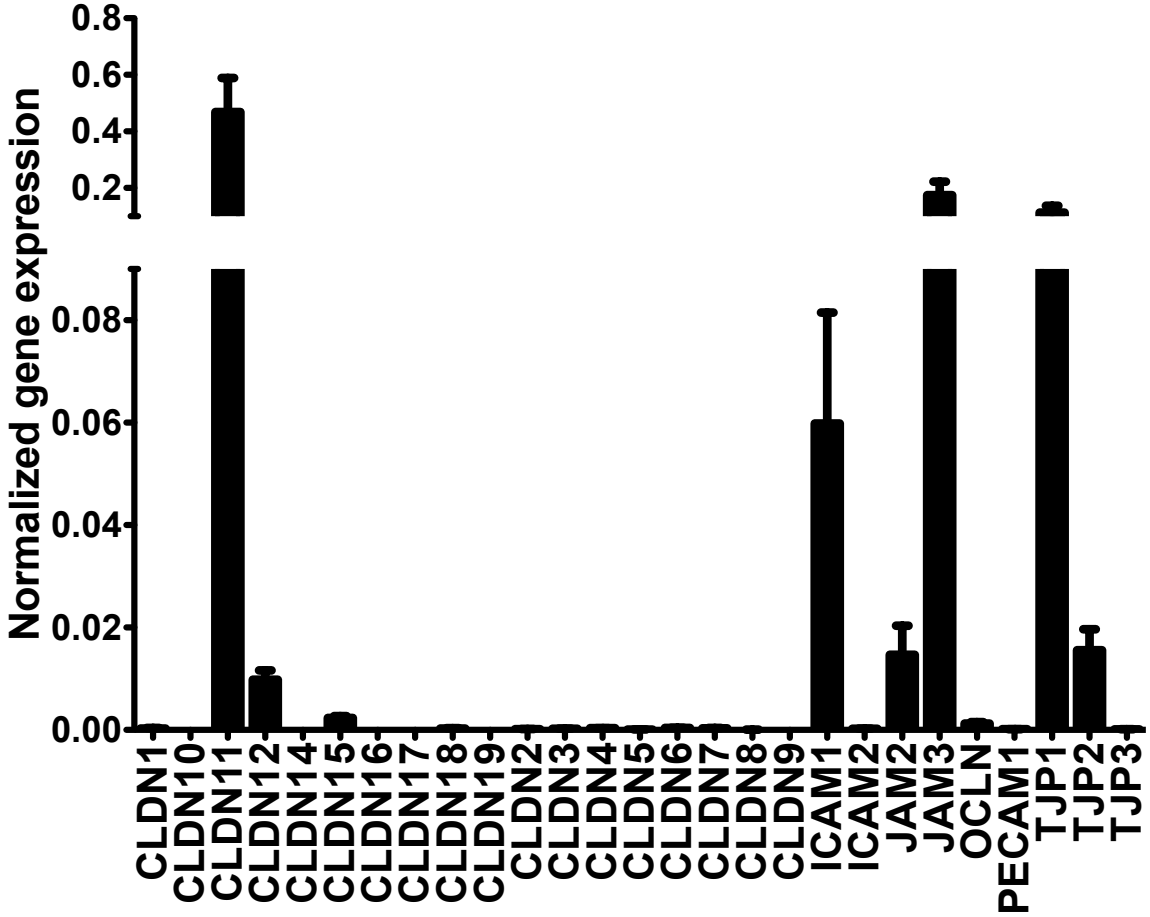

Figure 2.2: Microarray expression profile of junctional proteins in human SCEC.

The expression levels of various tight junction and adhesion junction associated proteins were assessed using the Human Tight Junctions RT^2 Profiler PCR array. Bar graphs represent $2^{-\Delta CT}$ relative expression levels of target transcripts from 4 separate SCEC strains, normalised to 5 different housekeeping genes, mean ± s.e.m.

Once the expression of these TJ components had been characterised at an mRNA level, it was desirable to further validate their role in the formation of endothelial barriers through confirmation of expression at a protein level. In order to do this, protein was extracted from primary cultured SCEC strains and used in western blot analysis, see fig. 2.3. These data agreed with the findings from the above microarray, showing that claudin-11 and ZO-1 were highly expressed in cultured human SCEC. We additionally showed here the presence of the TJ protein tricellulin, also known as MARVELD2, which was not included as a candidate in the original microarray. Tricellulin functions in the formation of TJs at tri-cellular endothelial junctions. We

also confirmed from this protein analysis that claudin-5 was indeed not expressed in SCECs.

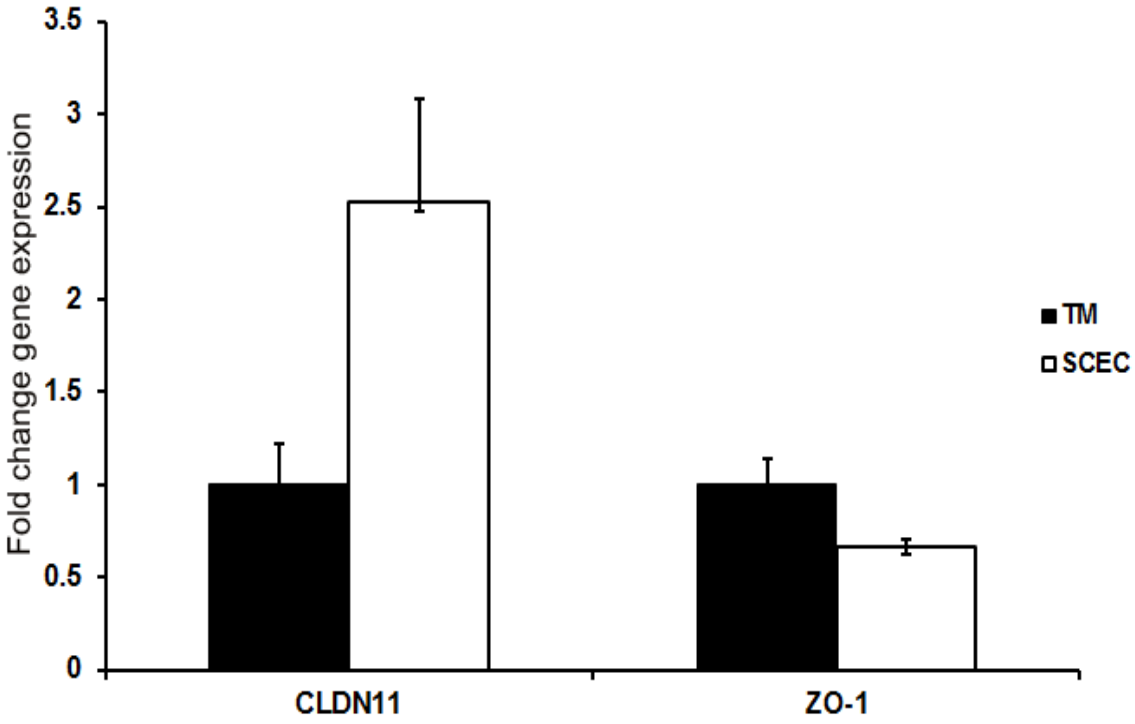

Figure 2.3: Comparison of claudin-11 and ZO-1 expression levels between TMC and SCEC.

The expression levels of claudin-11 and ZO-1 were determined using the Human Tight Junctions RT^2 Profiler PCR array, with relative expression between cultured TMC and SCEC shown as $2^{-\Delta\Delta CT}$, mean ± s.e.m. (N = 2).

Characterisation of expression of tight junction components in mouse and non-human primate outflow tissues

As there was an interest in applying this technique to both mouse and non-human primate model systems, similar characterization was also sought in these species. Cultured primary SCEC cell lines from these species were not available and microarray and western blot analysis were not feasible with dissected *ex vivo* tissues, due to the relatively small area of the outflow pathway of these eyes. Laser Capture Microdissection (LCM) of SC inner wall was attempted in fresh frozen murine eyes using the ArcturusXT LCM system, but was unsuccessful due to the insufficient resolution of the system preventing accurate dissection, and due to low RNA and

protein yields obtained from dissected material. Instead, immunohistochemistry (IHC) was used to analyse tissue sections from both mouse and primate for the presence and localisation of our proteins of interest. Figure 2.4 (a) shows the localisation of immunofluorescent signals corresponding to ZO-1 and tricellulin at the inner wall endothelial cells of SC in cryosectioned mouse eyes, with continuous junctional strands visible, indicating the presence of functional tight junctions. Staining for ZO-1 and tricellulin was also observed in the TM, but in this case was discontinuous, indicating the absence of a TJ controlled barrier to AH flow in the TM. In contrast to our results from human cells, we were unable to show the presence of claudin-11 or claudin-5 in the mouse SC inner wall endothelium, fig 2.5.

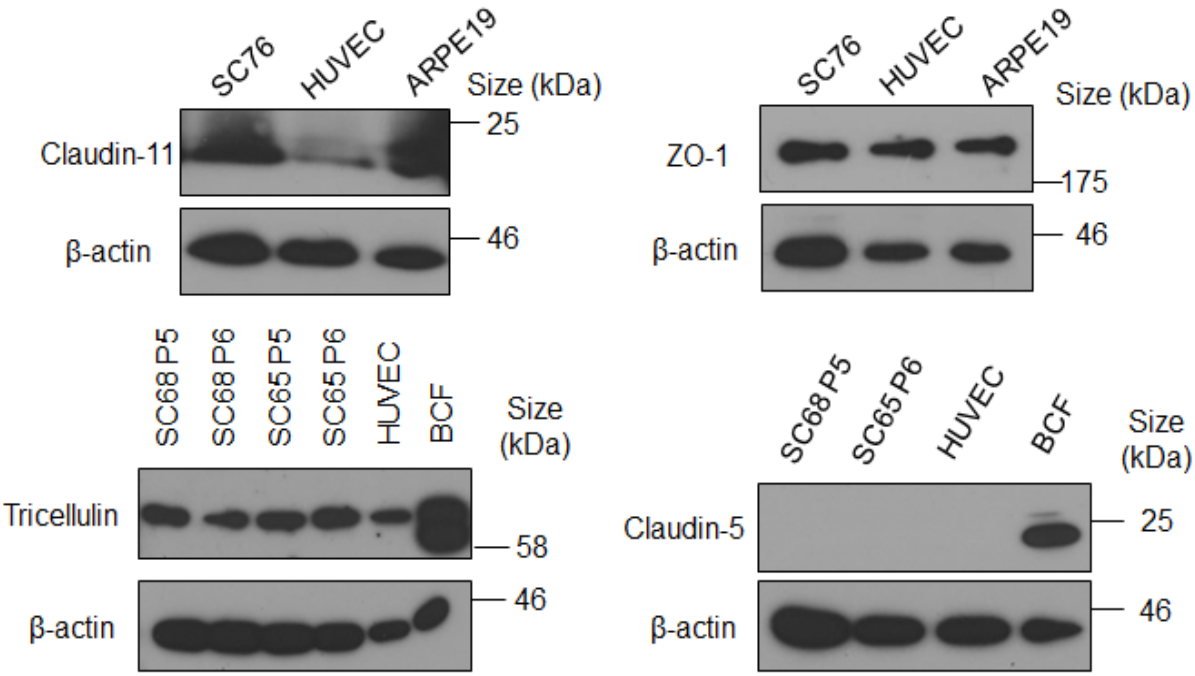

Figure 2.4: Analysis of protein expression of claudin-11, ZO-1, tricellulin, and claudin-5.

Protein expression was analysed by western blot of whole cell lysates of cultured SCEC of various strains, along with appropriate positive loading controls, human umbilical vein endothelial cells (HUVEC), murine brain capillary fractions (BCF), and human retinal pigment epithelium cells (ARPE19), with β-actin used as a loading control.

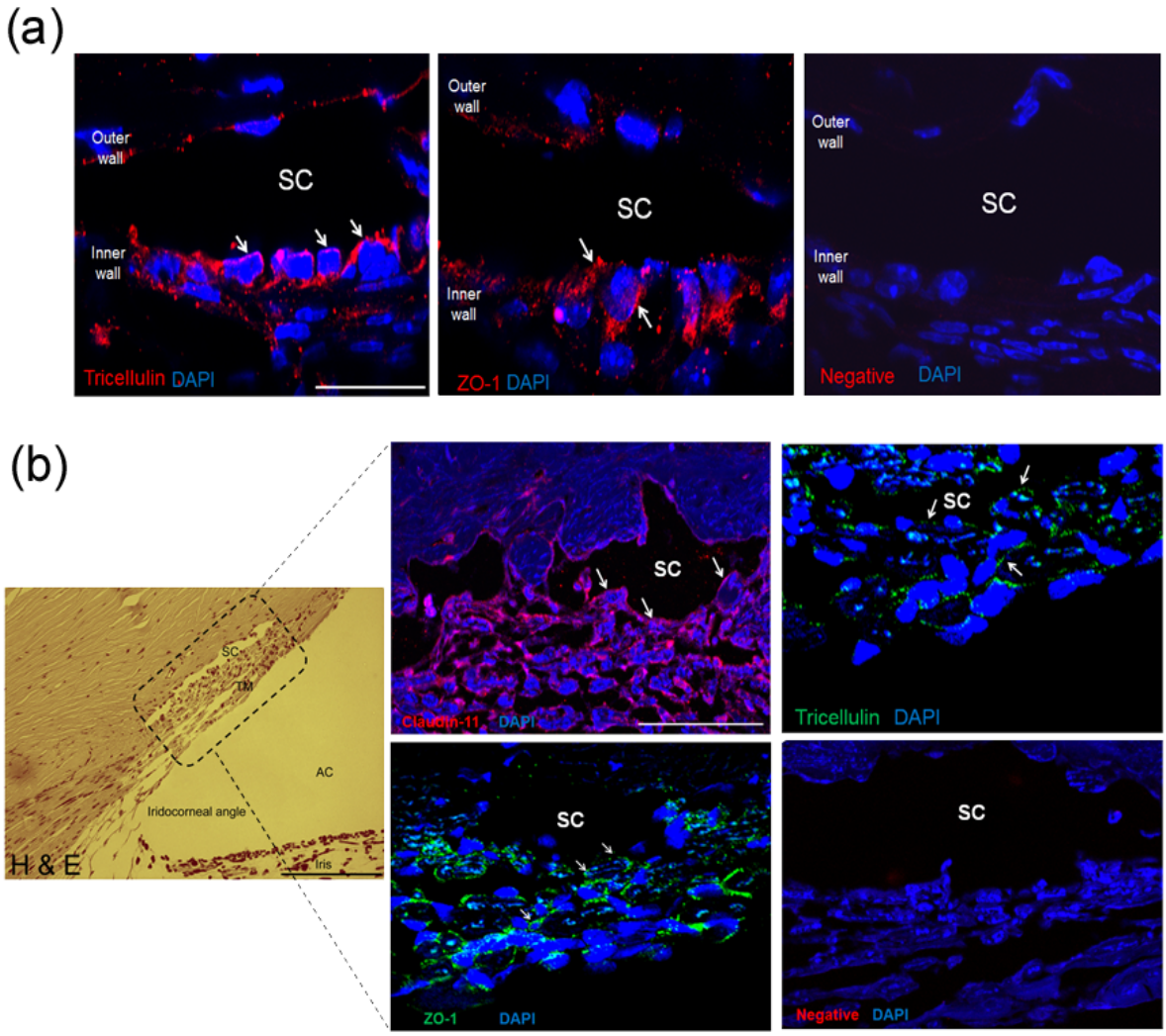

Figure 2.5: Immunohistochemical characterisation of TJ protein expression in murine and primate outflow pathways.

(a) *Immunohistochemical staining of cryosections of murine conventional outflow pathway, with ZO-1 and tricellulin labeled by Cy3 (red), and nuclei labeled with DAPI (blue). Negative control staining was carried out with no primary antibody. SC = Schlemm's canal lumen, scale bar = 50 µm.* ***(b) Left:*** *H&E staining of primate iridocorneal angle in paraffin section, with area enclosed in dotted box representing the region in inset immunohistochemical staining images. SC = Schlemm's canal lumen, AC = anterior chamber, TM = trabecular meshwork, scale bar = 200 µm.* ***Right:*** *Immunohistochemical staining of TJ proteins in the primate conventional outflow pathway. Claudin-11 is stained with Cy3 (red), while tricellulin and ZO-1 and stained with Cy2 (green), and nuclei are stained with DAPI (blue). Continuous TJ strands are identified by white arrowheads at SC inner wall. Negative control staining was carried out with no primary antibody. Scale bar = 50 µm.*

IHC was also used to characterise and localise the TJ components present in our non-human primate model, the African Green monkey (*Chlorocebus sabeus*), fig. 2.4 (b). This analysis showed the presence of continuous claudin-11 TJ strands at the endothelial cell boundaries of the inner wall cells of SC, indicating the role of these cells in the generation of outflow resistance through the maintenance of a TJ mediated endothelial barrier. In addition to this, the outer wall endothelial cells of SC were shown not to possess this strong claudin-11 staining. The same analysis was carried out for ZO-1 and tricellulin, and again an enrichment of expression was seen at the inner wall of SC, with continuous TJ strands visible in both cases. No continuous staining patterns were seen for any of our targets in the TM, indicating that TJ barrier formation in the TM is not likely to contribute greatly to the generation of outflow resistance. These data indicate that *in vivo* expression of TJ components in our non-human primate model matches well with the pattern seen in cultured primary human SCEC.

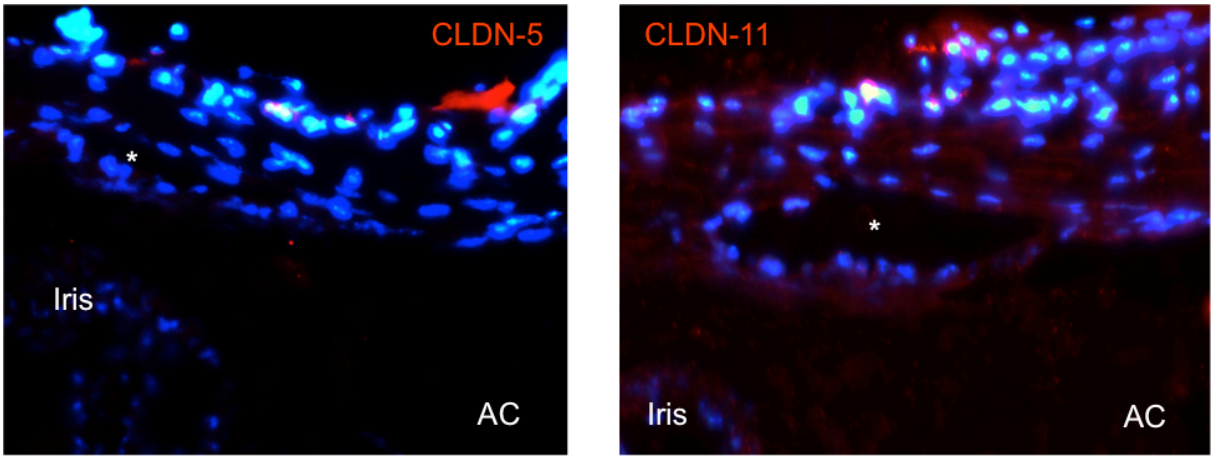

Figure 2.6: Immunohistochemical staining of murine conventional outflow tissue for claudin-11 and claudin-5.

Immunohistochemical staining of cryosections of murine conventional outflow pathway, with claudin-5 and claudin-11 labeled with Cy3 (red), and nuclei labeled with DAPI (blue). Asterisks (*) indicate the location of the SC lumen. AC =anterior chamber.

Validation of tight junction siRNAs

From this initial analysis, claudin-11, ZO-1, and tricellulin were selected as potential targets for siRNA mediated downregulation as part of our therapeutic approach. In order to begin the process of determining whether modulation of the expression of these proteins could have an IOP lowering effect through increased paracellular permeability at SC inner wall, we first had to demonstrate the ability to downregulate their expression. These proteins were downregulated using RNA interference (RNAi) technology, with short interfering RNAs (siRNAs) that were specific to the mRNA transcript sequence of our selected target proteins.

Primary human SCECs were treated with siRNA targeting our candidate TJ components, and protein was then extracted and analysed by western blot at 24, 48 and 72 hours post-treatment. This allowed the validation of effective downregulation of the target protein, and also the characterization of the time course of downregulation *in vitro*, with densitometric analysis being carried out to determine relative expression levels at each time point. Relative expression was calculated as compared to protein expression levels in SCEC treated with non-targeting (NT) siRNA. Time-dependent down-regulation of claudin-11 protein expression to 5 ± 3 % ($p < 0.0001$), 11 ± 1 % ($p < 0.0001$) and 9 ± 4 % ($p < 0.0001$) (mean ± standard error of mean, SEM) was achieved at 24, 48 and 72 hours post-transfection respectively, fig. 2.6 (N = 3). ZO-1 protein expression was reduced to 72 ± 3 % ($p = 0.005$), 64 ± 4 % ($p = 0.0004$) and 49 ± 18 % ($p = 0.02$) at 24, 48 and 72 hours post-transfection respectively, fig. 2.6. Furthermore, tricellulin protein expression was reduced to 75 ± 0.2 % ($p = 0.002$), 81 ± 6 % ($p = 0.012$) and 87 ± 8 % ($p > 0.05$, not significant) at 24, 48 and 72 hours respectively following siRNA treatment fig. 2.6. MTS based cell viability assays were also carried out to demonstrate that the downregulation of our selected target proteins did not have a significant cytotoxic effect on the viability of cultured SCEC, fig. 2.7.

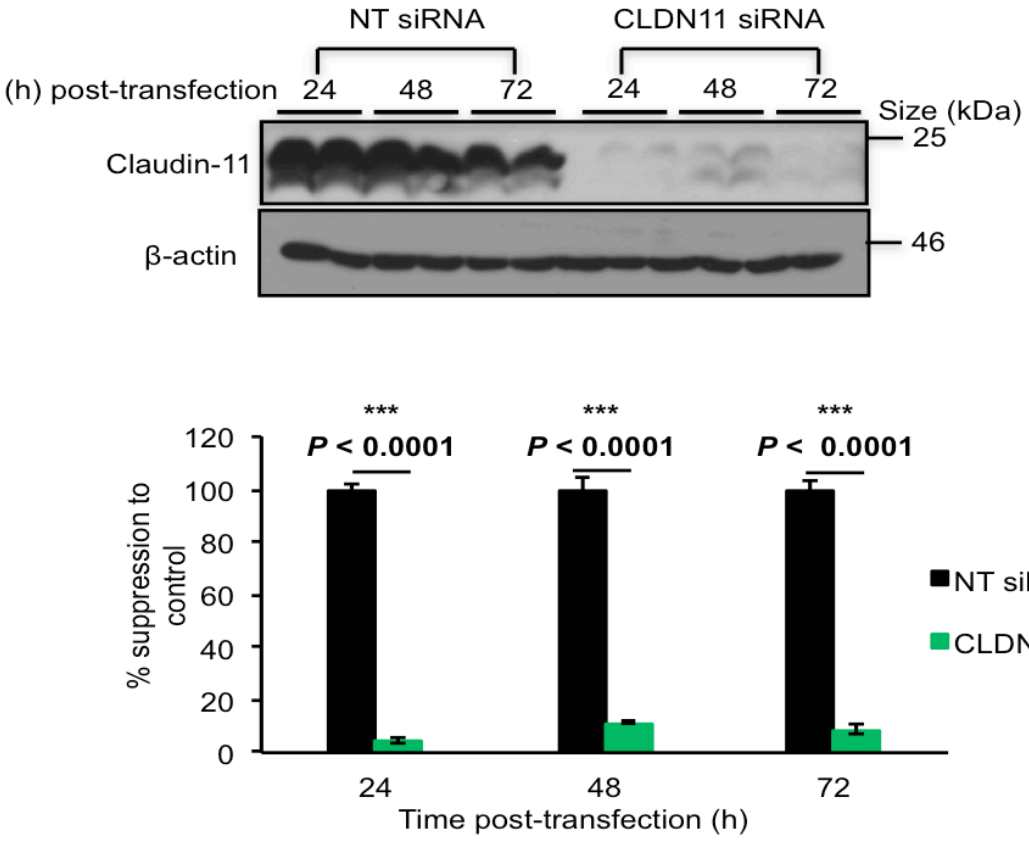
NT siRNA
CLDN11 siRNA
(h) post-transfection
24
48
72
24
48
72
Size (kDa)
Claudin-11
25
β-actin
46
***
***
***
P < 0.0001
P < 0.0001
P < 0.0001
120
100
80
60
40
20
0
% suppression to control
NT siRNA
CLDN11 siRNA
24
48
72
Time post-transfection (h)

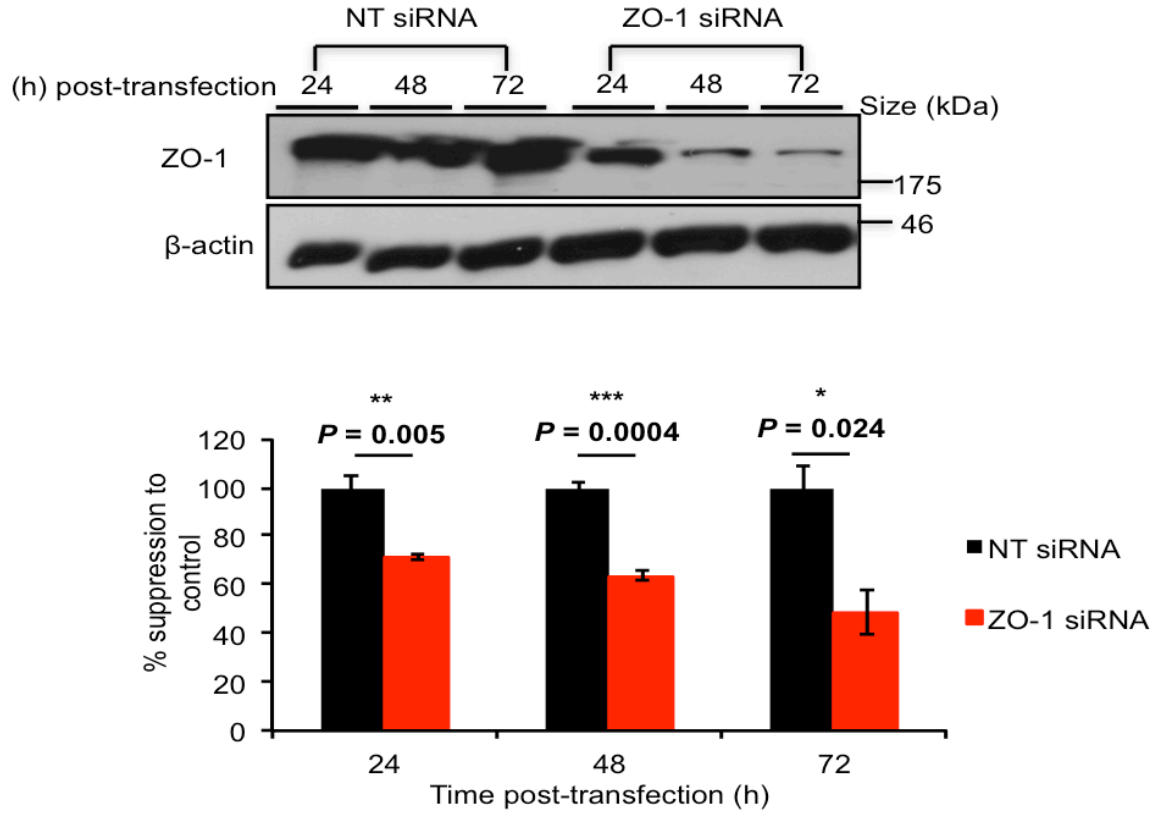
NT siRNA
ZO-1 siRNA
(h) post-transfection
24
48
72
24
48
72
Size (kDa)
ZO-1
175
β-actin
46
**
***
*
P = 0.005
P = 0.0004
P = 0.024
120
100
80
60
40
20
0
% suppression to control
NT siRNA
ZO-1 siRNA
24
48
72
Time post-transfection (h)

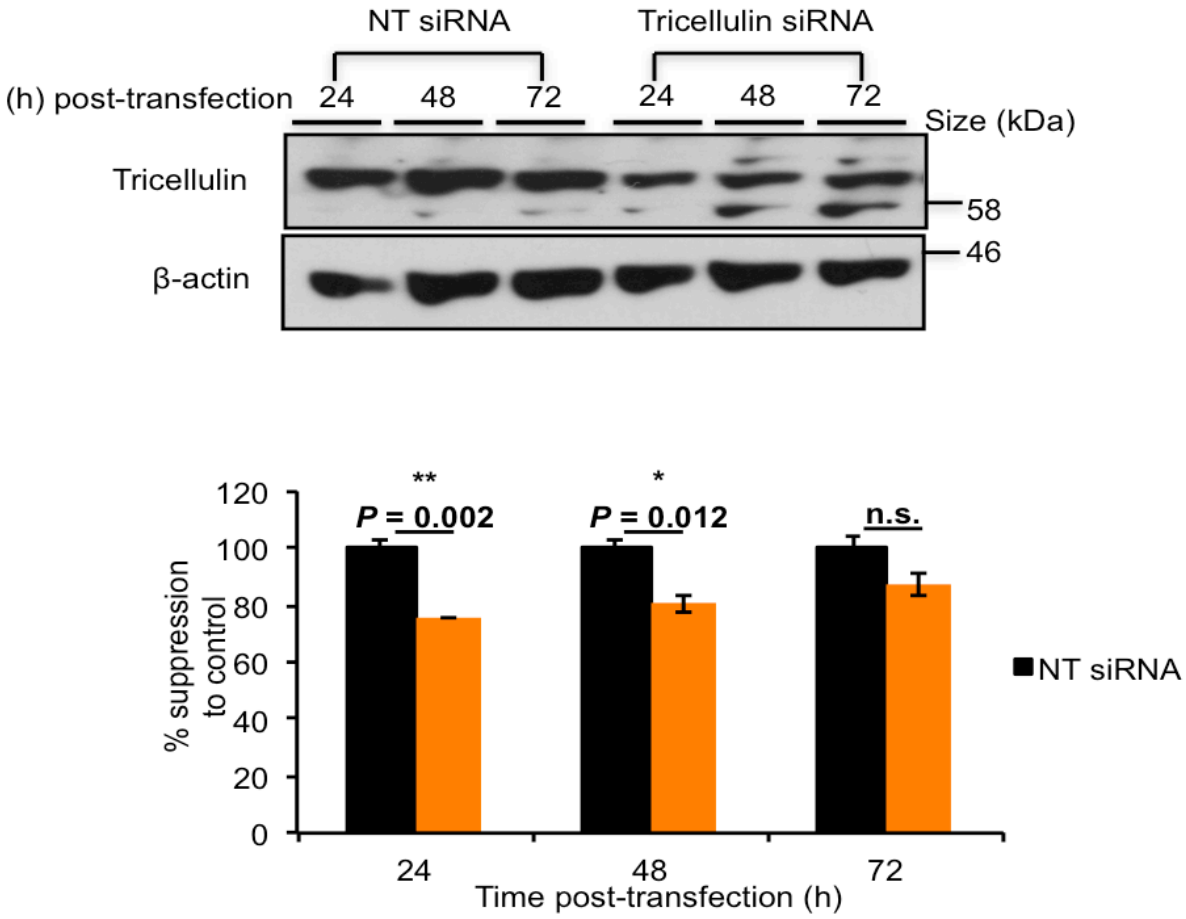

Figure 2.7: Western blot and densitometric analysis of siRNA mediated TJ protein downregulation.

Representative western blot images along with corresponding densitometric quantification of siRNA mediated downregulation of expression of claudin-11 (previous Page, upper), ZO-1 (previous page, lower), and tricellulin (above) in cultured SCEC at 24, 48 and 72 hours, normalised to β-actin loading control, and relative to non-targeting (NT) siRNA treated SCEC. Bar charts represent mean ± s.e.m, n.s. = $P \geq 0.05$. N = 4, unpaired t-test.

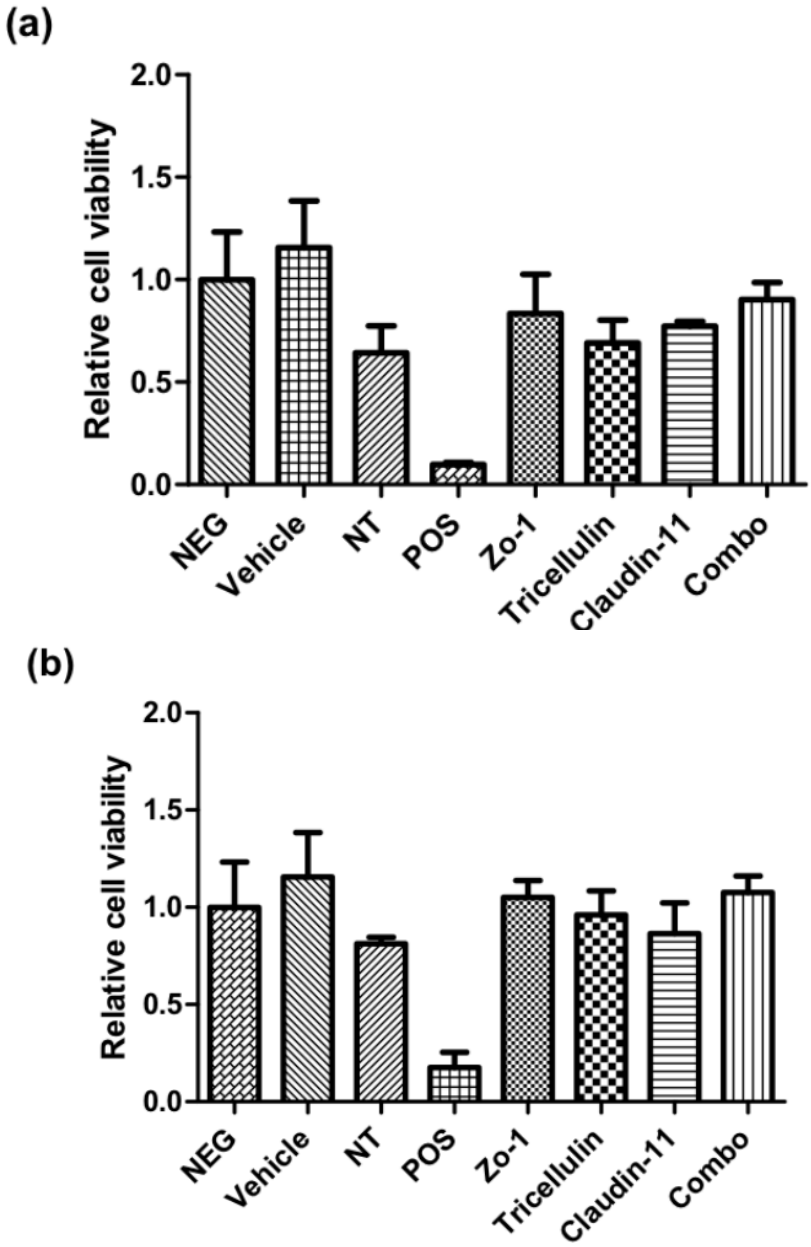

Figure 2.8: The effect of siRNA mediated downregulation of selected TJ components on cell viability.

Cultured human SCEC were treated with at (a) 40 nM siRNA and (b) 200 nM siRNA targeting our selected TJ targets, and the effect of the siRNA treatment on cell viability was assessed using an MTS based cell viability assay. No significant differences were detected in treated cells as compared to negative control (N = 4, one-way ANOVA with Tukey's post-test). NEG = untreated control, NT = non-targeting siRNA, POS = positive control, 1% SDS, Combo = combination treatment of all three siRNAs. Bar charts represent mean ± s.e.m.

Discussion

While TJs in general have been extensively studied in many different cell types, the TJ composition of SC cells had hitherto not been well characterised. As has been previously reported, ZO-1 was confirmed to be expressed in cultured human SC cells at an mRNA level by microarray and at a protein level by western blot (Underwood et al. 1999). Additionally, the expression of claudin-11 was shown by microarray and western blot of cultured cells also, while tricellulin expression was demonstrated by western blot alone, as it was not a candidate gene in the microarray. It was also demonstrated that the expression level of claudin-11 was 2.52 fold higher in cultured SC cells as compared to TM cells, while ZO-1 showed no significant difference in expression levels.

These data were reinforced by IHC staining showing continuous junctional strands of claudin-11, ZO-1, and tricellulin in paraffin sectioned primate outflow pathways, while ZO-1 and tricellulin alone were shown in cryosectioned murine outflow pathways. The staining pattern for these components was typified by enrichment at the inner wall of SC, where continuous strands were more frequently seen, with diffuse staining through the TM. This is consistent with models of outflow resistance generation in the conventional outflow pathway, where resistance to outflow in the TM is not generated through TJ mediated paracellular passage of AH, rather, it arises through heavy extracellular matrix deposition increasing the tortuosity of the pathway as AH approaches the JCT and SC inner wall (Overby et al. 2009). While some staining of TJ components was seen in the outer wall of SC, it was more diffuse and with less continuous strands than that seen in SC inner wall. This is as expected, as no fluid flow, and therefore no pressure drop, occurs across the SC outer wall, instead AH travels through the path of highest hydraulic conductivity, along the SC lumen to collector channels leading to the episcleral veins.

Claudin-5, an integral claudin protein, and occludin, a MARVELD family protein, both seen to be expressed in most ocular endothelia, were shown to not be significantly expressed in SC cells. This difference in expression profile is unsurprising, freeze fracture electron microscopy studies, as discussed, have shown that TJs in SC exhibit a different structure to vascular TJs, exhibiting less junctional strands and not forming complex networks, while the cell types also differ significantly in measured permeability *in vitro*.

Claudin-11, ZO-1, and tricellulin represent viable therapeutic targets for modulation to induce the desired increase in hydraulic conductivity of the conventional outflow pathway for several reasons. ZO-1 acts to stabilise TJ complexes by anchoring them to the cytoskeleton, and depletion of ZO-1 using siRNA in other cell types has been shown to destabilize TJs and increase solute permeability (Itallie et al. 2010; Fanning et al. 1998). Claudin-11 acts as a barrier to paracellular diffusion in myelin sheaths, and has been shown to be integral to TJ function in Sertoli cells, with silencing of claudin-11 alone decreasing TJ function by 55% in these cells (McCabe et al. 2016; Denninger et al. 2015). Similarly, tricellulin acts a barrier to macromolecular flux, and suppression of its expression via RNA interference leads to destabilization of tricellular TJs (Ikenouchi et al. 2005; Krug et al. 2009). While JAM3 was detected as being highly expressed in the microarray data, it was not included as potential therapeutic target as, while it forms a part of TJ complexes, it does not appear to be integral to TJ barrier function (Ebnet et al. 2004).

While murine SC sections were shown to possess similar staining patterns for ZO-1 and tricellulin, claudin-11 expression was not detected by IHC, suggesting differential claudin expression profiles may exist between murine SC cells and that seen in human and non-human primate. For this reason, only ZO-1 and tricellulin were suitable therapeutic targets for modulation in murine model systems.

Having selected the TJ proteins claudin-11, ZO-1, and tricellulin as potential therapeutic targets, these proteins were downregulated using siRNA in cultured SCEC, with protein levels assessed at 24, 48 and 72 hours. This brought about significant reductions in the levels of all three targets at 24 and 48 hours to varying extents, with claudin-11 and ZO-1 levels significantly reduced at 72 hours also. The differences seen in the extent of reduction of each protein's levels and in dynamics of downregulation are likely due to differences in mRNA stability and basal protein turnover rates. Cell viability assays confirmed that treatment of cultured SC cells with siRNAs targeting these TJ components did not have a cytotoxic effect. This demonstration of effective *in vitro* suppression of protein translation allowed for the movement of this approach in to *in vivo* models.

While the data herein has demonstrated the ability to downregulate TJ components, it is important to note that these data, which analyse expression only, do not take into account the phosphorylation state of TJ proteins, which affects both function and subcellular localisation. Further studies examining localisation via microscopy, and

phosphorylation state are necessary. Along with the data shown, work carried out by other lab members showed that downregulation of these proteins in cultured SCEC increased paracellular permeability to 70kDa dextran, and decreased transendothelial electrical resistance (TEER), a measure of ion permeability of cell layers, further demonstrating the suitability of these targets for therapeutic modulation.

Statement on collaboration

Microarray data and immunohistochemistry images in this chapter were prepared in collaboration with Dr. Lawrence Tam and Darragh Crosbie, both TCD.

Chapter 3: Investigating the therapeutic potential of RNAi mediated downregulation of tight junction proteins in Schlemm's canal

Introduction

As previously described, the pathological effects of POAG take the form of an increased resistance to the outflow of AH through the conventional outflow pathway, leading to elevated IOP and glaucomatous optic neuropathy. While current therapies largely focus on reducing AH production, and increasing unconventional outflow, the conventional outflow pathway remains an underused target for therapy. In Chapter 2, TJ components were identified as potential therapeutic targets for the modulation of paracellular permeability in cultured Schlemm's canal inner wall endothelial cells, and their potential to be downregulated at a protein level by selected siRNA was demonstrated. The relevance of these data to POAG is based on previous research in to endothelial tight junction modulation in other tissues.

Modulation of tight junction protein expression

It has been shown that systemic injection in mice of siRNA targeting the TJ protein claudin-5, which is highly expressed in vascular endothelial cells, leads to a decrease in expression of the protein, and a reversible opening of the blood-brain barrier. Barrier opening was size selective, allowing the transport of molecules up 742 Da into the brain from the bloodstream, but still excluding tracer molecules 4.4 kDa in size, allowing the systemic delivery of low molecular weight tracers to the brain that would otherwise be excluded by the TJ mediated endothelial barrier (Campbell et al. 2008). This process was later extended to the vascular endothelial cells of the inner blood-retinal barrier, again showing the siRNA mediated suppression of claudin-5, and in this case the systemic delivery of a low molecular weight drug to reduce photoreceptor cell death in a model of induced retinal damage (Campbell et al. 2009). After traumatic brain injury, fluid accumulates in the parenchyma of the brain at the site of injury, referred to as cerebral oedema. This results in elevated intracranial pressure, leading to increased morbidity and mortality post-injury. This same downregulation of claudin-5 after

experimentally induced cerebral oedema was shown to enhance clearance of water via a paracellular route across the blood-brain barrier and back in to peripheral circulation, reducing oedema volume and improving cognitive recovery in mice (Campbell et al. 2012). Downregulation of the TJ protein occludin has also been reported to increase vascular permeability (Keaney et al. 2015). These studies demonstrated that by direct modulation of the expression levels of TJ components in endothelial cells, the size selectivity of paracellular permeability to macromolecules can be increased. They also showed that the paracellular movement of water across a TJ mediated endothelial cell layer from an area of elevated pressure into the vessel lumen could be increased, leading to a therapeutic decrease in pressure. This has clear implications for the potential treatment of POAG, where elevated intraocular pressure is caused by reduced clearance of AH across the endothelial inner wall of SC into the SC lumen.

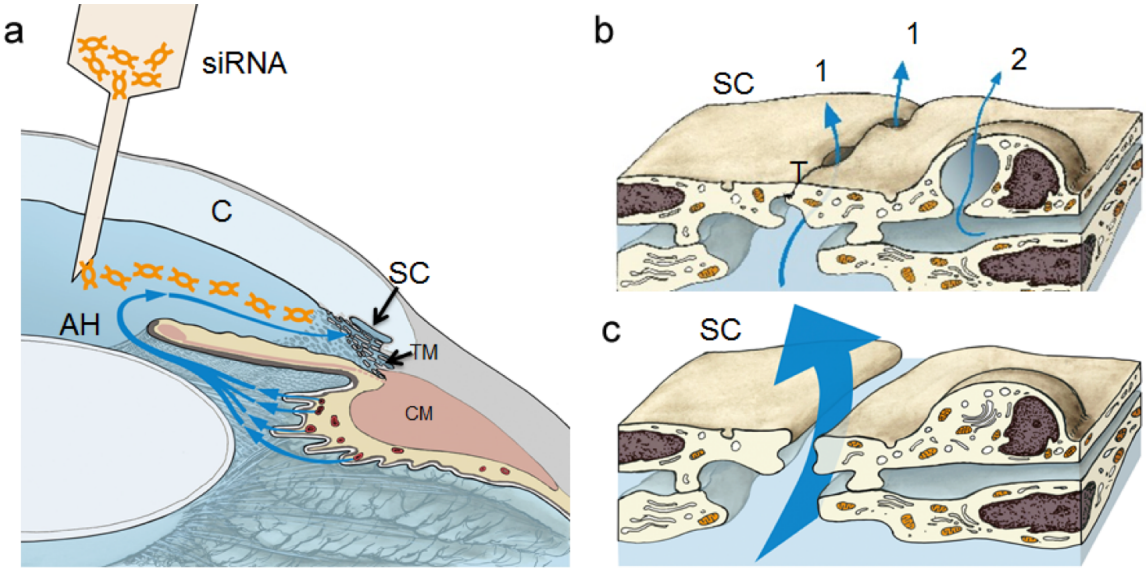

Figure 3.1: Therapeutic approach of siRNA mediated downregulation of Schlemm's canal tight junctions.

(a) *Intracameral injection of siRNA molecules into the AH leads to their movement to the conventional outflow pathway by normal AH flow dynamics, indicated by blue arrows. AH = aqueous humour; C = cornea; CM = ciliary muscle; SC = Schlemm's canal; TM = trabecular meshwork.* ***(b)*** *Normal AH pathways across SC inner wall endothelium, via (1) the paracellular route, between endothelial cells, or (2) the transcellular route, through larger pores in giant vacuole. T represents a tight junction mediated paracellular cleft.* ***(c)*** *siRNAs elicit knockdown of tight junction proteins, resulting in increased opening of paracellular clefts, increasing AH outflow facility.*

While siRNA was delivered systemically in the above studies, the therapeutic approach to *in vivo* delivery of these siRNA molecules here involves direct injection of unconjugated siRNA, targeting our selected TJ mRNA transcripts, through the cornea into the AH of the anterior chamber. From here, normal AH flow dynamics carry the siRNA to the iridocorneal angle where a portion will exit the eye via the conventional outflow pathway, thereby reaching the target tissue. This siRNA will be taken up by SC inner wall endothelial cells and subsequent downregulation of TJ components will bring about increased opening of paracellular pores, fig 3.1. This was hypothesised to lead to an increase in the hydraulic conductivity of the conventional outflow pathway.

Pressure dependence of aqueous humor outflow

AH outflow can occur via two distinct pathways, the conventional pathway, through the trabecular meshwork draining into SC, and the unconventional pathway, draining through interstitial spaces of ciliary muscle fibres. AH outflow through the conventional outflow pathway is described as pressure dependent, with flow driven by a pressure gradient existing between the pressure of AH in the anterior chamber, IOP, and the pressure in lumen of SC, which is maintained by episcleral venous pressure. The pressure drop between these two compartments occurs across the JCT and SC inner wall. AH flow rates through the conventional pathway increase linearly with increases in IOP in healthy eyes, demonstrating the pressure dependence of this flow (Alm & Nilsson 2009).

The unconventional outflow pathway is often described as a pressure independent outflow pathway, which means, while still driven by a pressure gradient, increases in IOP within the normal range do not readily increase the rate of uveoscleral outflow. This is due to the low hydraulic resistance generated by the ciliary muscle, the main site of resistance in this pathway necessitating only a small pressure gradient to drive flow (Emi et al. 1989). While rate of flow through this pathway is largely independent of pressure at physiological IOP, there is still a level of pressure dependence in the need for a pressure gradient between IOP and extraocular pressure to drive flow (Madekurozwa et al. 2017). If IOP is experimentally lowered below the threshold necessary to overcome the resistance of the ciliary muscle, the rate of unconventional outflow is greatly reduced, with studies by Anders Bill demonstrating a 63 % reduction in unconventional outflow at 2 mmHg, while no significant difference was observed at

4 mmHg (Bill 1967). For this reason, it is more appropriate to describe the unconventional pathway as pressure insensitive, rather than pressure independent. Truly pressure independent AH outflow, that is, outflow which is not driven by a pressure gradient, also exists in this pathway, with reabsorption of water into uveal veins occurring through an osmotic gradient rather than in any pressure dependent manner (Pederson et al. 1977).

In humans, the majority of AH outflow is pressure dependent, while in mice, pressure independent outflow represents the bulk of AH outflow (Overby et al. 2009).

Measuring aqueous humor outflow facility

In order to assess whether the planned delivery of siRNA to the anterior chamber has an effect of increasing the hydraulic conductivity of the conventional outflow pathway, the measurement of outflow facility, being the relationship between the outflow rate of AH from the anterior chamber and IOP, was necessary. This process is carried out through perfusion of cannulated eyes with a liquid, with several different perfusion approaches existing to measure outflow facility that are all based around a similar concept of the conservation of AH volume entering and exiting the eye, described by the following equation:

$$Q_f + Q = C\,(P - P_e) + Q_0$$

which is referred to as the Goldmann equation (Brubaker 2004). Here, Q_f is the formation rate of AH in the eye, while Q is the flow rate of fluid into the eye from the perfusion system, and Q_0 is pressure independent outflow. C is total outflow facility, being all outflow that is pressure dependent, comprising all conventional outflow facility, and any pressure dependent portion of unconventional outflow facility. P is IOP, while P_e is episcleral venous pressure, together defining the pressure gradient across the SC inner wall and JCT. For the purposes of perfusion measurements of outflow facility, it is often assumed that the values of Q_0, Q_f, P_e, and C itself are independent of IOP, leading to a linear model of the relationship between Q and P. This allows the measurement of the difference in rate of Q at two different levels of P as a method of calculating C, giving a value in the form of μL/min/mmHg, thereby

describing the relationship between outflow rate and IOP. This process is referred to as a two-step perfusion.

In the case of the perfusion of enucleated *ex vivo* eyes, P_e and Q_f are both zero, as all extraocular vessels have been severed. This allows the simplification of the above equation thus:

$$Q = CP + Q_0$$

It is common in enucleated eyes to measure Q at a range (3 – 5) of different values of P to improve the resolution of measurements, and since the relationship is assumed to be linear, the slope of the plotted values can be taken as C, while the Y-axis intercept of this line is sometimes taken as the rate of pressure independent outflow (Boussommier-Calleja et al. 2012; Lei et al. 2011). The use of this intercept value as representative of pressure independent outflow in *ex vivo* eyes has been challenged, due to the fact that the osmotic forces driving this outflow would be absent in enucleated eyes.

In order to utilize either of the above equations to calculate C, measurement of Q, the inflow rate of fluid during a perfusion, must be achieved, which has been approached in several manners. Syringe pumps have been used for this purpose, as the flow rate can be directly read and controlled. Constant flow rates can be applied with pressure measurements taken once pressure has reached a steady state, with pressure measured at multiple different flow rates. Alternatively, the flow rate can be actively controlled by a computer program to maintain a constant pressure, with the flow rate measured at several differing pressures (Stamer et al. 2011; Lei et al. 2011; Boussommier-Calleja et al. 2012). Another approach involves the cannulation of eyes to a small diameter reservoir containing fluid of known mass providing hydrostatic pressure. As fluid flows into the eye over time, the change in height of the reservoir meniscus represent the change in pressure over the time course of the perfusion, while the change in mass of the reservoir can be used to calculate the flow rate into the eye, allowing for two-step perfusion modelling (Aihara et al. 2003a; Camras et al. 2010). Constant pressure perfusion can also be carried out, whereby a large diameter reservoir is used to apply hydrostatic pressure, to negate change in pressure by drop in fluid level. Through measurement of the differential pressure either side of a capillary of known

diameter located between the reservoir and the eye, the flow rate into the eye can be calculated, while pressure is measured by a second pressure sensor (Ethier et al. 1993).

In vivo perfusions pose a greater problem, primarily as the value of P_e is non-zero and so cannot be removed from the equation describing AH volume conservation. This necessitates the direct measurement, or indirect estimation, of P_e in order to measure C. The measurement of P_e could be achieved through direct cannulation of episcleral veins to a pressure sensor, but this is a technically difficult process to achieve in larger eyes, and not possible in mice. Alternatively, IOP can be lowered until the pressure gradient is reversed and red blood cells are seen to flow in to SC lumen by gonioscopy, then IOP is slowly increased until no net flow is observed, thereby reaching an equilibrium between IOP and P_e, and indirectly measuring P_e (Aihara et al. 2003a).

Aims

The major aims of this research chapter are the assessment of the potential of siRNA mediated downregulation of tight junction components to increase pressure dependent outflow facility through the conventional pathway *ex* vivo and *in vivo* in model organisms, through implementation of appropriate outflow facility measurement techniques. The subsequent assessment of the effect of this treatment on *in vivo* IOP and SC ultrastructure was also carried out.

Results

Perfusion Systems

In order to assess the efficacy of siRNA mediated downregulation of TJ components, it was necessary to measure any changes in conventional outflow facility, termed *C*, in murine eyes. This was first approached using a modified version of the computerised, syringe pump based perfusion system describe by Boussommier-Calleja et al. 2012, fig 3.2. In this system, murine eyes are enucleated and *C* is measured *ex vivo*, with a single eye measured at a time, while the contralateral eye is stored in PBS at 4 ˚C. This system consists of a fluid filled cannula inserted through the cornea into the anterior chamber of the eye being perfused, and connected, by means of fluid filled pressure non-compliant tubing, to a computer controlled syringe pump, a wet-dry pressure transducer, and a manometric reservoir, together representing a closed system. Once the eye has been cannulated, the reservoir is used to apply a set pressure to the system as a whole, which therefore represents the IOP of the enucleated eye. After the pressure has been set, the reservoir is closed off from the system, a computer program takes readings from the pressure transducer, and the flow rate of the syringe pump is continually adjusted to maintain a constant pressure in the system. The average flow rate of the syringe pump at constant pressure here represents all fluid outflow out of the anterior chamber of the eye at that pressure, through both the conventional and unconventional pathways, and is recorded at steady state for 10 minutes at four separate pressure steps to create a linear plot of flow vs pressure.

With the aim of setting up and using this system to assess the effect of *in vivo* intracameral delivery of siRNA targeting ZO-1 and tricellulin on conventional outflow facility in *ex vivo* mouse eyes, we began preliminary perfusions to establish the accuracy of our measurements in wild type C57bl/6j mice, sample data shown in fig. 3.3(A). Unfortunately, despite prolonged efforts, we were unable to achieve consistent results for baseline conventional outflow facility in these untreated wild type mice, with *C* measurements higher than those reported in literature, representative data fig. 3.3(B), and varying significantly between contralateral eyes. Other issues that made this system unsuitable for continued use were the time taken to achieve measurements, with only one pair of eyes being assessed per day, the requirement for constant monitoring and manual adjustment during perfusion runs, and the high rate of failed perfusions due to

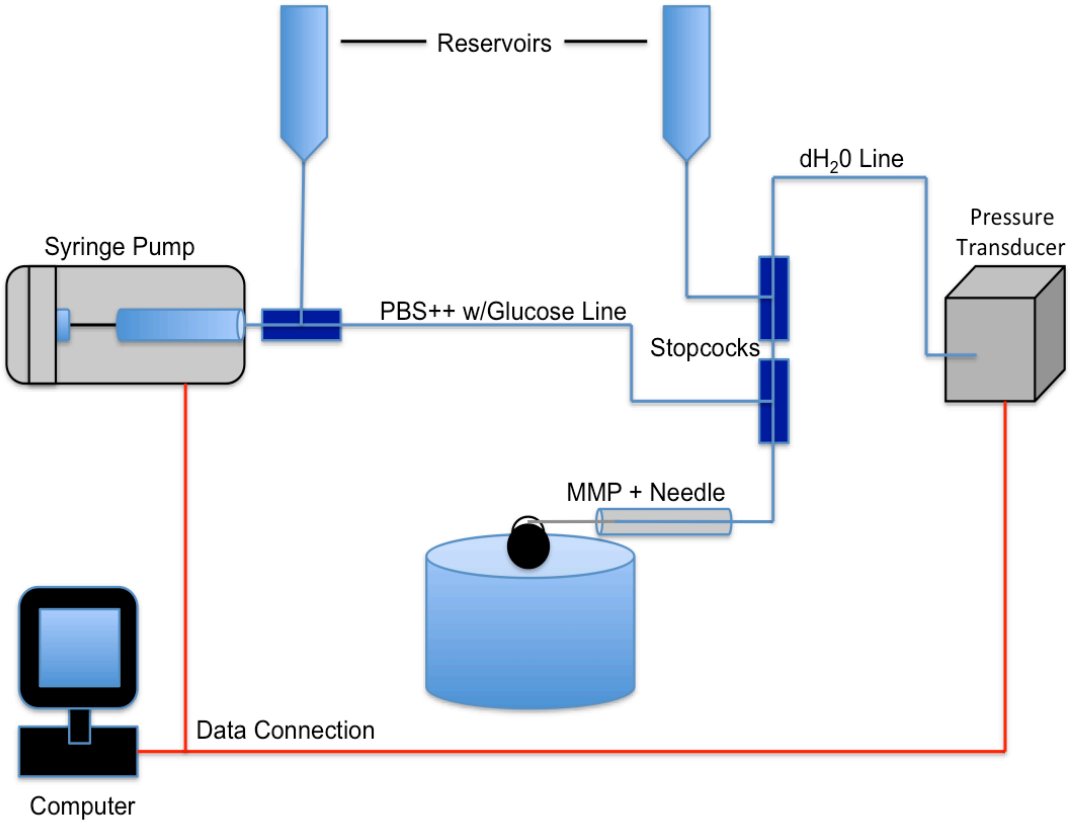

Figure 3.2: Pump based *ex vivo* murine perfusion system.

This figure shows the configuration of the ex vivo pump based perfusion system, with data connections between perfusion code on computer, pressure transducer, and syringe pump shown in red, and fluid filled pressure tubing shown in light blue. MMP = micromanipulator, PBS++ = phosphate buffered saline with divalent cations.

leaks or lack of stable flow data. Additionally, the stable data recorded included pressure drops or spikes that may have occurred in this time, which skewed results.

It was clear that a more sensitive and accurate perfusion system was needed in order to carry out assessment of the effect of the proposed modulation of conventional outflow facility. It was decided to instead pursue the use of the *iPerfusion* system which was in development in the Overby lab, Imperial College London, as described by Sherwood et al. 2016, fig. 3.4. This perfusion system differs from the previous pump based system in that it uses an actuator driven variable height reservoir to vary applied IOP in *ex vivo* eyes instead of a pump, and measures total fluid flow in to the eye directly using an extremely accurate thermal micro-flow sensor. It uses a wet-wet pressure transducer to measure IOP using external atmospheric pressure as a reference,

and also is contained within a sealed unit to prevent air currents from affecting pressure readings. This leads to extremely sensitive and accurate measurements of conventional outflow facility, with values reported as a reference facility at 8 mmHg, termed C_r. The system is semi-automated, with flow rate monitored continually, and set parameters of rate of change of flow rate defined to determine when steady state has been achieved and to automatically progress the perfusion to the next pressure step, removing the need for constant monitoring seen in the previous system. The increase in accuracy and sensitivity of measurements greatly increases the speed of the perfusion, meaning flow can be assessed over 8 pressure steps instead of the previous 4 steps. The system also allows for the simultaneous measurement of two eyes, overall increasing numbers of eyes measurable per day from 2 to 8. Sample trace data shown here clearly show this increase in measurement sensitivity, fig. 3.5, with no significant spiking of data.

Along with these mechanical changes to measurement, improved post measurement modeling and interpretation of perfusion data was implemented. Previous models assumed a linear relationship between flow and pressure, with C remaining constant across all ranges of pressure, which was shown to be incorrect (Sherwood et al. 2016). Instead, a power law fitting was applied to the data to account for greater increases in flow at higher pressure points. Another major change to the model was the removal of non-zero flow values at zero pressure. In an enucleated mouse eye, the absence of blood flow through ocular veins would remove the osmotic forces that drive pressure independent outflow *in vivo*, and no mechanism has been shown that would allow this pressure independent outflow to occur *ex vivo*. Instead the Y-axis intercept is forced through zero in the modeling of perfusion data. Variables were also added to account for deepening of the mouse anterior chamber during perfusions, which can increase flow through widening of the iridocorneal angle.

This system was clearly superior to the system previously used and would allow us to move forward with our investigation of the influence of tight junctions on AH outflow in *ex vivo* mouse eyes.

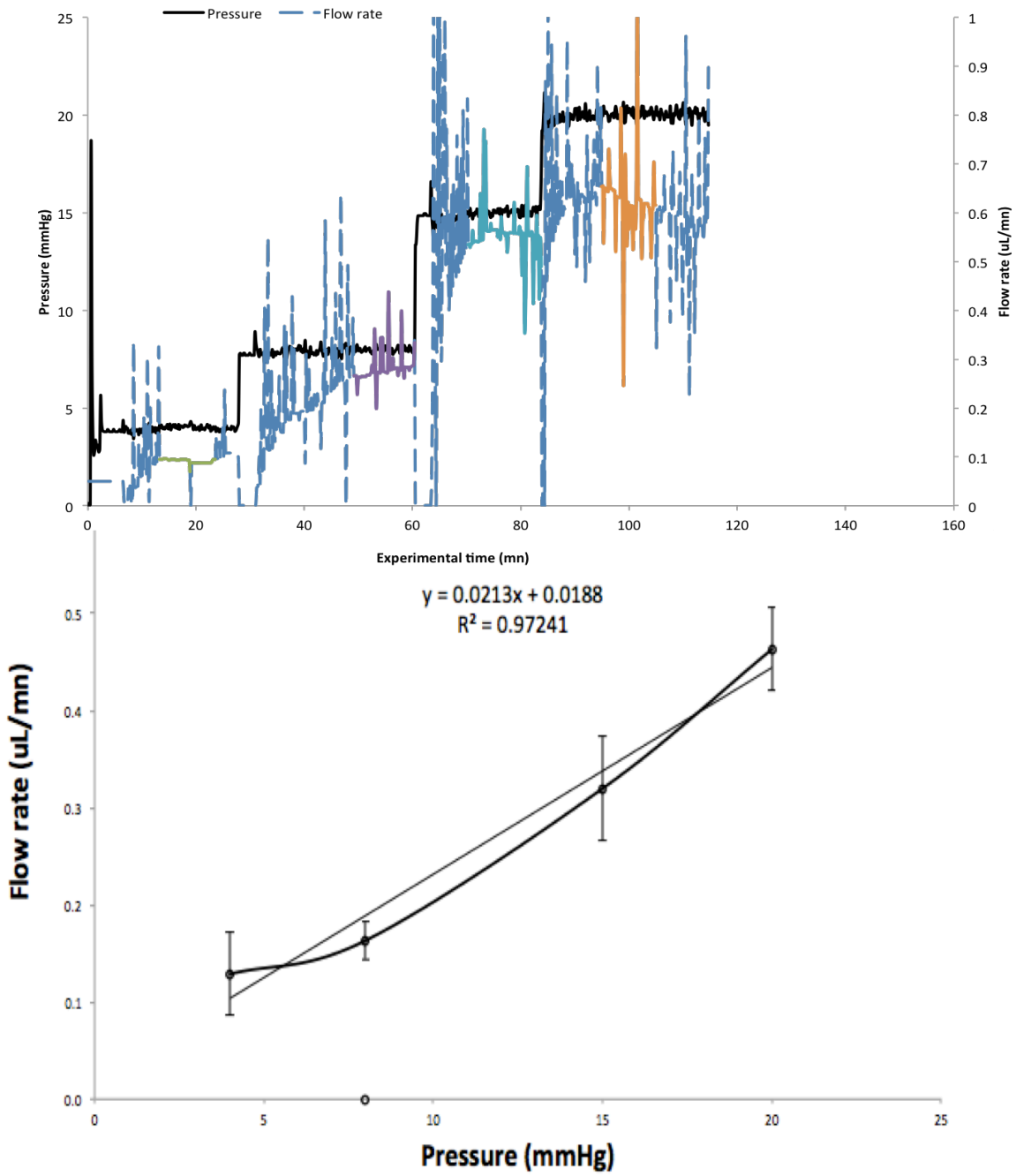

Figure 3.3: Representative data from pump based perfusion system.

(A) Representative raw data trace of pressure, left axis, black line, and flow, right axis, dark blue line, over the course of a perfusion. The four coloured areas (green, purple, light blue, orange) of the flow data line indicate the data that was deemed stable at each pressure step, and therefore included in analysis. (B) *Pooled flow vs pressure data at 4, 8, 15, and 20 mmHg, from a cohort of wild-type C57BL/6J mice (N=6), with linear best fit line. Conventional outflow facility is taken as the slope of this line, 0.0213 µL/min/mmHg here. Error bars represent SEM.*

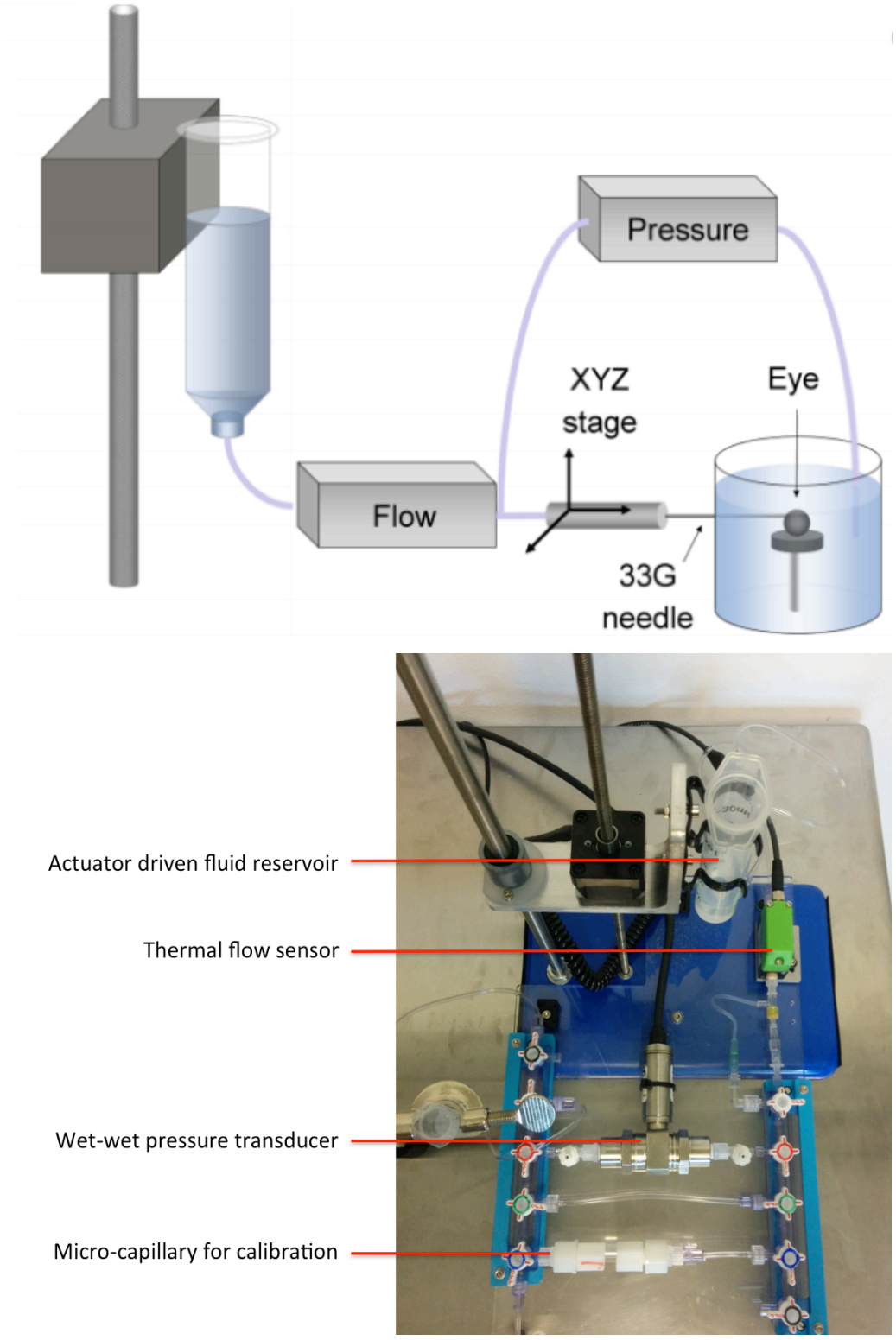

Figure 3.4: Schematic and photograph of iPerfusion system.

Top; schematic of iPerfusion system showing measurement of flow into eye from reservoir and applied pressure. Bottom; photograph of iPerfusion machinery with all relevant components labeled.

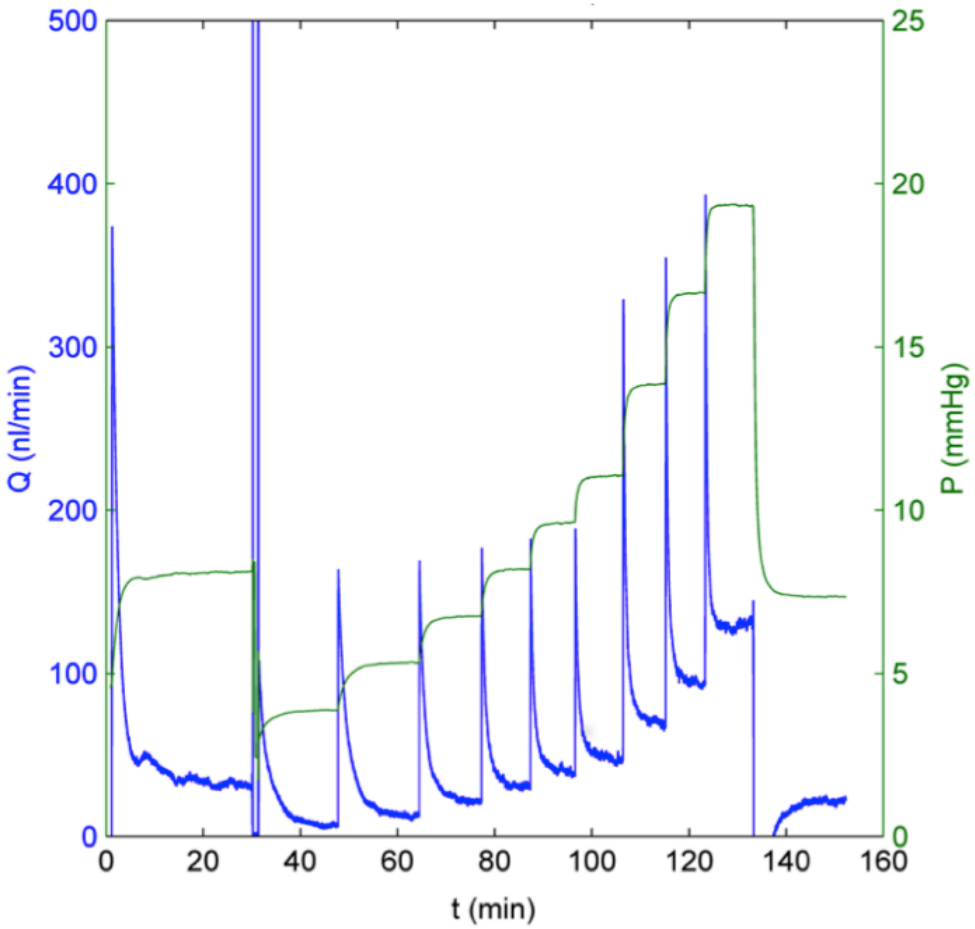

Figure 3.5: Representative trace of iPerfusion raw data.

A representative visualisation of the raw data generated by the iPerfusion system, showing pressure, right axis, green line, and flow, left axis, blue line, over the course of a perfusion. First 30 minutes represents pre-perfusion acclimatisation step at 8 mmHg, followed by 9 pressure steps.

Effect of siRNA modulation of tight junctions on murine conventional outflow

As acceptable assessment of the effectiveness of our proposed therapeutic approach to treating the pathology of glaucoma, by increasing AH outflow rates, and thereby decreasing IOP, was now possible, it was tested in wild type C57BL/6J mice. Mice were intracamerally injected with combination siRNA, containing 1µg each of ZO-1 and tricellulin siRNA, in one eye, with the contralateral control eye injected with 2µg non-targeting (NT) siRNA, using beveled pulled glass needles. Mice were sacrificed 48 hours post injection and the eyes were enucleated and immediately analysed using the *iPerfusion* system. The initial cohort of mice had issues with eye integrity that

precluded their use in perfusion studies, fig. 3.6. After injection, eyes exhibited nuclear cataracts, degraded corneas, and pigment dispersion. It was unclear whether these issues were due to the injection protocol, or due to the dosage of siRNA introduced to the AC. In order to investigate this, a series of control injections were carried out, with the injection buffer alone injected in to one group of mice, and corneal puncture alone, with no injection, performed on a second group. These mice still exhibited the previously observed ocular damage, indicating the injection protocol itself was causing the pathology. In order to address this, the protocol for intracameral injection was modified in several ways. Pulled glass needles were changed from beveled to unbevelled, to minimize the size of the puncture in the cornea and to allow for shallower injections, decreasing likelihood of needle contact with the lens. Sterility was also increased, with sterile surgical drapes used during procedures, topical fusidic acid applied to the injection site after injection, and subcutaneous antibiotics administered to the mice during the procedure. Corneal damage was believed to be due to water loss during anesthesia, and as such, an eye moistening gel was also introduced to the procedure, to reduce the effects of anesthetic-induced transcorneal water loss, and subsequent dehydration of the cornea. These protocol changes resulted in complete elimination of post injection pathology, and eyes appeared normal and healthy 48 hours after injection, fig. 3.6.

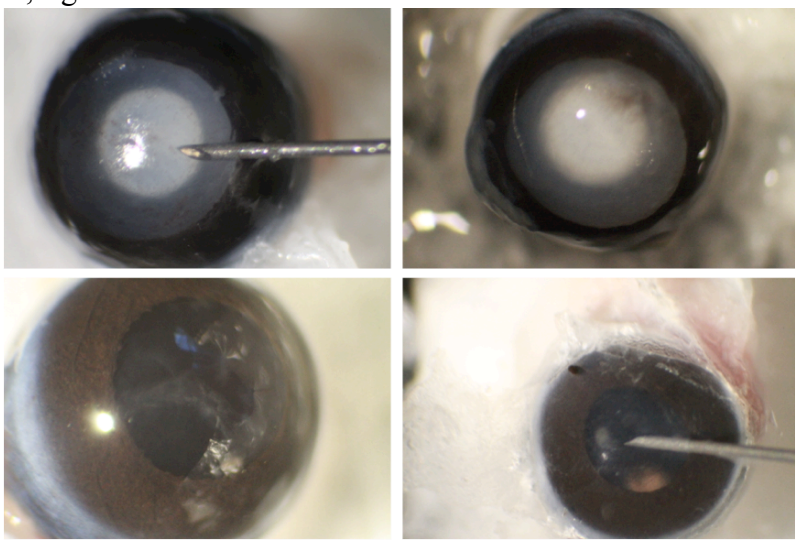

Figure 3.6: Mouse eye pathology after intracameral injection.

Upper images; damaged mouse eyes resulting from the original injection protocol, which were unsuitable for perfusion analysis. Eyes display nuclear cataracts, pigment dispersion, and weakened corneas. Lower images; eyes injected using the newer intracameral injection protocol, which showed no pathology.

Mice were again treated with combination ZO-1 and tricellulin siRNA, with contralateral NT controls, as described above, and eyes were enucleated and perfused after 48 hours. Figure 3.7 shows a representative flow-pressure trace from a single pair of eyes from this experiment, displaying a clear increase in outflow facility in the eye treated with targeting siRNA as compared with the contralateral NT siRNA treated control. Figure 3.8 shows the paired facility data for all 7 mice analysed in this experiment, with cello plots individual C_r values, being facility values as calculated at 8mmHg, of all treated vs control eyes in (a), while (b) shows of the paired facility data, with C_r of treated eye of each pair on the Y-axis, and of the control eye on the X-axis. As can be seen from this plot, in all treated eyes outflow facility was increased as compared to the contralateral control, with the average increase being 113 (35, 234) % (N = 7 pairs, p = 0.0064). This clearly shows that our approach of *in vivo* downregulation of selected TJ components of the conventional outflow tissues can increase outflow facility in *ex vivo* mouse eyes.

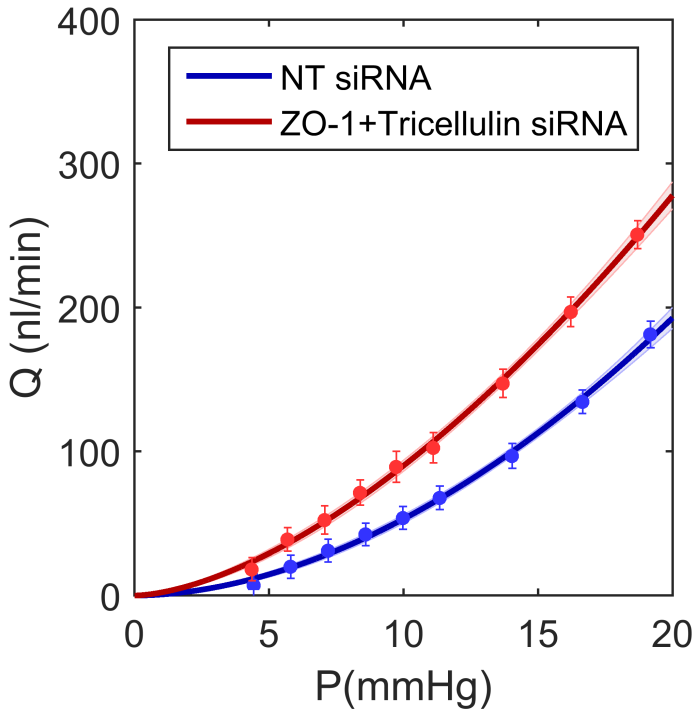

Figure 3.7: Representative flow-pressure plot from siRNA treated mouse

Flow (nL/min), y-axis, is shown against applied pressure, x-axis, (mmHg) in a representative pair of eyes from this experiment. Data from ZO-1 and tricellulin siRNA treated eye is shown in red, while non-targeting (NT) siRNA treated eye is shown in blue.

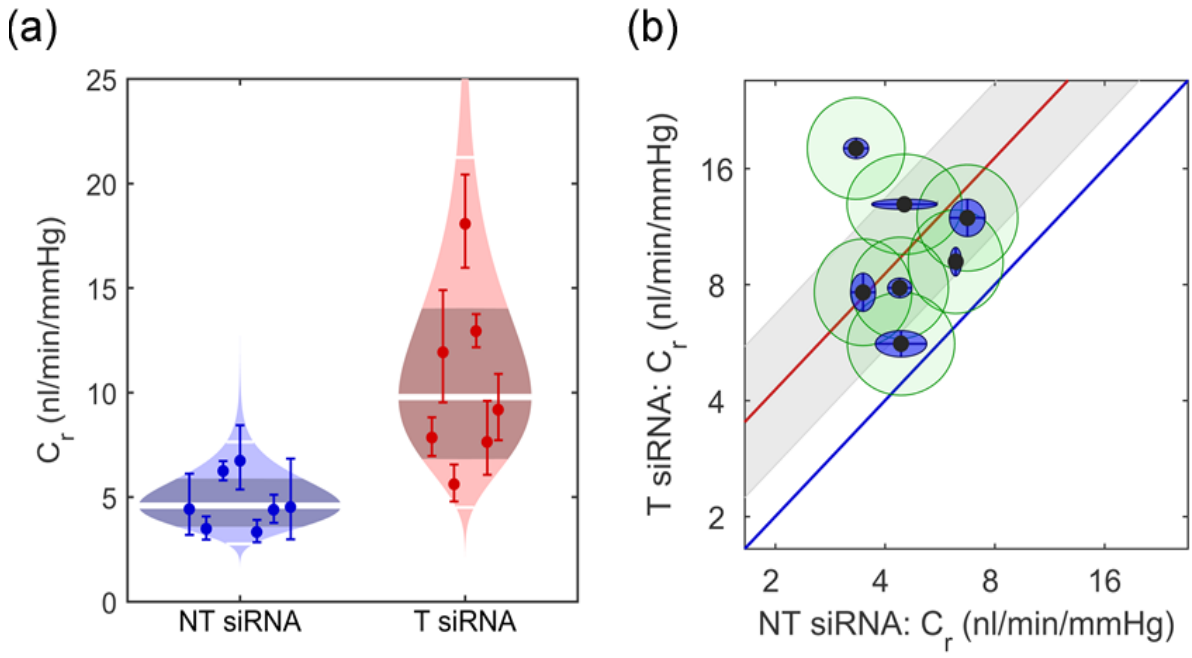

Figure 3.8: The effect of siRNA mediated downregulation of tight junctions on murine conventional outflow facility.

(a) Cello plots showing the individual values and distribution of outflow facility at 8 mmHg (C_r) for eyes treated with either non-targeting (NT) siRNA or a combination of ZO-1 and tricellulin targeting (T) siRNA. Each point represents a single eye, with error bars representing 95% confidence intervals on C_r. Shaded area represents predicted log normal distribution of data, middle white line represents mean, inner dark shading represents one standard deviation from mean, while outer white lines represent two standard deviations from mean.

(b) Paired facility plot: each data point represents one pair of eyes, with C_r for the treated T siRNA eye shown on the Y-axis and the C_r for contralateral control NT-siRNA eye on the X-axis. The red line represents the mean difference between contralateral eyes, with 95% confidence interval shown in grey, whilst the blue line represents the case of identical facility between contralateral eyes, corresponding to no effect due to T siRNA. Facility was higher in all treated eyes compared to the controls, with average increase being 113 (35, 234) % n = 7, p = 0.006. Inner blue ellipses show the 95% confidence intervals on C_r, whilst the green outer ellipses show additional uncertainty due variability between contralateral eyes, estimated from 10 pairs of C57BL/6J eyes perfused only with glucose supplemented PBS.

Effect of siRNA modulation of tight junctions on murine intraocular pressure

In order to assess the effect of siRNA mediated downregulation of ZO-1 and tricellulin on murine intraocular pressure, mice were anaesthetized and IOP was measured by rebound tonometry in both eyes at multiple time points post induction of anesthesia, and these IOP readings were interpolated to allow comparison of a reference IOP at 5 minutes post induction. Mice were injected as before with a combination of 1µg each of ZO-1 and tricellulin siRNA in one eye, with the contralateral control eye injected with 2µg NT siRNA, and IOP was again measured 48 hours post-injection. This measurement showed that eyes treated with siRNA targeting ZO-1 and tricellulin had a significant reduction in IOP after treatment of 2.3 ± 1.9 mmHg, p = 0.012, as compared to their IOP pre-treatment, while those eyes receiving NT siRNA showed no significant reduction in IOP at 48 hours, with a change of -0.7 ± 1.7 mmHg, p = 0.151 (N = 13), fig 3.8.

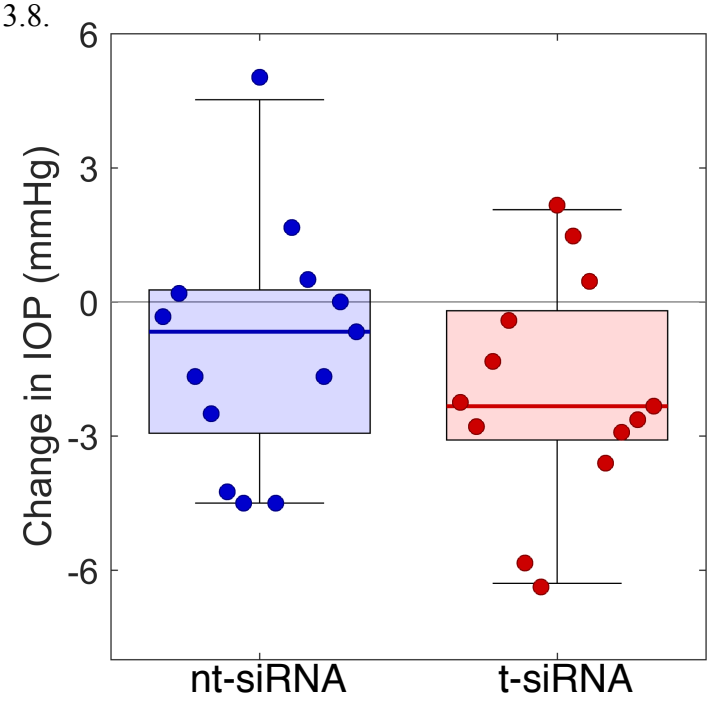

Figure 3.9: The effect of siRNA mediated downregulation of tight junctions on murine intraocular pressure.

IOP was measured before and after control, NT siRNA, or treated, ZO-1 and tricellulin siRNA, injection. Treated eyes had a significant reduction in IOP after injection, with a change of -2.3 ± 1.9 mmHg, p = 0.012, while control eyes showed no significant change in IOP, -0.7 ± 1.7 mmHg, p = 0.151. Data represents medians and median absolute deviations, error bars represent 5th and 95th percentiles, and data was analysed by 1-sample Wilcoxon signed-rank test against a theoretical mean of 0.

Ultrastructural analysis of Schlemm's Canal after siRNA modulation of selected tight junction components

In order to assess the effect of siRNA mediated downregulation of ZO-1 and tricellulin on the ultrastructure of Schlemm's canal endothelium, mice were again injected as before with 1μg each of ZO-1 and tricellulin siRNA in one eye, with the contralateral control eye injected with 2μg NT siRNA as before. Eyes were enucleated 48 hours after injection, immersion fixed, and sent to collaborators for analysis by transmission electron microscopy (TEM), fig. 3.10. Here, eyes were section sagittaly, stained, imaged, with images analysed to quantify open intercellular clefts between SC cells. Quantification of intercellular junctions was performed by 2 independent observers, who examined TEM sections at 80,000x along the anterior-posterior extent of the inner wall from 4 regions of each eye. These counts showed that a significant difference in open intercellular clefts between treated and control eyes, with eyes treated with siRNA targeting ZO-1 and tricellulin, on average 33 ± 25% of intercellular junctions were open, while in NT siRNA treated eyes, an average of only 1 ± 2 % of such junctions were open, fig. 3.11, ($p = 0.004$, unpaired Students t-test, $n = 6$ treated and 5 control). Thus, the data show that siRNA mediated downregulation of ZO-1 and tricellulin indeed disrupts TJs in SC endothelium, resulting in opening of the paracellular spaces between endothelial cells.

Additional examination of SEM images showed that while TJs were disrupted, adherens junctions were not impacted, with no visible disconnections between SC inner wall cells and sub-endothelial tissue observed in any eyes. No other signs of a pathological impact of TJ downregulation were observed.

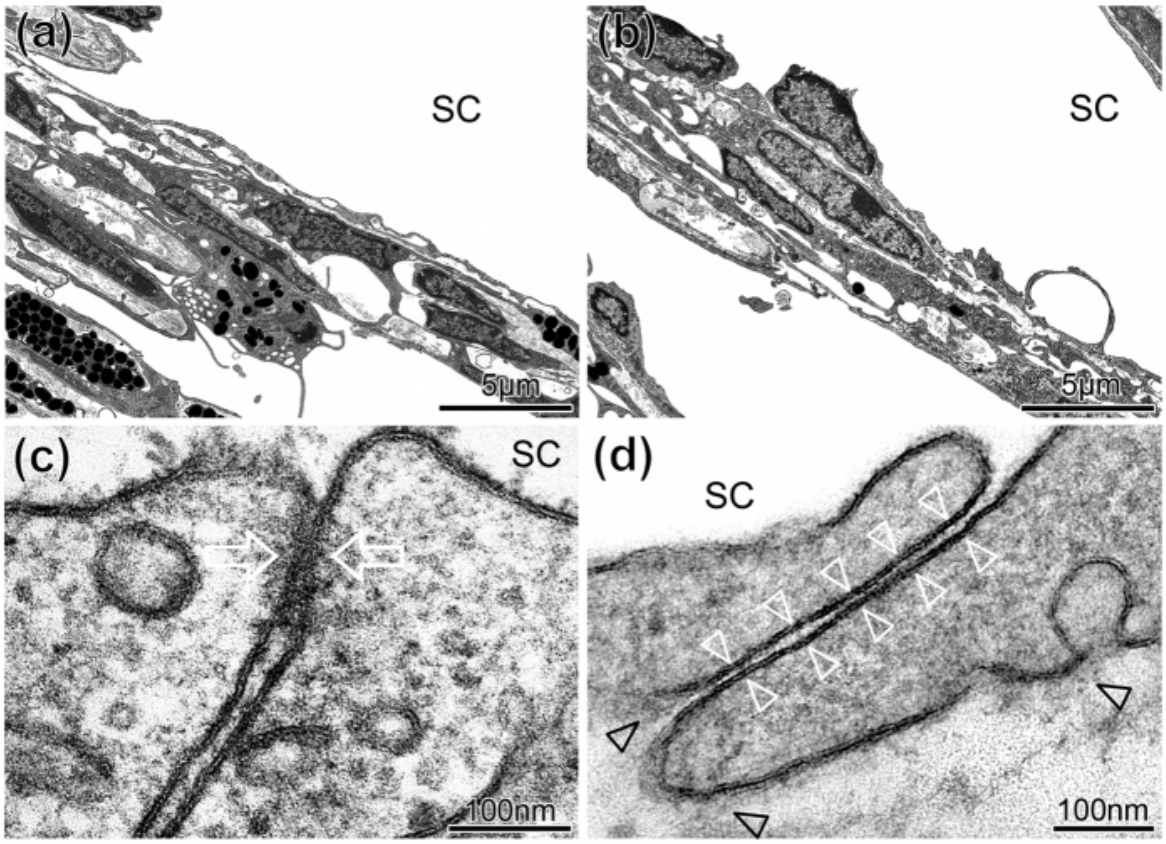

Figure 3.10: Transmission electron microscopic analysis of sagittal sections of the inner wall of SC following siRNA treatment.

(a) and (b) - Representative sections through the inner wall of Schlemm's canal (SC) and outer trabecular meshwork (TM) of a mouse eye treated with (a) non-targeting (NT) or (b) targeting (T) siRNA illustrating intact cells and an intact and continuous inner wall endothelium that appeared similar in both cases

(c) and (d) - Higher magnifications of sections through representative intercellular clefts along the inner wall endothelium of SC showing examples for tight junctions quantitatively evaluated as closed (c) with fusion between the neighbouring cell membranes, marked with white arrows, or open clefts (d) where the cell membranes of adjacent endothelial cells were clearly separated along the entire cleft length (white arrowheads). Black arrows mark intact adhesions to sub-endothelial matrix.

Sample	Region 1		Region 2		Region 3		Region 4		% open
	N total	N open	N total	N open	N total	N open	N total	N open	
C4 NEP T	15	4	17	3	21	5	24	9	27%
C4 REP T	18	15	14	3	22	17	10	5	63%
C4 LEP T	9	5	26	1	18	9	12	3	28%
C5 LEP T	26	10	15	3	24	4	20	4	25%
C6 LEP T	25	11	31	11	15	4	18	2	31%
C6 NEP T	25	2	29	9	16	4	30	8	23%
								Average	33%
								SD	25%

Sample	Region 1		Region 2		Region 3		Region 4		% open
	N total	N open	N total	N open	N total	N open	N total	N open	
C4 NEP NT	8	0	22	0	17	2	28	0	3%
C4 REP NT	17	1	20	0	13	0	18	0	1%
C5 LEP NT	21	0	26	0	14	0	19	0	0%
C6 LEP NT	11	1	30	0	26	0	9	0	1%
C6 NEP NT	20	1	17	0	29	0	31	1	2%
								Average	2%
								SD	1%

Figure 3.11: Quantification of open intercellular clefts in treated and control Schlemm's canal inner wall.

Top; Quantification of open intercellular clefts at four distinct regions of Schlemm's canal inner wall in eyes treated with siRNA targeting ZO-1 and tricellulin. On average 33 ± 25% of intercellular junctions were open in treated eyes.

Bottom; Quantification of open intercellular clefts at four distinct regions of Schlemm's canal inner wall in non-targeting siRNA treated eyes, an average of only 1 ± 2 % of such junctions were open, showing significant difference from treated eyes (p = 0.004, unpaired Students t-test, n = 6 treated and 5 control).

Adaptation of *iPerfusion* system to facilitate primate *in vivo* conventional outflow measurement

As the primary goal of this research was to develop a viable novel therapeutic approach that could be translated to the treatment of the reduced conventional outflow facility observed in human glaucomatous patients, assessment of siRNA-mediated down-regulation of SC tight junctions *in vivo* in non-human primates was carried out. For the purpose of this investigation, the African Green monkey (*Chlorocebus sabeus*) was used as a non-human primate model, with primate investigations carried out in collaboration with Professor Matthew Lawrence, Director of the St. Kitts Biomedical Research Foundation. For this study, it was decided to conduct *in vivo* perfusions, as they would represent a more biologically relevant measurement of change in outflow facility as compared to *ex vivo*, and the larger eye size would make this process easier to achieve than in mice. Initial calibration of the primate specific *iPerfusion* system was carried out in surplus *ex vivo* primate eyes to minimize the unnecessary use of animals, fig. 3.12. The *in vivo* measurement required adaptation of both the *iPerfusion* machinery and protocol. The main changes to the machinery involved the exchange of the original thermal flow sensor, which was optimized for the low flow rates seen in mouse eyes, for a flow sensor capable of reading the higher flow rates expected in primates, and the inclusion of a 31-gauge needle in line with the flow sensor, which acted as a pressure resistor, to negate the oscillatory flow effect of ocular pulse on recorded data. The system was also adapted to be smaller and more transportable, running off laptop computers, no longer requiring a large sealed cabinet, and having a lower maximum reservoir height. The protocol was altered from the previous single series of incrementing pressure steps, to an experimental protocol which comprised of an initial reading of IOP, termed spontaneous IOP (sIOP), by direct cannulation of anterior chamber to fluid filled pressure stable lines connected a pressure sensor, followed by a stepping cycle beginning at sIOP minus 6mmHg, stepping to sIOP minus 3mmHg, then plus 0, 4, 8, and 12mmHg respectively. This was carried out three times, with sIOP readings taken again before starting the second and third cycle, and after the third cycle, in order to account for temporal and pressure dependent responses to anesthesia. Initial perfusions in untreated animals showed that repeated sIOP measurement revealed a reduction in sIOP over time under anesthesia, representative data is shown in fig. 3.13.

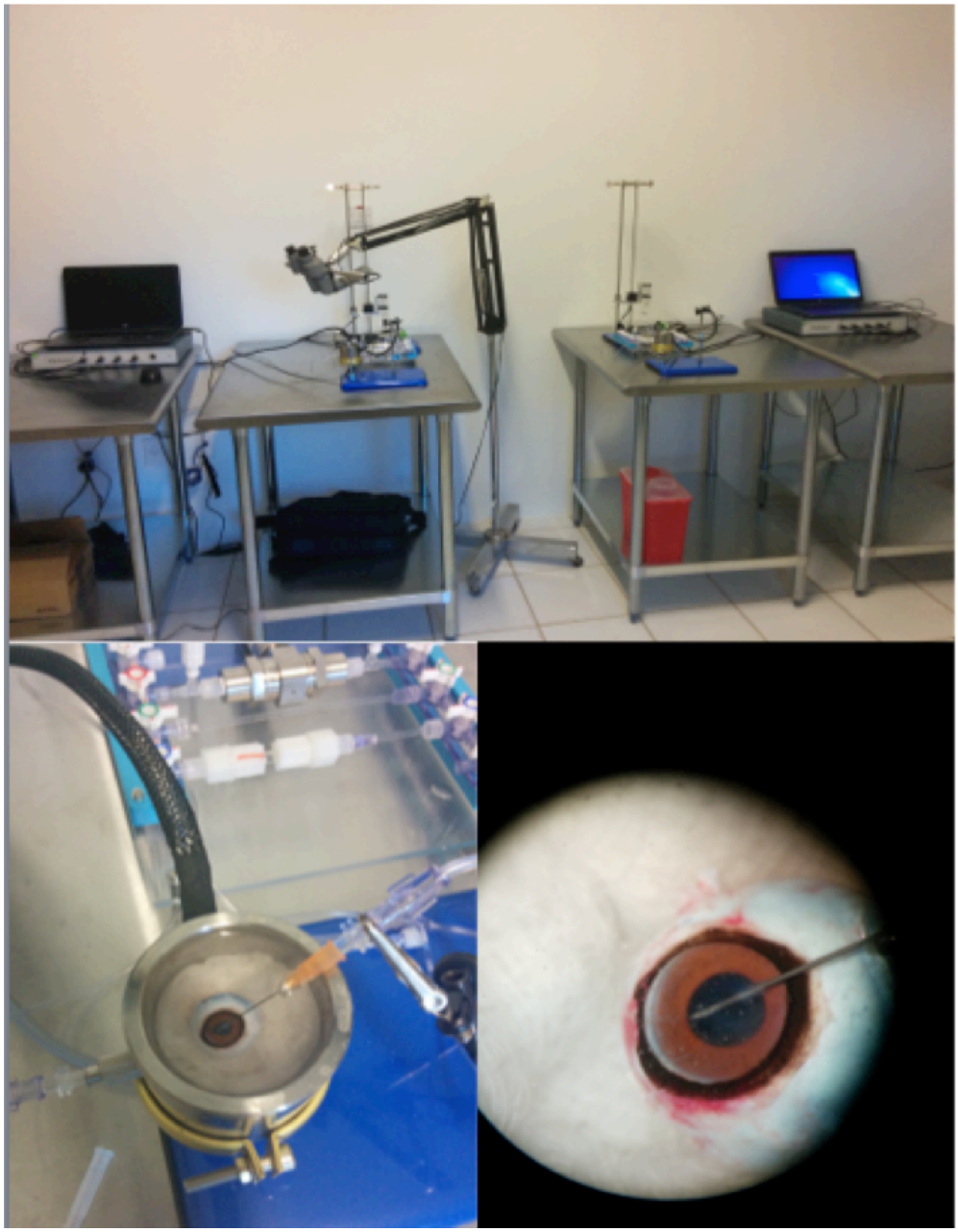

Figure 3.12: Primate *in vivo* and *ex vivo iPerfusion* set up.

Top; full iPerfusion set up, showing dual machinery for concurrent measurement of both eyes. An anesthetised primate is placed in a supine position on a platform between the two systems during perfusion measurements.

Bottom: images of ex vivo perfusion of primate eyes, carried out to validate and calibrate the system prior to in vivo use.

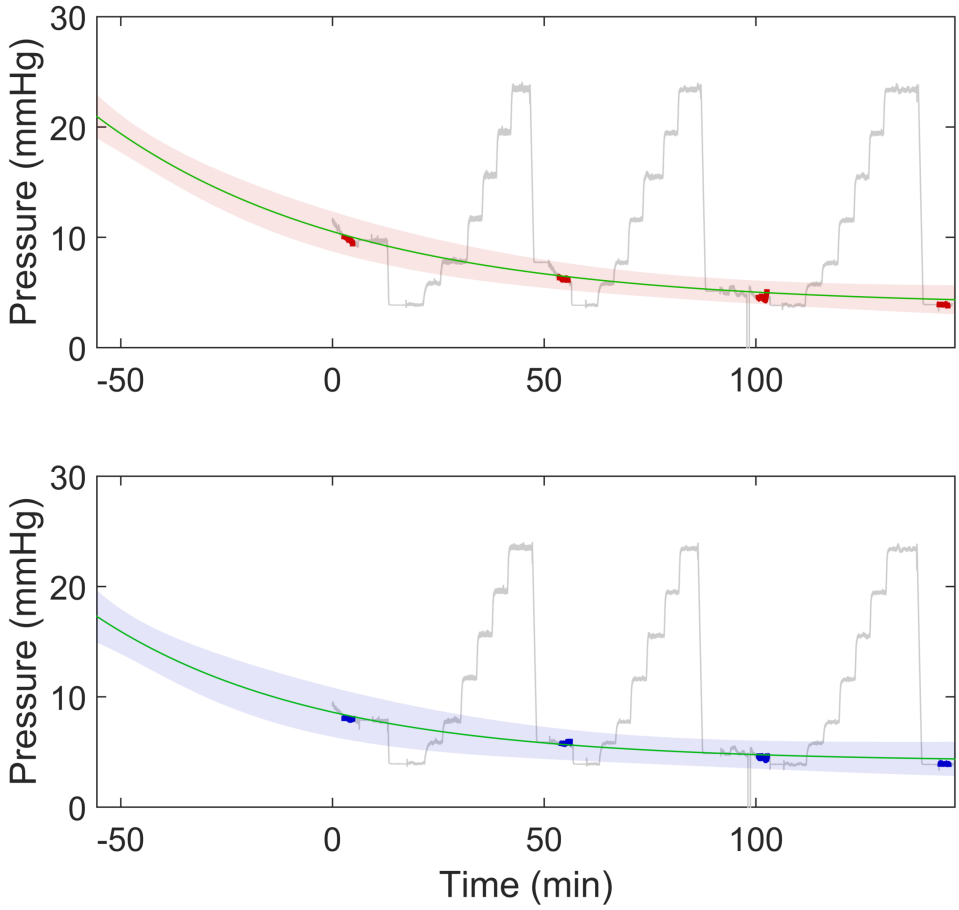

Figure 3.13: Effect of anesthesia on primate spontaneous intraocular pressure over time.

Representative data from a contralateral pair of perfused primate eyes showing repeated measurement of primate spontaneous IOP (sIOP) through direct cannulation of the anterior chamber to a pressure transducer until steady state pressure was achieved. This showed that sIOP decay occurred over time of anesthesia during three in vivo perfusion cycles. Pressure at -50 minutes was determined by tonometry before cannulation. Grey line represents measured intraocular pressure during the course of the perfusion, while red/blue line segments correspond to sIOP readings. Green line represents interpolated IOP over time of anesthesia, showing anesthesia induced IOP decay.

In this study, intracameral injections were then carried out delivering 100 µg each of siRNA targeting ZO-1, tricellulin, and claudin-11 transcripts in to one eye, with 300 µg NT siRNA injected in to the contralateral control eye, both delivered in a volume of 20 µL RNase free water. At 48 hours post injection, animals were anesthetized by intramuscular injection of ketamine and xylazine, IOP was measured through use of rebound tonometry in animals immediately prior to perfusion, with three measurements taken in each eye and median measurement used for analysis. Rebound tonometry showed that there was no significant difference in IOP between treated and control eyes, fig. 3.14, indicating that the treatment did not have an IOP lowering effect in this instance.

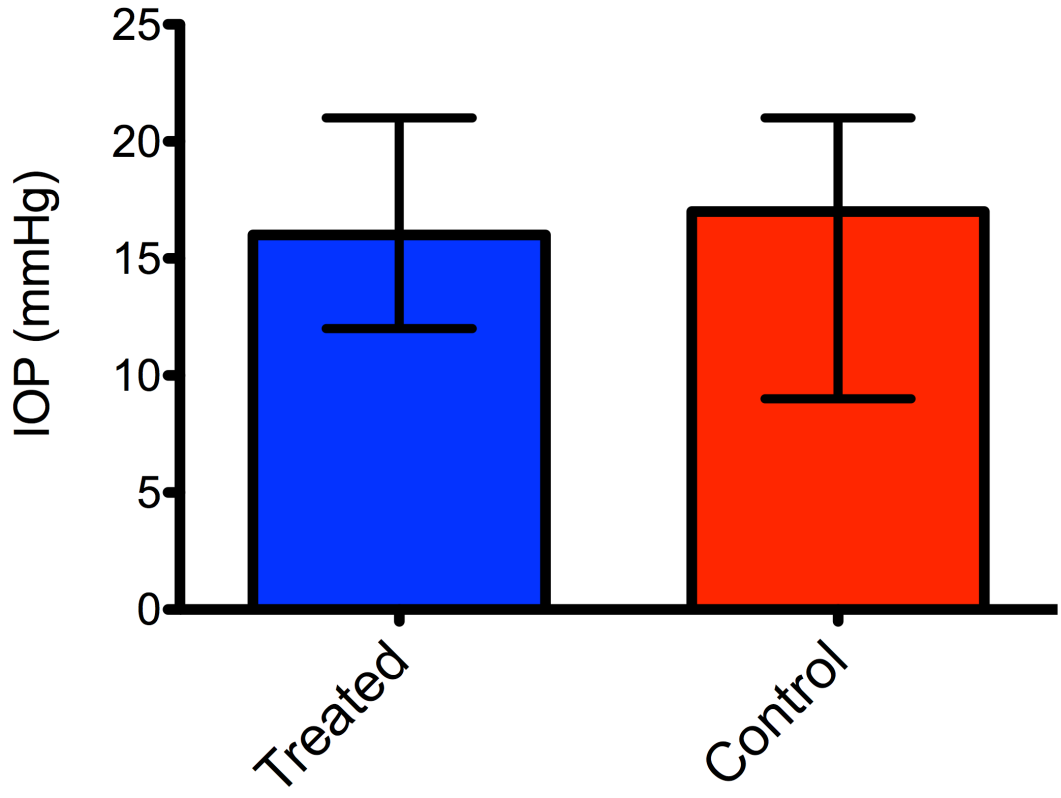

Figure 3.14: The effect of siRNA mediated downregulation of tight junctions on primate intraocular pressure.

IOP was measured by rebound tonometry 48 hours after injection in control eyes, 300 µg NT siRNA, or treated eyes, 100 µg each claudin-11, ZO-1 and tricellulin siRNA, in 20 µL. No significant difference in IOP was detected between control eyes, median 16 mmHg, and treated eyes, median 17 mmHg, p = 0.9054, N = 8, analysed by Wilcoxon Rank Sum test. Data represents median, error bars represents range of individual medians from triplicate IOP measurements.

After IOP measurements were taken, both eyes were cannulated and *in vivo iPerfusion* was carried out as described above, representative flow and pressure trace data from a pair of eyes from one animal is shown in fig. 3.15. Paired analysis of contralateral eyes showed no significant differences in outflow facility between treated and control eyes, with a high degree of pairedness observed between treated and control eyes, fig 3.16. This indicates that the treatment failed to have any conventional outflow facility increasing effect.

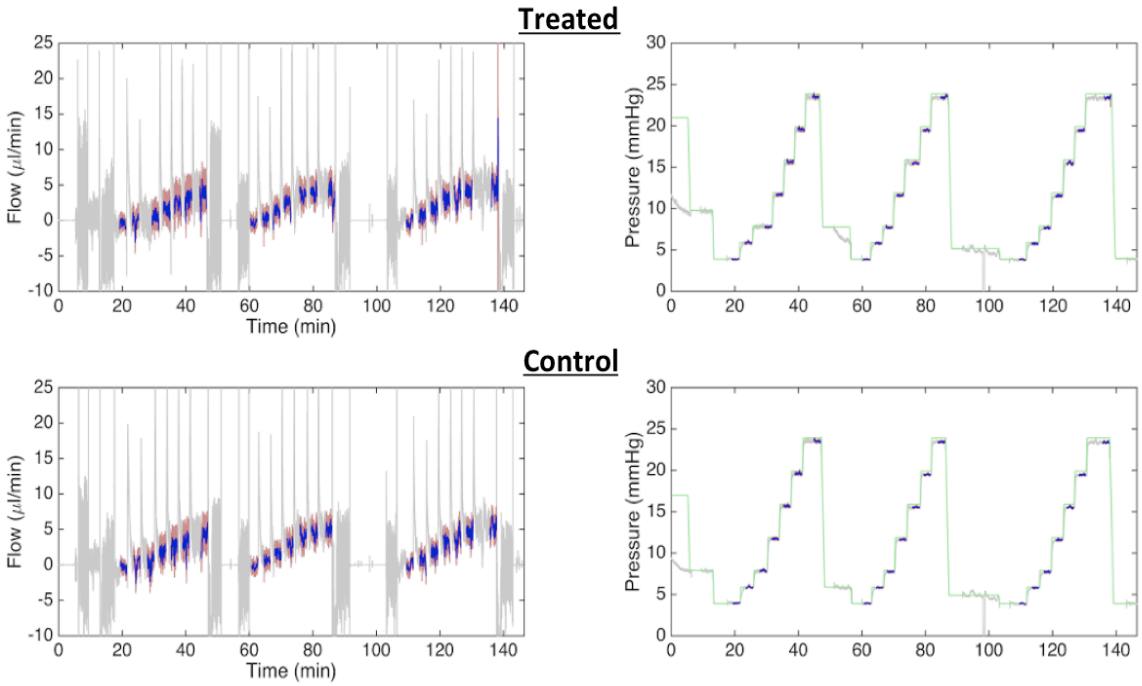

Figure 3.15: Representative flow and pressure trace data from a pair of primate eyes.

Flow and pressure trace data from contralateral injected control,300 µg NT siRNA, or treated eyes, 100 µg each claudin-11, ZO-1 and tricellulin siRNA, in 20 µL. Left panels show recorded flow data over the course of three cycles of an in vivo primate perfusion over time, with flow data shown as grey line, with stable data from each pressure step shown as blue line segments, while red areas represent data removed by computer filtering. Right panels show pressure data over the course of the perfusion, with recorded pressure data, which corresponds to IOP, shown as a grey line, with stable data from each pressure step shown as blue line segments, while red areas again represent data removed by computer filtering. The green line represents the intended applied hydrostatic pressure at each step.

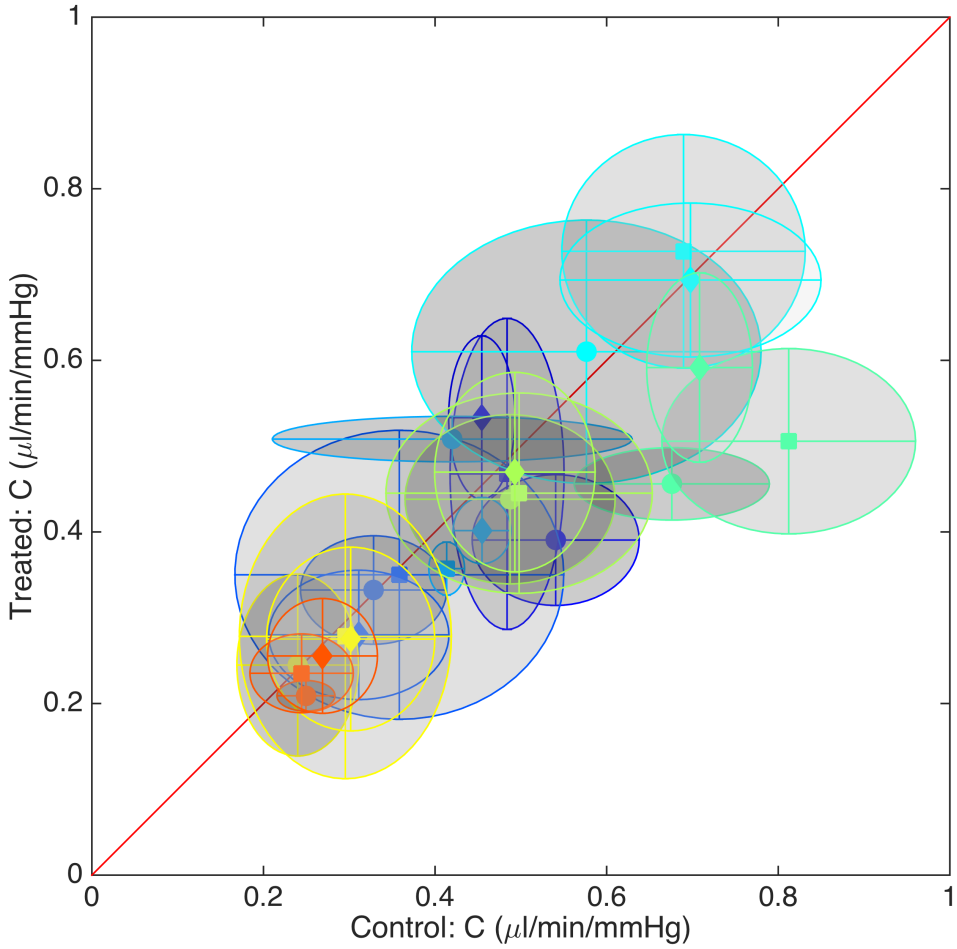

Figure 3.16: The effect of siRNA mediated downregulation of tight junctions on primate conventional outflow facility.

Paired facility plot of contralateral treated and control primate eyes. Each data point represents one of three cycles of perfusion from a pair of eyes, with all three cycles from the same animal coloured the same. C for the claudin-11, ZO-1, and tricellulin siRNA treated eye shown on the Y-axis and C for contralateral control NT siRNA eye on the X-axis. Large ellipses around each data point represent the uncertainty of measurements arising from known measurement uncertainty of flow and pressure sensors. The red line represents the case of identical facility between contralateral eyes, corresponding to no effect of treatment siRNA on conventional outflow facility. Facility was not significantly different in treated eyes compared to controls, N = 8.

A

MONKEY	OD TREATMENT	OS TREATMENT	Dose (per siRNA)	Total	FOLD change in gene expression (Control siRNA set at 1)		
					CLDN11 expression	ZO-1 expression	Tricellulin expression
Z634	siRNA	control	100 µg	300 µg	0.20	0.44	0.49
K247	control	siRNA	100 µg	300 µg	3.03	0.42	1.00
K217	control	siRNA	100 µg	300 µg	2.53	0.81	1.07
Z626	siRNA	control	100 µg	300 µg	3.52	0.71	0.70
Z803	control	siRNA	100 µg	300 µg	0.90	0.99	0.74
Z607	siRNA	control	100 µg	300 µg	1.69	0.62	0.55
Z497	siRNA	control	100 µg	300 µg	4.71	2.61	0.47
Z804	control	siRNA	100 µg	300 µg	1.08	1.89	1.28
Z606	siRNA	control	200 µg	600 µg	1.42	1.12	2.39
K119	control	siRNA	200 µg	600 µg	0.65	1.30	0.87

B

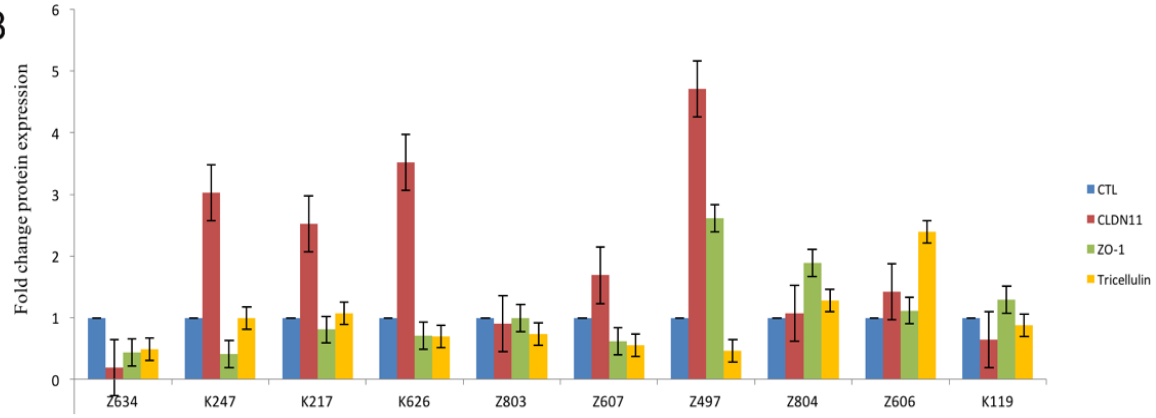

C

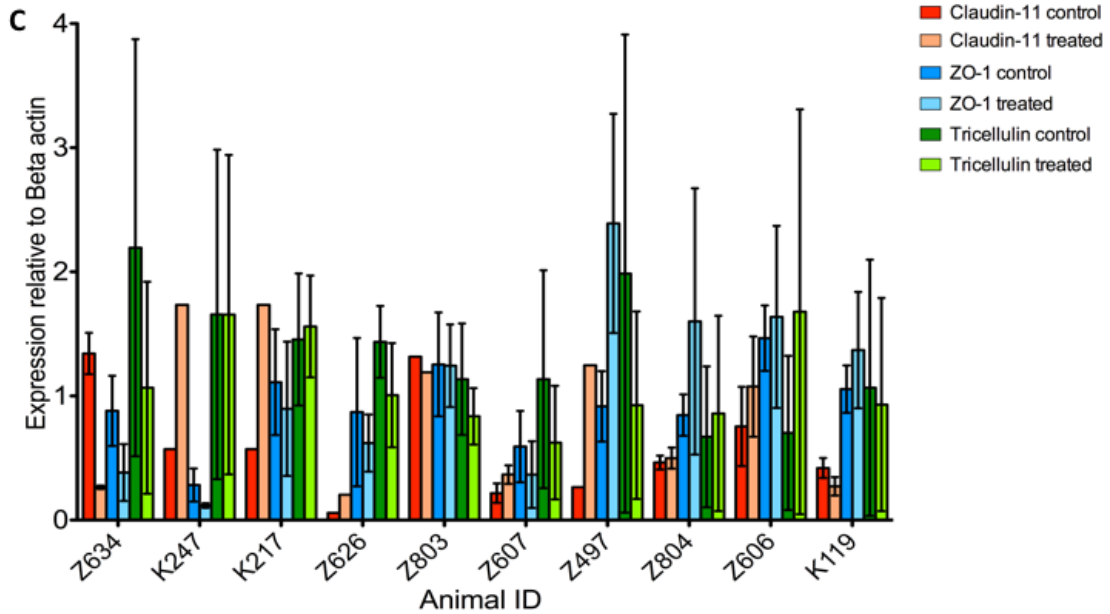

Figure 3.17: Assessment of effect of siRNA mediated downregulation of tight junction components on target protein levels.

A - Table detailing treatment received in each eye for each animal, OD = right eye, OS =left eye, along with siRNA dosage, and fold change in target protein expression relative to expression level in NT siRNA treated eye, as determined by densitometry.

B – Graphical representation of fold change in expression levels of claudin-11, ZO-1 and tricellulin in monkeys injected with normal dose (n=8; 100 μg per siRNA), and with high dose of siRNAs (n=2; 200 μg) per siRNA, with beta actin used as aloading control, and relative to expression level of the same protein in NT siRNA treated eye (600 μg), set to 1. Data represents mean ± s.e.m.
C – Graphical representation expression levels of claudin-11, ZO-1 and tricellulin in monkeys injected with normal dose (n=8; 100 μg per siRNA), and with high dose of siRNAs (n=2; 200 μg) per siRNA, relative to loading control beta actin. Data represents mean ± s.e.m.

Analysis of effect of delivery of siRNA targeting tight junction components on protein levels in dissected primate outflow tissues

In order to determine why this approach had failed in primates despite encouraging data in murine experiments, the effect of siRNA on protein expression levels of TJ targets was assessed. Additionally, two further animals were also injected with a double dose of each siRNA treatment, receiving 200 μg each of siRNA targeting ZO-1, tricellulin, and claudin-11 transcripts in to one eye, with 600 μg NT siRNA injected in to the contralateral control eye. Due to larger outflow tissue size in primate eyes allowing for surgical dissection not possible in murine eyes, animals were sacrificed, and conventional outflow tissues were dissected out, and then snap frozen. Protein was later extracted from these tissues and analysed by western blot to determine levels of down regulation of target proteins. This analysis revealed that downregulation was inconsistent with regards to both targets downregulated and levels of downregulation, fig. 3.17, with only a single animal showing downregulation of all three targets, and some animals showing upregulation of targets, particularly claudin-11. Monkeys receiving a higher dose of siRNA did not show any difference in levels of downregulation. This may offer an explanation as to the lack of effect of treatment on both IOP and conventional outflow facility.

Mouse *in vivo* measurement of spontaneous IOP

As the adapted *in vivo* primate *iPerfusion* protocol had been shown to be capable of detecting spontaneous IOP through direct cannulation of the anterior chamber to a

pressure transducer, an attempt was made to carry out a similar procedure in mice in order to obtain further data on the effect of our siRNA based treatment on IOP reduction. For this, mice were injected with ketamine and xylazine via a catheter placed intraperitoneally, re-dosed throughout the perfusion to maintain anesthesia, and placed on a palate bar head holder on a heated platform. IOP was measured after induction of anesthesia by rebound tonometry prior to cannulation, then both anterior chambers were cannulated with pulled glass needles attached to the *iPerfusion* system with reservoir set to the tonometric IOP reading, and eyes were covered with lubricant to retain moisture, see fig. 3.18. After cannulation, the anterior chamber fluid line was switched to directly connect to the pressure transducer, giving a reading of sIOP as above in primates, mice were than perfused, and a second sIOP reading was taken after perfusion. A representative example of pressure trace data generated from this protocol can be seen in fig. 3.19. As can be seen from this representative data, murine IOP decays rapidly under injectable ketamine and xylazine anesthesia, and steady state readings of sIOP took quite some time to achieve, and in several cases sIOP didn't stabilize within reasonable time limits, so data was not obtained. There were also difficulties in maintaining full pressure seal at needle cannulation site, as is demonstrated by sIOP reading dropping below 0 mmHg in the second sIOP reading in the control eye of this animal. Pooled pre- and post-perfusion sIOP measurements for all mice can be seen in fig. 3.20. Pre-perfusion sIOP showed no significant difference between treated and control eyes, $p = 0.756$, $N = 8$ for control, 10 for treated. Similarly, no significant difference was observed between treated and control groups for post-perfusion sIOP, $p = 0.477$, $N = 6$ for control, 7 for treated.

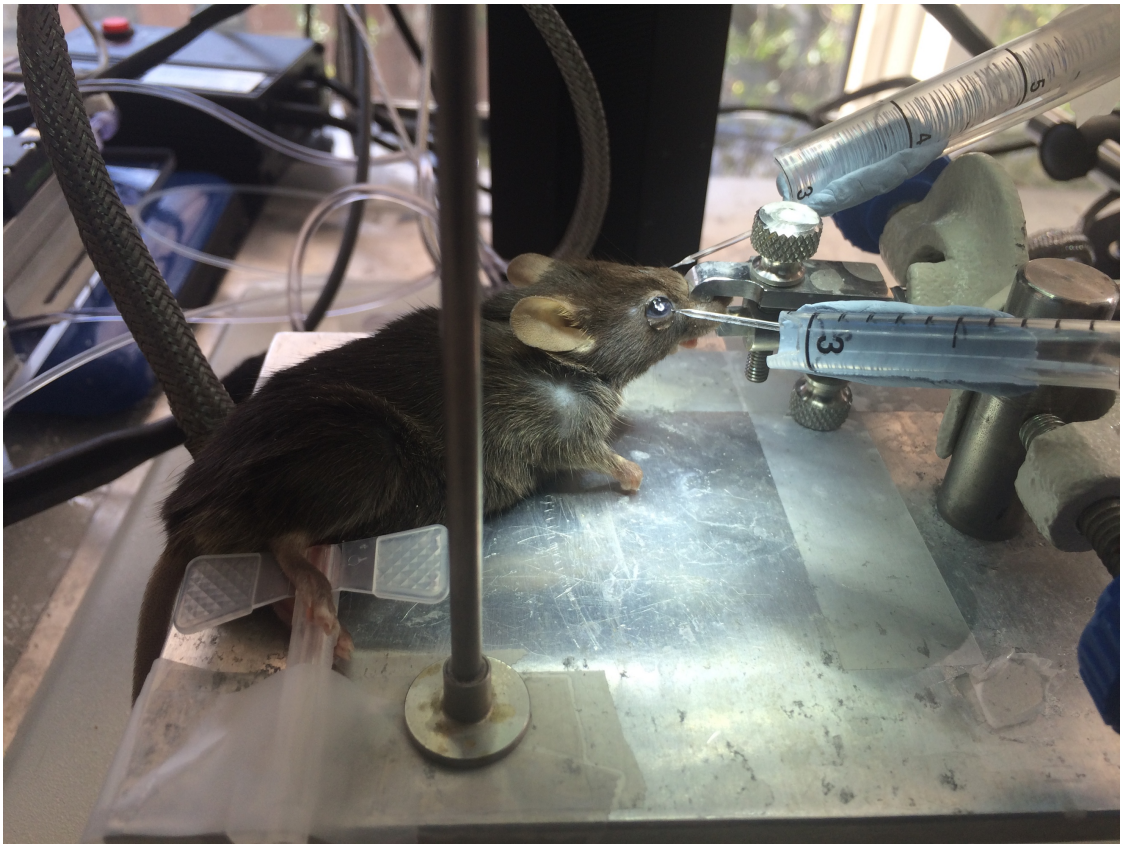

Figure 3.18: Murine *in vivo* spontaneous IOP and perfusion set up.

Demonstration of mouse in vivo spontaneous IOP and perfusion set up. Animals were anesthetized with intraperitoneal ketamine and xylazine, with re-dosing throughout experiment to maintain anesthesia, and mounted on a palate bar head holder on a heated platform, with temperature probe visible in foreground. Both eyes were cannulated with fluid filled pulled glass micropipettes attached to two independent iPerfusion systems, and eyes were covered with lubricant.

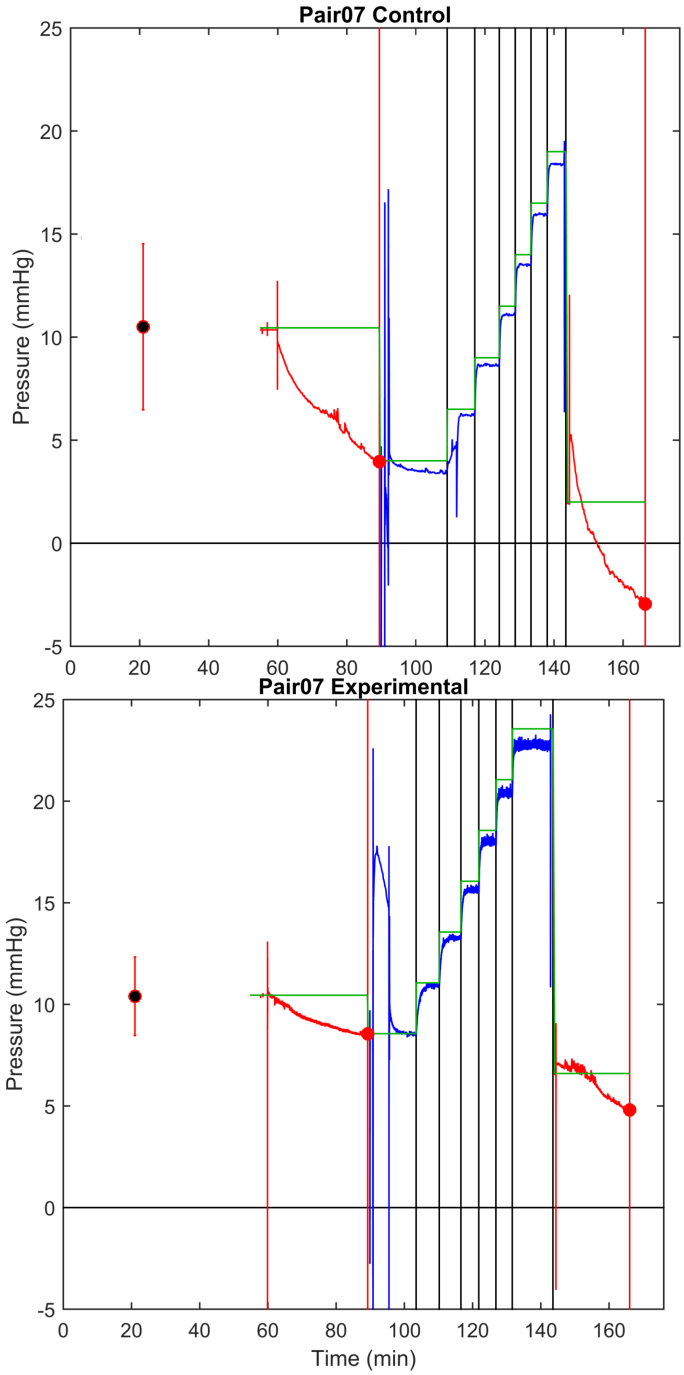

Figure 3.19: Representative pressure measurement data from mouse spontaneous IOP and *in vivo* perfusion.

Representative pressure data from a pair of contralateral control, 2 µg NT siRNA, and treated, 1 µg each ZO-1 and tricellulin siRNA, injected eyes. Black data points represents tonometric IOP measured to determine cannulation pressure, green line represents applied hydrostatic pressure during perfusion while blue line represents directly recorded pressure. Red line segments represent time of spontaneous IOP measurement before and after perfusion cycle, while red data points represent the point at which spontaneous IOP reached a steady state and pressure reading was taken.

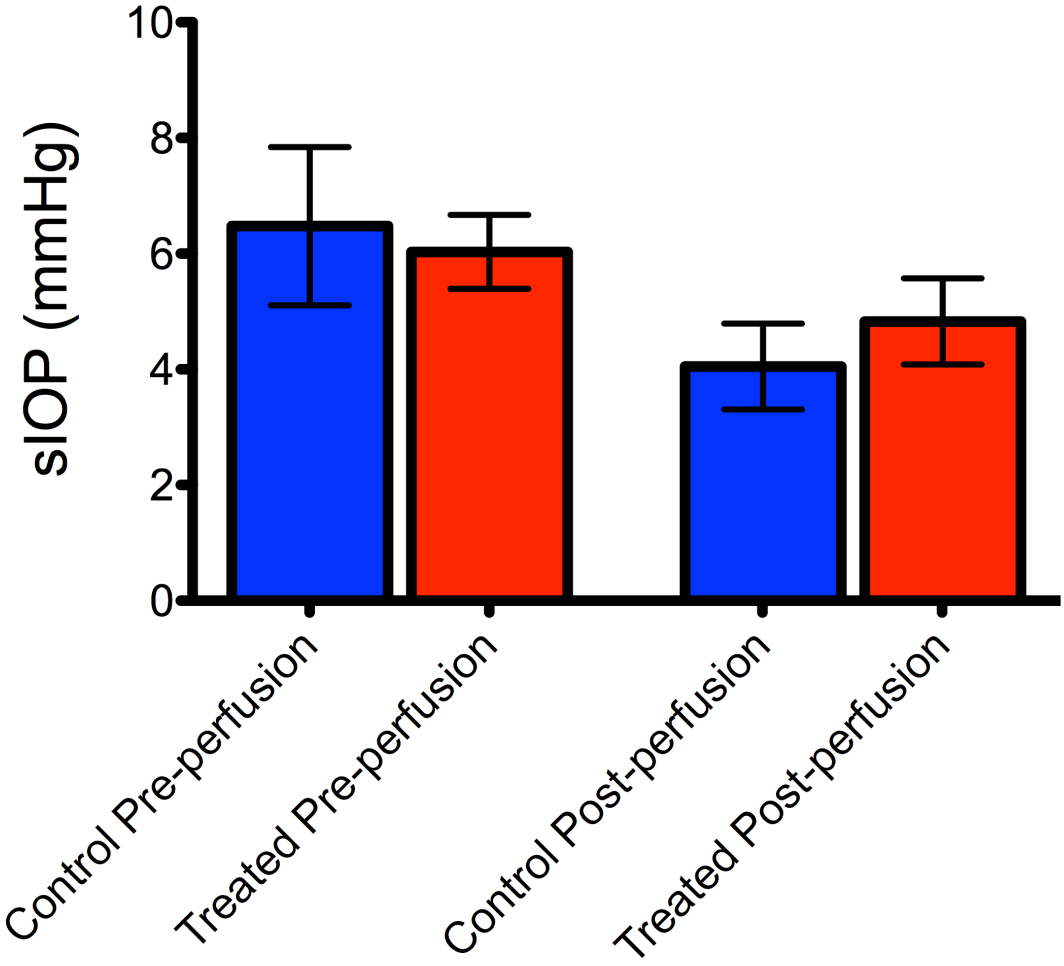

Figure 3.20: Spontaneous IOP measurement before and after *in vivo* murine perfusion.

Comparison of spontaneous IOP measurement between treated and control eyes before and after in vivo perfusion. No significant differences were detected between groups in pre-perfusion, p = 0.756, (N = 8 for control, 10 for treated), or post-perfusion sIOP, p = 0.477, (N = 6 for control, 7 for treated). Data represents mean ± s.e.m.

Discussion

A major aim of this research chapter was to establish appropriate means of measuring potential changes to conventional outflow in our model organisms, mouse and non-human primate. Initial attempts were to establish a pump based perfusion system as previously described in the literature (Boussommier-Calleja et al. 2012; Chang et al. 2015). Despite extensive efforts, data generated from this system was inconsistent, and did not agree with expected outflow facility values in untreated wildtype mice reported in the literature, with values of *C* consistently higher than 0.02 μL/min/mmHg recorded, while reported normal values ranged from 0.005 – 0.015 μL/min/mmHg. In order to more accurately and repeatedly measure *C* through perfusion studies, and through collaboration with the Overby lab in Imperial College London, investigations began involving in the early stage use of the novel *iPerfusion* system (Sherwood et al. 2016). This system, composed of a thermal flow sensor, an actuated pressure reservoir, a high-resolution differential pressure transducer and a temperature regulated bath that holds the *ex vivo* murine eye, the system yielded significant improvements in accuracy, repeatability and reliability over the previous perfusion system used. *In vivo* delivery of siRNA to murine anterior chambers was optimised to prevent ocular pathology post injection, thereby allowing the use of the system and experimental procedure together to assess the effect of our therapeutic approach of siRNA mediated downregulation of ZO-1 and tricellulin on conventional outflow facility.

Measurement of conventional outflow facility using *iPerfusion* and subsequent paired analysis showed that the downregulation of ZO-1 and tricellulin in the conventional outflow pathway led to a significant increase in outflow facility. This increase in the AH clearance capacity of the conventional outflow pathway would be expected to bring about a concurrent decrease in IOP. In order to assess if this was the case, a further cohort of mice was injected with same siRNA treatment, with tonometric IOP determine before treatment, and 48 hours post injection. This showed that, as expected, eyes injected with siRNA targeting ZO-1 and tricellulin and had significantly reduced IOP 48 hours after treatment as compared to those injected with NT siRNA. In order to show that the therapeutic approach here was effective in opening TJ clefts, and in the absence of *in vivo* downregulation data, a further cohort of mice was treated with siRNA as before, and eyes were prepared for TEM analysis. This analysis looked at

distinct regions of the SC inner wall and determined the number of open intercellular clefts between SC endothelial cells as well as the total number of clefts observed, and the percentage of open clefts was compared between eyes treated with ZO-1 and tricellulin siRNA and those treated with NT siRNA. These counts showed that there was a significant increase in open intercellular clefts in treated eyes as compared to control eyes, reinforcing the idea that siRNA mediated downregulation of these TJ protein components is increasing conventional outflow facility through opening of tight junctions and increasing AH flow across the paracellular route into SC lumen. Other studies that disrupt TJs of the SC endothelium in a non-specific manner, through the use of EDTA for example, show signs of pathology in SC inner wall (Bill et al. 1980; Hamanaka & Bill 1987), while eyes treated with siRNA here showed no signs of apoptosis, necrosis, or any pathology. Together these data represent successful demonstration of the potential of siRNA mediated downregulation of selected SC TJ components as a therapeutic to the treatment of primary open angle glaucoma through increase in outflow facility and decrease in IOP in mice.

As a follow on to this study, a similar approach was attempted in a non-human primate model, *Chlorocebus sabeus*, again with siRNA delivered intracamerally, but differing in that targets for downregulation were expanded to include claudin-11, detected in sectioned primate outflow tissue, as well as ZO-1 and tricellulin as used in mice. IOP was measured by rebound tonometry 48 hours after injection, and no significant difference in IOP was observed between treated and control eyes. *In vivo* perfusions were then carried out, with *iPerfusion* protocol adapted to include measurement of sIOP, with this reading used to calibrate the range of each perfusion cycle, as described above. Similar to the tonometric IOP data above, no effect of siRNA treatment on outflow facility was observed between paired treated and control primate eyes 48 hours after injection. After perfusion, animals were sacrificed and dissected outflow tissues were analysed to determine whether siRNA mediated downregulation of the selected targets had been effective. This analysis showed that downregulation was inconsistent between animals, with only a single animal having downregulation of all three targets, and significant upregulation of targets occurring in some animals after treatment. Reasons for these data may be related to tissue dissection, with protein analysis controlled by beta actin to ensure even loading of cell material, but not controlled specifically for amount of protein from our target tissues. It is important to note the shortcomings of assessing the effect of this treatment through protein levels

alone. While this method is expected to provide accurate measurements of the protein levels in assayed samples, it does not account for post –translational modifications of proteins that may influence their function, and no data on subcellular localisation of the target proteins is obtained. Additionally, as tissue is dissected prior to analysis, differences in dissection accuracy may give rise to variance between samples. Future studies should include immunohistochemical analysis to investigate any potential changes to protein localisation, and also directly assess the phosphorylation state of the target proteins. Another likely explanation for the lack of observed effect is that in mice, 1.5 μL of siRNA solution injected in to an approximately 2.5 μL volume anterior chamber, with paracentesis prior to injection to accommodate the injection volume, meaning the injected siRNA fills the anterior chamber and the majority of the outflow pathway is likely exposed to the injected siRNA. In primates, 20 μL of siRNA solution was injected in to an approximately 100 - 120 μL anterior chamber, with no paracentesis. Segmental outflow occurs in the anterior chamber of mammalian eyes, with regions of the conventional outflow pathway having high rates of AH clearance, while other regions carry little AH in to the SC lumen (de Kater et al. 1989). Additionally, regions of high flow have been shown to co-localise with increased density of open paracellular pores in SC inner wall (Braakman et al. 2015). It is therefore possible that, with lower relative injection volume in primates, the delivered siRNA failed to reach the entire circumference of the conventional outflow pathway, and instead passed through high flow regions of the pathway. These regions would be expected to have basal high density of open paracellular pores, and therefore siRNA would have the least potential effect on opening of pores. As delivery of siRNA to the target tissue is clearly an issue here, future primate investigations will involve the retro-perfusion of siRNA, fig 3.21. In this process, episcleral veins are occluded on the surface of the globe, causing them to engorge, and are then cannulated. The siRNA solution is then injected under pressure into these veins, where it travels upstream and through collector channels into the SC lumen, thereby reaching the full circumference of SC inner wall endothelial cells at their apical surface, negating the effect of segmental outflow on delivery.

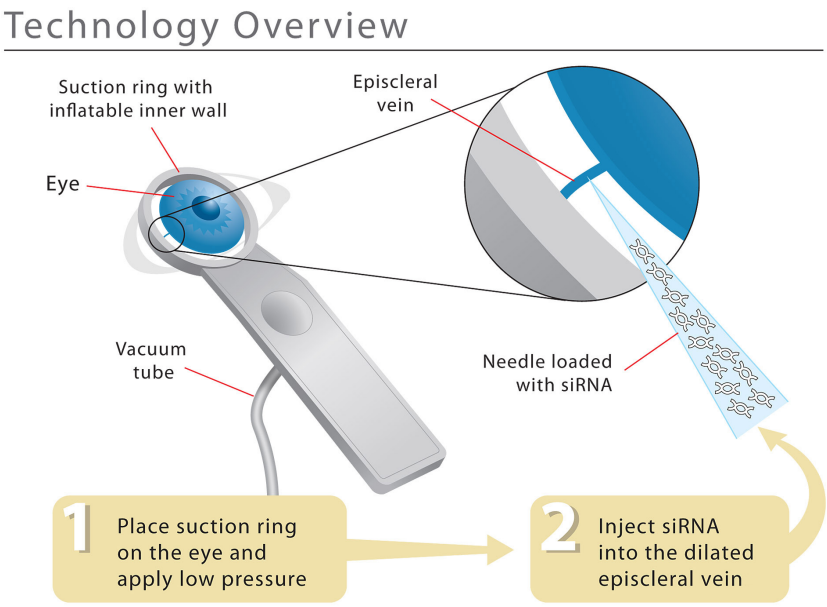

Figure 3.21: Episcleral delivery of siRNA.

Schematic of Retroject™ device for episcleral vein injection. Suction is applied by a vacuum ring at the limbus, and the device is inflated to occlude the episcleral veins. After veins become engorged, siRNA will be injected, travelling upstream to the SC lumen. Shown with permission from Retroject Inc.

A potential alternative future mechanism for delivery of siRNA to SC inner wall endothelial cells is the virally mediated expression of a short hairpin RNA (shRNA) in these cells. Such a system has been previously used to deliver shRNA targeting TJ components to the murine retina, with adeno-associated virus (AAV) used to transduce the target cells, while expression of the shRNA was controlled through the use of a doxycycline inducible promote (Campbell et al. 2011). AAV are the most widely used viral vector for human therapy today, having been used extensively in human gene therapy trials. While AAV serotypes do not appear to readily transduce the conventional outflow pathway, reports have shown that self-complementary AAV and AAVs with modified capsid proteins are capable of transducing the TM and SC inner wall (Buie et al. 2010; Wang et al. 2017). Alternatively, adenoviral vectors have also been shown to efficiently transduce the conventional outflow pathway, although these viruses hold less potential in human gene therapy due to potential immune response issues (Li et al. 2013). Implementation of such a system, whereby SC inner wall cells are transduced by intracamerally injected virus, would allow for the long-term expression of shRNA

necessary for therapeutic efficacy, rather than the transient downregulation demonstrated here, with scAAV reported to maintain expression for more than 2.3 years in primates (Buie et al. 2010). Additionally, use of an inducible promoter would allow for the topical administration of an inducer of viral expression, enabling controlled expression of shRNA, potentially in response to patients reaching a defined threshold of ocular hypertension, giving greater overall control of the therapies IOP lowering effects, and avoiding any potential hypotony.

Finally, a second measurement method for IOP was attempted *in vivo* in mice, through replication of the primate spontaneous IOP measurement process. This process was made difficult through instability of measured pressure data, and data obtained showed no significant difference between ZO-1 and tricellulin siRNA treated eyes and contralateral NT siRNA treated control eyes. The drastic reduction in IOP brought about by injectable anaesthesia here likely masked any IOP reducing effects of the siRNA treatment, with sIOP readings of approximately 6 mmHg obtained early in anaesthesia, while readings of 4 – 5 mmHg were seen later in the process. This contrasts from usual tonometric IOP readings obtained under isoflurane gas anaesthesia of 12 – 14 mmHg in untreated mice. Thus, this process was not suitable for measuring IOP lowering effects of novel therapeutic approaches.

While the data shown in this chapter is encouraging, a thorough investigation of potential side effects resulting from siRNA mediated downregulation of TJ proteins is essential to the further translation of this research to a therapy. As yet, data regarding changes in expression of other TJ components after downregulation has not been obtained. Additionally, the targeted TJ components are expressed in other AC tissues, such as the corneal endothelium and iris. EM data did not show any deleterious effects in these tissues, but a more thorough investigation in to off target effects is required. Although other lab members have demonstrated that outflow facility values return to normal levels several weeks after treatment in mice, the dynamics of this are yet to be characterised.

Statement on collaboration

Mouse siRNA perfusions and IOP measurements were carried out in collaboration with Dr. Ester Reina-Torres, Imperial College London and TCD. Primate perfusions were carried out with Dr. Joseph Sherwood, Imperial College London, at RxGen Inc., St. Kitts. After injection, EM imaging was carried out by Dr. Elke Lütjen-Drecoll at University of Erlangen-Nürnberg. Analysis of protein levels in primate tissue was carried out with Dr. Lawrence Tam, TCD.

Chapter 4: Investigation of a murine model of ocular hypertension

Introduction

In the previous chapter, the potential of the therapeutic downregulation of TJ components to treat elevated IOP in POAG was investigated in wildtype mice, showing an increase in conventional outflow facility and a decrease in IOP in these normotensive animals. In order to better characterise the efficacy of this treatment, it was desired to examine the effect of this same treatment in animals in a state of ocular hypertension, representing a better model of POAG. The proposed siRNA-based treatment functions to increase the permeability of the SC inner wall through destabilisation of TJ mediated paracellular clefts, leading to the opening of paracellular pores. It has been shown previously that, while transcellular pore density is unaffected by pressure, paracellular pores are responsive to pressure, with pore density increasing at the inner wall in a pressure dependent manner, implying a pressure driven mechanical opening of these pores (Ethier et al. 1998). It is therefore reasonable to infer that siRNA mediated downregulation of TJ components at the SC inner wall, shown in the previous chapter to increase the number of open clefts in normotensive mice, would have an even greater effect on the number of open pores in murine models of ocular hypertension.

Selecting a murine model of ocular hypertension

While there are many different murine model systems utilised in POAG research, it is important to carefully consider the suitability of different model systems to a particular approach. As glaucomatous optic neuropathy represents the primary concern in the development and progression of POAG, a significant proportion of murine models used in POAG research are concerned with retinal degeneration alone. While ocular hypertension is commonly used as a means to induce this degeneration, the means by which IOP is elevated is not of relevance to the study of optic neuropathy . As a result, the mechanisms by which ocular hypertension arises in these models does not well represent that seen in POAG, discounting the use of these models in investigations involving AH dynamics and modulation of the outflow pathways. For

this reason it was necessary to implement a murine model of ocular hypertension that occurred through increased resistance in the inner portion of the conventional outflow pathway, at the JCT or SC inner wall. While ocular hypertension induced retinal damage is clearly an important factor in POAG, for the purpose of the validation of this approach IOP reduction and conventional outflow facility increase were viewed as primary experimental goals, and glaucomatous optic neuropathy were not essential in the selected murine model.

The DBA/2J mouse

The DBA/2J strain of mouse represents a spontaneous genetic model of ocular hypertension and glaucomatous optic neuropathy (John et al. 1998). These mice exhibit significantly elevated IOP at around 6 - 8 months of age, with axonal loss in the optic nerve observed soon after the development of ocular hypertension, while RGC loss occurring in a retrograde fashion from the damaged ONH axons in the months following this (Libby et al. 2005; Schlamp et al. 2006). DBA/2J have homozygous mutations in two genes that are responsible for the observed IOP elevation, *Tyrp1*^{b}, a melanosomal structural protein, and *Gpnmb*^{R150X}, a transmembrane glycoprotein also expressed in melanosomes, the latter mutation being a premature stop codon, with DBA/2J mice homozygous for wildtype forms of these genes reported as having no glaucoma symptoms (Howell et al. 2007). Mechanistically, IOP is elevated through pigment dispersion from the iris into the AH, leading to the accumulation of pigment in the iridocorneal angle, blocking the outflow of AH. As such, these mice represent a model of pigmentary glaucoma. There is also evidence that pigment dispersion alone may not be the only factor in the development of glaucoma in these mice, as the replacement of DBA/2J bone marrow with that of mice with wildtype versions of the above genes also prevents disease development, indicating a systemic or immune role of these genes in neurodegeneration as well as a local role in IOP elevation (Anderson et al. 2005). As the increased resistance to AH outflow in these mice is caused by physical blocking of the outflow pathways they were not considered as a potential model.

Induced models of ocular hypertension

Aside from spontaneous mouse models of ocular hypertension, an elevation in IOP can be induced in mice through various means, all requiring an increase in the resistance to AH outflow. One approach to increasing this resistance involves targeting of the episcleral veins, these being the downstream drainage site of the conventional outflow pathway. Through occlusion of some of these veins, outflow resistance is increased by reducing the potential outflow routes for AH from the lumen of SC. This episcleral vein occlusion can be created through cauterisation, or laser photocoagulation (Ruiz-Ederra & Verkman 2006; Gross et al. 2003; Ji et al. 2005). Laser energy has also been used to induce ocular hypertension through applying burns directly to the trabecular meshwork (Aihara et al. 2003b). While these laser induced methods are effective in elevating IOP, as they take effect in the distal outflow regions of the conventional pathway, or in the case of TM burns, the outer regions of the TM, they do not well represent the increase in resistance at the JCT and SC inner wall as observed in POAG.

Elevated IOP can also be induced in mice through intracameral injection of 10 μM polystyrene microbeads. These beads accumulate at the iridocorneal angle in a manner similar to pigment particles in the DBA/2J mice, blocking the passage of AH in to the outflow pathways, thereby increasing outflow resistance (Chen et al. 2011). Greater increases in IOP and retinal damage are attained through the injection of a mixture of 6 μM and 1 μM microbeads, together with a viscoelastic binding material (Cone et al. 2012). As this process obstructs the passage of AH upstream of the site of therapeutic activity of the siRNA approach being assessed, these models were also not deemed suitable. A further mechanism to induce an elevation in murine IOP involves the placement of a circumlimbal suture, providing continuous inward pressure on the limbus (Liu et al. 2017). This likely causes IOP elevations through compression of the ciliary muscle, blocking the unconventional outflow pathway, and as such is an inadequate model of POAG.

Models of ocular hypertension with increased outflow resistance in the trabecular meshwork

Two mouse models of ocular hypertension exist that closely resemble the increase in ocular hypertension seen in human POAG, with the AH outflow resistance increase

occurring primarily in the JCT in both cases. The first of these models came arose from the study of a Mendelian form of human POAG, which arises from mutations in the myocilin gene (*MYOC*), previously known as trabecular meshwork induced glucocorticoid response gene (*TIGR*). While wildtype MYOC is secreted from TM cells, in its mutant forms it instead accumulates in the TM, with over 90 % of identified human mutations occurring in the olfactamedin domain, and being predicted to affect protein structure (Resch & Fautsch 2009; Jacobson et al. 2001). Expression of human mutant $MYOC^{Y437H}$, a mutation found in juvenile onset POAG patients, via an adenoviral vector transducing the iridocorneal angle was shown to cause ocular hypertension (Shepard et al. 2007). Subsequently, a transgenic mouse model was generated, *Tg*-$MYOC^{Y437H}$, which showed accumulation of the mutant protein in the TM, along with ocular hypertension, RGC loss, and axonal degeneration at the ONH. Ocular hypertension manifested in these animals from three months of age. Reduction of endoplasmic reticulum (ER) stress in the TM, through treatment with phenylbutyric acid, was associated with an amelioration of glaucomatous optic neuropathy, linking ER stress to disease pathology in human patients (Zode et al. 2011). These mice also exhibit reduced AH outflow facility, and abnormal intracellular accumulation of ECM components in the TM, while cultured TM cells expressing the mutant gene showed a reduction in active MMP-2 and MMP-9 (Kasetti et al. 2016). This murine model of ocular hypertension and POAG therefore represents an acceptable replication of the human condition.

The second murine model that has an IOP elevating site of action in the TM is the glucocorticoid induced ocular hypertension model. Glucocorticoids (GCs) are a widely prescribed class of steroids used in the treatment of inflammation and immune related disorders, which, while extremely effective, have significant ocular side effects, chief among these the elevation of IOP, leading to GC-induced glaucoma (Overby & Clark 2015). GC-induced glaucoma presents clinically in the same manner as POAG, with elevated IOP in patients with open iridocorneal angles, requiring a known patient history of GC use for diagnosis. While ocular hypertension desists after GC treatment is discontinued, any resultant glaucomatous optic neuropathy is irreversible. GC treatment does not give rise to ocular hypertension in all patients, with affected patients referred to as ‘steroid responders’, and from 11 – 79 % of patients in one meta-analysis shown to have elevated IOP after long-term intravitreal GC treatment, with differences based on specific GC type and dosage used (Kiddee et al. 2013). Another study reported

that 45 % of eyes receiving long term GC implantation treatment required surgical intervention to address the resultant GC-induced glaucoma (Bollinger et al. 2011). Analysis of post mortem human eyes diagnosed with GC-induced glaucoma showed an increased deposition of the ECM components collagen IV, heparan sulfate proteoglycan, and fibronectin in the JCT (Tawara et al. 2008). In perfused human organ culture, ECM accumulation is seen ultrastructurally in steroid responder eyes, with narrowing of intercellular spaces in the JCT, while non-responder eyes showed no change (Clark et al. 1995). GC treatment also modifies the cytoskeleton of TM cells, causing the formation of cross-linked actin networks (CLANs), potentially increasing resistance to outflow through alterations of the mechanical properties of these cells (Overby & Clark 2015). As is seen in humans, GC-induced hypertension also occurs in mice, with long-term subcutaneous delivery of dexamethasone (DEX) by osmotic mini-pump shown to elevate IOP significantly within 2 weeks of treatment, with a concomitant reduction in conventional outflow facility of 50 % (Whitlock et al. 2010; Darryl R. Overby, Bertrand, Tektas, Boussommier-Calleja, Schicht, Ross Ethier, Woodward, Daniel Stamer & Lütjen-Drecoll 2014). Mice treated with DEX are also known to have a similar increase in ECM deposition in the TM, with increased levels of collagen I, fibronectin, and α-smooth muscle actin reported (Patel et al. 2017). Also, of particular relevance to our TJ modulation based approach, GC treatment of cultured human SC endothelial cells has been shown to significantly increase ZO-1 expression, and to increase the number of TJ-containing intercellular contacts (Underwood et al. 1999). Murine GC-induced ocular hypertension therefore represents a further acceptable model of ocular hypertension caused by increased resistance to AH outflow in the JCT. As such, this model represents a suitable means to assess the modulation of outflow facility through the siRNA based approach previously described, acting as a model of POAG in general, and more specifically, of human GC-induced glaucoma.

While both of these models are suitable for evaluation of the effect of siRNA mediated downregulation of TJ transcripts on IOP and outflow facility in ocular hypertensive mice, for the purpose of this investigation, the murine GC-induced ocular hypertension model was used, as IOP elevation was seen in this model within 2 weeks in wildtype mice, while the use of $MYOC^{Y437H}$, which is in fact also being currently pursued, required first the establishment of an in-house breeding colony, followed by a delay of three months before animals are expected to show significant IOP increases.

Aims

The aims of this thesis research chapter were to implement a DEX induced murine model of ocular hypertension, and to investigate the effect of siRNA mediated downregulation of selected TJ proteins at SC inner wall on IOP and outflow facility in these hypertensive mice. This would enable analysis of whether higher IOP prior to siRNA treatment would result in a greater decrease in IOP and increase in outflow facility post-treatment, as would be expected by pressure driven opening of weakened paracellular pores at the inner wall of SC.

Results

Evolution of elevated intraocular pressure in dexamethasone treated mice

Wildtype C57BL/6J were implanted subcutaneously with osmotic mini-pumps delivering DEX at 2 different dosages, a low dose of 0.13 mg/kg/day (N = 6), and a high dose of 2 mg/kg/day (N = 14). Two mice in the high-dose treatment group were excluded from all analysis, one due to GC side effect related death, and the second due to congenital ocular malformation. A third mouse in this group was sacrificed prior to the final IOP measurement due to GC induced illness, but is included in the preceding IOP time points. IOP was measured by rebound tonometry in one eye and mice were weighed one day prior to pump implantation, and these measurements were repeated weekly thereafter for 4 weeks. Figure 4.1 shows the recorded IOP measurements for low dose and high dose DEX treated mice.

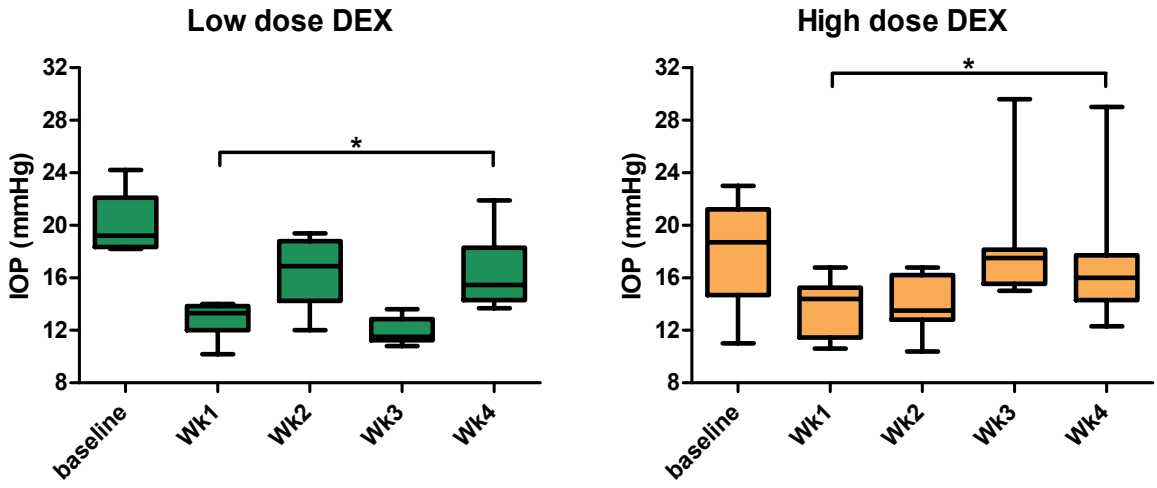

Figure 4.1: Evolution of intraocular pressure in dexamethasone treated mice

*Weekly IOP measurements in low dose (left) and high dose (right) DEX treated mice. Box plots represent 25th to 75th percentile, centre line of box plots represent the median IOP, while whiskers show the 5th and 95th percentile. * represents statistical significance ($p \leq 0.05$, t-test).*

As is clear from this figure, baseline IOP measurements prior to pump implantation are exceptionally high, with these high initial IOP values masking any ocular hypertension inducing effects of DEX treatment, potential causes of this are discussed further below. For the low dose group, baseline IOP was measured as 20.10 [17.65,

22.55] (mean [95% confidence interval]) mmHg (N = 6), while at week 4, the mean IOP for this group was 16.35 [13.24, 19.46] mmHg (N = 6). For the high dose treatment group, baseline IOP was recorded as 17.75 [15.34, 20.16] mmHg (N = 12), while at week 4 the mean IOP for the group was measured as 16.75 [13.74, 19.75] mmHg (N = 11). If the anomalous high baseline IOP readings are excluded from analysis, a significant increase in IOP is detected from week 1 to week 4 in both low dose and high dose treatment groups, fig. 4.1. The mean increase in IOP was 3.12 [6.18, 0.07] mmHg (p = 0.046) in the high dose treatment group and for the low dose group the mean increase was 3.48 [7.00, 0.03] mmHg (p = 0.05).

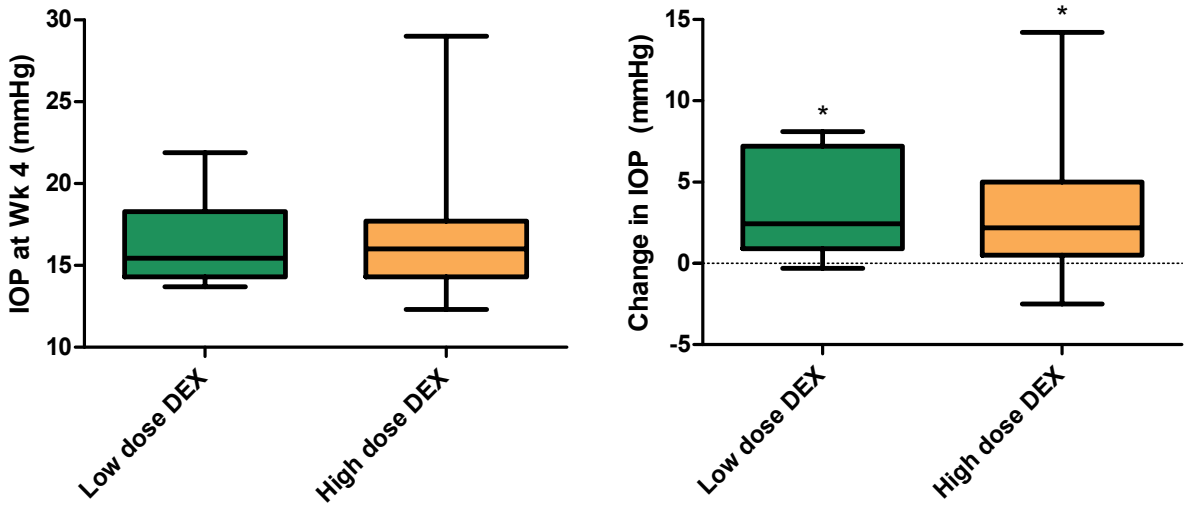

Figure 4.2: Intraocular pressure change in low dose and high dose dexamethasone treated mice.

*The final IOP readings for low dose and high dose DEX treated mice (left) showed no significant difference in IOP between dosage groups, while a significant increase in IOP from week 1 to week 4 was observed in both groups (right). Box plots represent 25th to 75th percentile, centre line of box plots represent the median IOP, while whiskers show the 5th and 95th percentile. * represents statistical significance from no change to IOP ($p \leq 0.05$, one sample t-test, theoretical mean of 0).*

Interestingly, when analysing IOP measurements in this manner, no significant difference was detected between the effects of low dose and high dose DEX in mean IOP at week 4, with a mean difference in IOP at week 4 between the two groups of 0.40 [-4.76, 3.97] mmHg, (p = 0.85, unpaired t test), fig. 4.2. Similarly, while both groups showed a significant increase in IOP from week 1 to week4, there was no difference in

the level of IOP elevation between groups 0.36 [-4.17, 4.88] mmHg (p = 0.87, unpaired t test). This is useful for future studies, as the lower DEX dosage is better tolerated by mice.

Potential reasons for high baseline IOP readings

High baseline IOP readings are a confounding factor in this analysis of DEX induced IOP elevation. It was noticed after DEX treatment had been completed that temperatures within the animal facility that housed these mice had been unstable during the course of the study, fig. 4.3. In order to determine whether these temperature fluctuations could have impacted tonometric IOP readings, all IOP measurements carried out on untreated wildtype mice were collated and analysed with respect to the average temperature recorded in the room these mice were housed in on the day of IOP measurement.

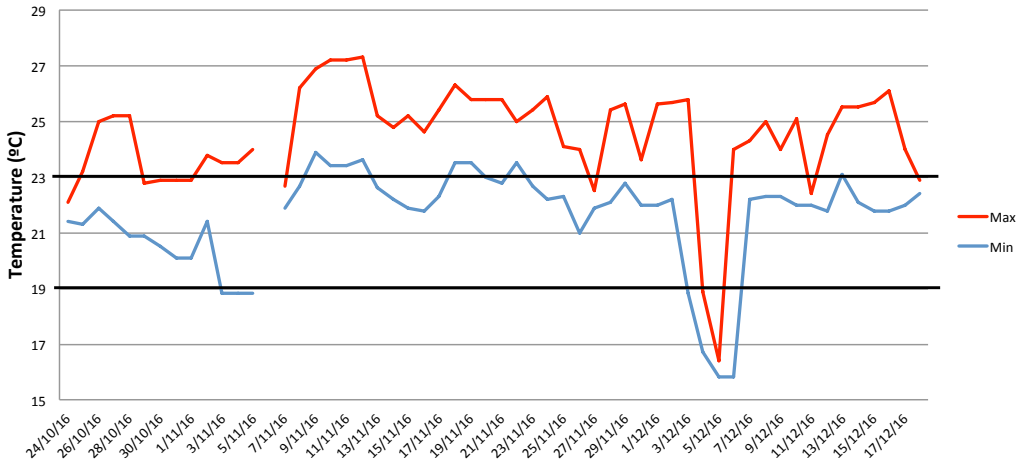

Figure 4.3: Temperature fluctuations in animal housing facility

This plot shows the maximum (red) and minimum (blue) temperatures recorded in the room where mice were housed over the duration of their housing for this study. Black line represent the recommend temperature range for the animal facility

This analysis showed a correlation between housing temperature and measured IOP, $R^2 = 0.461$, with higher IOP recorded at lower temperatures, fig 4.4. A similar effect was seen in pooled IOP measurements taken in all DEX treated animals, $R^2 = 0.479$, fig. 4.5. As baseline IOP measurements were obtained in early November, when housing temperature was notably lower than following weeks, this may account for observed differences between the baseline IOP readings and those measured in later in

the study. In addition to the effects of temperature fluctuation, it was also discovered that the cyclic lighting system in the animal facility had malfunctioned and lights had been on for 24 hours a day, as opposed to the usual 12/12 hour light/dark cycle. As IOP has a strong circadian component this likely also played a role in the IOP data reported.

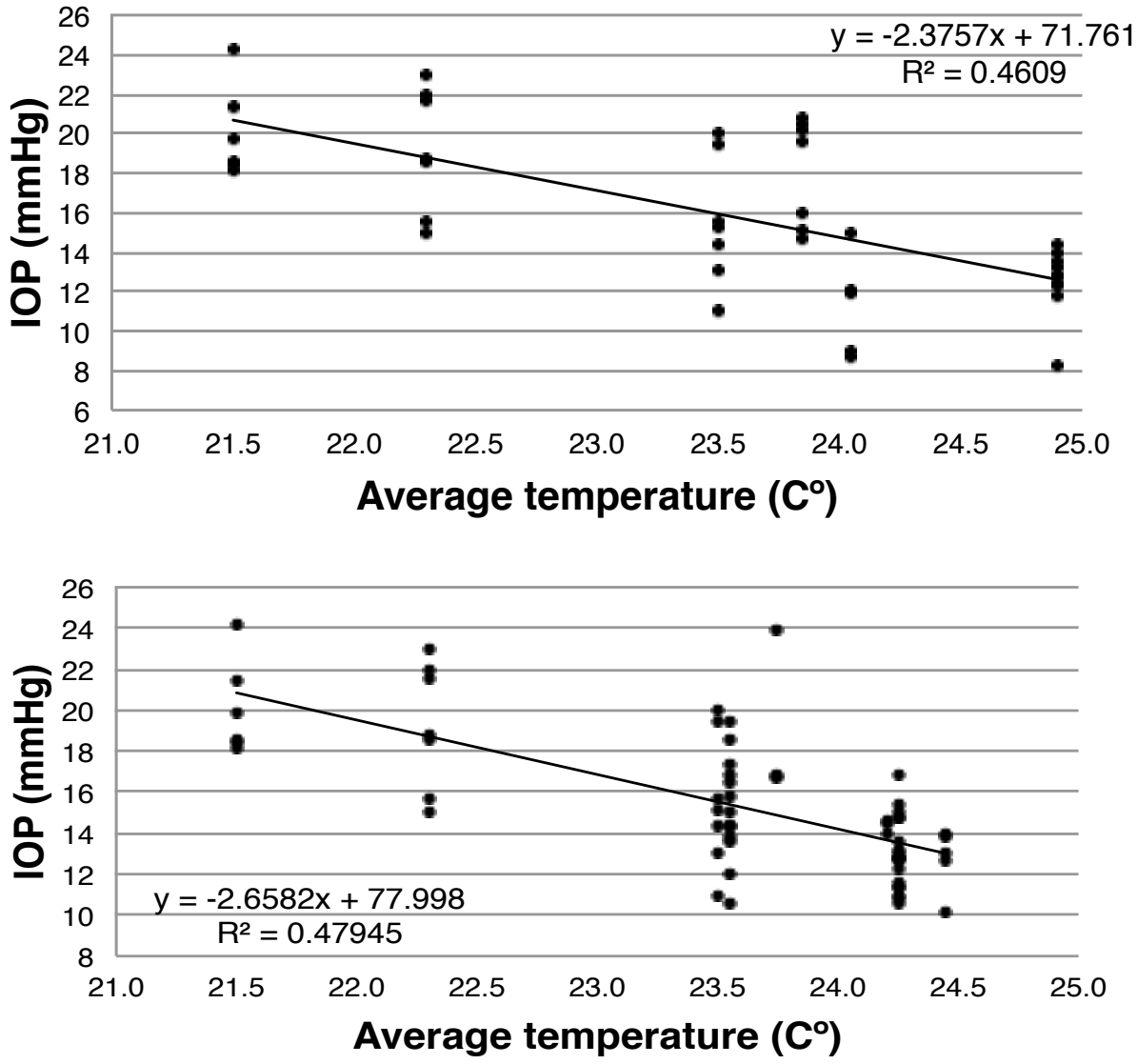

Figure 4.4: Correlation between intraocular pressure and temperature in untreated and dexamethasone treated mice

The recorded tonometric IOP from untreated wildtype mice(top), not included in this study, and DEX treated mice (bottom) is shown here against the average temperature in the room they were housed in on the day of IOP measurement ((Max + Min)/2).

Effect of siRNA treatment on intraocular pressure in dexamethasone treated mice

After DEX treatment, all mice were injected intracamerally with 1 μg each ZO-1 and tricellulin siRNA in one eye, while contralateral control eyes received NT siRNA injections, as in normotensive mice in chapter 3. At 48 hours post-injection, mice were anesthetised and IOP was measured again by rebound tonometry.

In low dose DEX treated mice, pre-injection IOP was measured as 16.45 [13.68, 19.22] mmHg, while at 48 hours it was 14.95 [10.06, 19.84] mmHg with no significant change in IOP detected, -1.5 [-6.13, 9.13] mmHg ($p = 0.635$, $N = 6$). For eyes injected with treatment siRNA, targeting ZO-1 and tricellulin, the mean IOP before the injection was 16.05 [13.21, 18.89] mmHg, while mean IOP at 48 hours was 13.55 [10.52, 16.58] mmHg, with no significant change in IOP detected again in this case, -2.50 [-2.50, 7.50] mmHg ($p = 0.255$, $N = 6$), fig. 4.5.

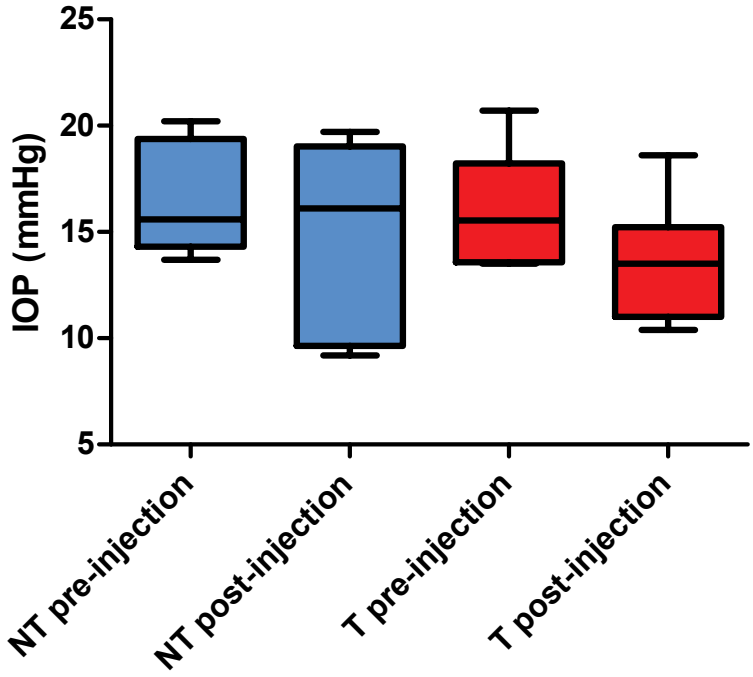

Figure 4.5: Effect of siRNA downregulation of ZO-1 and tricellulin on intraocular pressure in low dose dexamethasone treated mice.

This figure shows the IOP of low dose DEX treated mice before siRNA injection, and 48 hours after injection. Eyes receiving non-targeting (NT) siRNA injections are shown in blue, while eye injected with ZO-1 and tricellulin siRNA (T) are shown in red. Box plots represent 25th to 75th percentile, centre line of box plots represent the median IOP, while whiskers show the 5th and 95th percentile.

In high dose DEX treated mice, control eyes had a mean IOP before injection of 14.48 [11.81, 17.15] mmHg, which at 48 hours post-injection was measured as 13.10 [11.66, 14.54] mmHg, with no significant change in IOP detected, -1.38 [-0.73, 3.50] mmHg ($p = 0.174$, $N = 10$). For eyes injected with treatment siRNA, the mean IOP prior to injection was 14.17 [13.17, 15.17] mmHg, which was reduced to 12.11 [10.62, 13.60] mmHg after siRNA injection. This is a significant mean reduction of 2.06 [0.40, 3.72] mmHg ($p = 0.020$, $N = 10$), fig. 4.6.

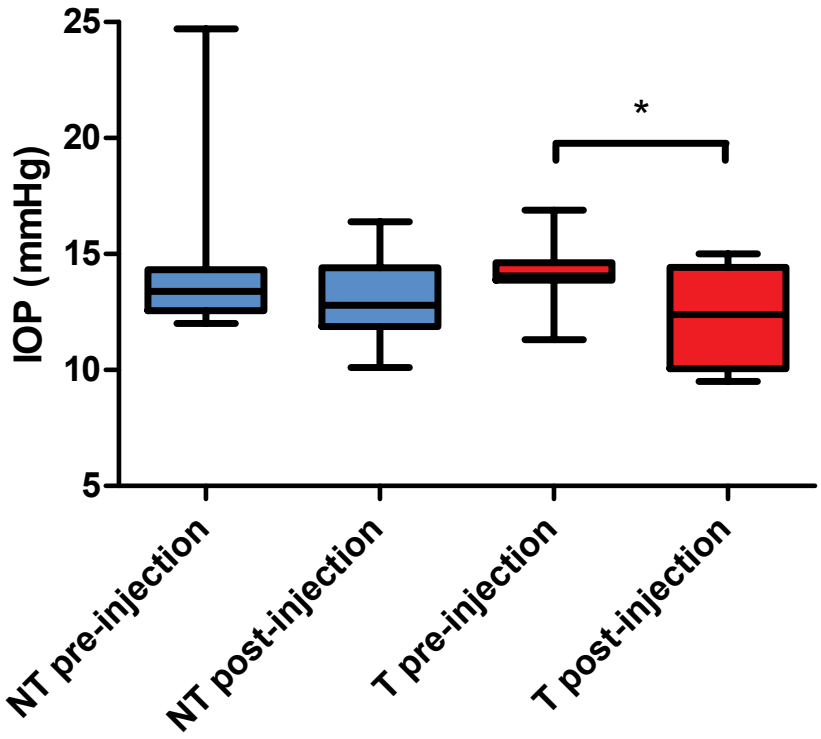

Figure 4.6: Effect of siRNA downregulation of ZO-1 and tricellulin on intraocular pressure in high dose dexamethasone treated mice.

*This figure shows the IOP of high dose DEX treated mice before siRNA injection, and 48 hours after injection. Eyes receiving non-targeting (NT) siRNA injections are shown in blue, while eye injected with ZO-1 and tricellulin siRNA (T) are shown in red. Box plots represent 25th to 75th percentile, centre line of box plots represent the median IOP, while whiskers show the 5th and 95th percentile. * represents statistically significant difference ($p = 0.020$, $N = 10$).*

As it was shown above that both high and low dose DEX treatment had the same effect on the level of IOP elevation from week 1 to week 4, and that no significant difference was present in mean IOP between the two treatment groups, the change in

IOP induced by ZO-1 and tricellulin siRNA was also analysed for both treatment groups together, fig. 4.7. This analysis showed that when all eyes are considered together, mean IOP in control eyes was 15.22 [13.40, 17.04] mmHg prior to injection and 13.79 [12.07, 15.52] mmHg 48h after injection, showing no significant change in IOP, -1.42 [-1.12, 3.97] mmHg (p = 0.25). For eyes injected with targeting siRNA, pre-injection mean IOP was measured as 14.88 [13.74, 16.01] mmHg and 48 hours post-injection, mean IOP was 12.65 [11.36, 13.94] mmHg, representing a significant reduction of 2.22 [0.47, 3.98] mmHg (p = 0.016).

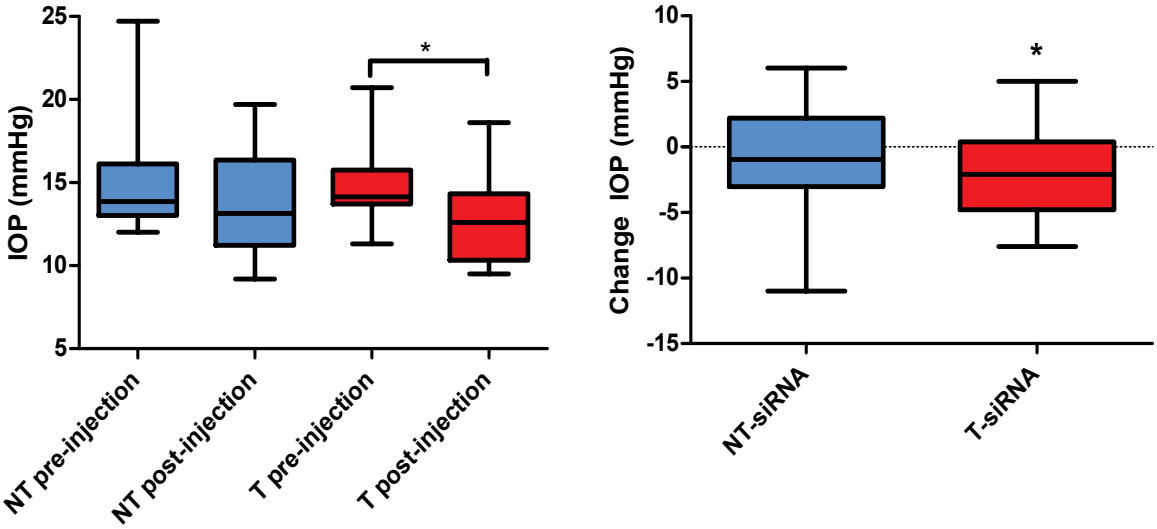

Figure 4.7: Effect of siRNA downregulation of ZO-1 and tricellulin on intraocular pressure in all dexamethasone treated mice.

*This figure shows the IOP of both low dose and high DEX treated mice before siRNA injection, and 48 hours after injection (left), and the change in IOP for each group (right). Data for eyes receiving non-targeting (NT) siRNA injections are shown in blue, while eyes injected with ZO-1 and tricellulin siRNA (T) are shown in red. Box plots represent 25th to 75th percentile, centre line of box plots represent the median IOP, while whiskers show the 5th and 95th percentile. * represents statistically significant difference (p = 0.016, N = 16).*

Effect of siRNA treatment on outflow facility in dexamethasone treated mice

Outflow facility (*C*) was assessed using the *iPerfusion* system in these same animals, in this case 72 hours after siRNA injection, with *C* compared between contralateral

control and treated *ex vivo* eyes, fig. 4.8. In low does DEX treated mice, a non-significant mean increase in *C* of 42 [-14, 136] % was observed (p = 0.12, N = 5 pairs). Similarly, in high dose DEX treated mice, no significant increase in *C* was measured, 39 [-9, 113] % (p = 0.10, N = 6 pairs). As it was demonstrated above that treating with either high or low DEX dosage had no significant effect on the level of IOP elevation, and no significant difference was detected in mean IOP between treatment groups, the facility data for both groups were analysed together. This analysis of all DEX treated animals showed a significant increase in *C* of 41 [9, 82] % (p = 0.015, N = 11 pairs) in treated eyes as compared to their contralateral controls.

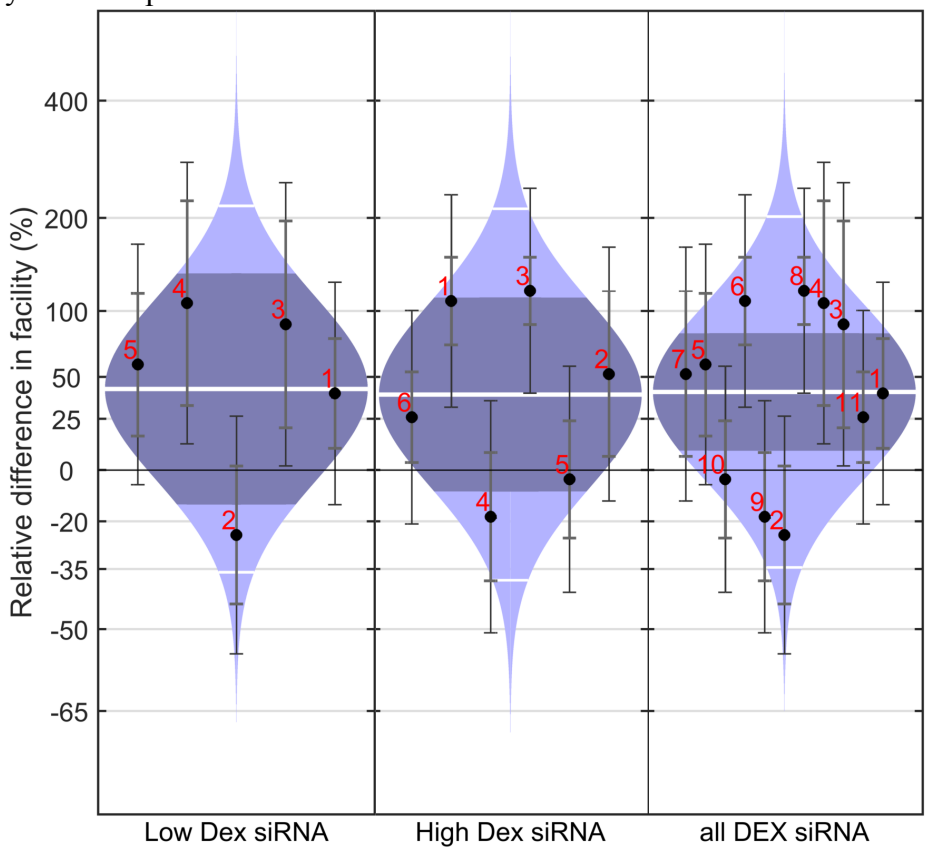

Figure 4.8: Effect of siRNA downregulation of ZO-1 and tricellulin on outflow facility in dexamethasone treated mice.

Cello plots showing the relative increase in C between paired control and treated contralateral eyes in mice receiving low dose (left) or high dose (middle) DEX, as well as combined data for both groups of DEX treated mice (right). Each data point is a pair of eyes, error bars represent one and two standard deviations. Shaded area shows predicted log normal distribution of data, white line represents mean, inner shading represents 95% CI of mean, while outer white lines represent two standard deviations from mean.

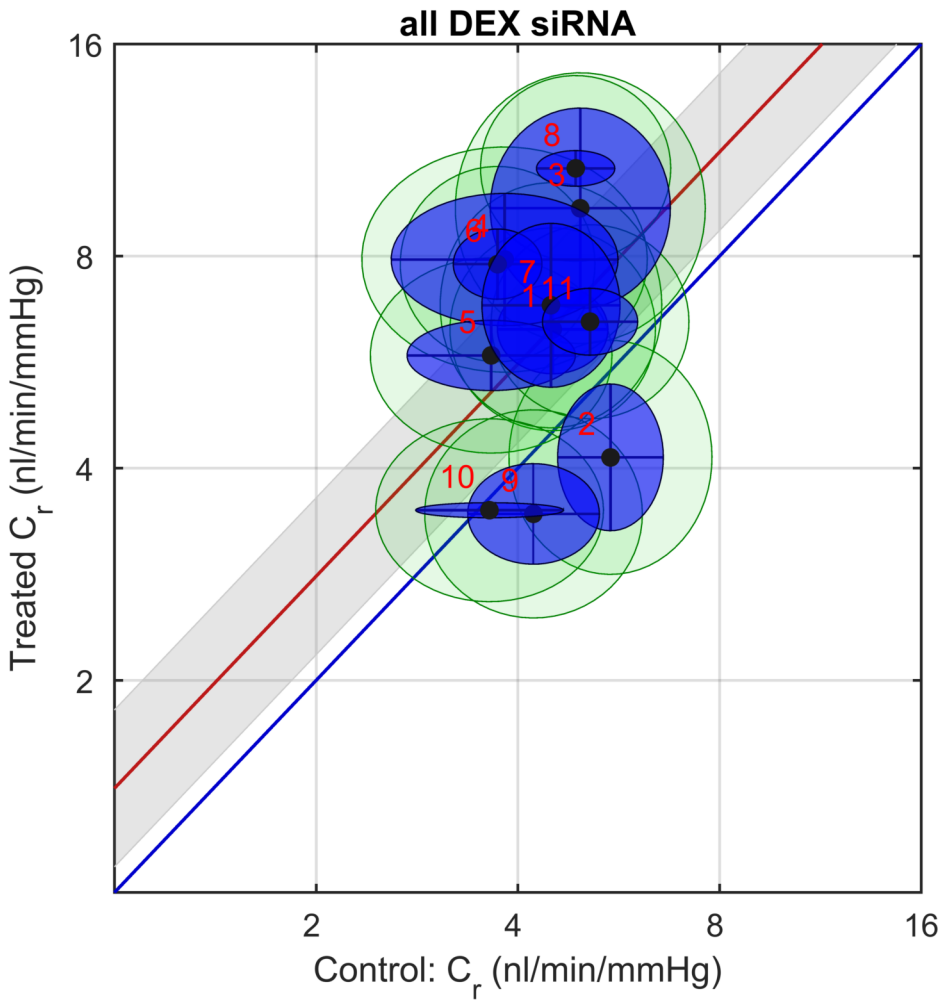

Figure 4.9: Effect of siRNA downregulation of ZO-1 and tricellulin on outflow facility in dexamethasone treated mice.

Paired facility plot showing the reference outflow facility at 8 mmHg (C_r) for all eyes included in this study. Each point represents a pair of eyes from one mouse, with C_r values for eyes receiving ZO-1 and tricellulin siRNA on the X-axis, and control eyes receiving NT siRNA on the Y-axis. The red line shows the average difference between contralateral eyes, with its confidence interval in grey, whilst the blue line represents the case of identical facility between contralateral eyes, corresponding to no effect due to siRNA. Inner blue ellipses show the 95% confidence intervals on C_r, whilst the green outer ellipses show additional uncertainty due variability between contralateral eyes, estimated from 10 pairs of C57BL/6J eyes perfused only with glucose supplemented PBS.

Discussion

The aim of this chapter was to assess the effect of siRNA targeting ZO-1 and tricellulin on IOP and outflow facility in a murine model of ocular hypertension. Anomalously high baseline IOP measurements in both low dose and high dose DEX treated mice made characterisation of the increase in IOP from prior to pump implantation to the end of the study difficult. However, if baseline measurements are excluded, significant increases in IOP were observed in both groups from one week to 4 weeks post DEX treatment.

IOP measurements for untreated wildtype C57BL/6J mice under isoflurane anaesthesia normally fall in the range of 12 – 14 mmHg, in our own recordings and in published reports (Ding et al. 2011). While it is not completely clear the reason for the high baseline IOP readings obtained, a correlation was shown between IOP and environmental housing temperature in both wildtype and DEX treated mice, with lower housing temperatures correlating with higher measured IOP. As the cornea is avascular and has a low metabolic rate, its temperature is heavily dependent on environmental temperature, with a linear relationship demonstrated between the two (Mapstone 1968; Kessel et al. 2010). Additionally, it has been reported that the corneas elastic potential energy is dependent on corneal temperature, with higher elastic potential energy occurring at lower corneal temperatures (Lucia et al. 2016). As IOP measurements in this study were obtained using a rebound tonometer, which involves the bouncing of a magnetized probe off the mouse's central cornea and measurement of the speed of its deflection, any increases in corneal elastic potential energy brought about by lower environmental temperature may indeed cause an artificial elevation of recorded IOP (Jorge et al. 2008). A further factor that made the interpretation of IOP data difficult was the discovery that light cycles within the animal housing facility had been disrupted, with mice housed under constant light conditions for at least some portions of the study. It is known that there is a strong circadian pattern of IOP, with lower IOP, 13.3 ± 1.3 mmHg, observed during the day and higher IOP observed in the late evening, 18.2 ± 1.6 mmHg, in mice housed in 12 hour light/dark cycles (Aihara et al. 2003c). When mice are exposed to constant light conditions, entrainment of this circadian pattern of IOP is lost, and mean IOP does not lower during the day , remaining constantly high, 19.2 ± 0.4 mmHg (Sugimoto et al. 2006). It is not known when or for how long this issue persisted during this study, so it is not possible to draw any

conclusions with regards to measured IOP data, however if constant light conditions occurred during baseline line IOP measurements, followed by restoration of a normal 12 hour light cycle, a similar effect on measured IOP would be expected. As a result of the above factors confounding baseline IOP measurements, it would be expected that actual IOP at baseline would be lower than week 1 measurements.

Despite these confounding factors in the analysis of IOP elevation, siRNA treatment was carried out as in normotensive mice. While no significant IOP reducing effect was detected in low dose DEX treated animals treated with ZO-1 and tricellulin siRNA, this was likely a result of the low sample size of this group rather than a lack of effect of treatment. High dose DEX treated mice showed a significant decrease in IOP in eyes injected with treatment siRNA over control siRNA injected eyes. The dosage level of DEX treatment was not observed to influence the level of increase in IOP, and there was no significant difference in pre-injection IOP between the two DEX treatment groups. As the effects of DEX treatment itself was not a concern, and ocular hypertension alone was of interest in this mouse model, both groups were analysed together with regards to the IOP lowering effect of ZO-1 and tricellulin siRNA. This again showed a significant reduction in IOP, in this case a reduction of 2.22 mmHg, closely matching the 2.3 mmHg reduction seen in normotensive mice in chapter 3. Ideally, it would be possible to detect a significant difference in mean IOP between control and treated eyes after injection as well as a significant decrease in IOP in treated eyes. IOP readings in control eyes injected with non-targeting siRNA, while not significantly reduced, do appear lower after injection, making detection of differences between the groups more difficult. This is likely due to subtle changes in the mechanical properties of the cornea induced by injection and possibly mild corneal scarring effecting tonometric IOP measurement. This could be avoided through use of a viral shRNA delivery system, as discussed in chapter 3, to allow greater time for corneal healing after injection and before the measurement of IOP.

The effect of siRNA treatment on conventional outflow facility was also assessed in these mice 72 hours after siRNA injection. While increases in *C* were not statistically significant when low dose and high dose DEX cohorts were analysed separately, when both cohorts were analysed together for the same reason as mentioned above, a significant increase in *C* of 41 % was detected in eyes injected with ZO-1 and tricellulin siRNA as compared to paired controls. While this is a more modest increase than was seen in normotensive mice in chapter 3, that being 113 %, the outflow facility

measurements here were carried out 72 hours post injection, while those in normotensive mice were carried out 48 hours post-injection. The peak of the treatment's IOP lowering effect was predicted from *in vitro* protein downregulation and permeability data to be at 48 hours, while at 72 hours some protein levels had begun to increase, see chapter 1, possibly explaining the observed difference.

A primary aim of this chapter was to determine whether destabilisation of the TJs of the murine SC inner wall, through the use of ZO-1 and tricellulin siRNA, would have a greater effect on IOP reduction and increase in outflow facility in a model of ocular hypertension than was observed in normotensive mice. While the above data do not support this hypothesis, they still demonstrate the efficacy of this approach, serving as a further demonstration of the potential of modulation of TJ expression in the conventional outflow pathway as a means to lower IOP and increase outflow facility. It has been reported that *in vitro* DEX treatment of SC cells results in an increased expression of ZO-1, and an 8-fold decrease in open paracellular clefts (Underwood et al. 1999). This has clear implications for IOP reduction and outflow facility increase with this siRNA therapy, as it indicates DEX treatment would have a stabilising effect on paracellular contacts at the SC inner wall, and would increase the expression of target proteins before siRNA injection.

It is also important to consider that, while DEX treated animals represent a model of ocular hypertension, and showed significant IOP increases from week 1 to week 4 in this study, the level of IOP increase was relative low, with pre-injection IOP being approximately 15 mmHg. As the hypothesised increase in effect of this treatment is based on pressure-driven opening of paracellular pores at destabilised TJs, it may be the case that this level of IOP increase is insufficient to observe this effect. The *Tg-MYOC*^{Y437H} mouse, of which a colony is currently being established for use in a follow up investigation, is reported to exhibit mean IOP measurements of approximately 18 mmHg at 8 months of age, which may allow for detection of a greater effect of siRNA treatment (Kasetti et al. 2016). Additionally, mice exhibit a circadian pattern of IOP, and both *Tg-MYOC*^{Y437H} and DEX treated mice are reported to have IOP of approximately 25 mmHg at night, (Zode et al. 2012; Patel et al. 2017). Measurement of the effect of siRNA treatment on night time IOP in these models may provide a means to better examine the differences in effect between normotensive and hypertensive mice.

Statement on collaboration

All work in this chapter was carried out in direct partnership with Dr. Ester Reina-Torres, Imperial College and TCD.

Chapter 5: The effect of IL-18 on Schlemm's canal endothelial permeability and conventional outflow facility

Introduction

Interleukin-18 (IL-18) is a cytokine in the IL-1 family of interleukins. This family of interleukins perform immune related functions in response to infection and sterile tissue damage. While sterile inflammation and increases in IL-18 expression have been reported in glaucoma animal models and human glaucoma patients, little is known of the effect of IL-18 on SC permeability and conventional outflow facility.

The innate immune system and sterile inflammation

The innate immune system, often referred to as the non-specific immune system, acts primarily as a first line of defence against pathogens in the human body. The innate immune system activates a generalised response upon the detection of pathogens in order to inhibit the spread of an infection. One of the primary generalised responses to the presence of a pathogen is induction of an inflammatory response, brought about by the release of cytokines and chemokines, which leads to the movement of blood derived fluids and proteins in to infected tissue. Pro-inflammatory chemokines also aid in the clearance of infection through recruitment of systemic immune cells from the blood into infected tissue to directly destroy the pathogen present. Additionally, inflammation increases the flow of lymphatic fluid from the affected tissue to nearby lymph nodes, where any pathogens or antigen presenting cells carried in the lymphatic fluid can more effectively activate the more specialised adaptive immune response (Murphy 2014). As the innate immune system is non-specific, in that it activates the same general response for all pathogens, it must be able to recognise a broad range of molecular signals carried by bacterial, viral and fungal pathogens, referred to as pathogen-associated molecular patterns (PAMPs), using a limited number of receptors called pattern-recognition receptors (PRRs). Toll-like receptors (TLRs) are the most well characterised PRRs, with ten human TLRs and 13 murine TLRs identified to date. These TLRs all share a similar structure, with a leucine-rich extracellular domain responsible for recognition of PAMPs, a transmembrane domain, and an intracellular domain that functions to

propagate downstream signalling. Upon binding of ligands to the extracellular domain, the intracellular domain becomes activated and recruits adapter proteins that activate a signalling cascade culminating in transcription of pro-inflammatory cytokines, interferons, and other innate immune response proteins (Doyle & O'Neill 2006).

While the innate immune system was first characterised as being involved in pathogen recognition alone, it has become clear that it can also initiate an inflammatory response in the absence of pathogens. This occurs through the ability of PRRs to also detect and respond to molecular patterns that are not of pathogenic origin, but rather, are endogenous intracellular molecules. Since this inflammation occurs in the absence of any infection, it is referred to as sterile inflammation. Under normal conditions, these molecules cannot induce an inflammatory response, due to their intracellular sequestration, but when cells undergo necrosis or otherwise lose plasma membrane integrity, the molecules are released and can bind to cell surface PRRs (Rock et al. 2010; Chen & Nuñez 2010). For this reason these molecules are referred to as damage associated molecular patterns, (DAMPs). Additionally, intracellular reserves of pro-inflammatory cytokines can be liberated from necrotic cells, further initiating sterile inflammation (Cayrol & Girard 2009). TLRs are primarily mediators of the innate immune response to PAMPs, and while they do exhibit some DAMP recognition activity, another group of intracellular PRRs called NOD-like receptors (NLRs) have a significant role in DAMP perception during sterile inflammation. NLRs are characterised by having a central nucleotide binding NACHT domain, flanked by a C-terminal region containing leucine rich repeats (LRR), and usually a pyrin domain (PYD) at the N-terminus. In humans, 23 NLR genes have been identified, while 34 murine NLR genes have been reported (Schroder & Tschopp 2010). Components of the innate immune system appear to hold an important role in neural inflammation following glaucomatous optic neuropathy (Soto & Howell 2014).

The NLRP3 inflammasome

An inflammasome is a multi-unit protein complex that is activated in response to various stimuli, leading to the downstream maturation of pro-inflammatory cytokines to their bioactive forms. Several inflammasomes have been identified which become activated in response to different ligands, with the NLRP3 inflammasome being responsible for promoting inflammation in response to sterile cellular damage. The

NLRP3 inflammasome consists of three different proteins, NLRP3, an NLR family PRR, apoptosis-associated speck-like protein containing a caspase recruitment domain (ASC), an adapter protein with PYD and a caspase recruitment domain (CARD), and pro-caspase-1, an inactive cysteine protease, also containing a CARD. Upon activation of NLRP3, individual NLRP3 subunits oligomerise at their NACHT domains, which causes PYD domain clustering. These clustered PYD domains induce the recruitment of ASC through homotypic PYD domain interaction. Upon ASC binding to the NLRP3 PYD domain, pro-caspase-1 is recruited to the inflammasome through CARD-CARD interaction with ASC. This recruitment causes clustering of pro-caspase-1, allowing for auto-cleavage of the protease to its bioactive form, caspase-1, (Schroder & Tschopp 2010; Davis et al. 2011). Active caspase-1 forms a tetrameric complex that functions to cleave pro-IL-1β and pro-IL-18 to their respective mature forms.

The activation of this innate immune sterile inflammatory response is a two-step process with the first step referred to as priming, whereby DAMPs are recognised by TLRs, leading to nuclear factor kappa B (NF-κB) signalling. This signalling leads to upregulation of NLRP3, and pro-IL-1β and pro-IL-18, necessary for inflammasome formation and inflammation (Shao et al. 2015). The second step is the activation of the inflammasome itself through NLRP3 activation and oligomerisation. The precise mechanism of NLRP3 activation by DAMPs is not yet known. NLRP3 is an intracellular protein so cannot interact directly with extracellular DAMPs that result from sterile cell damage. As such, an indirect activation must be occurring, with three main models for this activation process having been proposed. The first model states that extracellular ATP, released from necrotic cells, can bind to a purinergic receptor named P2X7, stimulating the opening of an ATP gated channel leading to an efflux of K^+ ions (Kahlenberg & Dubyak 2004). This cationic efflux has been reported to stimulate the opening of Pannexin-1 plasma membrane pore (Kanneganti et al. 2007) The opening of this pore could facilitate the entry of extracellular DAMPs into the cytosol of the cell, allowing NLRP3 activation. Activation of NLRP3 is unlikely to occur through direct interaction of the DAMPs with NLRP3, due to the diverse structure of DAMPs capable of NLRP3 activation, making activation through interaction with upstream signalling molecules more reasonable (Schroder & Tschopp 2010). Activation could also occur through an as yet unknown mechanism in this model, such as direct NLRP3 activation due to cellular K+ depletion. Evidence for this model comes

from the inhibition of NLRP3 activation by high extracellular levels of K+ (Chen & Nuñez 2010). According to the second model, DAMPs cause the generation of reactive oxygen species (ROS), which then interact through a common pathway which brings about the formation of the NLRP3 inflammasome. All major NLRP3 activating DAMPs have been reported to induce the production of ROS, however, some ROS inducing cytokines do not activate NLRP3, indicating that while ROS is necessary for inflammasome formation, it is not necessarily capable of doing this alone (Schroder & Tschopp 2010). The third model states that crystalline or particulate DAMPs are phagocytosed by cells, after which they cause lysosomal damage. This damage allows the leakage of cathepsin B, a lysosomal protease, into the cytosol, where it then activates a direct ligand of NLRP3. Inhibition of cathepsin B has been reported to prevent inflammasome activation in response to DAMPs, supporting this model (Shao et al. 2015). However, mice deficient in cathepsin B can still form functional NLRP3 inflammasomes, so it is not clear the extent to which cathepsin B or other lysosomal components are involved in this process, (Schroder and Tschopp, 2010, Davis et al., 2011). The most likely explanation is that none of these three models are independently responsible for NLRP3 inflammasome activation, and their combined activity may represent a mechanism by which NLRP3 can be activated by a diverse range of DAMPs, fig 5.1.

Interleukin-18

IL-18 is a member of the IL-1 family of cytokines, containing 11 different related interleukins which have primary roles in mediating inflammatory response to infection and sterile insult (Lukens et al. 2012). IL-18 is expressed in an inactive form, as 24 kDA pro-IL-18, and must be cleaved by caspase-1 after NLRP3 inflammasome activation to its active 17 kDa form. Pro-IL-18 can also be activated through non-canonical caspase-8 based inflammasome formation (Gringhuis et al. 2012). Following cleavage, mature IL-18 is secreted from cells (Dinarello et al. 2013). Pro-IL-18 is constitutively expressed in macrophages, dendritic cells, and endothelial cells, amongst other cell types. Upon secretion, IL-18 induces interferon-γ production from natural killer (NK) cells, along with activation and recruitment of inflammatory immune cells such as macrophages and neutrophils (Lukens et al. 2012). IL-18 signalling occurs

through the binding of IL-18 to cell surface IL-18 receptor alpha (IL-18Rα), followed by the recruitment of IL-18 receptor beta (IL-18Rβ), forming a heterotrimer which activates the respective Toll-IL-1 receptor (TIR) domains of IL-18Rα and IL-18Rβ, promoting downstream NF-κB signalling (Dinarello et al. 2013). Both IL-18 and IL-18 receptors have been shown to be expressed in vascular endothelial cells (Gerdes et al. 2002). IL-18 induces an inflammatory response upon IL-18 receptor signalling, causing increases in cellular adhesion molecules, nitric oxide synthesis, and chemokine production (Dinarello et al. 2013). Secreted IL-18 is activity is inhibited by a soluble protein known as IL-18 binding protein (IL-18bp), present in serum at a 20-fold higher concentration than IL-18,which may function to prevent aberrant over-activity of IL-18 (Novick et al. 1999; Novick et al. 2001). IL-18bp expression is driven by interferon-γ, representing a negative feedback loop for IL-18 activity (Dinarello et al. 2013).

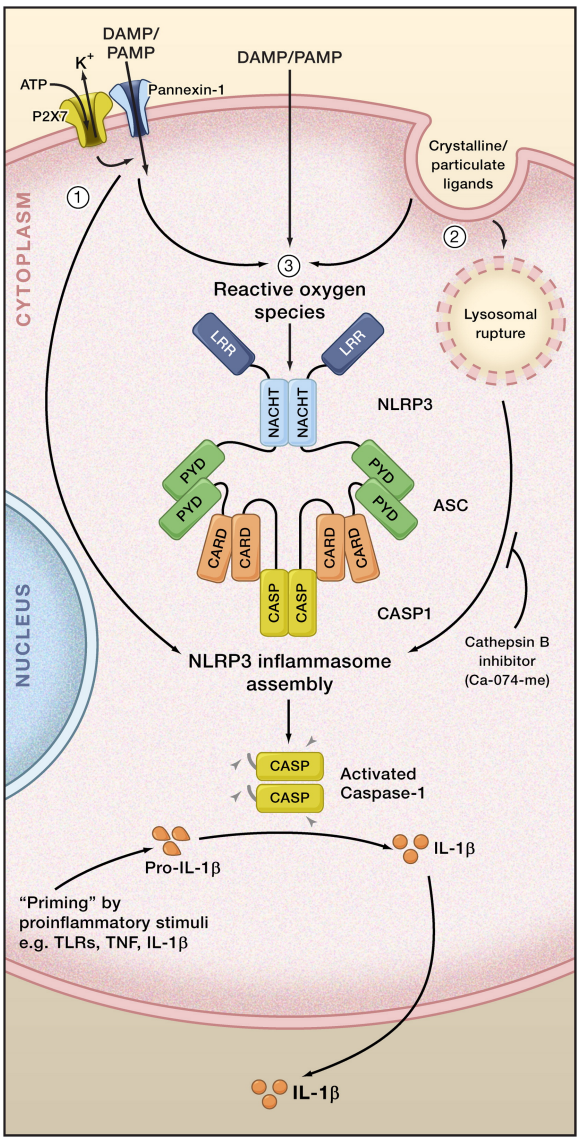

Figure 5.1: Activation of the NLRP3 inflammasome.

This figure shows the three proposed models for the activation of the NLRP3 inflammasome, being 1. Extracellular ATP, 2. Phagocytosis of NLRP3 agonists, and 3. ROS generation by DAMPs. These triggers lead to NLRP3 dimerisation, and inflammasome assemble, activating caspase-1 which in turn activates IL-1beta and IL-18.

Sterile inflammation and primary open-angle glaucoma

Glaucomatous optic neuropathy is typified by damage to the RGC layer and its afferent ONH axons, primarily brought about by elevated IOP, thus representing sterile damage to the retina. DAMP release is thought to occur as a result of this damage, with elevated levels of intracellular heat shock proteins reported in glaucomatous retinas, and in response to elevated IOP (Soto & Howell 2014). Similarly, tenascin-C, a DAMP that activates TLR4 signalling, is reported to be expressed by astrocytes in the ONH of POAG patients (Pena et al. 1999). Transcriptional profiling studies have also shown upregulation of genes involved in inflammatory pathways, including TLRs, downstream signalling adapters, and pro-inflammatory cytokines in human glaucomatous retinas (Luo et al. 2010; Yang et al. 2011). Oxidative stress, resulting in ROS generation, also occurs under glaucomatous hypoxic conditions in the retina, leading to further inflammasome activation (Vohra et al. 2013). In animal models of glaucoma, similar inflammatory gene expression is observed. Models of mechanically induced acute RGC axonal damage show NLRP3 upregulation in retinal microglia, leading to NLRP3 inflammasome assembly and caspase-1 activation, along with upregulation of IL-18 at the ONH (Puyang et al. 2016; Menge et al. 2001). In the DBA/2J mouse model of glaucoma, IL-18 is reported to be highly upregulated in the retina and AH in parallel with progressive optic neuropathy (Zhou et al. 2005; Zhou et al. 2009). Thus, it is clear that glaucomatous optic neuropathy results in the induction of a sterile inflammatory response in the eye.

Potential relevance of interleukin-18 to outflow facility

IL-1 family cytokines have long been known to have an effect on the paracellular permeability of endothelial and epithelial cells, with IL-1α and IL-1β both reported to increase permeability through suppression of expression of the TJ protein occludin (Capaldo & Nusrat 2010). IL-18 has also been reported to downregulate TJ proteins, namely claudins and occludin in different cell types (Yang et al. 2015; Lapointe & Buret 2012). Contrastingly, IL-18 has also been reported to reduce vascular endothelial permeability in models of choroidal neovascularisation (Doyle et al. 2014). Investigations in to anti-VEGF based therapies showed that suppression of VEGF

activity brought about a significant increase in IL-18 expression, and that IL-18 reduced vascular permeability through increasing expression of claudin-5 in TJs of vascular endothelial cells at the iBRB (Shen et al. 2014). Anti-VEGF therapy has been shown to reduce outflow facility in AMD patients, and VEGF itself has been shown to increase outflow facility through increasing permeability of the SC inner wall (Reina-Torres et al. 2017; Wen et al. 2017). Additionally, IL-18 is known to induce the synthesis of nitric oxide (NO), while NO has been shown to increase outflow facility in mice (Bogdan 2001; Chang et al. 2015). It is clear that the effect of IL-18 on TJ expression permeability is dependent on cell type. As yet, the effect of IL-18 on SC inner wall permeability has not been studied, but it is likely that through TJ modulation or induction of NO synthesis, a modulation of outflow facility would occur.

Aims

As is clear, sterile inflammation is induced in the retina in response to glaucomatous optic neuropathy, with NLRP3 activation and IL-18 expression seen in the retina and AH of mouse models of glaucoma. Il-18 is also know to influence TJ protein expression and endothelial permeability in different cell types. The aim of this research chapter was to assess the effect of IL-18 on SC endothelial cells, through investigation of changes to their *in vitro* permeability to ions and macromolecules, as well as their TJ protein expression. In addition, the *in vivo* effect of IL-18 on conventional outflow facility was to be investigated.

Results

Effect of interleukin-18 on Schlemm's canal endothelial paracellular permeability

As it was an objective to evaluate the effects of IL-18 on the paracellular permeability of inner wall of SC, primary human SCECs were cultured on permeable transwell membranes, and subsequently treated with recombinant human IL-18 at a range of concentrations. After 24 hours of IL-18 treatment, the paracellular permeability of the monolayer to ions was determined by measuring transendothelial electrical resistance (TEER), fig. 5.1. This measurement showed that IL-18 brought about a significant increase in resistance to paracellular ion flux at 50 ng/ml of 22.7 (3.5, 41.9) %, (mean (95% confidence interval)), $p < 0.05$, and at 100 ng/ml of 41.6 (21.3, 62) %, $p < 0.0001$, as compared to untreated cells (N = 5 untreated, 4 treated, ANOVA with Tukey's post-test).

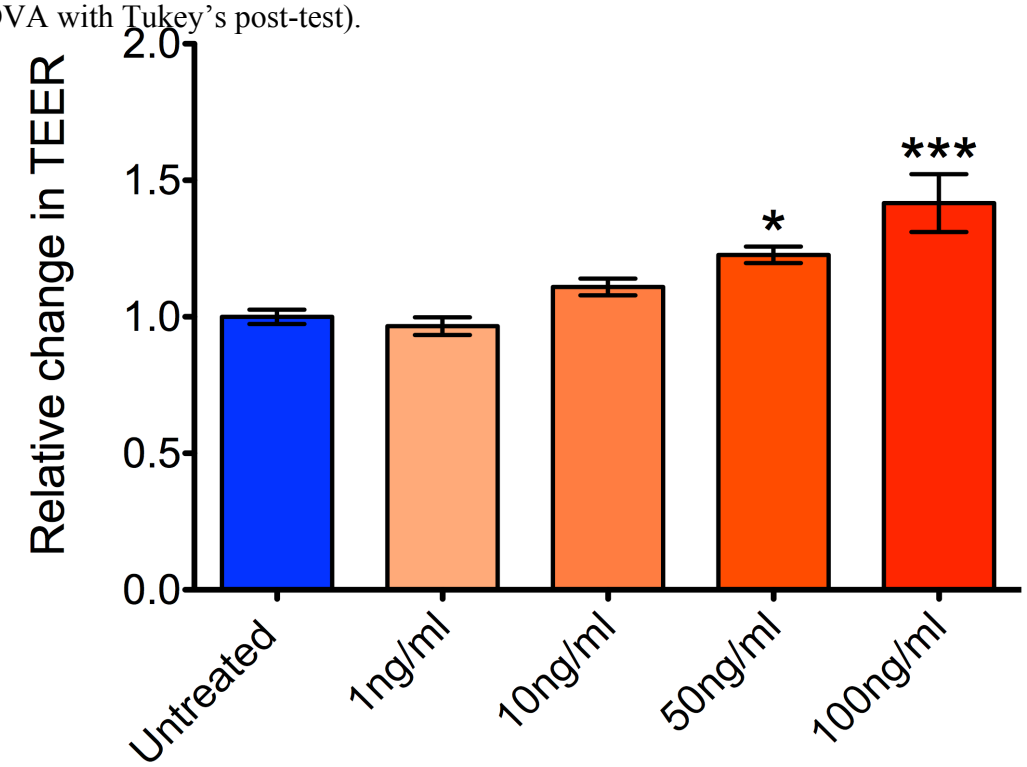

Figure 5.2: Transendothelial electrical resistance of IL-18 treated primary human Schlemm's canal endothelial cells.

*Primary human SCEC were grown on transwell membranes to confluency, before being treated for 24 hours with recombinant human IL-18 diluted in cell culture media at a range of concentrations, or with cell culture media alone. Data represents mean ± s.e.m., relative to untreated, N= 5 for untreated, N = 4 for all treatment concentrations, one way ANOVA with Tukey's post-test, *p < 0.05, ***p < 0.0001.*

As well as assessing the effect of IL-18 on paracellular permeability to ions through TEER measurements, its effect on paracellular transport of larger macromolecules was also assessed. This was carried out through measurement of the basal to apical flux of fluorescein isothiocyanate (FITC) labeled 70 kDa dextran protein across cultured primary human SCEC grown on permeable transwell membranes, as above, carried out 24 hours after treatment with recombinant human IL-18, fig. 5.2. This showed that IL-18 had a similar paracellular permeability reducing effect to larger molecules. At a concentration of 1 ng/ml, apparent permeability coeffficient, P_{app}, was reduced by $1.951x10^{-9}$ ($1.524x10^{-9}$, $2.37x10^{-9}$) cm/s, $p < 0.0001$, at 10 ng/ml it was reduced by $2.711x10^{-9}$ ($2.283x10^{-9}$, $3.13x10^{-9}$) cm/s, $p < 0.0001$, while at 50 ng/ml it was reduced by $8.027x10^{-10}$ ($3.998x10^{-10}$, $1.206x10^{-9}$) cm/s , $p < 0.0001$. Interestingly, this flux assay did not show a decrease in permeability at 100 ng/ml.

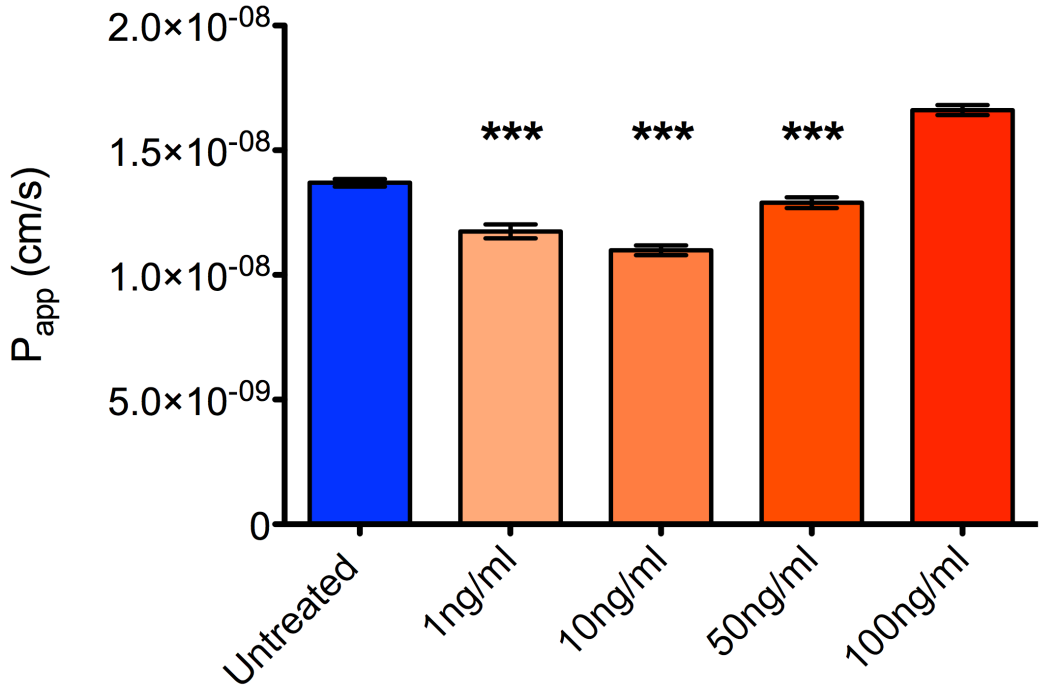

Figure 5.3: 70 kDa FITC-dextran flux assay of IL-18 treated primary human Schlemm's canal endothelial cells.

*Primary human SCEC were grown on transwell membranes to confluence, before being treated for 24 hours with recombinant human IL-18 diluted in cell culture media at a range of concentrations, or with cell culture media alone. Media was replaced flux of 70 kDa from basal to apical chambers was measured over 120 minutes. N= 5 for untreated, N = 4 for all treatment concentrations, one way ANOVA with Tukey's post-test, ***p < 0.0001.*

Effect of interleukin-18 on Schlemm's canal endothelial cell viability

In order to determine if treatment with Il-18 had a cytotoxic effect at these concentrations, and therefore a possible effect on paracellular permeability, an *in vitro* MTS cell viability assay was performed, with cultured primary human SCEC treated with recombinant IL-18 at the same concentrations as used in the above permeability assays. This assay showed that cells retained 90% viability up to a concentration of 92 ng/ml, N= 8, fig. 5.3. This result precludes the use of data on IL-18 induced alteration of paracellular permeability at 100 ng/ml above, but reinforces the validity of the data generated at lower concentrations.

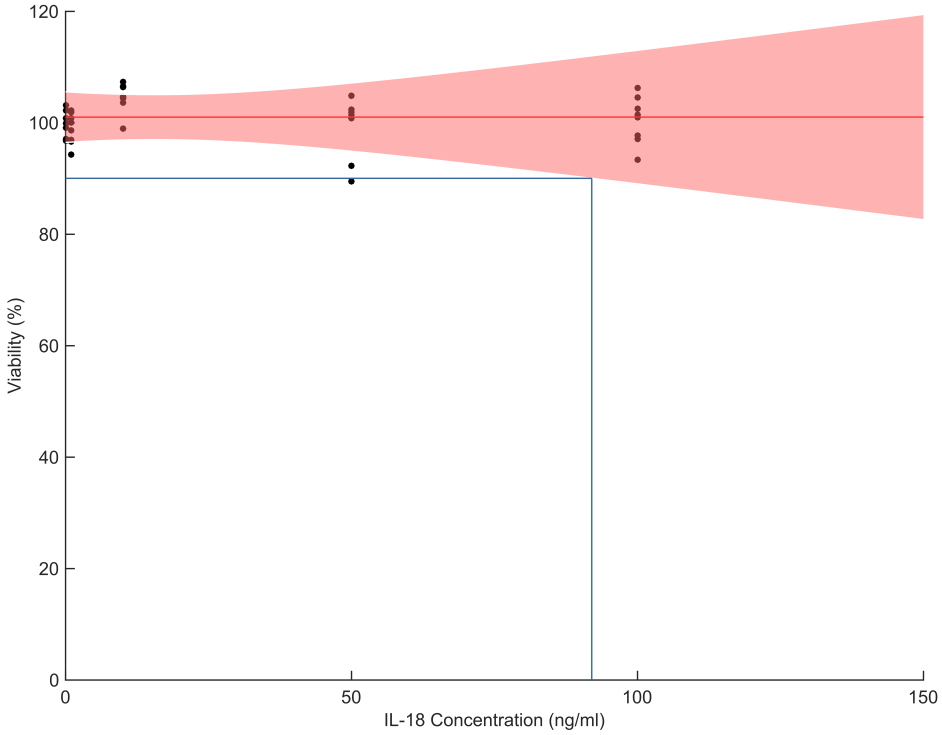

Figure 5.4: Viability of IL-18 treated primary human Schlemm's canal endothelial cells.

Primary human SCEC were grown in a 96-well plate to confluence, before being treated for 24 hours with recombinant human IL-18 diluted in cell culture media at a range of concentrations, or with cell culture media alone. Cell viability was maintained above 90% for all concentrations up to 92 ng/ml.

Effect of interleukin-18 on Schlemm's canal endothelial cell tight junction expression

In order to determine whether the paracellular permeability reducing effect of IL-18 on human SCEC was related to TJ expression in these cells, cells were grown to confluency and treated with recombinant human IL-18 at a range of doses for 24 hours, then lysed, with protein isolated and analysed by western blot. This showed that for ZO-1, no significant change to protein levels were induced by IL-18 treatment at 1, 10, or 50 ng/ml (N = 4, one sample t-test), fig. 5.4.

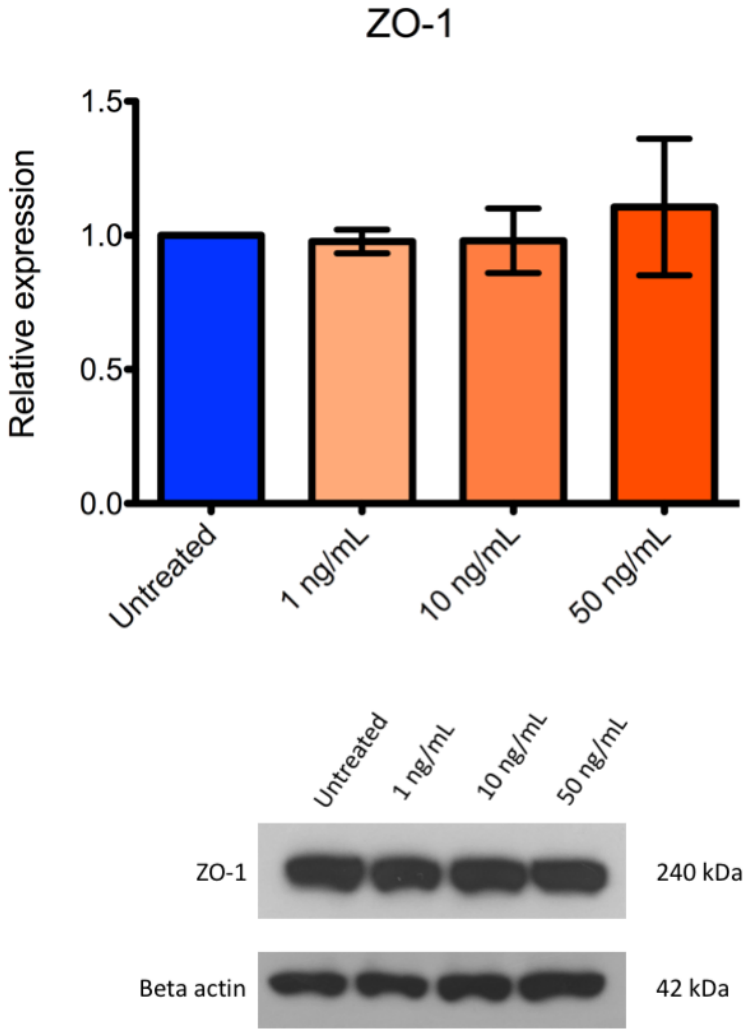

Figure 5.5: Effect of interleukin-18 on ZO-1 expression in cultured human Schlemm's canal endothelial cells.

Densitometric analysis of ZO-1 protein expression level (top), controlled to the house keeping gene β-actin, relative to mean untreated expression level (N = 4), with a representative western blot included (bottom).

Similarly, the expression level of the TJ protein tricellulin was also assessed in response to recombinant IL-18 treatment in human SCEC, fig. 5.5. This revealed a significant increase in tricellulin protein levels in cells treated with IL-18 at 10 ng/ml, p = 0.0195, and 50 ng/ml, p = 0.0076, (N = 3, one sample t-test)

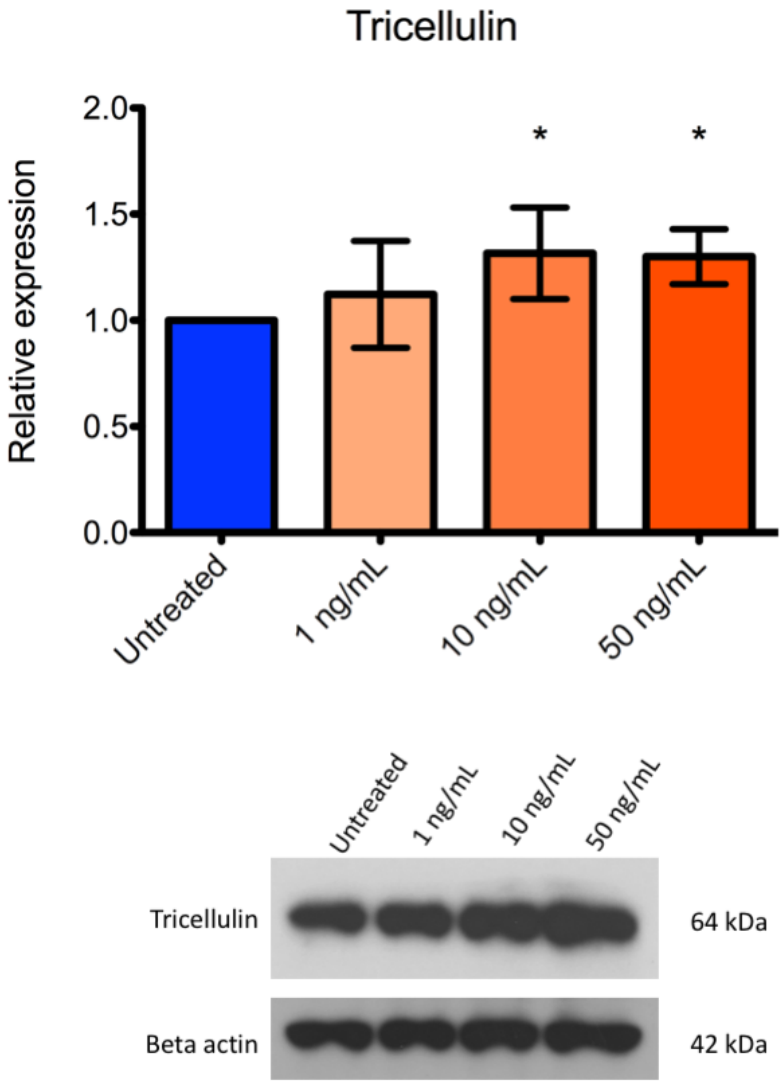

Figure 5.6: Effect of interleukin-18 on tricellulin expression in cultured human Schlemm's canal endothelial cells.

*Densitometric analysis of tricellulin protein expression level (top), controlled to the house keeping gene β-actin, relative to mean untreated expression level (N = 3), with a representative western blot included (bottom). * denotes statistical significance, p < 0.05, one sample t-test.*

Effect of interleukin-18 on conventional outflow facility

As the above data had determined that IL-18 had the effect of significantly reducing paracellular permeability to both ions and macromolecules at 50 ng/ml, the *in vivo* effect of recombinant IL-18 at this concentration was assessed. Recombinant mouse IL-18 was injected intracamerally in one eye of wild type C57BL/6J mice, while the contralateral eyes received a vehicle injection. At 48 hours post-injection, eyes were enucleated and immediately perfused in pairs to determine *ex vivo* conventional outflow facility at 8mmHg, C_r, using *iPerfusion*. Briefly, *iPerfusion* measures flow rates in to cannulated *ex vivo* murine eyes, maintained in a temperature controlled bath, over a range of applied pressure steps, with treated eyes compared to vehicle injected eyes. Figure 5.6 shows that IL-18 treated eyes had an average reduction in C_r of 34 (10, 52) % as compared to contralateral control eyes ($p = 0.0162$, $N = 10$ pairs). These data thus reinforces the *in vitro* data above, showing that reductions in *in vitro* permeability of human SCEC are mirrored by reduction in the *ex vivo* hydraulic conductivity of the conventional outflow pathway.

Conventional outflow facility in knockout mice deficient in active interleukin-18

As it had been demonstrated that *in vivo* injected exogenous IL-18 reduced conventional outflow facility in *ex vivo* murine eyes, the influence of endogenous IL-18 on the regulation of outflow facility was also investigated. This was carried out initially through investigation of the basal conventional outflow facility in untreated $ASC^{-/-}$ C57BL/6J mice, which, due to knockout of the ASC gene, could not undergo NLRP3 inflammasome assembly, and therefore were unable to process the inactive pro-IL-18 or pro-IL-1β to their mature, bioactive forms. These mice therefore would be lacking any conventional outflow facility modulating effects of active IL-18 or IL-1β. As above, C_r was determined using *iPerfusion* in *ex vivo* eyes from these mice, and due to paired analysis of eyes not being possible in knockout animals, unpaired analysis was carried out, comparing conventional outflow facility in $ASC^{-/-}$ eyes to a reference population of wild type C57BL/6J mice, fig. 5.7. This unpaired analysis showed that $ASC^{-/-}$ had 40 (8, 82) % higher C_r than wild type controls ($p = 0.0148$, $N = 11$ for $ASC^{-/-}$, $N = 14$ for wild type).

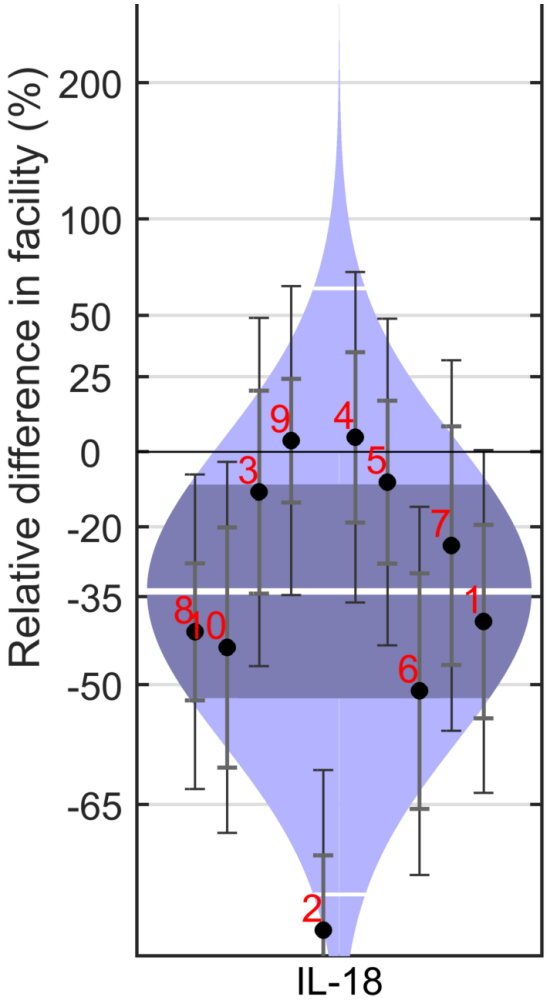

Figure 5.7: Cello plot of effect of intracameral injection of 50 ng/ml IL-18 on conventional outflow facility.

Wild type C57BL/6J mice were intracamerally injected with 50 ng/ml recombinant mouse IL-18 in one eye, with contralateral vehicle injections. 48 hours post-injection conventional outflow facility was measured using iPerfusion and treated eyes were shown to have an average reduction in C_r of 34 (10, 52) % ($p = 0.0162$, $N = 10$ pairs). Each data point represents a pair of eyes, error bars represent one and two standard deviations. Shaded area represents predicted log normal distribution of data, middle white line represents mean, inner shading represents 95% CI of mean, while outer white lines represent two standard deviations from mean.

This observed increase in conventional outflow facility could be attributed to the absence of both mature Il-18 and mature IL-1β, so in order to better characterise the effects of endogenous IL-18 alone, similar measurements were carried out using IL-18$^{-/-}$ mice. In these animals, rather than inability to convert pro-IL-18 to its bioactive

state, IL-18 is not expressed in any form. Figure 5.8 shows that measurements of IL-18$^{-/-}$ C_r using *iPerfusion* revealed the same mean reduction as seen above, with IL-18$^{-/-}$ mice also showing a 40 (5, 86) % increase in facility over wild type controls (p = 0.0215, N = 16 for IL-18$^{-/-}$, N = 14 for wild type).

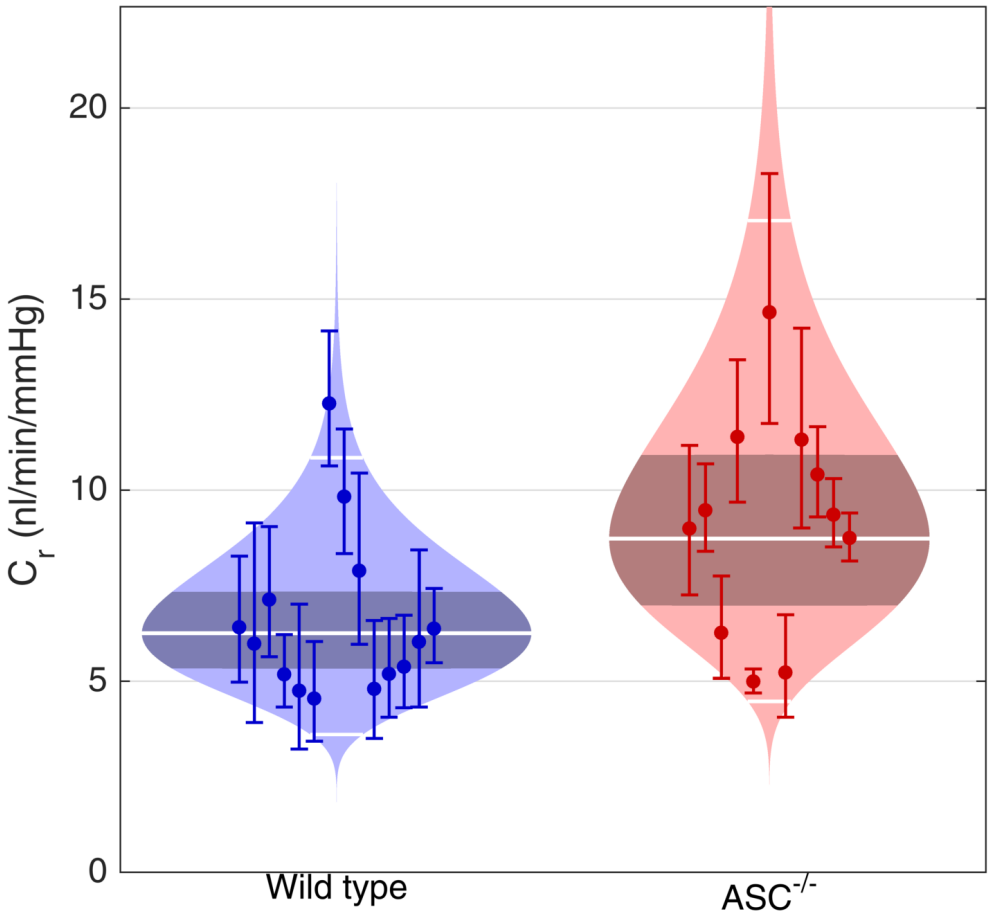

Figure 5.8: Cello plot of conventional outflow facility comparison between wild type and ASC$^{-/-}$ mice.

Cello plot of distribution of data for C_r of wild type and ASC$^{-/-}$ C57BL/6J ex vivo murine eyes. Each data point represents a single eye, error bars represent 95% CI. Shaded area represents predicted log normal distribution of data, middle white line represents mean, inner dark shading represents 95% CI of mean, while outer white lines represent two standard deviations from mean. ASC$^{-/-}$ had 40 (8, 82) % higher C_r, mean = 8.73 mmHg, than wild type controls, mean = 6.26 mmHg (p = 0.0148, N = 11 for ASC$^{-/-}$, N = 14 for wild type).

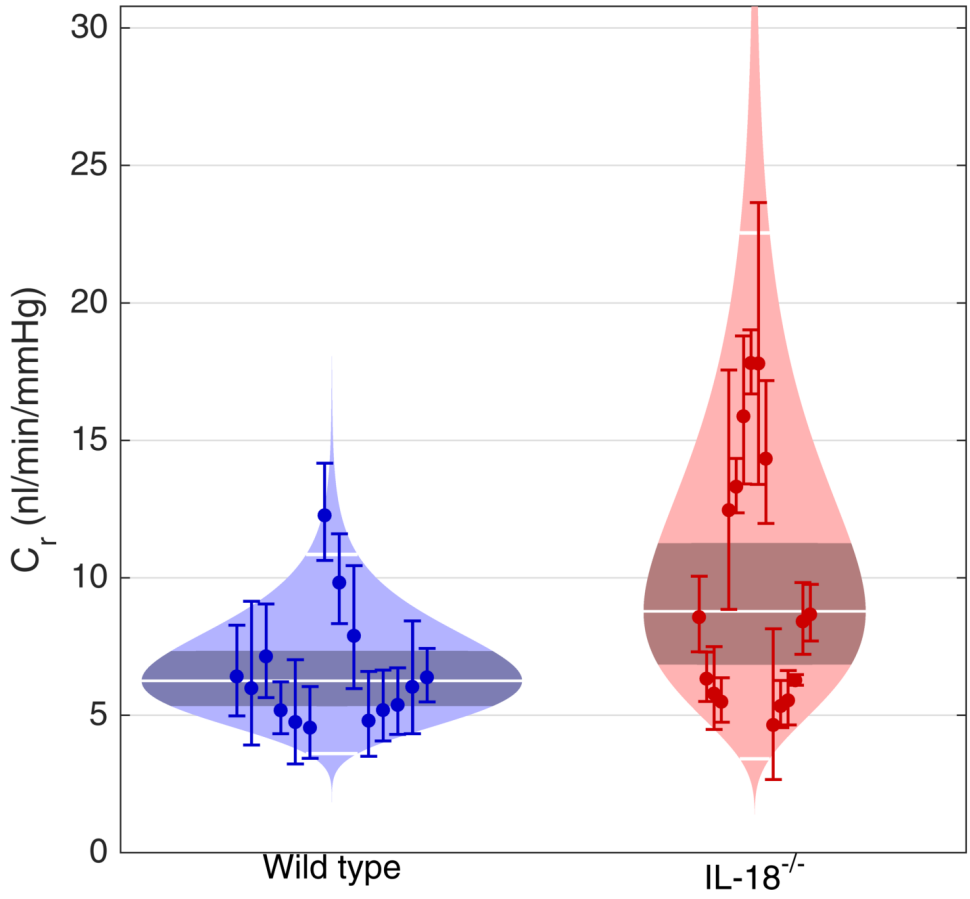

Figure 5.9: Cello plot of conventional outflow facility comparison between wild type and IL-18$^{-/-}$ mice.

Cello plot of distribution of data for C_r of wild type and IL-18$^{-/-}$ C57BL/6J ex vivo murine eyes. Each data point represents a single eye, error bars represent 95% CI. Shaded area represents predicted log normal distribution of data, middle white line represents mean, inner dark shading represents 95% CI of mean, while outer white lines represent two standard deviations from mean. IL-18$^{-/-}$ had 40 (5, 86) % higher C_r, mean = 8.78 mmHg, than wild type controls, mean = 6.26 mmHg ($p = 0.0215$, $N = 16$ for IL-18$^{-/-}$ $N = 14$ for wild type).

Interleukin-18 levels in aqueous humor in a model of axonal damage

NLRP3 inflammasome activation in the retina has been shown to be induced by optic nerve crush (ONC), a model of glaucomatous insult. Anterior diffusion of activated IL-18 from the retina to the AH could potentially induce a reduction in outflow facility

after axonal damage, exacerbating the glaucomatous condition. In order to determine whether this may be a factor in POAG, the level of IL-18 in the AH after mechanical damage to the RGC axons of the optic nerve by ONC was investigated. Wild type C57BL/6J mice were anesthetized and ONC was performed in one eye, carried out as per published protocols, with the contralateral control eye subject to conjunctival incision only (Templeton & Geisert 2012). At 24 hours post-ONC, animals were sacrificed and AH was collected, with IL-18 levels assessed by ELISA, fig. 5.9. In order to carry out this analysis, it was necessary to pool AH samples from four eyes to attain sufficient AH to run the assay in duplicate. This ELISA showed that there was no significant increase in IL-18 levels in eyes subject to ONC as compared to undamaged controls, p = 0.737 (N = 3 samples (4 eyes/sample), t-test).

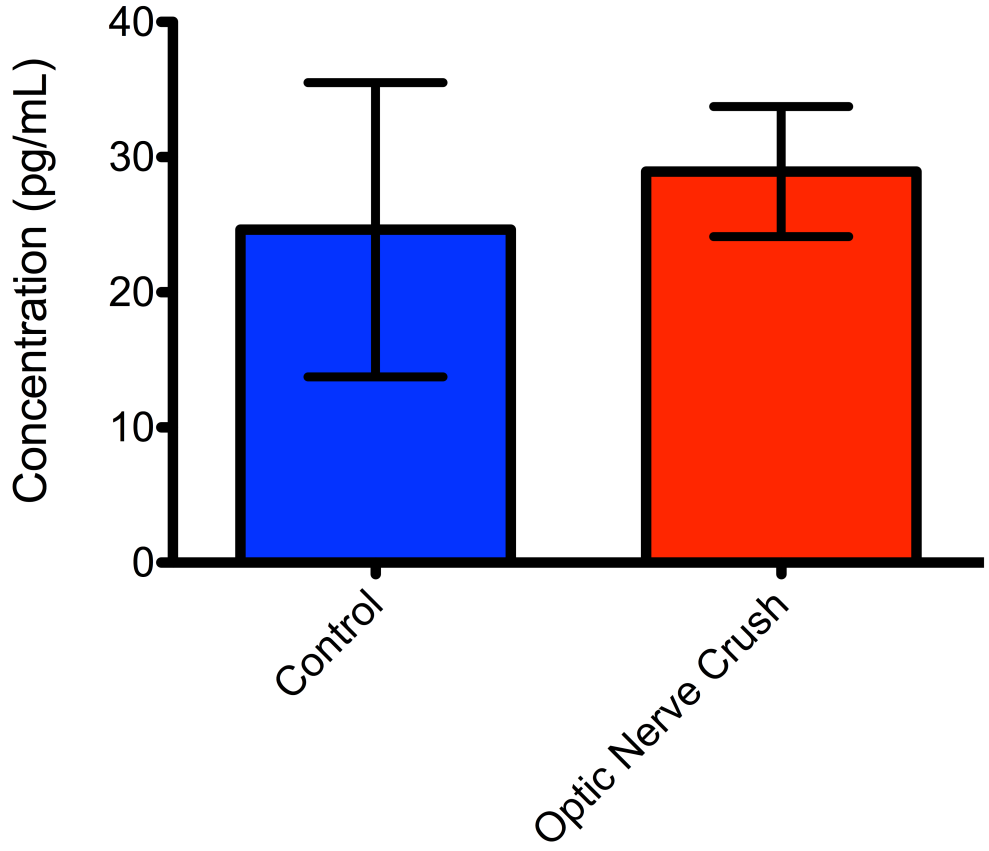

Figure 5.10: Effect of optic nerve crush on interleukin-18 levels in murine aqueous humor.

IL-18 levels in AH as determined by ELISA are shown for control (blue) and ONC (red) eyes. No significant difference was detected, p = 0.737 (N = 3 samples (4 eyes/sample), t-test). Data and error bars represent mean with s.e.m.

Interleukin-18 levels in human glaucomatous aqueous humor

The level of IL-18 in human aqueous humor obtained from POAG patients undergoing cataract surgery was also assessed by ELISA, with non-glaucomatous AH as a control, fig 5.10. This analysis showed no significant difference in IL-18 concentration between POAG and control AH, with very low, < 1.5 pg/ml, levels recorded in both, $p = 0.571$ ($N = 8$, t-test).

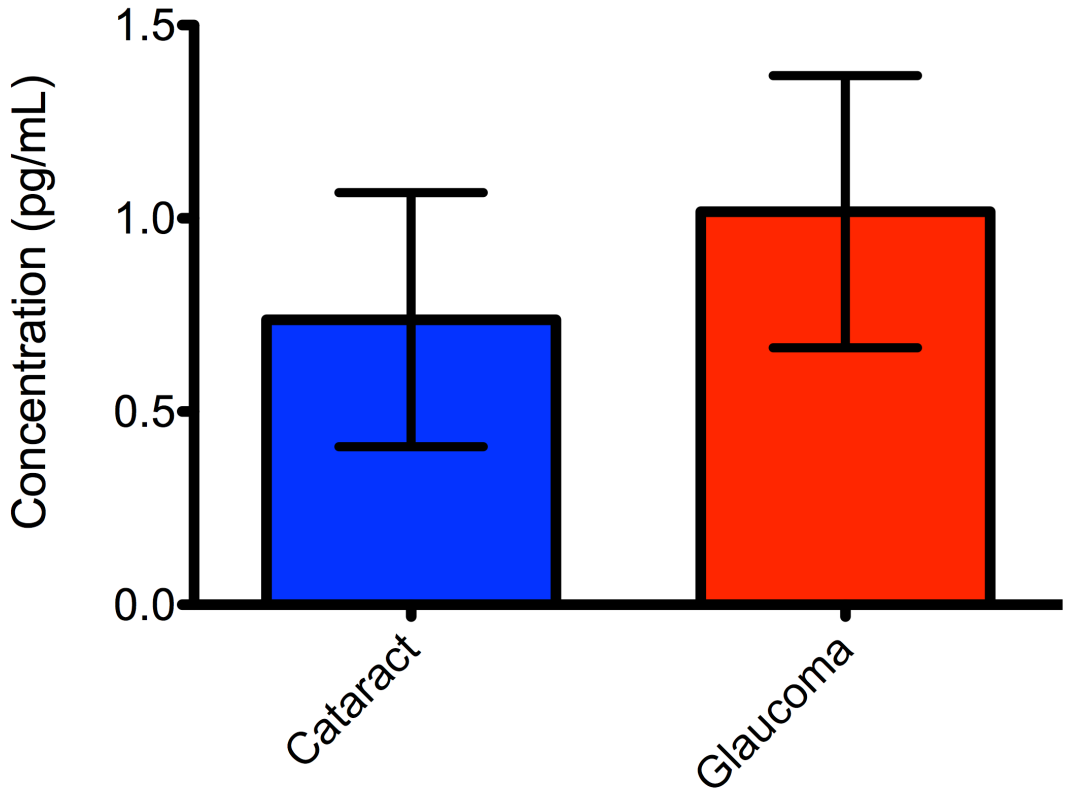

Figure 5.11: Level of interleukin-18 in aqueous humor from primary open-angle glaucoma patients.

IL-18 levels in AH as determined by ELISA are shown for cataract control (blue) and POAG (red) patients. No significant difference was detected, $p = 0.571$ ($N = 8$, t-test). Data and error bars represent mean with s.e.m.

Discussion

The aim of this chapter was to investigate the effect of IL-18 on SC permeability and outflow facility. Treatment of cultured primary human SCEC with IL-18 showed a significant increase in TEER at concentrations of 50 and 100 ng/ml, representing a decrease in the permeability of the SC monolayer to ions. IL-18 treatment of these cells was also shown to induce a decrease in permeability of human SCEC to the basal-to-apical flux of macromolecules, as represented by a significant reduction in flux of a 70 kDa fluorescently labeled protein tracer in cells treated with 1, 10, and 50 ng/ml IL-18. These data together show that IL-18 reduces the *in vitro* permeability of human SCEC. The effect of IL-18 on the viability of these cells was investigated, showing that SCEC retained 90 % viability up to 92 ng/ml, potentially explaining the increase in macromolecular permeability observed in cells treated with 100 ng/ml IL-18. As IL-18 is known to influence the expression of TJ proteins, the effect of IL-18 on ZO-1 and tricellulin protein expression in human SCEC was assessed. This showed that while IL-18 had no significant effect on the expression of ZO-1, it caused a significant increase in tricellulin protein levels in cells treated with a concentration of 10 or 50 ng/ml IL-18. As it was previously shown that downregulation of tricellulin via RNA interference brought about an increase in *in vitro* SCEC permeability, as measured by TEER and flux assays, this observed increase in tricellulin protein levels is likely to contribute to the IL-18 mediated decrease in SCEC permeability shown here.

As IL-18 was demonstrated to reduce permeability of SCEC *in vitro*, its effect on conventional outflow facility was assessed. This investigation showed that the intracameral injection of recombinant IL-18 brought about a significant reduction in outflow facility in wildtype mice, as would be predicted by reduction to permeability of the SC inner wall. Similarly, the potential role of IL-18 in conventional outflow facility regulation was examined through the use of knockout mice. $ASC^{-/-}$ mice, are deficient in ASC, the inflammasome adapter protein necessary for caspase-1 activation. These mice therefore cannot cleave pro-IL-1β or pro-IL-18 to their mature, bioactive form, preventing any signaling by these cytokines. Measurement of outflow facility in untreated $ASC^{-/-}$ showed they had significantly higher outflow facility values as compared to untreated wildtype mice. As increased outflow facility in $ASC^{-/-}$ could be due to the absence of active IL-18 or IL-1β signaling, outflow facility was also

measured in IL-18$^{-/-}$ mice. This showed an almost identical increase in outflow facility over wildtype control levels in these mice as was observed in ASC$^{-/-}$, indicating that IL-18 likely has an outflow facility decreasing effect in wildtype mice.

The mechanism by which IL-18 reduces outflow facility is as yet uncharacterized. IL-18-induced increases in tricellulin levels at SC inner wall may function to stabilize TJs at tri-cellular contacts. This would be expected to reduce paracellular pore formation, thereby increasing outflow resistance through increased funneling of AH. Additionally, IL-18 has been reported to induce the expression tissue inhibitor of MMP-1 (TIMP-1) and TIMP-2, which function to inhibit MMP activity (Zhang et al. 2004). Such increased inhibition could potentially cause increased ECM accumulation, leading to a reduction in outflow facility. IL-18 is reported to suppress the production of VEGF (Shen et al. 2014). VEGF has been shown to be an endogenous regulator of outflow facility, being secreted from the TM in response to mechanical deformation and binding to VEGF receptors at the SC inner wall, while anti-VEGF therapies have been reported to increase IOP (Reina-Torres et al. 2017; Wen et al. 2017; Bracha et al. 2017). Suppression of VEGF expression by IL-18 may be responsible for the outflow facility reduction reported here. Homeostatic suppression of VEGF expression by IL-18 could also provide a potential explanation for the increased outflow facility measured in the absence of IL-18 signaling in ASC$^{-/-}$ and IL-18$^{-/-}$ mice. Further studies will be required to determine the mechanistic role of IL-18 in outflow facility modulation, such as characterisation of IL-18 receptor expression in the conventional outflow pathway, and assessment of the effect of IL-18 treatment on VEGF expression.

In order to determine whether the above data held any relevance to POAG, the level of IL-18 in AH was measured after mechanical axonal damage in a murine model of glaucomatous optic neuropathy. This showed no significant difference in IL-18 concentration in AH as compared to contralateral control eyes. The concentration of IL-18 in samples of human POAG patient AH was also assessed, and again no increase in IL-18 concentration was detected between glaucomatous and control AH. Together these data indicate that, while IL-18 has a clear effect on the *in vitro* permeability of SCEC, and on conventional outflow facility, it may not be of relevance to the pathologically increased conventional outflow resistance seen in POAG.

As intraocular IL-18 been proven as an effective means of reducing choroidal neovascularization in mice and cynomolgus monkeys, the potential outflow facility lowering and IOP increasing effects of IL-18 administration will require further study,

with monitoring of patient IOP likely to be necessary (Doyle et al. 2014; Doyle et al. 2015).

The above data may also represent a means to generate a novel model of murine ocular hypertension. We have previously shown the ability to virally transfect the corneal endothelium with AAV-2/9 expressing the secretory protein MMP-3. Upon transfection, MMP-3 is expressed and secreted apically into the AH, where it is carried to the outflow tissues. Here, it mediates the degradation of ECM components, thereby reducing outflow resistance and increasing *C* (O'Callaghan et al. 2017, included in appendix). Similar viral delivery and secretion of IL-18, in its active form, from the corneal endothelium could hypothetically be used to chronically reduce *C*, leading to ocular hypertension. The implementation of such a potential model would require further evaluation of the mechanism of IL-18 mediated outflow facility reduction, but may represent a novel means to elevate IOP chronically in a murine model.

Statement on collaboration

Mouse perfusion after intracameral injection of IL-18 was carried out in collaboration with Dr. Ester Reina-Torres, Imperial College London and TCD.

Conclusion

POAG is one of the most prevalent blinding diseases worldwide, and is of great economic importance due to the high costs associated with long-term disease management. The main goal of this thesis was to investigate a novel approach to the treatment of POAG through targeting of the conventional outflow pathway. In chapter 2, the TJ composition of primary human SCECs was characterised, allowing the selection of potential TJ proteins, ZO-1, tricellulin, and claudin-11, as therapeutic targets. The expression of these proteins was also shown at the inner wall of SC in sectioned primate eyes, while ZO-1 and tricellulin alone were shown to be expressed in the murine conventional outflow pathway. The ability to downregulate these proteins *in vitro* with siRNA was also demonstrated. In chapter 3 the potential of these TJ proteins as therapeutic targets was investigated. The aim of this novel therapy was to downregulate TJ protein expression at the SC inner wall, leading to increased paracellular permeability through opening of paracellular pores. This pore opening would increase overall pore density at the inner wall, reducing the effect of funneling on AH outflow resistance generation. This study showed that *in vivo* injection of siRNA targeting ZO-1 and tricellulin into the murine anterior chamber resulted in lowered IOP and increased outflow facility. In addition, affirming the hypothesis that downregulation of TJ proteins at the inner wall would increase paracellular pore formation, EM data showed that treated eyes had significantly increased open paracellular clefts as compared to control eyes. Together, these data represent a successful demonstration of the siRNA mediated downregulation of TJ proteins as a potential novel therapeutic approach to the treatment of POAG. This therefore represents a novel approach to the treatment of POAG through targeting of the conventional outflow pathway has been investigated and demonstrated to hold therapeutic potential through its outflow increasing and IOP lowering effect in murine models. In chapter 4 the siRNA mediated downregulation of TJ proteins was investigated in a murine model of dexamethasone induced OHT. While baseline IOP measurements made the interpretation of data difficult, a reduction in IOP and an increase in outflow facility was also observed in these mice. This gave further support to the siRNA based approach for the of POAG.

While the data shown is an encouraging step towards the development of a novel therapeutic avenue for the treatment of POAG, there are certain shortcomings to the approaches taken that could be corrected in future studies. All data obtained in these studies with regards to protein downregulation by RNAi gives information only on the overall level of a specific protein within a given sample. As a result, there is a dearth of information on a variety of potential effects of target protein downregulation on other cellular components, and indeed on the remaining target proteins. It would be essential to carry out studies on the effect of siRNA treatment on the sub-cellular localisation of target proteins, for example, as downregulation may induce cytoplasmic sequestration of targeted TJ components, which would not be detected by western blot analysis. The effect of downregulation on the expression of non-targeted TJ components would also need to be assessed. TJs represent diverse multi-protein complexes which can form in many combinations of TJ proteins, and any downregulation of targeted TJ components could potentially result in the compensatory upregulation of alternate TJ components. A further unknown aspect of this approach is the potential long-term efficacy. All experiments thus far have shown that transient protein downregulation can reduce IOP and increase outflow facility, however as IOP homeostasis is a dynamic and as yet not fully understood process, long-term downregulation may not prove to be as effective. The potential for side effects from this approach is also not fully characterised. While TEM data did not reveal any structural abnormalities in treated eyes, the targeted TJ proteins are likely expressed in other tissues that form a blood-aqueous barrier, such as the iris, and in the corneal endothelium. Off target downregulation in these tissues could possibly compromise these barriers. Aside from ultrastructural alterations, the effect of downregulation of these TJ components on factors such as cytoskeletal stability or actin filament organization is not known. As TJs are anchored at the plasma membrane to the cytoskeleton through adapter proteins, such as ZO-1, downregulation of these proteins will likely influence cytoskeletal structure in some form, which in turn could be expected to affect factors such as cellular stiffness and contractility, among others.

This approach was also investigated in a non-human primate model, through adaptation of the *iPerfusion* machinery for *in vivo* primate use, with no reduction in IOP or increase in outflow facility measured after siRNA injection. Subsequent analysis showed that consistent downregulation of target TJ proteins had been unsuccessful. The measurement of spontaneous IOP in siRNA treated mice was also unsuccessfully attempted, largely due to anesthesia induced lowering of IOP. As discussed in chapter

3, there are several possible explanations for the lack of consistent downregulation seen in these animals. While murine siRNA injections consist of a 1.5 μL injection into an anterior chamber volume of approximately 4.5 μL, with paracentesis prior to injection draining much of the AH present, primate injections were 20 μL of siRNA solution inoculated into an anterior chamber volume of approximately 120 μL, with no paracentesis. This would mean that in mice it would be expected that siRNA would reach all of the circumference of the conventional outflow pathway, while in primates the lower relative injection volume may result in siRNA reaching only high-flow regions of the pathway, lessening its effects.

In order to progress this therapeutic approach towards human use, primate studies will need to be repeated to demonstrate the efficacy of TJ downregulation on *C* increase and IOP decrease. This may be better achieved through episcleral vein retro-injection of siRNA, to overcome the inconsistencies in downregulation previously observed. While demonstration efficacy of the treatment in non-human primates will be of benefit, ultimately, the transient nature of an RNAi based approach is a major issue. Viral transduction of the SC inner wall cells of the conventional outflow pathway to induce the expression of shRNA targeting TJ components may represent a means of long term delivery. Self-complementary AAV and AAV with modified capsid proteins have been shown to transduce the conventional outflow pathway, with expression lasting more than 2.3 years in primates (Wang et al. 2017; Buie et al. 2010). Further studies will be required to investigate whether virally delivered shRNA can lower IOP and increase *C*, but a greatly increased duration of effect would be expected. If this can successfully be demonstrated, this therapeutic approach will hold significant value as a novel treatment for POAG. While many patients respond well to topical interventions to lower IOP, some patients fail to achieve adequate IOP reduction with this treatment. The development of novel approaches to IOP reduction is essential to allow for alternate treatment approaches. This approach could also be used in conjunction with current treatments for greater overall effect. Virally delivered shRNA, if implemented, would also address the problem of patient compliance to topical eye drop administration, replacing daily drops necessary for IOP management with intraocular injection of AAV which could remain effective for up to two years. A potential negative to this would be the lack of control of downregulation. This could be negated through topical administration of an inducer of expression, which would result in patient compliance

issues. Alternately, a topical repressor of expression could be implemented in cases where the treatment needed to be discontinued due to pathological effects.

A secondary aim of this thesis was to assess the effect of IL-18 on conventional outflow facility. In chapter 5 it was shown that IL-18 reduced the *in vitro* permeability of human SCEC to ions and macromolecules, and increased the expression of tricellulin. The intracameral injection of IL-18 was shown to reduce outflow facility, while outflow facility was shown to be increased in knockout mice deficient in active IL-18. The mechanism by which IL-18 increases outflow facility remains to be fully elucidated, but upregulation of tricellulin likely plays a role through reduction of paracellular pore density. While these data represent an interesting observation on the potential effects of IL-18 on conventional outflow, much further work is required. The investigation by IHC of the distribution of IL-18 receptors in the anterior chamber, particularly in the JCT and SC inner wall, would give important information on the site of effect of IL-18's outflow reducing effect. It would also be essential to assess the effect of IL-18 on IOP directly to validate the outflow facility findings. The effect of IL-18 on SC cells would also need to be better characterised, as only data on permeability and TJ expression has thus far been generated. Alterations in cytoskeletal organization in particular should be investigated, along with the downstream signaling pathways that become activated through IL-18 binding it's receptor.

These data could allow for the generation of a novel model of chronic ocular hypertension, through viral secretion of IL-18 from the corneal endothelium into AH. Such a model would be useful as it would not require transgenic mouse lines, and may represent a better model for the study of conventional outflow facility modulation than those currently available. Further studies, along with a thorough understanding of the molecular mechanisms of such a model, would be required to assess the suitability of this potential model.

Assessment of IL-18 levels in murine AH after axonal damage, and human POAG patient AH both showed no significant increase in IL-18 over controls, indicating IL-18 is not likely to play a role in POAG. As IL-18 is being developed as a therapeutic agent for the treatment of AMD, it will be important to fully characterise its effect on AH outflow prior to human use. As the murine data was generated through intracameral injection, it would be helpful to replicate it with intravitreal injection to better represent the AMD treatment approach, and to assess if this still reduces outflow facility.

In conclusion, the studies in this thesis contribute to a greater overall understanding of the mechanisms by which the SC inner wall, and specifically the TJ proteins which control intercellular junctions and influence pore formation, contribute to the generation of outflow resistance. While these findings may allow for the generation of a novel therapy for POAG in the future, with the continuation of the necessary work discussed herein, they also are of value to the overall understanding of conventional outflow physiology. With the continued development of therapies targeting the conventional outflow pathway, the future of medical treatment for POAG is encouraging.

Materials and Methods

Cell culture

Human SCEC and TM cells were obtained from the Stamer lab at Duke Eye Centre, and were isolated, cultured and characterised as previously described (Stamer et al. 1995; Stamer et al. 1998). SCEC strains used in this study were SC65, SC68, SC73, SC74, SC76, SC77, SC79, SC82 and SC83. TM93 was used for RNA analysis. All SCEC and TM cells were used between passages 2 and 6. Prior to experimental use, cells were characterised as described in Perkumas et al, 2012. Briefly, cells were confirmed to be fusiform and contact inhibited, and to form linearly arranged monolayers. SC and TM cells were both assayed for expression of VEGF-R1/2, eNOS, Tie2, and neurophilin-1. SC lines were also demonstrated to express SC marker proteins fibulin-2, and VE-cadherin, distinguishing them from TM cells. SCEC were cultured in low glucose Dulbecco's modified Eagle medium (Gibco, Life Sciences) supplemented with 10% *Performance Plus* foetal bovine serum (FBS) (Gibco, Life Sciences), 1% Pen/Strep glutamine (Gibco, Life Sciences), in a 5% CO_2 incubator at 37 °C. TM cells underwent a differentiation step by plating at full confluency for one week in media containing 10% FBS, and changed over to media containing 1% FBS for an additional week prior to experimentation. Cultured cells were passaged with trypsin-EDTA (Gibco-BRL) to maintain exponential growth.

Human tight junction PCR array

Analysis of TJ mRNA expression levels was carried out using the human TJ RT^2 Profiler PCR array (PAHS-143ZA, Qiagen), which profiled the expression of 84 key genes encoding proteins that are involved in intercellular junctions between both epithelial and endothelial cells. Total RNA was extracted from four different human SCEC strains (SC65, 68, 76 and 77) at passages 3 to 5 using RNEasy Mini Kit (Qiagen) according to manufacturer's protocol. Genomic DNA contamination was eliminated by DNase treatment. Total RNA was reverse-transcribed into cDNA using RT^2 First Strand Kit (Qiagen). The Threshold cycle (Ct) values of different passage numbers from each SCEC strain were determined and averaged using ABI Prism 7700 Sequence

Detector. The mean normalised expression ($2^{-\Delta Ct}$) of genes encoding claudin and adhesion junctional proteins was determined and analysed using the online Qiagen RT^2 Profiler PCR Array Data Analysis software. Normalised gene expression was calculated by using the equation: $2^{-\Delta Ct} = 2^{-[Ct(\text{gene of interest}) - Ct(\text{Housekeeping genes})]}$. Normalisation was carried out with five housekeeping genes (*ACTB, B2M, GAPDH, HPRT1 and RPLP0*) included in the PCR array. The $2^{-\Delta\Delta CT} = 2^{-\Delta Ct\ \text{treated}}/2^{-\Delta Ct\ \text{control}}$ method was used to calculate fold changes for each gene as difference in gene expression.

Western blotting

Protein lysates were isolated from cultured cells in protein lysis buffer containing 1 M Tris pH 7.5, 1 M NaCl, 1% NP-40, 10% SDS, 1X protease inhibitor cocktail (Roche). The homogenate was centrifuged at 12,000 r.p.m. (IEC Micromax microcentrifuge, 851 rotor) at 4 °C for 15 min and the supernatant was stored at −80 °C until use. Protein concentration was determined by BCA Protein assay kit (Pierce, IL, USA) with bovine serum albumin (BSA) at 2 mg/ml as standards on 96-well plates according to the manufacturer's protocol. Dissected primate tissue was snap frozen for shipping. Upon arrival protein was extracted using NP-40 protein lysis buffer and protein concentration was determine by nanodrop. 30–50 μg of total protein was loaded in each lane. Protein samples were separated by electrophoresis on 10-12% SDS–PAGE under reducing conditions and electro-transferred to PVDF membranes. After transferring, blots were washed in TBST and then blocked with 5% blotting grade non-fat dry milk in TBS for 1 h at room temperature. Membranes were incubated overnight at 4 °C with the following Rabbit polyclonal primary antibodies: anti-oligodendrocyte specific protein antibody (1:500; Abcam); anti-ZO-1 antibody (1:250; Invitrogen), anti-tricellulin C-terminal antibody (1:125; Invitrogen), anti-claudin-5 antibody (1:500, Invitrogen. Blots were washed with TBS and incubated with horse radish peroxidase-conjugated polyclonal rabbit IgG secondary antibody (Abcam). The blots were developed using enhanced chemiluminescent kit (Pierce Chemical Co.) and exposed to Fuji X-ray film. Each blot was stripped with Restore Western Blot Stripping Buffer (Pierce) and probed with rabbit polyclonal antibody to β-actin as loading controls. Protein band intensities were quantified by scanning with a HP Scanjet Professional 10000 Mobile Scanner and analysed using *Image J* (Version 1.50c). In the case of

siRNA treatment, the percentage reduction in band intensity was calculated relative to the control non-targeting siRNA, which was standardised to represent 100% and normalised against β-actin. For IL-18 treated SCEC, change in expression was calculated relative to untreated cells, standardised to 1, and normalised against β-actin. For primate tissues, change in expression was calculated relative to NT siRNA injected tissues, standardised to 1, and normalised against β-actin.

Immunohistochemistry

Mouse: Enucleated mouse eyes were immersion fixed in 4% paraformaldehyde (pH 7.4) overnight at 4 °C on a rotating device. Posterior segments of the eye and the lens were removed and anterior segments were then washed with PBS for 15 min and dehydrated through sequentially immersion in 10, 20 and 30% sucrose. Dissected anterior segments were then suspended in specimen blocks with OCT solution (Tissue-Tek) and frozen in a bath of isopropanol submerged in liquid nitrogen to prevent tissue deformation. Frozen anterior segments were sectioned using a cryostat (Leica CM 1900) to 12 µm thickness. Sections were collected on Polysine® coated slides (Menzel-Glazer). To detect TJ proteins, sections were blocked for 20 min at room temperature in PBS containing 5% goat serum and 1% BSA, and incubated with the corresponding antibodies at 1:100 dilutions overnight at 4 °C in a humidity chamber. All sections were then washed three times in PBS and incubated with Cy-3 labelled anti-rabbit IgG antibody at 1:500 (Abcam) for 2 h at room temperature in a humidity chamber. Following incubation, sections were washed with PBS and mounted with aqua-polymount (Polyscience) after nuclei-counterstaining with DAPI. Anterior segments were visualised using a confocal microscope (Zeiss LSM 710).

Primate: Paraffin sections of African green monkey (*Chlorocebus Sabeus*) anterior segments were rehydrated by immersion in the following solutions: twice for 2 min each in Histoclear solution; 100% ethanol for 1 min; 95% ethanol for 1 min; 70% ethanol for 1 min; deionised water for 1 min; washing twice for 5 min in PBS. For antigen retrieval, paraffin sections were heated to 95 °C for 10 min in citrate buffer (Sodium citrate, pH 6). Paraffin sections were then blocked and stained as described above.

siRNA

All *in vivo* predesigned siRNAs used in this study were synthesised by Ambion and reconstituted as per manufacturer's protocol. siRNA identification numbers are as follows: human claudin-11 siRNA (ID number: s9925), human ZO-1 siRNA (ID number: s14156), human MARVELD2 siRNA (ID number: s45794), mouse ZO-1 siRNA (ID number: s75175), mouse MARVELD2 siRNA (ID number: ADCSU2H). Silencer Negative control siRNA (Ambion) was used as a non-targeting control in knockdown studies. For validation of *in vitro* knockdown, SCEC were transfected with 40 nM (1 pmol/well) siRNA using Lipofectamine RNAi max as per manufacturers protocol.

Cell viability

For assessment of SCEC viability after siRNA treatment, cells were grown to confluency on a 96-well plate and subsequently transfected with siRNA in quadruplicate using Lipofectamine RNAiMax reagent as per manufacturers protocol (Life Technologies) at both 1 pmol/well (40 nM) and 5 pmol/well (200 nM) for 48 hours. For assessment of SCEC viability after IL-18 treatment cells were grown to confluency on a 96-well plate and subsequently treated with recombinant human IL-18 (Glaxosmithkline) at 1, 10, 50, and 100 ng/mL for 24 hours. CellTitre 96 AQ_{ueous} One Solution Reagent (Promega) was thawed and mixed with culture medium at a 1:5 dilution. Cells were incubated with this mixture for a period of 2 hours, before transferring the media to a fresh 96-well plate. Absorbance of each well was recorded at 450 nm on a spectrophotometer (Multiskan FC, Thermo Scientific) and each reading was blanked against wells with reagent and no cells. For siRNA, each treatment group was presented relative to a negative control containing no siRNA. A positive control was achieved by incorporating 1% SDS into the media-reagent mixture to induce cytotoxicity. A one-way ANOVA with a Tukey's post-test was performed on the data set. For IL-18, viability was defined as was defined at an average of 90 % viability over eight cell samples, with untreated cells normalised to 100 % viability. A linear model was fitted to normalised data, with the lower 95 % confidence interval used to determine when cell viability reached to 90 % threshold.

Pump based perfusion

Pump based perfusions were carried out as per Boussommier-Calleja et al. 2012. Briefly, mouse eyes were enucleated after sacrifice by cervical dislocation, with one eye perfused immediately while the second was stored in PBS at 4 °C for perfusion after the first eye. Eyes to be perfused were placed in a humidified chamber and cannulated with 33-gauge steel needles connected to tubing filled with PBS containing Ca^{2+}, Mg^{2+}, and 5.5 mM glucose, using a micromanipulator. Pressure was set using a manometric reservoir, and the system was closed, with pressure maintained through software controlled pressure monitoring via a pressure transducer, with automatic adjustment of inflow rate from a Harvard Apparatus PHD200 syringe pump. This was carried out at sequential pressure steps of 4, 8, 15, and 20 mmHg, with 10 minutes of stable flow rate data required before movement to the next pressure step.

iPerfusion

Outflow facility measurement with *iPerfusion* were carried out as described in Sherwood et al. 2016. Mice were culled by cervical dislocation, eyes were enucleated immediately and stored in PBS at room temperature to await perfusion (~20 min). Both eyes were perfused simultaneously using two independent perfusion systems as described previously. Briefly, each eye was affixed to a support using a small amount of cyanoacrylate glue and submerged in a PBS bath regulated at 35 °C. The eye was cannulated via the anterior chamber with a 33-gauge bevelled needle (NanoFil, #NF33BV-2, World Precision Instruments) under a stereomicroscope using a micromanipulator. The iPerfusion system comprises an automated pressure reservoir, a thermal flow sensor (SLG64-0075, Sensirion) and a wet-wet pressure transducer (PX409, Omegadyne) in order to apply a desired pressure, measure flow rate out of the system and measure the intraocular pressure respectively. The perfusate was PBS containing Ca^{2+}, Mg^{2+}, and 5.5 mM glucose, and was filtered through a 0.22 μm filter (VWR international) prior to use. Following cannulation, eyes were perfused for 30 min at 8 mmHg to allow the eye to acclimatis. Subsequently, nine discrete pressure steps were applied from 4.5 to 21 mmHg, while flow and pressure were recorded. Stability was defined programmatically, and data were averaged over 4 min at steady state. A non-linear model was fit to flow-pressure data to account for the pressure dependence

of outflow facility in mouse eyes. This model was of the form $Q = C_r P (P/P_r)^{\beta}$. where Q and P and are the flow rate and pressure respectively, and C_r is the outflow facility at reference pressure P_r, which is selected to be 8 mmHg (the approximate physiological pressure drop across the outflow pathway). The power law exponent β quantifies the non-linearity in the Q-P response and thus the pressure dependence of outflow facility. The data analysis methodology described in Sherwood et al. 2016 was applied in order to analyse the treatment effect, whilst accounting for measurement uncertainties, and statistical significance was evaluated using the paired weighted t-test described therein.

Intracameral injection

For siRNA injection, adult C57BL/6J mice of 10 to 12 weeks of age were anaesthetised by intra-peritoneal injection of medetomidine hydrochloride (Domitor) and ketamine (0.66 and 66.6 mg/kg body weight, respectively). Pupils were dilated with 2.5% tropicamide and 2.5% phenylephrine eye drops. Glass micro-capillaries (outer diameter = 1 mm, inner diameter = 0.58 mm; World Precision Instruments) were pulled using a micropipette puller (Narishige PB-7). Under microscopic control, a pulled blunt-ended micro-glass needle (tip diameter ~100 μm) was first used to puncture the cornea to withdraw AH. Immediately after puncture, a pulled blunt-ended micro-glass needle attached to a 10 μl syringe (Hamilton, Bonaduz) held in a micromanipulator (World Precision Instruments) was inserted through the puncture, and 1.5 μl of PBS containing 1 μg of ZO-1 siRNA and 1 μg of tricellulin siRNA was administered into the anterior chamber to give a final concentration of 16.84 μM. Contralateral eyes received an identical injection of 1.5 μl containing the same concentration of NT siRNA. Following surgery, a reversing agent (1.5 mg/kg body weight, atipamezole hydrochloride) was delivered by intra-peritoneal injection. Fusidic gel was applied topically to the eye as antibiotic and Vidisic gel was also applied topically as a moisturiser. Furthermore, 5 mg/kg enrofloxacin antimicrobial (Baytril; Bayer Healthcare) was injected subcutaneously. For IL-18 injection, adult C57BL/6J mice of 10 to 12 weeks of age were anaesthetized with 3 % isoflurane at 1 litre/min and injection was carried out as above, with 1.5 μl PBS containing 50 ng/ml recombinant mouse IL-18 (Glaxosmithkline).

Rebound tonometry

For analysis of the effect of siRNA in chapter 3, IOP measurements were performed by rebound tonometry (TonoLab, Icare). Readings were taken 10 min after the intra-peritoneal administration of mild general anaesthetic (53.28 mg/kg ketamine and 0.528 mg/kg domitor). with each reading representing the average IOP values of five tonometric events. Two readings were taken for one eye, then the other. This was repeated for a total of four readings per eye. Due to a minimum reading of 7 mmHg by the tonometer, a non-parametric approach was taken in the analysis of the readings. The median IOP was calculated for each eye, and MAD (median absolute deviation) values were used as a measure of dispersion. For comparing median values in a paired population, the Wilcoxon matched-pairs signed-rank test was employed to test for changes in IOP pre- and post-injection. For analysis of the effect of DEX on IOP weekly, mice were anaesthetized with 3 % isoflurane at 1 litre/min for 2 minutes in an induction chamber, and then moved to a headholder delivering isoflurane at the same rate. At 3 minutes, 5 measurements of IOP were carried out in the right eye and averaged. For measurement of pre- and post-siRNA injection IOP, mice were anaesthetized as above and 3 IOP measurements were made at 3 different time points in both eyes (eye 1: minute 3, 5 and 7, eye 2: minute 4, 6 and 8). The average IOP at each time point was used to fit a line and interpolate IOP at minute 5, to allow for measurement of IOP in both eyes while accounting for the IOP lowering effect of anaesthesia.

Transmission electron microscopy

48 hours after siRNA injection, all eyes were enucleated, punctured at their posterior, immersion fixed in Karnovsky's solution initially and post-fixed in Ito's solution, and shipped to the Lütjen-Drecoll lab at University of Erlangen-Nürnberg for EM analysis. There, eyes were embedded in Epon and semi-thin sagittal sections were cut through the whole globe. Ultrathin sections of SC and TM were cut sagitally from one side of the eye first, and then another ultrathin section approximately 1mm deeper was cut. If possible, this section was taken from the other side of the eye. In the small mouse eye, this process could be repeated four times. In this way, different parts of the circumference of the eye were evaluated. Different staining methods were investigated

to visualise cell membranes, and the best results were obtained using UAR-EMS (Science Services, Munich, Germany). In ultrathin sections of the entire anterior posterior length of the inner wall from all four regions of treated eyes and their controls, we investigated whether there was any ballooning of the inner wall endothelium, necrosis or apoptosis of endothelial cells or adherence of platelets to the inner wall endothelium. Intercellular gaps were counted at magnifications of 80.000x by two independent observers.

Primate *in vivo* iPerfusion

The setup of the primate *iPerfusion* system was similar to that of the murine *ex vivo* system, with notable exceptions being lower reservoir height, for easier transport, and higher range flow sensors (Sensirion). The protocol for primate *in vivo iPerfusion* involved measurement of tonometric IOP in intramuscular ketamine and xylazine anaesthetized animals immediately prior to perfusion. Needles are placed in the tear film of primate eyes and reference manometric reservoirs adjusted to achieve measurement of a reference pressure, based on height of the eye during perfusion. Cannulation of both anterior chambers was then performed at mean tonometric IOP with 30-gauge needles connected to tubing containing standard *iPerfusion* perfusate. After cannulation, the anterior chamber ass connected directly to a pressure sensor to measure sIOP for 5 minutes of stability (pressure slope < 0.2 mmHg/min), and then perfusion was performed, beginning at sIOP – 8 mmHg, with 6 increments of 4 mmHg carried out. After a perfusion cycle, the pressure was set to sIOP – 1 mmHg, and a second measurement of sIOP was taken. This was repeated for three total cycles of *iPerfusion* measurement.

Murine spontaneous IOP measurement

Murine sIOP was measured in a manner similar to that in primates, with mice anaesthetized using intraperitoneal (IP) ketamine and xylazine, with an IP catheter placed to allow redosing throughout the perfusion protocol. Tonometric IOP was measured after onset of anaesthesia. Mice were mounted on a palate bar and held on a temperature controlled platform at 35 °C. Both anterior chambers were cannulated at

tonometric IOP to two separate *iPerfusion* systems using beveled, pulled glass micropipettes, and eyes were coated in lubricant (Vidisic) to maintain corneal moisture. After cannulation, anterior chambers were connected directly to pressure transducers and sIOP measured once steady state had been achieved. A single perfusion cycle was carried out as in *ex vivo iPerfusion*, followed by a second measurement of sIOP.

Dexamethasone micro-osmotic pump implantation

DEX micro-osmotic pump (Model 1004, Alzet) were implanted as in Whitlock et al. 2010. The DEX was water-soluble (D2915; Sigma-Aldrich), contained cyclodextrin (1.36 g per 100 mg DEX), and was dissolved in PBS. DEX was delivered at 2 mg/kg/day in high dose mice, and 0.13 mg/kg/day in low dose mice. Adult C57BL/6J mice of 10 to 12 weeks of age were anaesthetized with 3 % isoflurane at 1 litre/min, and surgical site was shaved and disinfected with chlorhexidine swabs. Mice were injected intramuscularly with 0.05 mg/kg buprenorphine (Buprecare, Animalcare) and subcutaneously with 5 mg/kg enfloroxacine (Enrocare, Animalcare). An incision was made between the scapulae and a subcutaneous pocket was created by blunt dissection and the pump was inserted. The incision was closed using surgical glue (Surgibond, RayVet). After pump implantation, mice were housed singly and diet was supplemented with Complan to prevent GC induced weight loss. Weight was monitored weekly, with any mice losing more than 20 % body weight overall, or 10 % body weight in one week required to be sacrificed.

Trans-endothelial electrical resistance measurement

TEER was used as a measure of TJ integrity by human SCEC monolayers. Human SCEC were grown to confluency on Costar HTS Transwell-polyester membrane inserts with a pore size of 0.4 μm. The volume of the apical side (inside of the membrane inserts) was 0.1 ml and that of the basal side (outside of the membrane inserts) was 0.6 ml. Baseline TEER values were determined using an EVOM resistance meter with Endohm Chamber (World Precision Instruments) and a Millicell-Electrical Resistance System. For measurement of TEER, both the apical and basolateral sides of the endothelial cells were bathed in fresh growth medium at 37 °C, and a current was passed across the monolayer with electrical resistance recorded, which was reported as Ω.cm2

after correcting for the surface area of the membrane (1.12 cm). The inherent resistance of a blank transwell was subtracted from the values obtained for the endothelial cells. For IL-18 treatment, confluent cells were treated with IL-18 at 1, 10, 50, and 100 ng/ml in quadruplicate, with 5 replicate wells of untreated cells. 24 hours post-treatment, TEER was measured again as above, and the change in TEER after treatment determined. The change in untreated cells was normalised to 1, with IL-18 induced changes reported relative to untreated cells.

Cell permeability assay using FITC-dextran

Human SCEC were prepared and treated as for TEER measurement as described above. 70 kDa fluorescein isothiocyanate (FITC)-conjugated dextran (FD) (Sigma) was applied at 1 mg/ml to the basal compartment of the transwells. Sampling aliquots of 0.1 ml were collected every 15 min for a total of 120 min from the apical side for fluorescence measurements and the same volume of culturing media was added to replace the medium removed. FITC fluorescence was determined using a spectrofluorometer (Optima Scientific) at an excitation wavelength of 485 nm and an emission wavelength of 520 nm. Relative fluorescence units (RFU) were converted to values of nanograms per millilitre using FITC-dextran standard curves, and were corrected for background fluorescence and serial dilutions over the course of the experiment. The apparent permeability co-efficient (Papp, cm/s) for each treatment was calculated using the following equation: $P_{app} = (dM/dT)/(A\ xC_0)$ where dM/dt (µg/s) is the rate of appearance of FD on the apical side from 0 min to 120 min after application of FD. C_0 (µg/ml) is the initial FD concentration on the basal side, and A (cm2) is the effective surface area of the insert. dM/dt is the slope calculated by plotting the cumulative amount of (M) versus time.

Optic nerve crush

Optic nerve crush was carried out as per published protocols (Templeton & Geisert 2012). Briefly, adult C57BL/6J mice of 10 to 12 weeks of age were anaesthetized with 3 % isoflurane at 1 litre/min. Following induction of anaesthesia, they were placed on a head holder delivering isoflurane as above with one eye facing upwards towards a dissection microscope. The conjunctiva was held with surgical forceps and an incision

was made. The eye was then rotated nasally using forceps holding the conjunctiva, allowing access to the posterior aspects of the glove. The optic nerve was grasped approximately 2 mm from the globe using self-closing forceps (Dumont #7, World Precision Instruments) for 10 seconds. After this crush, the forceps were removed, a drop of 0.5 % proparacaine hydrochloride was delivered, and eyes were coated with the anti-microbial fusidic acid (Fucithalmic, Concordia).

ELISA

ELISA assays were carried out to determine concentration of IL-18 in human POAG patient AH and murine AH after ONC. For human, 8 POAG and 8 cataract control AH samples were diluted 1 in 4 and run in duplicate using a RayBio Human IL-18 ELISA kit (ELH-IL-18) as per manufacturers protocol. For mouse, 3 pooled AH samples from four treated and four control eyes were diluted 1 in 10 and run in duplicate as per manufacturers protocol using a mouse IL-18 ELISA kit from R&D systems (#7625, Biotechne Ltd). ELISA data was read using a spectrophotometer at 450 nm.

References

Abu-Amero, K., Kondkar, A.A. & Chalam, K. V., 2015. An updated review on the genetics of primary open angle glaucoma. *International Journal of Molecular Sciences*, 16(12), pp.28886–28911.

Abu-Hassan, D., Acott, T. & Kelley, M., 2014. The trabecular meshwork: A basic review of Form and Function. *Journal of ocular biology*, 2(1).

Acott, T.S. et al., 2014. Intraocular pressure homeostasis: maintaining balance in a high-pressure environment. *Journal of ocular pharmacology and therapeutics : the official journal of the Association for Ocular Pharmacology and Therapeutics*, 30(2–3), pp.94–101. Available at: http://www.ncbi.nlm.nih.gov/pubmed/24401029%5Cnhttp://www.pubmedcentral.nih.gov/articlerender.fcgi?artid=PMC3991985.

Ahmed, I.I.K. et al., 2014. Prospective evaluation of microinvasive glaucoma surgery with trabecular microbypass stents and prostaglandin in open-angle glaucoma. *Journal of Cataract and Refractive Surgery*, 40(8), pp.1295–1300.

Aihara, M., Lindsey, J.D. & Weinreb, R.N., 2003a. Aqueous Humor Dynamics in Mice. *Investigative Ophthalmology and Visual Science*, 44(12), pp.5168–5173.

Aihara, M., Lindsey, J.D. & Weinreb, R.N., 2003b. Experimental mouse ocular hypertension: Establishment of the model. *Investigative Ophthalmology and Visual Science*, 44(10), pp.4314–4320.

Aihara, M., Lindsey, J.D. & Weinreb, R.N., 2003c. Twenty-four-hour pattern of mouse intraocular pressure. *Experimental Eye Research*, 77(6), pp.681–686.

Allingham, R.R., Liu, Y. & Rhee, D.J., 2009. The genetics of primary open-angle glaucoma: A review. *Experimental Eye Research*, 88(4), pp.837–844. Available at: http://dx.doi.org/10.1016/j.exer.2008.11.003.

Alm, A. & Nilsson, S.F.E., 2009. Uveoscleral outflow - A review. *Experimental Eye Research*, 88(4), pp.760–768.

Alvarado, J.A., Wood, I. & Polansky, J.R., 1982. Human trabecular cells. II. Growth pattern and ultrastructural characteristics. *Investigative Ophthalmology and Visual Science*, 23(4), pp.464–478.

Amasheh, S. et al., 2002. Claudin-2 expression induces cation-selective channels in tight junctions of epithelial cells. *Journal of cell science*, 115(Pt 24), pp.4969–

4976.

Anderson, J.M. & Van Itallie, C.M., 2009. Physiology and function of the tight junction. *Cold Spring Harbor perspectives in biology*, 1(2).

Anderson, M.G. et al., 2005. High-dose radiation with bone marrow transfer prevents neurodegeneration in an inherited glaucoma. *Proceedings of the National Academy of Sciences of the United States of America*, 102(12), pp.4566–71. Available at: http://www.pubmedcentral.nih.gov/articlerender.fcgi?artid=555465&tool=pmcentrez&rendertype=abstract%0Ahttp://www.ncbi.nlm.nih.gov/pubmed/15758074%0Ahttp://www.pubmedcentral.nih.gov/articlerender.fcgi?artid=PMC555465.

Asrani, S. et al., 2000. Large diurnal fluctuations in intraocular pressure are an independent risk factor in patients with glaucoma. *Journal of Glaucoma*, 9(2), pp.134–142. Available at: http://eutils.ncbi.nlm.nih.gov/entrez/eutils/elink.fcgi?dbfrom=pubmed&id=10782622&retmode=ref&cmd=prlinks%5Cnpapers2://publication/uuid/6BC7D52D-1B3B-4783-8CFD-D0CB289BB1E6.

Bellezza, A.J. et al., 2003. Deformation of the lamina cribrosa and anterior scleral canal wall in early experimental glaucoma. *Investigative Ophthalmology and Visual Science*, 44(2), pp.623–637.

Ben-Yosef, T. et al., 2003. Claudin 14 knockout mice, a model for autosomal recessive deafness DFNB29, are deaf due to cochlear hair cell degeneration. *Human Molecular Genetics*, 12(16), pp.2049–2061.

Bhatt, K., Gong, H. & Freddo, T.F., 1995. Freeze-fracture studies of interendothelial junctions in the angle of the human eye. *Investigative Ophthalmology and Visual Science*, 36(7), pp.1379–1389.

Bill, A., 1967. Further studies on the influence of the intraocular pressure on aqueous humor dynamics in cynomolgus monkeys. *Investigative Ophthalmology and Visual Science*, 6, pp.364–372.

Bill, A., 1965. The Aqueous Humor Drainage Mechanism in the Cynomolgus Monkey (Macaca irus) with Evidence for Unconventional Routes. *Investigative ophthalmology & visual science*, pp.911–919.

Bill, A., Lutjen-Drecoll, E. & Svedbergh, B., 1980. Effects of intracameral Na2EDTA and EGTA on aqueous outflow routes in the monkey eye. *Investigative Ophthalmology and Visual Science*, 19(5), pp.492–504.

Blasig, I.E. et al., 2006. On the self-association potential of transmembrane tight junction proteins. *Cellular and Molecular Life Sciences*, 63(4), pp.505–514.

Bogdan, C., 2001. Nitric oxide and the immune response. *Nature immunology*, 2(10), pp.907–16. Available at: http://www.ncbi.nlm.nih.gov/pubmed/11577346.

Bollinger, K. et al., 2011. Intraocular pressure outcome of patients with fluocinolone acetonide intravitreal implant for noninfectious uveitis. *Ophthalmology*, 118(10), pp.1927–1931.

Boussommier-Calleja, A. et al., 2012. Pharmacologic manipulation of conventional outflow facility in ex vivo mouse eyes. *Investigative Ophthalmology and Visual Science*, 53(9), pp.5838–5845.

Braakman, S.T. et al., 2014. Biomechanical strain as a trigger for pore formation in Schlemm's canal endothelial cells. *Experimental Eye Research*, 127, pp.224–235.

Braakman, S.T. et al., 2015. Colocalization of outflow segmentation and pores along the inner wall of Schlemm's canal. *Experimental Eye Research*, 130, pp.87–96.

Braakman, S.T. et al., 2016. Transport across Schlemm's canal endothelium and the blood-aqueous barrier. *Experimental Eye Research*, 146, pp.17–21.

Bracha, P. et al., 2017. The acute and chronic effects of intravitreal anti-vascular endothelial growth factor injections on intraocular pressure: A Review. *Survey of ophthalmology*, 8(0), pp.743–747. Available at: http://www.ncbi.nlm.nih.gov/pubmed/28882597.

Bradley, J.M.B. et al., 1998. Effect of matrix metalloproteinases activity on outflow in perfused human organ culture. *Investigative Ophthalmology and Visual Science*, 39(13), pp.2649–2658.

Braunger, B.M., Fuchshofer, R. & Tamm, E.R., 2015a. The aqueous humor outflow pathways in glaucoma: A unifying concept of disease mechanisms and causative treatment. *European Journal of Pharmaceutics and Biopharmaceutics*, 95, pp.173–181. Available at: http://dx.doi.org/10.1016/j.ejpb.2015.04.029.

Braunger, B.M., Fuchshofer, R. & Tamm, E.R., 2015b. The aqueous humor outflow pathways in glaucoma: A unifying concept of disease mechanisms and causative treatment. *European Journal of Pharmaceutics and Biopharmaceutics*, 95, pp.173–181.

Brilakis, H.S. & Johnson, D.H., 2001. Giant vacuole survival time and implications for aqueous humor outflow. *Journal of glaucoma*, 10, pp.277–283.

Brooks, A.M. & Gillies, W.E., 1992. Ocular beta-blockers in glaucoma management.

Clinical pharmacological aspects. *Drugs & aging*, 2(3), pp.208–21. Available at: http://www.ncbi.nlm.nih.gov/pubmed/1351412.

Brubaker, R.F., 1997. Chapter 9 Clinical Measurements of Aqueous Dynamics: lmplications for Addressing Glaucoma. *Current Topics in Membranes and Transport*, 45(C), pp.233–284.

Brubaker, R.F., 2004. Goldmann's equation and clinical measures of aqueous dynamics. *Experimental Eye Research*, 78(3), pp.633–637.

Buie, L.K.K. et al., 2010. Self-complementary AAV virus (scAAV) safe and long-term gene transfer in the trabecular meshwork of living rats and monkeys. *Investigative Ophthalmology and Visual Science*, 51(1), pp.236–248.

Burgoyne, C.F., 2011. A biomechanical paradigm for axonal insult within the optic nerve head in aging and glaucoma. *Experimental eye research*, 93(2), pp.120–32. Available at: http://www.pubmedcentral.nih.gov/articlerender.fcgi?artid=3128181&tool=pmcentrez&rendertype=abstract [Accessed July 13, 2014].

Campbell, M. et al., 2009. An experimental platform for systemic drug delivery to the retina. *Proceedings of the National Academy of Sciences of the United States of America*, 106(42), pp.17817–17822.

Campbell, M. et al., 2008. RNAi-mediated reversible opening of the blood-brain barrier. *Journal of Gene Medicine*, 10(8), pp.930–947.

Campbell, M. et al., 2011. Systemic low-molecular weight drug delivery to pre-selected neuronal regions. *EMBO Molecular Medicine*, 3(4), pp.235–245.

Campbell, M. et al., 2012. Targeted suppression of claudin-5 decreases cerebral oedema and improves cognitive outcome following traumatic brain injury. *Nature communications*, 3(May), p.849. Available at: http://www.ncbi.nlm.nih.gov/pubmed/22617289.

Campbell, M. & Humphries, P., 2012. The blood-retina barrier tight junctions and barrier modulation. *Advances in Experimental Medicine and Biology*, 763, pp.70–84.

Camras, C.B., 1996. Comparison of latanoprost and timolol in patients with ocular hypertension and glaucoma: a six-month masked, multicenter trial in the United States. The United States Latanoprost Study Group. *Ophthalmology*, 103(1), pp.138–47. Available at: http://linkinghub.elsevier.com/retrieve/pii/S0161642096307495%5Cnhttp://ww

w.ncbi.nlm.nih.gov/pubmed/8628544.

Camras, L.J. et al., 2010. Duration of anesthesia affects intraocular pressure, but not outflow facility in mice. *Current eye research*, 35(9), pp.819–827.

Capaldo, C.T. & Nusrat, A., 2010. Cytokine regulation of tight junctions. *Biochim Biophys Acta*, 1788(4), pp.864–871. Available at: http://dx.doi.org/10.1016/j.bbamem.2008.08.027.

Cayrol, C. & Girard, J.-P., 2009. The IL-1-like cytokine IL-33 is inactivated after maturation by caspase-1. *Proceedings of the National Academy of Sciences*, 106(22), pp.9021–9026. Available at: http://www.pnas.org/cgi/doi/10.1073/pnas.0812690106.

Challa, P., 2009. Glaucoma genetics. *International Ophthalmology*, 48(4), pp.1–18.

Chang, I.L. et al., 1991. Expression of Modified Low-Density-Lipoprotein Receptors by Trabecular Meshwork Cells. *Current Eye Research*, 10(12), pp.1101–1112.

Chang, J.Y.H. et al., 2015. Role of nitric oxide in murine conventional outflow physiology. *American Journal of Physiology - Cell Physiology*, 309(4), pp.C205–C214. Available at: http://ajpcell.physiology.org/lookup/doi/10.1152/ajpcell.00347.2014.

Chen, G.Y. & Nuñez, G., 2010. Sterile inflammation: sensing and reacting to damage. *Nature Reviews Immunology*, 10(12), pp.826–837. Available at: http://www.nature.com/doifinder/10.1038/nri2873.

Chen, H. et al., 2011. Optic neuropathy due to microbead-induced elevated intraocular pressure in the mouse. *Investigative Ophthalmology and Visual Science*, 52(1), pp.36–44.

Civan, M.M. & Macknight, A.D.C., 2004. The ins and outs of aqueous humour secretion. *Experimental Eye Research*, 78(3), pp.625–631.

Clark, A.F. et al., 1995. Dexamethasone-induced ocular hypertension in perfusion-cultured human eyes. *Investigative Ophthalmology and Visual Science*, 36(2), pp.478–489.

Claude, P. & Goodenough, D.A., 1973. FRACTURE FACES OF ZONULAE OCCLUDENTES FROM " TIGHT " AND " LEAKY " EPITHELIA From the Department of Neurobiology and the Department of Anatomy , Harvard Medical School ,. , 58, pp.390–400.

Cone, F.E. et al., 2012. The effects of anesthesia, mouse strain and age on intraocular pressure and an improved murine model of experimental glaucoma. *Experimental*

Eye Research, 99(1), pp.27–35.

Crowston, J.G. et al., 2004. Effect of latanoprost on outflow facility in the mouse. *Investigative Ophthalmology and Visual Science*, 45(7), pp.2240–2245.

Davis, B.K., Wen, H. & Ting, J.P.-Y., 2011. The Inflammasome NLRs in Immunity, Inflammation, and Associated Diseases. *Annual Review of Immunology*, 29(1), pp.707–735. Available at: http://www.annualreviews.org/doi/10.1146/annurev-immunol-031210-101405.

Denninger, A.R. et al., 2015. Claudin-11 Tight Junctions in Myelin Are a Barrier to Diffusion and Lack Strong Adhesive Properties. *Biophysical Journal*, 109(7), pp.1387–1397.

Dinarello, C.A. et al., 2013. Interleukin-18 and IL-18 binding protein. *Frontiers in Immunology*, 4(OCT).

Ding, C., Wang, P. & Tian, N., 2011. Effect of general anesthetics on IOP in elevated IOP mouse model. *Experimental Eye Research*, 92(6), pp.512–520.

Doyle, S.L. et al., 2014. IL-18 Attenuates Experimental Choroidal Neovascularization as a Potential Therapy for Wet Age-Related Macular Degeneration. *Science Translational Medicine*, 6(230), p.230ra44-230ra44. Available at: http://stm.sciencemag.org/cgi/doi/10.1126/scitranslmed.3007616.

Doyle, S.L. et al., 2015. IL-18 immunotherapy for neovascular AMD: Tolerability and efficacy in nonhuman primates. *Investigative Ophthalmology and Visual Science*, 56(9), pp.5424–5430.

Doyle, S.L. & O'Neill, L. a J., 2006. Toll-like receptors: From the discovery of NFKappaB to new insights into transcriptional regulations in innate immunity. *Biochemical Pharmacology*, 72(9 SPEC. ISS.), pp.1102–1113.

Ebnet, K. et al., 2004. Junctional adhesion molecules (JAMs): more molecules with dual functions? *Journal of cell science*, 117, pp.19–29.

Emi, K., Pederson, J.E. & Toris, C.B., 1989. Hydrostatic pressure of the suprachoroidal space. *Investigative Ophthalmology and Visual Science*, 30(2), pp.233–238.

Epstein, D.L. & Rohen, J.W., 1991. Morphology of the trabecular meshwork and inner-wall endothelium after cationized ferritin perfusion in the monkey eye. *Investigative Ophthalmology and Visual Science*, 32(1), pp.160–171.

Ethier, C.R. et al., 1986. Calculations of flow resistance in the juxtacanalicular meshwork. *Investigative Ophthalmology and Visual Science*, 27(12), pp.1741–1750.

Ethier, C.R. et al., 1998. Two pore types in the inner-wall endothelium of Schlemm's canal. *Investigative Ophthalmology and Visual Science*, 39(11), pp.2041–2048.

Ethier, C.R., Ajersch, P. & Pirog, R., 1993. An improved ocular perfusion system. *Current eye research*, 12(8), pp.765–770.

Ethier, C.R. & Chan, D.W.H., 2001. Cationic ferritin changes outflow facility in human eyes whereas anionic ferritin does not. *Investigative Ophthalmology and Visual Science*, 42(8), pp.1795–1802.

Fanning, A.S. et al., 1998. The tight junction protein ZO-1 establishes a link between the transmembrane protein occludin and the actin cytoskeleton. *Journal of Biological Chemistry*, 273(45), pp.29745–29753.

Farquhar, M.G. & Palade, G.E., 1963. Junctional complexes in various epithelia. *The Journal of cell biology*, 17, pp.375–412.

Fechtner, R. & Weinreb, R., 1994. Mechanisms of optic nerve damage in primary open angle glaucoma. *Survey of Ophthalmology*, 39(1), pp.23–42. Available at: http://www.sciencedirect.com/science/article/pii/S0039625705800426%5Cnhttp://www.sciencedirect.com/science?_ob=MiamiImageURL&_cid=271199&_user=5674931&_pii=S0039625705800426&_check=y&_origin=article&_zone=toolbar&_coverDate=31-Aug-1994&view=c&originConten.

Fingert, J.H. et al., 1999. Analysis of myocilin mutations in 1703 glaucoma patients from five different populations. *Human molecular genetics*, 8(5), pp.899–905. Available at: http://www.ncbi.nlm.nih.gov/pubmed/10196380.

Fingert, J.H., 2011. Primary open-angle glaucoma genes. *Eye*, 25(5), pp.587–595. Available at: http://www.nature.com/doifinder/10.1038/eye.2011.97.

Flammer, J. & Orgül, S., 1998. Optic nerve blood-flow abnormalities in glaucoma. *Progress in Retinal and Eye Research*, 17(2), pp.267–289.

Freddo, T.F., 2013. A contemporary concept of the blood-aqueous barrier. *Progress in Retinal and Eye Research*, 32(1), pp.181–195.

French, A.D. et al., 2009. PKC and PKA Phosphorylation Affect the Subcellular Localization of Claudin-1 in Melanoma Cells. *International Journal of Medical Sciences*, 6(2), pp.93–101.

Fujimoto, K., 1995. Freeze-fracture replica electron microscopy combined with SDS digestion for cytochemical labeling of integral membrane proteins. Application to the immunogold labeling of intercellular junctional complexes. *Journal of cell science*, 108, pp.3443–3449.

Furuse, M. et al., 1998. Claudin-1 and -2: novel integral membrane proteins localizing at tight junctions with no sequence homology to occludin. *The Journal of Cell Biology*, 141(7), pp.1539–1550.

Furuse, M., Sasaki, H. & Tsukita, S., 1999. Manner of interaction of heterogeneous claudin species within and between tight junction strands. *Journal of Cell Biology*, 147(4), pp.891–903.

Gaton, D.D. et al., 2001. Increased matrix metalloproteinases 1, 2, and 3 in the monkey uveoscleral outflow pathway after topical prostaglandin F(2 alpha)-isopropyl ester treatment. *Archives of Ophthalmology*, 119(8), pp.1165–70. Available at: http://www.ncbi.nlm.nih.gov/pubmed/11483084.

Gerdes, N. et al., 2002. Expression of Interleukin (IL)-18 and Functional IL-18 Receptor on Human Vascular Endothelial Cells, Smooth Muscle Cells, and Macrophages: Implications for Atherogenesis. *J. Exp. Med*, 12451300(2), pp.245–257. Available at: http://www.jem.org/cgi/content/full/195/2/245.

Goel, M. et al., 2010. Aqueous humor dynamics: a review. *The open ophthalmology journal*, 4, pp.52–9. Available at: http://www.pubmedcentral.nih.gov/articlerender.fcgi?artid=3032230&tool=pmcentrez&rendertype=abstract.

Gong, H. et al., 2002. A new view of the human trabecular meshwork using quick-freeze, deep-etch electron microscopy. *Exp Eye Res*, 75(3), pp.347–358. Available at: http://www.ncbi.nlm.nih.gov/pubmed/12384097.

Gonzalez-Mariscal, L., Garay, E. & Quiros, M., 2010. *Regulation of Claudins by Posttranslational Modifications and Cell-Signaling Cascades*,

Gordon, M.O. et al., 2002. The Ocular Hypertension Treatment Study: baseline factors that predict the onset of primary open-angle glaucoma. *Archives of ophthalmology*, 120(6), pp.714-20-30. Available at: http://www.ncbi.nlm.nih.gov/pubmed/12049575.

Gringhuis, S.I. et al., 2012. Dectin-1 is an extracellular pathogen sensor for the induction and processing of IL-1β via a noncanonical caspase-8 inflammasome. *Nature Immunology*, 13(3), pp.246–254. Available at: http://www.nature.com/doifinder/10.1038/ni.2222.

Gross, R.L. et al., 2003. A mouse model of elevated intraocular pressure: retina and optic nerve findings. *Transactions of the American Ophthalmological Society*, 101, pp.163-9-71. Available at:

http://www.ncbi.nlm.nih.gov/pubmed/14971574%5Cnhttp://www.pubmedcentral.nih.gov/articlerender.fcgi?artid=PMC1358985.

Gunzel, D. & Yu, A.S.L., 2013. Claudins and the Modulation of Tight Junction Permeability. *Physiological Reviews*, 93(2), pp.525–569. Available at: http://physrev.physiology.org/cgi/doi/10.1152/physrev.00019.2012.

Hamanaka, T. & Bill, A., 1987. Morphological and functional effects of Na2EDTA on the outflow routes for aqueous humor in monkeys. *Experimental Eye Research*, 44(2), pp.171–190.

Harris, A. et al., 1998. Regulation of Retinal and Optic Nerve Blood Flow. *Arch Ophthalmol*, 116(11), pp.1491–1495. Available at: http://archopht.ama-assn.org/cgi/content/abstract/116/11/1491%5Cnhttp://archopht.ama-assn.org/cgi/reprint/116/11/1491.pdf.

Harris, A. et al., 2005. The role of optic nerve blood flow in the pathogenesis of glaucoma. *Ophthalmology Clinics of North America*, 18(3), pp.345–353.

He, M. et al., 2006. Angle-closure glaucoma in East Asian and European people. Different diseases? *Eye (London, England)*, 20(1), pp.3–12.

Heijl, A. et al., 2002. Reduction of intraocular pressure and glaucoma progression: results from the Early Manifest Glaucoma Trial. *Archives of ophthalmology (Chicago, Ill. : 1960)*, 120(10), pp.1268–1279.

Heys, J.J. & Barocas, V.H., 2002. A Boussinesq model of natural convection in the human eye and the formation of Krukenberg's spindle. *Annals of Biomedical Engineering*, 30(3), pp.392–401.

Hoehn, R. et al., 2013. Distribution of intraocular pressure and its association with ocular features and cardiovascular risk factors: The gutenberg health study. *Ophthalmology*, 120(5), pp.961–968.

Howell, G.R. et al., 2007. Absence of glaucoma in DBA/2J mice homozygous for wild-type versions of Gpnmb and Tyrp1. *BMC Genetics*, 8(1), p.45. Available at: http://bmcgenet.biomedcentral.com/articles/10.1186/1471-2156-8-45.

Ikari, A. et al., 2008. Claudin-16 is directly phosphorylated by protein kinase A independently of a vasodilator-stimulated phosphoprotein-mediated pathway. *Journal of Cellular Physiology*, 214(1), pp.221–229.

Ikenouchi, J. et al., 2005. Tricellulin constitutes a novel barrier at tricellular contacts of epithelial cells. *Journal of Cell Biology*, 171(6), pp.939–945.

Ishizaki, T. et al., 2003. Cyclic AMP induces phosphorylation of claudin-5

immunoprecipitates and expression of claudin-5 gene in blood-brain-barrier endothelial cells via protein kinase A-dependent and -independent pathways. *Experimental Cell Research*, 290(2), pp.275–288.

Itallie, C.M. et al., 2010. ZO-1 Stabilizes the Tight Junction Solute Barrier through Coupling to the Perijunctional Cytoskeleton. *Molecular biology of the cell*, 21(22), pp.4042–4056.

Van Itallie, C.M. et al., 2006. Two splice variants of claudin-10 in the kidney create paracellular pores with different ion selectivities. *American journal of physiology. Renal physiology*, 291(6), pp.F1288–F1299.

Jackson, T.L. et al., 2006. Human scleral hydraulic conductivity: Age-related changes, topographical variation, and potential scleral outflow facility. *Investigative Ophthalmology and Visual Science*, 47(11), pp.4942–4946.

Jacobson, N. et al., 2001. Non-secretion of mutant proteins of the glaucoma gene myocilin in cultured trabecular meshwork cells and in aqueous humor. *Human molecular genetics*, 10(2), pp.117–125.

Janssen, S.F. et al., 2013. The vast complexity of primary open angle glaucoma: Disease genes, risks, molecular mechanisms and pathobiology. *Progress in Retinal and Eye Research*, 37, pp.31–67.

Ji, J. et al., 2005. Effects of elevated intraocular pressure on mouse retinal ganglion cells. *Vision Research*, 45(2), pp.169–179.

John, S.W.M. et al., 1998. Essential iris atrophy, pigment dispersion, and glaucoma in DBA/2J mice. *Investigative Ophthalmology and Visual Science*, 39(6), pp.951–962.

Johnson, M. et al., 1992. Modulation of outflow resistance by the pores of the inner wall endothelium. *Investigative Ophthalmology and Visual Science*, 33(5), pp.1670–1675.

Johnson, M. et al., 2002. The pore density in the inner wall endothelium of Schlemm's canal of glaucomatous eyes. *Investigative Ophthalmology and Visual Science*, 43(9), pp.2950–2955.

Johnson, M., 2006. What controls aqueous humour outflow resistance? *Experimental Eye Research*, 82(4), pp.545–557.

Johnson, M., McLaren, J.W. & Overby, D.R., 2015. Unconventional aqueous humor outflow: A review. *Experimental Eye Research*, pp.1–18. Available at: http://dx.doi.org/10.1016/j.exer.2016.01.017.

Jorge, J.M.M. et al., 2008. Correlations between corneal biomechanical properties measured with the ocular response analyzer and ICare rebound tonometry. *Journal of glaucoma*, 17(6), pp.442–8. Available at: http://www.ncbi.nlm.nih.gov/pubmed/18794677.

Kahlenberg, J.M. & Dubyak, G.R., 2004. Mechanisms of caspase-1 activation by P2X7 receptor-mediated K+ release. *American journal of physiology. Cell physiology*, 286(5), pp.C1100-8. Available at: http://www.ncbi.nlm.nih.gov/pubmed/15075209.

Kanneganti, T.D. et al., 2007. Pannexin-1-Mediated Recognition of Bacterial Molecules Activates the Cryopyrin Inflammasome Independent of Toll-like Receptor Signaling. *Immunity*, 26(4), pp.433–443.

Kasetti, R.B. et al., 2016. Expression of mutant myocilin induces abnormal intracellular accumulation of selected extracellular matrix proteins in the trabecular meshwork. *Investigative Ophthalmology and Visual Science*, 57(14), pp.6058–6069.

Kass, M.A. et al., 2002. The Ocular Hypertension Treatment Study: a randomized trial determines that topical ocular hypotensive medication delays or prevents the onset of primary open-angle glaucoma. *Archives of ophthalmology (Chicago, Ill. : 1960)*, 120(6), pp.701–730.

de Kater, A.W., Melamed, S. & Epstein, D.L., 1989. Patterns of aqueous humor outflow in glaucomatous and nonglaucomatous human eyes. A tracer study using cationized ferritin. *Archives of ophthalmology (Chicago, Ill. : 1960)*, 107(4), pp.572–6. Available at: http://www.ncbi.nlm.nih.gov/pubmed/2705927.

Keaney, J. et al., 2015. Autoregulated paracellular clearance of amyloid-β across the blood-brain barrier. *Sci Adv.*, 1(8), pp.1–24.

Keller, K.E. et al., 2011. Segmental versican expression in the trabecular meshwork and involvement in outflow facility. *Investigative Ophthalmology and Visual Science*, 52(8), pp.5049–5057.

Kessel, L. et al., 2010. The relationship between body and ambient temperature and corneal temperature. *Investigative Ophthalmology and Visual Science*, 51(12), pp.6593–6597.

Kiddee, W. et al., 2013. Intraocular Pressure Monitoring Post Intravitreal Steroids: A Systematic Review. *Survey of Ophthalmology*, 58(4), pp.291–310.

Krohn, J. & Bertelsen, T., 1997. Corrosion casts of the suprachoroidal space and uveoscleral drainage routes in the human eye. *Acta ophthalmologica*

Scandinavica, 75(1), pp.32–5. Available at: http://www.ncbi.nlm.nih.gov/pubmed/9088397.

Krug, S.M. et al., 2012. Claudin-17 forms tight junction channels with distinct anion selectivity. *Cellular and Molecular Life Sciences*, 69(16), pp.2765–2778.

Krug, S.M. et al., 2009. Tricellulin forms a barrier to macromolecules in tricellular tight junctions without affecting ion permeability. *Molecular biology of the cell*, 20(16), pp.3713–24. Available at: http://www.pubmedcentral.nih.gov/articlerender.fcgi?artid=2777931&tool=pmcentrez&rendertype=abstract.

Kwon, Y.H. et al., 2009. Primary open-angle glaucoma. *The New England Journal of Medicine*, 360(11), pp.1113–1124. Available at: http://www.pubmedcentral.nih.gov/articlerender.fcgi?artid=3207715&tool=pmcentrez&rendertype=abstract.

Lapointe, T.K. & Buret, a. G., 2012. Interleukin-18 facilitates neutrophil transmigration via myosin light chain kinase-dependent disruption of occludin, without altering epithelial permeability. *AJP: Gastrointestinal and Liver Physiology*, 302(3), pp.G343–G351.

Lee, D.A. & Higginbotham, E.J., 2005. Glaucoma and its treatment : A review. , 62, pp.691–699.

Lee, R.K., 2008. The molecular pathophysiology of pseudoexfoliation glaucoma. *Current opinion in ophthalmology*, 19(2), pp.95–101.

Lei, Y. et al., 2011. Outflow physiology of the mouse eye: pressure dependence and washout. *Investigative ophthalmology & visual science*, 52(3), pp.1865–71. Available at: http://www.pubmedcentral.nih.gov/articlerender.fcgi?artid=3101677&tool=pmcentrez&rendertype=abstract [Accessed June 9, 2014].

Li, G. et al., 2013. Optimizing gene transfer to conventional outflow cells in living mouse eyes. *Experimental eye research*, 109, pp.8–16. Available at: http://www.pubmedcentral.nih.gov/articlerender.fcgi?artid=3615119&tool=pmcentrez&rendertype=abstract [Accessed July 8, 2014].

Li, T. et al., 2016. Comparative Effectiveness of First-Line Medications for Primary Open-Angle Glaucoma: A Systematic Review and Network Meta-analysis. *Ophthalmology*, 123(1), pp.129–140. Available at: http://dx.doi.org/10.1016/j.ophtha.2015.09.005.

Libby, R.T. et al., 2005. Inherited glaucoma in DBA/2J mice: Pertinent disease features for studying the neurodegeneration. *Visual Neuroscience*, 22(5), pp.637–648. Available at: http://www.journals.cambridge.org/abstract_S0952523805225130.

Liu, H.-H. et al., 2017. A Mouse Model of Chronic Ocular Hypertension Induced by Circumlimbal Suture. *Doi.Org*, 151(1), p.353. Available at: http://iovs.arvojournals.org.proxy.library.adelaide.edu.au/article.aspx?articleid=2599711.

Liu, Y. & Allingham, R.R., 2017. Major review: Molecular genetics of primary open-angle glaucoma. *Experimental Eye Research*, 160, pp.62–84.

Llobet, A., Gasull, X. & Gual, A., 2003. Understanding trabecular meshwork physiology: a key to the control of intraocular pressure? *News in physiological sciences : an international journal of physiology produced jointly by the International Union of Physiological Sciences and the American Physiological Society*, 18, pp.205–9. Available at: http://www.ncbi.nlm.nih.gov/pubmed/14500801.

Lu, Z. et al., 2008. The mechanism of increasing outflow facility by rho-kinase inhibition with Y-27632 in bovine eyes. *Experimental Eye Research*, 86(2), pp.271–281.

Lucia, U. et al., 2016. Constructal approach to bio-engineering: the ocular anterior chamber temperature. *Scientific Reports*, 6, p.31099. Available at: http://dx.doi.org/10.1038/srep31099%5Cnhttp://www.nature.com/articles/srep31099.

Lukens, J.R., Gross, J.M. & Kanneganti, T.D., 2012. IL-1 family cytokines trigger sterile inflammatory disease. *Frontiers in Immunology*, 3(OCT).

Luo, C. et al., 2010. Glaucomatous tissue stress and the regulation of immune response through glial Toll-like receptor signaling. *Investigative ophthalmology & visual science*, 51(11), pp.5697–707. Available at: http://www.pubmedcentral.nih.gov/articlerender.fcgi?artid=3061506&tool=pmcentrez&rendertype=abstract.

Madekurozwa, M. et al., 2017. Direct measurement of pressure-independent aqueous humour flow using iPerfusion. *Experimental Eye Research*, 162, pp.129–138. Available at: http://linkinghub.elsevier.com/retrieve/pii/S0014483517301410.

Mäepea, O. & Bill, A., 1989. The pressures in the episcleral veins, Schlemm's canal and the trabecular meshwork in monkeys: Effects of changes in intraocular

pressure. *Experimental Eye Research*, 49(4), pp.645–663.

Mallick, J. et al., 2016. Update on Normal Tension Glaucoma. *Journal of ophthalmic & vision research*, 11(2), pp.204–8. Available at: http://www.ncbi.nlm.nih.gov/pubmed/27413503.

Mapstone, R., 1968. DETERMINANTS OF CORNEAL TEMPERATURE. *Brit. J. Ophthal*, 52, pp.729–741.

De Marco, N. et al., 2006. Optineurin increases cell survival and translocates to the nucleus in a Rab8-dependent manner upon an apoptotic stimulus. *Journal of Biological Chemistry*, 281(23), pp.16147–16156.

Mark, H.H., 2010. Aqueous Humor Dynamics in Historical Perspective. *Survey of Ophthalmology*, 55(1), pp.89–100.

Mastropasqua, R. et al., 2014. Trans-conjunctival aqueous humor outflow in glaucomatous patients treated with prostaglandin analogues: an in vivo confocal microscopy study. *Graefe's archive for clinical and experimental ophthalmology = Albrecht von Graefes Archiv f??r klinische und experimentelle Ophthalmologie*, 252(9), pp.1469–1476.

McCabe, M.J. et al., 2016. Claudin-11 and occludin are major contributors to Sertoli cell tight junction function, in vitro. *Asian journal of andrology*, 18(4), pp.620–6. Available at: http://www.ncbi.nlm.nih.gov/pubmed/26585695%5Cnhttp://www.pubmedcentral.nih.gov/articlerender.fcgi?artid=PMC4955190%5Cnhttp://www.ajandrology.com/article.asp?issn=1008-682X;year=2016;volume=18;issue=4;spage=620;epage=626;aulast=McCabe.

Melamed, S., Ben Simon, G.J. & Levkovitch-Verbin, H., 2003. Selective laser trabeculoplasty as primary treatment for open-angle glaucoma: a prospective, nonrandomized pilot study. *Archives of ophthalmology*, 121(7), pp.957–960.

Menge, T., Jander, S. & Stoll, G., 2001. Induction of the proinflammatory cytokine interleukin-18 by axonal injury. *Journal of Neuroscience Research*, 65(4), pp.332–339.

Michelessi, M. & Lindsley, K., 2016. Peripheral iridotomy for pigmentary glaucoma. *Cochrane Database of Systematic Reviews*, 2016(2).

Morita, K. et al., 1999. Endothelial claudin: Claudin-5/TMVCF constitutes tight junction strands in endothelial cells. *Journal of Cell Biology*, 147(1), pp.185–194.

Mousa, S. & Beidoe, 2012. Current primary open-angle glaucoma treatments and future

directions. *Clinical Ophthalmology*, p.1699.

Mozaffarieh, M. & Flammer, J., 2013. New insights in the pathogenesis and treatment of normal tension glaucoma. *Current Opinion in Pharmacology*, 13(1), pp.43–49. Available at: http://dx.doi.org/10.1016/j.coph.2012.10.001.

Murphy, K., 2014. *Janeway's immunobiology*,

Nitta, T. et al., 2003. Size-selective loosening of the blood-brain barrier in claudin-5-deficient mice. *Journal of Cell Biology*, 161(3), pp.653–660.

Noecker, R.J., 2006. The management of glaucoma and intraocular hypertension: current approaches and recent advances. *Therapeutics and clinical risk management*, 2(2), pp.193–206.

Nongpiur, M.E., Ku, J.Y.F. & Aung, T., 2011. Angle closure glaucoma: a mechanistic review. *Current Opinion in Ophthalmology*, 22(2), pp.96–101. Available at: http://www.ncbi.nlm.nih.gov/pubmed/21252671.

Novick, D. et al., 2001. A NOVEL IL-18BP ELISA SHOWS ELEVATED SERUM IL-18BP IN SEPSIS AND EXTENSIVE DECREASE OF FREE IL-18. *Cytokine*, 14(6), pp.334–342. Available at: http://linkinghub.elsevier.com/retrieve/pii/S1043466601909147.

Novick, D. et al., 1999. Interleukin-18 binding protein: A novel modulator of the Th1 cytokine response. *Immunity*, 10(1), pp.127–136.

O'Callaghan, J. et al., 2017. Therapeutic potential of AAV-mediated MMP-3 secretion from corneal endothelium in treating glaucoma. *Human Molecular Genetics*, 26(7), pp.1230–1246.

Overby, D. et al., 2002. The mechanism of increasing outflow facility during washout in the bovine eye. *Investigative Ophthalmology and Visual Science*, 43(11), pp.3455–3464.

Overby, D.R., Zhou, E.H., Vargas-Pinto, R., Pedrigi, R.M., Fuchshofer, R., Braakman, S.T., Gupta, R., Perkumas, K.M., Sherwood, J.M., et al., 2014. Altered mechanobiology of Schlemm's canal endothelial cells in glaucoma. *Proceedings of the National Academy of Sciences of the United States of America*, 111(38), pp.13876–81. Available at: http://www.pubmedcentral.nih.gov/articlerender.fcgi?artid=4183270&tool=pmcentrez&rendertype=abstract.

Overby, D.R., Bertrand, J., Tektas, O.Y., Boussommier-Calleja, A., Schicht, M., Ross Ethier, C., Woodward, D.F., Daniel Stamer, W. & Lütjen-Drecoll, E., 2014.

Ultrastructural changes associated with dexamethasone-induced ocular hypertension in mice. *Investigative Ophthalmology and Visual Science*, 55(8), pp.4922–4933.

Overby, D.R. & Clark, A.F., 2015. Animal models of glucocorticoid-induced glaucoma. *Experimental Eye Research*, 141, pp.15–22.

Overby, D.R., Stamer, W.D. & Johnson, M., 2009. The changing paradigm of outflow resistance generation: towards synergistic models of the JCT and inner wall endothelium. *Experimental eye research*, 88(4), pp.656–70. Available at: http://www.pubmedcentral.nih.gov/articlerender.fcgi?artid=2744486&tool=pmcentrez&rendertype=abstract [Accessed July 8, 2014].

Pasutto, F. et al., 2012. Variants in ASB10 are associated with open-angle glaucoma. *Human Molecular Genetics*, 21(6), pp.1336–1349.

Patel, G.C. et al., 2017. Dexamethasone-Induced Ocular Hypertension in Mice. *The American Journal of Pathology*, 187(4), pp.713–723. Available at: http://linkinghub.elsevier.com/retrieve/pii/S0002944017300263.

Pederson, J.E., Gaasterland, D.E. & MacLellan, H.M., 1977. Uveoscleral aqueous outflow in the rhesus monkey: Importance of uveal reabsorption. *Investigative Ophthalmology and Visual Science*, 16(11), pp.1008–1017.

Pedrigi, R.M. et al., 2011. A model of giant vacuole dynamics in human Schlemm's canal endothelial cells. *Experimental Eye Research*, 92(1), pp.57–66.

Pena, J.D.O. et al., 1999. Enhanced Tenascin Expression Associated with Reactive Astrocytes in Human Optic Nerve Heads with Primary Open Angle Glaucoma. *Experimental Eye Research*, 68(1), pp.29–40. Available at: http://linkinghub.elsevier.com/retrieve/pii/S0014483598905772.

Perkumas, K.M. & Stamer, W.D., 2012. Protein markers and differentiation in culture for Schlemm's canal endothelial cells. *Experimental Eye Research*, 96(1), pp.82–87.

Polansky, J.R. et al., 1979. Human trabecular cells. I. Establishment in tissue culture and growth characteristics. *Investigative ophthalmology & visual science*, 18(10), pp.1043–1049.

Polansky, J.R., Fauss, D.J. & Zimmerman, C.C., 2000. Regulation of TIGR/MYOC gene expression in human trabecular meshwork cells. *Eye (Lond)*, 14 (Pt 3B, pp.503–514. Available at: http://www.ncbi.nlm.nih.gov/pubmed/11026980.

Polansky, J.R., Weinreb, R. & Alvarado, J.A., 1981. Studies on human trabecular cells

propagated in vitro. *Vision Research*, 21(1), pp.155–160.

Poulsen, P.B. et al., 2005. Cost analysis of glaucoma-related-blindness in Europe. *International Congress Series*, 1282, pp.262–266. Available at: http://linkinghub.elsevier.com/retrieve/pii/S0531513105008484 [Accessed July 13, 2014].

Prum, B.E. et al., 2016. Primary Open-Angle Glaucoma Preferred Practice Pattern® Guidelines. *Ophthalmology*, 123(1), pp.P41–P111. Available at: http://linkinghub.elsevier.com/retrieve/pii/S0161642015012762.

Purves, D. et al., 2001. Neuroscience. 2nd edition. *Sunderland (MA): Sinauer Associates; 2001.*, pp.109–12.

Puyang, Z. et al., 2016. Retinal Ganglion Cell Loss is Delayed Following Optic Nerve Crush in NLRP3 Knockout Mice. *Scientific reports*, 6, p.20998. Available at: http://www.nature.com/articles/srep20998%5Cnpapers3://publication/doi/10.1038/srep20998.

Quigley, H.A. et al., 2000. Retrograde axonal transport of BDNF in retinal ganglion cells is blocked by acute IOP elevation in rats. *Investigative Ophthalmology and Visual Science*, 41(11), pp.3460–3466.

Raviola, G. & Raviola, E., 1981. Paracellular route of aqueous outflow in the trabecular meshwork and canal of Schlemm. A freeze-fracture study of the endothelial junctions in the sclerocorneal angle of the macaque monkey eye. *Investigative Ophthalmology and Visual Science*, 21(1 II), pp.52–72.

Reina-Torres, E. et al., 2017. VEGF as a paracrine regulator of conventional outflow facility. *Investigative Ophthalmology and Visual Science*, 58(3), pp.1899–1908.

Ren, R. et al., 2016. Outflow facility in human eyes through multiple mechanisms. *Investigative Ophthalmology and Visual Science*, 57(14), pp.6197–6209.

Resch, Z.T. & Fautsch, M.P., 2009. Glaucoma-associated myocilin: A better understanding but much more to learn. *Experimental Eye Research*, 88(4), pp.704–712.

Rezaie, T., 2002. Adult-Onset Primary Open-Angle Glaucoma Caused by Mutations in Optineurin. *Science*, 295(5557), pp.1077–1079. Available at: http://www.sciencemag.org/cgi/doi/10.1126/science.1066901.

Rock, K.L. et al., 2010. The Sterile Inflammatory Response. *Annual Review of Immunology*, 28(1), pp.321–342. Available at: http://www.annualreviews.org/doi/10.1146/annurev-immunol-030409-101311.

Ruiz-Ederra, J. & Verkman, A.S., 2006. Mouse model of sustained elevation in intraocular pressure produced by episcleral vein occlusion. *Experimental Eye Research*, 82(5), pp.879–884.

Rulli, E. et al., 2013. Efficacy and Safety of Trabeculectomy vs Nonpenetrating Surgical Procedures. *JAMA Ophthalmology*, 131(12), p.1573. Available at: http://archopht.jamanetwork.com/article.aspx?doi=10.1001/jamaophthalmol.2013.5059.

Sagara, T. et al., 1999. Topical prostaglandin F2alpha treatment reduces collagen types I, III, and IV in the monkey uveoscleral outflow pathway. *Archives of Ophthalmology*, 117(6), pp.794–801.

Scherer, W.J., 2002. A retrospective review of non-responders to latanoprost. *Journal of ocular pharmacology and therapeutics : the official journal of the Association for Ocular Pharmacology and Therapeutics*, 18(3), pp.287–91. Available at: http://www.ncbi.nlm.nih.gov/pubmed/12099549.

Schlamp, C.L. et al., 2006. Progressive ganglion cell loss and optic nerve degeneration in DBA/2J mice is variable and asymmetric. *BMC neuroscience*, 7, p.66.

Schlötzer-Schrehardt, U. & Naumann, G.O.H., 2006. Ocular and Systemic Pseudoexfoliation Syndrome. *American Journal of Ophthalmology*, 141(5).

Schneeberger, E.E. & Karnovsky, M.J., 1976. Substructure of intercellular junctions in freeze-fractured alveolar-capillary membranes of mouse lung. *Circulation research*, 38(5), pp.404–411.

Schroder, K. & Tschopp, J., 2010. The Inflammasomes. *Cell*, 140(6), pp.821–832.

Shao, B.Z. et al., 2015. NLRP3 inflammasome and its inhibitors: A review. *Frontiers in Pharmacology*, 6(NOV).

Shen, J. et al., 2014. Interleukin-18 has antipermeablity and antiangiogenic activities in the eye: Reciprocal suppression with VEGF. *Journal of Cellular Physiology*, 229(8), pp.974–983.

Shepard, A.R. et al., 2007. Glaucoma-causing myocilin mutants require the Peroxisomal targeting signal-1 receptor (PTS1R) to elevate intraocular pressure. *Human Molecular Genetics*, 16(6), pp.609–617.

Sherwood, J.M. et al., 2016. Measurement of outflow facility using iPerfusion. *PLoS ONE*, 11(3).

Sit, A.J. et al., 1997. Factors affecting the pores of the inner wall endothelium of Schlemm's canal. *Investigative Ophthalmology and Visual Science*, 38(8),

pp.1517–1525.

Snyder, R.W. et al., 1993. Corticosteroid Treatment and Trabecular Meshwork Proteases in Cell and Organ Culture Supernatants. *Experimental Eye Research*, 57(4), pp.461–468.

Soto, I. & Howell, G.R., 2014. The complex role of neuroinflammation in glaucoma. *Cold Spring Harbor Perspectives in Medicine*, 4(8), p.14.

Stamer, D.W. et al., 2000. Isolation of primary open-angle glaucomatous trabecular meshwork cells from whole eye tissue. *Current eye research*, 20(5), pp.347–350.

Stamer, W.D. et al., 2015. Biomechanics of Schlemm's canal endothelium and intraocular pressure reduction. *Progress in Retinal and Eye Research*, 44, pp.86–98.

Stamer, W.D. et al., 2011. eNOS, a pressure-dependent regulator of intraocular pressure. *Investigative ophthalmology & visual science*, 52(13), pp.9438–44. Available at: http://www.pubmedcentral.nih.gov/articlerender.fcgi?artid=3293415&tool=pmcentrez&rendertype=abstract [Accessed May 26, 2014].

Stamer, W.D. et al., 1998. Isolation, culture, and characterization of endothelial cells from Schlemm's canal. *Investigative Ophthalmology and Visual Science*, 39(10), pp.1804–1812.

Stamer, W.D. et al., 1995. Isolation and culture of human trabecular meshwork cells by extracellular matrix digestion. *Current eye research*, 14(7), pp.611–7. Available at: http://www.ncbi.nlm.nih.gov/pubmed/7587308%5Cnhttp://www.tandfonline.com/doi/abs/10.3109/02713689508998409.

Stamer, W.D., 2012. The cell and molecular biology of glaucoma: mechanisms in the conventional outflow pathway. *Investigative ophthalmology & visual science*, 53(5), pp.2470–2. Available at: http://www.ncbi.nlm.nih.gov/pubmed/22562843 [Accessed July 8, 2014].

Stamer, W.D. & Acott, T.S., 2012. Current understanding of conventional outflow dysfunction in glaucoma. *Current Opinion in Ophthalmology*, 23(2), pp.135–143.

Stein, J.D. & Challa, P., 2007. Mechanisms of action and efficacy of argon laser trabeculoplasty and selective laser trabeculoplasty. *Current opinion in ophthalmology*, 18(2), pp.140–5. Available at: http://www.ncbi.nlm.nih.gov/pubmed/17301616.

Stevenson, B.R. et al., 1986. Identification of ZO-1: A high molecular weight polypeptide associated with the tight junction (Zonula Occludens) in a variety of epithelia. *Journal of Cell Biology*, 103(3), pp.755–766.

Stone, E.M., 1997. Identification of a Gene That Causes Primary Open Angle Glaucoma. *Science*, 275(5300), pp.668–670. Available at: http://www.sciencemag.org/cgi/doi/10.1126/science.275.5300.668.

Sugimoto, E. et al., 2006. Effect of light cycle on 24-hour pattern of mouse intraocular pressure. *J Glaucoma*, 15(6), pp.505–511. Available at: http://www.ncbi.nlm.nih.gov/pubmed/17106363%5Cnhttp://graphics.tx.ovid.com/ovftpdfs/FPDDNCOBMFAOMO00/fs046/ovft/live/gv023/00061198/00061198-200612000-00006.pdf%5Cnhttp://content.wkhealth.com/linkback/openurl?sid=WKPTLP:landingpage&an=00061198-200612000-0.

Suzuki, H. et al., 2015. Model for the architecture of claudin-based paracellular ion channels through tight junctions. *Journal of Molecular Biology*, 427(2), pp.291–297.

Svedbergh, B. & Bill, A., 1972. Scanning electron microscopic studies of the corneal endothelium in man and monkeys. *Acta ophthalmologica*, 50(3), pp.321–36. Available at: http://www.ncbi.nlm.nih.gov/pubmed/4628789.

Tamm, E.R., 2014. Functional Morphology of the Trabecular Meshwork Outflow Pathways. In *Glaucoma: Second Edition*. pp. 40–46.

Tamm, E.R., 2009. The trabecular meshwork outflow pathways: Structural and functional aspects. *Experimental Eye Research*, 88(4), pp.648–655.

Tanaka, M., Kamata, R. & Sakai, R., 2005. EphA2 phosphorylates the cytoplasmic tail of claudin-4 and mediates paracellular permeability. *Journal of Biological Chemistry*, 280(51), pp.42375–42382.

Tawara, A. et al., 2008. Immunohistochemical evaluation of the extracellular matrix in trabecular meshwork in steroid-induced glaucoma. *Graefe's Archive for Clinical and Experimental Ophthalmology*, 246(7), pp.1021–1028.

Templeton, J.P. & Geisert, E.E., 2012. A practical approach to optic nerve crush in the mouse. *Molecular vision*, 18(July), pp.2147–52. Available at: http://www.pubmedcentral.nih.gov/articlerender.fcgi?artid=3413441&tool=pmcentrez&rendertype=abstract.

Tham, Y.C. et al., 2014. Global prevalence of glaucoma and projections of glaucoma

burden through 2040: A systematic review and meta-analysis. *Ophthalmology*, 121(11), pp.2081–2090. Available at: http://dx.doi.org/10.1016/j.ophtha.2014.05.013.

Toris, C.B., Gabelt, B.T. & Kaufman, P.L., 2008. Update on the Mechanism of Action of Topical Prostaglandins for Intraocular Pressure Reduction. *Survey of Ophthalmology*, 53(6 SUPPL.).

Trope, G.E. & Clark, B., 1982. Beta adrenergic receptors in pigmented ciliary processes. *The British journal of ophthalmology*, 66, pp.788–792.

Underwood, J.L. et al., 1999. Glucocorticoids regulate transendothelial fluid flow resistance and formation of intercellular junctions. *The American journal of physiology*, 277(2 Pt 1), pp.C330-42. Available at: http://www.ncbi.nlm.nih.gov/pubmed/10444410.

Vegge, T., 1967. The fine structure of the trabeculum cribriforme and the inner wall of Schlemm's canal in the normal human eye. *Zeitschrift f??r Zellforschung und Mikroskopische Anatomie*, 77(2), pp.267–281.

Vohra, R., Tsai, J.C. & Kolko, M., 2013. The Role of Inflammation in the Pathogenesis of Glaucoma. *Survey of Ophthalmology*, 58(4), pp.311–320.

Vranka, J.A. et al., 2015. Mapping molecular differences and extracellular matrix gene expression in segmental outflow pathways of the human ocular trabecular meshwork. *PLoS ONE*, 10(3).

Wang, L. et al., 2017. Single stranded adeno-associated virus achieves efficient gene transfer to anterior segment in the mouse eye. *PLoS ONE*, 12(8), pp.1–12.

Wang, N., Wu, H. & Fan, Z., 2002. Primary angle closure glaucoma in Chinese and western populations. *Chinese Medical Journal*, 115(11), pp.1706–1715.

Watson, P. et al., 1996. A six-month, randomized, double-masked study comparing latanoprost with timolol in open-angle glaucoma and ocular hypertension. *Ophthalmology*, 103(1), pp.126–137. Available at: http://www.embase.com/search/results?subaction=viewrecord&from=export&id=L26046169%5Cnhttp://sfxhosted.exlibrisgroup.com/sfxtul?sid=EMBASE&issn=01616420&id=doi:&atitle=A+six-month%2C+randomized%2C+double-masked+study+comparing+latanoprost+with+timolol+in+.

Weinreb, R.N., Aung, T. & Medeiros, F.A., 2014. The Pathophysiology and Treatment of Glaucoma. *Jama*, 311(18), p.1901. Available at: http://www.pubmedcentral.nih.gov/articlerender.fcgi?artid=4523637&tool=pmce

ntrez&rendertype=abstract%5Cnhttp://jama.jamanetwork.com/article.aspx?doi=10.1001/jama.2014.3192.

Weinreb, R.N. & Khaw, P.T., 2004. Primary open-angle glaucoma. *Lancet (London, England)*, 363(9422), pp.1711–20. Available at: http://www.sciencedirect.com/science/article/pii/S0140673604162570.

Wen, J.C. et al., 2017. Intravitreal anti-VEGF injections reduce aqueous outflow facility in patients with neovascular age-related macular degeneration. *Investigative Ophthalmology and Visual Science*, 58(3), pp.1893–1898.

Whitlock, A. et al., 2010. Increased intraocular pressure in mice treated with dexamethasone. *Investigative Ophthalmology and Visual Science*, 51(12), pp.6496–6503.

Yamaguchi, Y. et al., 2006. Localization and ontogeny of aquaporin-1 and -4 expression in iris and ciliary epithelial cells in rats. *Cell and Tissue Research*, 325(1), pp.101–109.

Yamauchi, K. et al., 2004. Disease-causing mutant WNK4 increases paracellular chloride permeability and phosphorylates claudins. *Proceedings of the National Academy of Sciences of the United States of America*, 101(13), pp.4690–4. Available at: http://www.pubmedcentral.nih.gov/articlerender.fcgi?artid=384808&tool=pmcentrez&rendertype=abstract.

Yang, X. et al., 2011. Neurodegenerative and inflammatory pathway components linked to TNF-α/TNFR1 signaling in the glaucomatous human retina. *Investigative Ophthalmology and Visual Science*, 52(11), pp.8442–8454.

Yang, Y. et al., 2015. Interleukin-18 enhances breast cancer cell migration via down-regulation of claudin-12 and induction of the p38 MAPK pathway. *Biochemical and Biophysical Research Communications*, 459(3), pp.379–386.

Ye, W. et al., 1997. Interendothelial junctions in normal human schlemm's canal respond to changes in pressure. *Investigative Ophthalmology and Visual Science*, 38(12), pp.2460–2468.

Zhang, B. et al., 2004. IL-18 increases invasiveness of HL-60 myeloid leukemia cells: Up-regulation of matrix metalloproteinases-9 (MMP-9) expression. *Leukemia Research*, 28(1), pp.91–95.

Zhou, X. et al., 2009. Anti-inflammatory effect of pigment epithelium-derived factor in DBA/2J mice. *Molecular vision*, 15(December 2008), pp.438–50. Available at:

http://www.pubmedcentral.nih.gov/articlerender.fcgi?artid=2647972&tool=pmcentrez&rendertype=abstract.

Zhou, X. et al., 2005. Involvement of inflammation, degradation, and apoptosis in a mouse model of glaucoma. *Journal of Biological Chemistry*, 280(35), pp.31240–31248.

Zihni, C. et al., 2016. Tight junctions: from simple barriers to multifunctional molecular gates. *Nature Reviews Molecular Cell Biology*, 17(9), pp.564–580. Available at: http://www.nature.com/doifinder/10.1038/nrm.2016.80.

Zode, G.S. et al., 2011. Reduction of ER stress via a chemical chaperone prevents disease phenotypes in a mouse model of primary open angle glaucoma. *Journal of Clinical Investigation*, 121(9), pp.3542–3553.

Zode, G.S. et al., 2012. Topical ocular sodium 4-phenylbutyrate rescues glaucoma in a myocilin mouse model of primary open-angle glaucoma. *Investigative Ophthalmology and Visual Science*, 53(3), pp.1557–1565.

Appendix

This appendix contains four papers prepared over the course of this PhD to which I have contributed, two research papers, and two reviews, as follows:

1. Tam *et al*. Enhancement of Outflow Facility in the Murine Eye by Targeting Selected Tight-Junctions of Schlemm's Canal Endothelia. *Scientific Reports,* **7**, 40717; doi: 10.1038/srep40717 (2017).

2. O'Callaghan *et al.* Therapeutic potential of AAV-mediated MMP-3 secretion from corneal endothelium in treating glaucoma. *Human Molecular Genetics,* 26(7): 1230–1246; 10.1093/hmg/ddx028 (2017)

3. Campbell *et al.* Manipulating ocular endothelial tight junctions: applications in treatment of retinal disease pathology and ocular hypertension. Proceedings in Retinal and Eye Research, accepted for publication.

4. O'Callaghan *et al.* Open-angle Glaucoma: Therapeutically Targeting the Extracellular Matrix of the Conventional Outflow Pathway. Expert Opinions on Therapeutic Targets, under review.

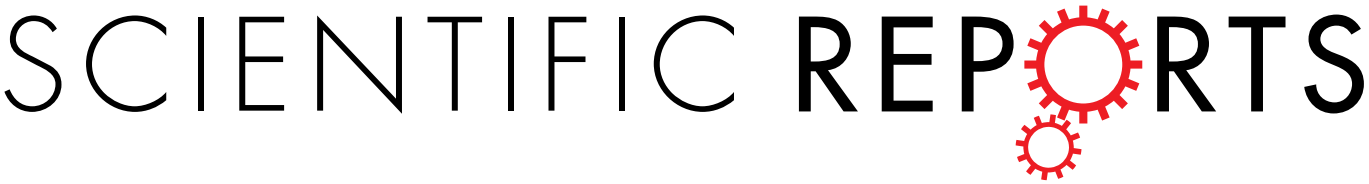

OPEN

Enhancement of Outflow Facility in the Murine Eye by Targeting Selected Tight-Junctions of Schlemm's Canal Endothelia

Received: 05 August 2016
Accepted: 09 December 2016
Published: 16 January 2017

Lawrence C. S. Tam[1,*], Ester Reina-Torres[1,2,*], Joseph M. Sherwood[2], Paul S. Cassidy[1], Darragh E. Crosbie[1], Elke Lütjen-Drecoll[3], Cassandra Flügel-Koch[3], Kristin Perkumas[4], Marian M. Humphries[1], Anna-Sophia Kiang[1], Jeffrey O'Callaghan[1], John J. Callanan[5], A. Thomas Read[6], C. Ross Ethier[7], Colm O'Brien[8], Matthew Lawrence[9], Matthew Campbell[1], W. Daniel Stamer[4], Darryl R. Overby[2] & Pete Humphries[1]

The juxtacanalicular connective tissue of the trabecular meshwork together with inner wall endothelium of Schlemm's canal (SC) provide the bulk of resistance to aqueous outflow from the anterior chamber. Endothelial cells lining SC elaborate tight junctions (TJs), down-regulation of which may widen paracellular spaces between cells, allowing greater fluid outflow. We observed significant increase in paracellular permeability following siRNA-mediated suppression of TJ transcripts, claudin-11, zonula-occludens-1 (ZO-1) and tricellulin in human SC endothelial monolayers. In mice claudin-11 was not detected, but intracameral injection of siRNAs targeting ZO-1 and tricellulin increased outflow facility significantly. Structural qualitative and quantitative analysis of SC inner wall by transmission electron microscopy revealed significantly more open clefts between endothelial cells treated with targeting, as opposed to non-targeting siRNA. These data substantiate the concept that the continuity of SC endothelium is an important determinant of outflow resistance, and suggest that SC endothelial TJs represent a specific target for enhancement of aqueous movement through the conventional outflow system.

Under physiological conditions, the majority of aqueous humour (AH) exits the anterior chamber through the conventional outflow pathway in humans[1–3]. In this pathway, AH filters sequentially through the trabecular meshwork (TM), including the juxtacanalicular tissue (JCT), and the endothelial lining of Schlemm's canal (SC) before entering the SC lumen and draining into the episcleral veins. Electron microscopic evidence has indicated that AH drainage across SC endothelium occurs through micron-sized pores that pass either through (transcellular) or between (paracellular) individual SC cells[4–9]. In particular, a significant fraction of AH crosses the inner wall of SC via paracellular pores[10]. Moreover, the presence of tight-, adherens- and gap-junctions in SC endothelial cells provides a mechanism by which the conventional outflow pathway is dynamically responsive to constantly changing physiological conditions while still preserving the blood-aqueous barrier[11–17]. It has long been recognised that elevated intraocular pressure (IOP) associated with primary open-angle glaucoma (POAG) is due to elevated resistance to AH outflow through the conventional outflow pathway[18], although the cause of elevated outflow resistance in glaucoma remains to be fully elucidated. Previous studies support the concept that outflow

[1]Neurovascular Genetics, Smurfit Institute of Genetics, Trinity College, University of Dublin, Dublin 2, Ireland. [2]Department of Bioengineering, Imperial College London, London, UK. [3]Department of Anatomy, University of Erlangen-Nürnberg, Erlangen, Germany. [4]Department of Ophthalmology, Duke University, Durham, NC, USA. [5]Ross University School of Veterinary Medicine, P. O. Box 334, Basseterre, St. Kitts, West Indies. [6]Department of Ophthalmology and Vision Sciences, University of Toronto, Canada. [7]Coulter Department of Biomedical Engineering, Georgia Institute of Technology and Emory University, Atlanta, USA. [8]Ophthalmology, Mater Hospital, UCD School of Medicine, Dublin, Ireland. [9]RxGen, Hamden, CT, USA. *These authors contributed equally to this work. Correspondence and requests for materials should be addressed to L.C.S.T. (email: lawrenct@tcd.ie) or W.D.S. (email: william.stamer@duke.edu) or P.H. (email: pete.humphries@tcd.ie)

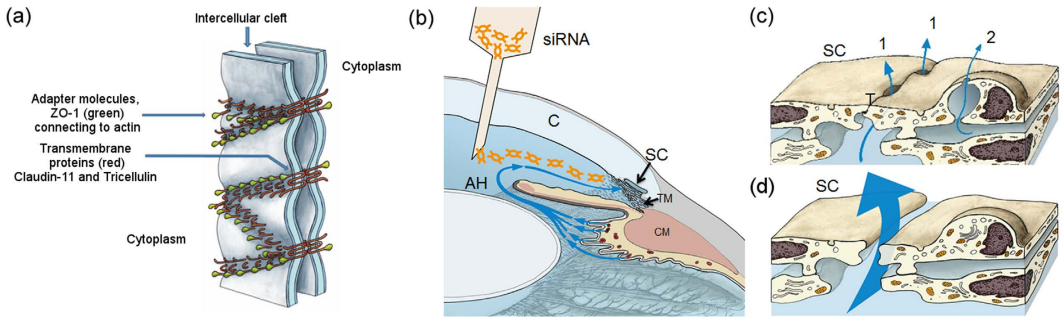

Figure 1. Schematic illustration of the therapeutic strategy addressed in this study. (a) Schematic representation of adapter molecules and transmembrane proteins connecting neighbouring SCEC. **(b)** Intracameral delivery enables siRNAs to be transported towards the conventional outflow pathway by following the natural flow dynamics of aqueous humour in the anterior chamber. AH = aqueous humour; C = cornea; CM = ciliary muscle; SC = Schlemm's canal; TM = trabecular meshwork. **(c)** AH crosses the inner wall endothelium of SC via (1) the intercellular pathway through gaps in tight junctions (T) and, or via (2) the intracellular pathway through a giant vacuole with a pore. **(d)** siRNAs taken up by endothelial cells of the inner wall of SC elicit knockdown of tight junction proteins, resulting in the opening of intercellular clefts with concomitant increase in aqueous outflow facility.

resistance is modulated through a synergistic hydrodynamic interaction between JCT and SC endothelium such that inner wall pore density may influence outflow resistance generation by defining the regions of filtration through the JCT[19–21]. As glaucomatous eyes have reduced SC inner wall pore density, decreased porosity of the inner wall appears to contribute to elevated outflow resistance and increased IOP[22–24].

Prolonged elevation of IOP results in progressive degeneration of retinal ganglion cell axons, and hence to irreversible vision loss. Treatment of POAG by lowering IOP remains the only approach to limiting disease progression. Topically applied medications that either reduce AH production or increase drainage through the unconventional (uveoscleral) outflow pathway are widely used in management of IOP in patients with POAG[25]. However, a proportion of patients do not respond optimally to such medications and, therefore, there is a clear need to investigate novel approaches to reduce outflow resistance by identifying specific targets within the conventional outflow pathway through which this might be achieved. Owing to the fact that a major fraction of AH filtration at the level of SC appears to largely pass through paracellular routes[10], strategies specifically targeting cell-cell junctions between endothelial cells of the inner wall of SC may be effective at decreasing outflow resistance. Hence, we hypothesised that down-regulation of selected tight junction (TJ) components of endothelial cells lining the inner wall of SC may increase the paracellular spaces between these cells, facilitating flow of AH across the inner wall into the SC (Fig. 1), thus reducing outflow resistance and IOP.

In this report, we have identified TJ components in human primary cultures of SC endothelial cells (SCEC), and also in mouse and non-human primate outflow tissues. We show that siRNA-mediated down-regulation of such components increases the paracellular permeability of human primary SCEC monolayers to 70 kDa FITC-dextran, and decreases transendothelial electrical resistance. Furthermore, intracameral delivery of siRNAs targeting selected TJ components is shown to increase intercellular open spaces between SC inner wall endothelial cells as observed by transmission electron microscopy (TEM) and elevates outflow facility (the mathematical inverse of outflow resistance) in normotensive mice. In summary, our findings clearly identify a specific approach to promoting AH outflow by direct manipulation of selected TJs within the conventional outflow pathway.

Results

Characterisation of tight junction expression in human SC endothelial cells. We examined the TJ expression profile in primary cultures of human SCEC isolated from four individual donors, with the objective of determining key junctional components that regulate permeability and selectivity of the inner wall of SC. The mean normalised expression ($2^{-\Delta\Delta Ct}$) of genes encoding claudin and adhesion junctional proteins from four different SCEC strains is shown in Fig. 2a. The complete expression pattern can be found as Supplementary Fig. S1. The expression profile shows that claudin-11 (or oligodendrocyte specific protein) was amongst the highest expressed claudin-based TJ protein in cultured SCEC (Fig. 2a). In addition, zonula-occludens-1 protein (ZO-1, also known as *TJP1*), a key component of junctional complexes that regulate TJ formation, was also expressed at high levels in cultured SCEC. The cell-cell adhesion molecule, junctional adhesion molecule-3 (JAM3) was also highly expressed in human SCEC monolayers. In contrast, occludin and claudin-5, which are major TJ components of human and mouse brain and inner retinal vascular endothelium[26,27] were expressed at low levels in human SCEC. Collectively, these data indicate that claudin-11 is the dominant claudin in the TJs of cultured SCEC, and that ZO-1 is a major junctional associated protein of cultured SCEC. We also compared transcript levels of claudin-11 and ZO-1 in cultured monolayers of human SCEC (SC77) against those of human TM cells (TM93), and observed expression levels of claudin-11 to be 2.52-fold higher in SCEC than in TM cells (Supplementary Fig. S2). However, no significant difference in ZO-1 transcript expression was observed between TM and SCEC.

Claudin-11 and ZO-1 protein expression was detected in cultured SCEC by Western blot (Fig. 2b). In addition, we also detected expression of another TJ protein, tricellulin (also known as MARVELD2) in cultured SCEC,

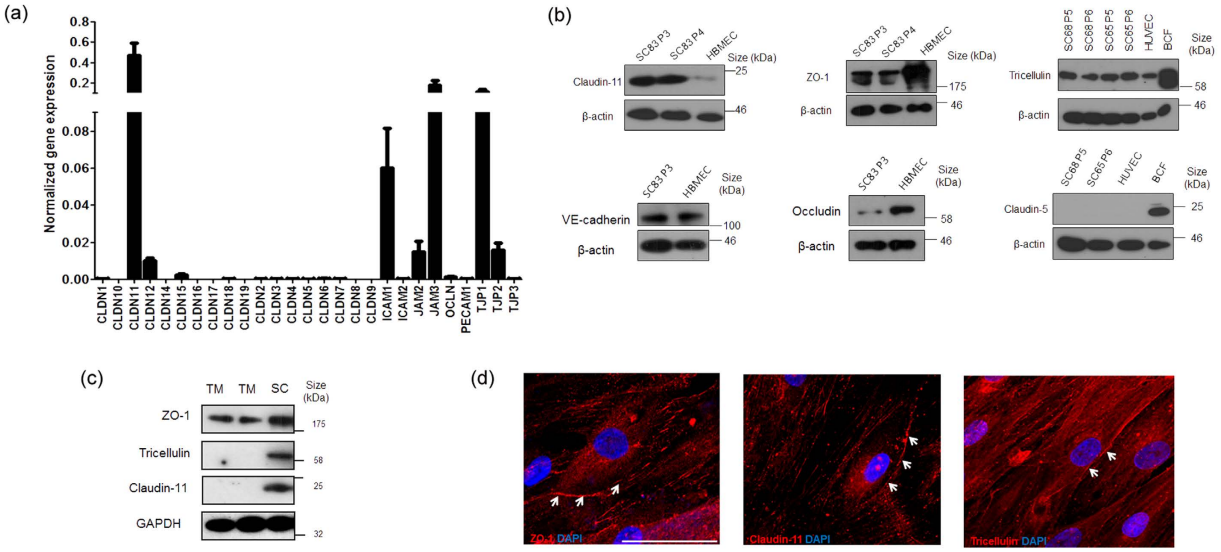

Figure 2. Characterisation of tight junction expression in human Schlemm's canal endothelial cells. **(a)** The human TJs RT^2 Profiler PCR array was used to profile the expression of claudin and adhesion junctional proteins. Bar graphs illustrate average relative gene expression ($2^{-\Delta CT}$) normalised to 5 housekeeping genes from 4 different human SCEC strains. Data are mean ± s.e.m. Note the break in scale for normalised gene expression. **(b)** Protein analysis of claudin-11, ZO-1, tricellulin, VE-cadherin, occludin and claudin-5 in cultured human SCEC. HBMEC = human brain microvascular endothelial cells; BCF = Mouse brain capillary fraction; B-actin as loading control. Different SCEC strains are denoted followed by passage (P) number. **(c)** Tight junction protein expression in TM (TM120 and TM130) and SCEC. GAPDH as loading control. **(d)** White arrow heads illustrate immuno-detection of ZO-1, claudin-11 and tricellulin (Cy3) in cultured human SCEC. Blue = DAPI nuclei staining. Scale bar, 50 μm.

which was not included in the PCR array. Consistent with previous studies[14,28], expression of vascular endothelial (VE)-cadherin was also identified in cultured SCEC (Fig. 2b). However, we did not detect claudin-5 protein expression in cultured SCEC, and only low levels of occludin protein expression were detected, an observation consistent with the PCR array data. Furthermore, we did not detect claudin-11 and tricellulin expression in TM cells (TM120 and 130), whereas both TM and SCEC (SC82) were shown to express ZO-1 protein (Fig. 2c). This is consistent with a previous finding showing that both TM and SCEC express the junction-associated protein, ZO-1[29]. Immunocytochemistry was then undertaken to examine the expression patterns of TJ proteins in confluent SCEC monolayers. We observed discontinuous membrane-specific staining patterns for ZO-1, claudin-11 and tricellulin in cultured SCEC monolayers (Fig. 2d).

Characterisation of expression of tight junction and tight junction associated components in mouse and non-human primate outflow tissues. We performed immunohistochemistry (IHC) on frozen sections of mouse anterior segments to localise the expression of TJ proteins in the outflow region comprising the TM and the inner wall of SC. Immunofluorescent images show tricellulin and ZO-1 staining predominantly localising in the inner wall endothelium of SC (Fig. 3a). In particular, we observed ZO-1 staining to be diffusely distributed in the cytoplasm of SCEC. In regions where part of the endothelium was cut obliquely to the inner wall of SC, continuous junctional strands were displayed around SCEC margins. ZO-1 and tricellulin staining were also detected in the TM region and in the outer wall. In both regions the endothelial cells were connected by TJs. However, we did not detect claudin-11 or claudin-5 staining in the inner wall of SC and TM with the antibodies used in this study (Supplementary Fig. S3). These data indicate that murine outflow tissues may possess a different junctional composition at the inner wall of SC as compared to humans, with the possible absence of claudin-based tight junctional proteins in TM and SCEC. However, the presence of ZO-1 and tricellulin along the inner wall in mice indicates that these proteins may be suitable targets for assessment of effects of TJ down-regulation in mice.

IHC was performed on paraffin sections of African green monkey anterior segments to identify the junctional composition of the outflow region. Hematoxylin and eosin staining (H&E) of the anterior chamber clearly identified the iridocorneal angle and conventional outflow tissues (Fig. 3b). Superimposed immunofluorescent imaging showed strong continuous claudin-11 staining along the endothelial cell margins of the inner wall of SC, highly indicative of TJ barrier function (Fig. 3b). Claudin-11 immunostaining was also present along the outer wall of SC and between TM cells. Similarly, ZO-1 and tricellulin staining were observed in the inner wall endothelium of SC. All three TJ proteins were present between TM endothelial cells, but the staining was less intense than in the inner wall endothelium. In addition, we did not detect claudin-5 expression in SCEC isolated from non-human primates (Supplementary Fig. 4). These data indicate that SCEC in non-human primates possess a similar TJ barrier composition to that found in humans.

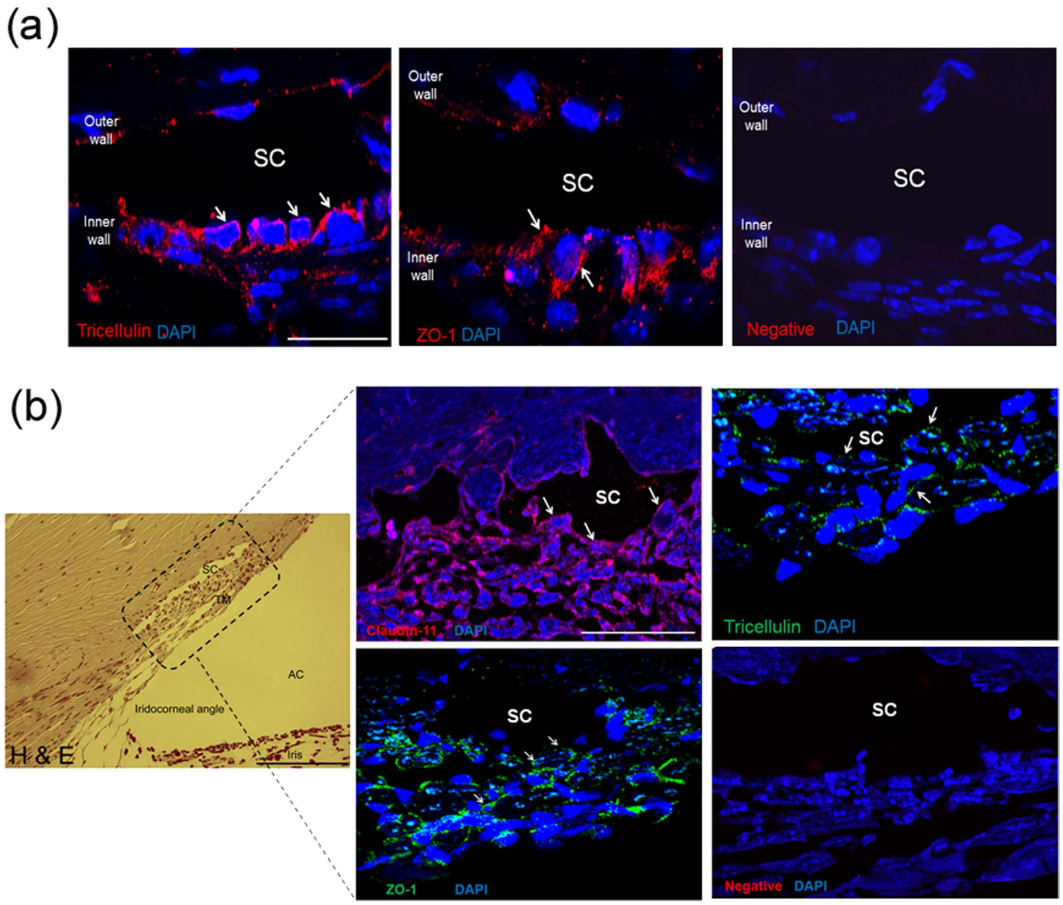

Figure 3. Characterisation of tight junction expression in mouse and non-human primate outflow tissues. (**a**) Immunostaining of tricellulin and ZO-1 in frozen sections of mouse anterior segments. ZO-1 and tricellulin = Cy3 (red); DAPI = blue; SC = Schlemm's canal lumen. Scale bar, 50 μm. (**b**) H&E staining of paraffin monkey anterior segments (left panel). Boxed area depicts superimposed regions shown in immunofluorescence images. AC = anterior chamber; SC = Schlemm's canal lumen; TM = trabecular meshwork. Scale bar, 200 μm. Immunofluorescent images of claudin-11, ZO-1 and tricellulin staining in the inner wall endothelium of SC. White arrows indicate detection of corresponding tight junctions at the inner wall of SC endothelium. Negative = no primary antibody. Scale bar, 50 μm.

Validation of tight junction siRNAs. In order to validate the suppression efficiency of pre-designed siRNAs targeting the human transcripts of claudin-11, ZO-1 and tricellulin, cultured SCEC were separately transfected with 40 nM of each siRNA, and levels of endogenous TJ expression were assessed in a time-dependent manner by Western blot. Time-dependent down-regulation of claudin-11 expression to $5 \pm 3\%$ ($p < 0.0001$), $11 \pm 1\%$ ($p < 0.0001$) and $9 \pm 4\%$ ($p < 0.0001$) (mean ± s.e.m.), was achieved at 24, 48 and 72 h post-transfection respectively, as compared to non-targeting (NT) siRNA (Fig. 4a). ZO-1 expression was reduced to $72 \pm 3\%$ ($p = 0.005$), $64 \pm 4\%$ ($p = 0.0004$) and $49 \pm 18\%$ ($p = 0.02$) at 24, 48 and 72 h post-transfection respectively (Fig. 4b). Furthermore, tricellulin expression was reduced to $75 \pm 0.2\%$ ($p = 0.002$), $81 \pm 6\%$ ($p = 0.012$) and $87 \pm 8\%$ ($p > 0.05$) at 24, 48 and 72 h respectively following siRNA treatment (Fig. 4c). The difference in knockdown efficiencies likely indicates that ZO-1 and tricellulin have slower protein turnover rates than claudin-11 in cultured SCEC. A cell viability assay was performed on transfected SCEC and no change in viability due to siRNA treatment was detected when cells were treated with either 40 or 200 nM of siRNA (Supplementary Fig. S5). siRNAs targeting mouse ZO-1 and tricellulin were also validated and show efficient knockdown of gene expression *in vitro* (Supplementary Fig. S6).

The efficacy of siRNA inhibition *in vivo* was tested in retinas from mice injected intravitreally with siRNA against ZO-1 and tricellulin. RT-PCR carried out on RNA extracted from mouse retinas showed that 12 hr post-injection, tricellulin RNA was significantly reduced to 0.32 fold ($p = 0.049$; Supplementary Fig. S7) compared to eyes injected with NT-siRNA while ZO-1 was reduced to 0.57 fold ($p = 0.048$; Supplementary Fig. S7). This approach using retina was taken because of the difficulty in isolating SC endothelium from mouse eyes to perform a reliable quantification analysis.

We performed cell death assays to assess SCEC viability following siRNA inoculation *in vivo* in mouse outflow tissues. Immunohistochemistry was performed on eyes 48 hours post injection with either targeting or NT siRNA. Approximately 30–40 12 μm sections were each stained by TUNEL and complemented by cleaved

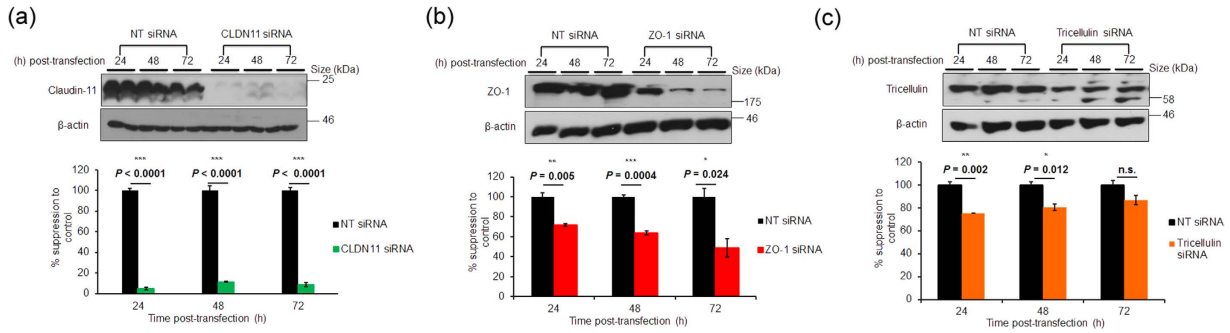

Figure 4. siRNA-mediated down-regulation of tight junction RNA transcripts in cultured human SCEC. Representative Western blots of (**a**) claudin-11, (**b**) ZO-1 and (**c**) tricellulin knockdown in cultured human SCEC over a 72 h period. Corresponding bar graphs depict densitometric analysis of percentage protein normalised to β-actin. NT siRNA = non-targeting siRNA. Data are mean ± s.e.m.; n.s. = $P \geq 0.05$ (n = 4, unpaired *t*-test).

caspase-3 staining as markers of apoptosis for representatives of targeting and non-targeting siRNA. For TUNEL staining, most sections displayed some apoptotic damage in the corneal epithelium. Parts of the ciliary body were also the site of minor labelling, regardless of treatment received. Closer inspection of the angle and outflow tissue itself provided no evidence of any apoptotic cell death in either targeting or NT controls. Cleaved caspase-3 was sparsely detected in the ciliary body, and effectively absent in the angle or outflow tissue in either treatment, correlating with observations by TUNEL (Supplementary Fig. S8).

Effect of down-regulation of tight junctions on SCEC monolayer permeability. In order to address the hypothesis that down-regulation of TJ components in SCEC could be used as a means of modulating the resistance of SC inner wall, transendothelial electrical resistance (TEER) was measured to assess changes in endothelial barrier function in confluent SCEC monolayers following TJ knockdown. SCEC monolayers transfected with claudin-11 or ZO-1 siRNAs showed significant reduction in TEER compared to NT siRNAs at 48 and 72 h post-transfection ($p < 0.001$; Fig. 5a). Furthermore, transfection with a combination of claudin-11 and ZO-1 siRNAs elicited a significant decrease in TEER, and the magnitude of decrease was more profound than those treated with single siRNAs at 48 h post-transfection ($p < 0.001$, Fig. 5a). Similarly, treatment with tricellulin siRNA alone also showed significant reduction of TEER at 48 h post-transfection, and the effect was sustained up to 72 h ($p < 0.001$, Fig. 5b). We next treated SCEC monolayer simultaneously with a combination of three siRNAs targeting claudin-11, ZO-1 and tricellulin, and observed significant reduction in TEER from 24 to 72 h post-transfection as compared to control ($p < 0.001$, Fig. 5c). Measured TEER values can be seen in Supplementary Table S1.

The effect of TJ down-regulation on endothelial permeability was tested in confluent SCEC monolayers using non-ionic macromolecular tracer, FITC-dextran (FD), which can only transverse via the paracellular route. To investigate the size selectivity of paracellular permeability in SCEC monolayers, we first determined the flux of 4, 70 and 150 kDa FD in the basal to apical direction following treatment of monolayers with siRNAs targeting tricellulin. At 24 h post-transfection, we observed no difference between control and treated in apparent permeability co-efficient (P_{app}) to the 4 kDa FD ($\approx 3.66 \times 10^{-6}$ cm/s), which readily passes through the monolayer. In contrast, the 150 kDa FD did not readily cross the monolayer ($\approx 1.23 \times 10^{-8}$ cm/s). The largest decrease in barrier tightness as measured by P_{app} was observed with the 70 kDa FD ($p < 0.0001$, Fig. 5d). These data indicate that down-regulation of tricellulin in SCEC monolayers selectively opens the paracellular route to macromolecules of 70 kDa. Following this, we treated SCEC monolayers with siRNAs targeting other TJs, and observed that down-regulation of claudin-11 ($p < 0.0001$), ZO-1 ($p < 0.0001$), as well as tricellulin ($p < 0.0001$) significantly increased paracellular flux of 70 kDa FD, as compared to controls (Fig. 5e,f). In addition, P_{app} (70 kDa FD) was observed to be significantly greater in monolayers treated with a combination of ZO-1 and tricellulin siRNAs than control ($p < 0.0001$), and compared to those treated singly with either ZO-1 or tricellulin siRNA ($p < 0.001$) (Fig. 5f). Furthermore, treatment with a combination of siRNAs targeting three TJs simultaneously also increased P_{app} of SCEC to 70 kDa FD ($p = 0.0004$ vs. control; Fig. 5g). We used primary SCEC strains from different donor eyes for flux assays in Fig. 5e–g, and as a consequence, we observed natural variability in baseline P_{app} values and responses to TJ down-regulation from different strains. Collectively, these data demonstrate that claudin-11, ZO-1 and tricellulin contribute to the barrier function of cultured human SCEC, and that siRNA-mediated down-regulation of these cellular junctional proteins significantly alters endothelial cell barrier integrity and permeability.

Ultrastructural analysis of the inner wall endothelium of SC following treatment with siRNAs. To examine how siRNA treatment affects the continuity of the inner wall of SC, ultrastructural investigation of TJs between SC cells was performed by TEM. Six wild type C57BL/6J mice were intracamerally injected with a combination of 1 μg ZO-1 siRNA and 1 μg of tricellulin siRNA, and contralateral eyes were injected with 2 μg of NT siRNA. 48 h post-injection, all animals were sacrificed with eyes enucleated immediately after death and immersed for TEM investigation. As can be seen in Fig. 6a,b, the inner wall of SC in both treated and control

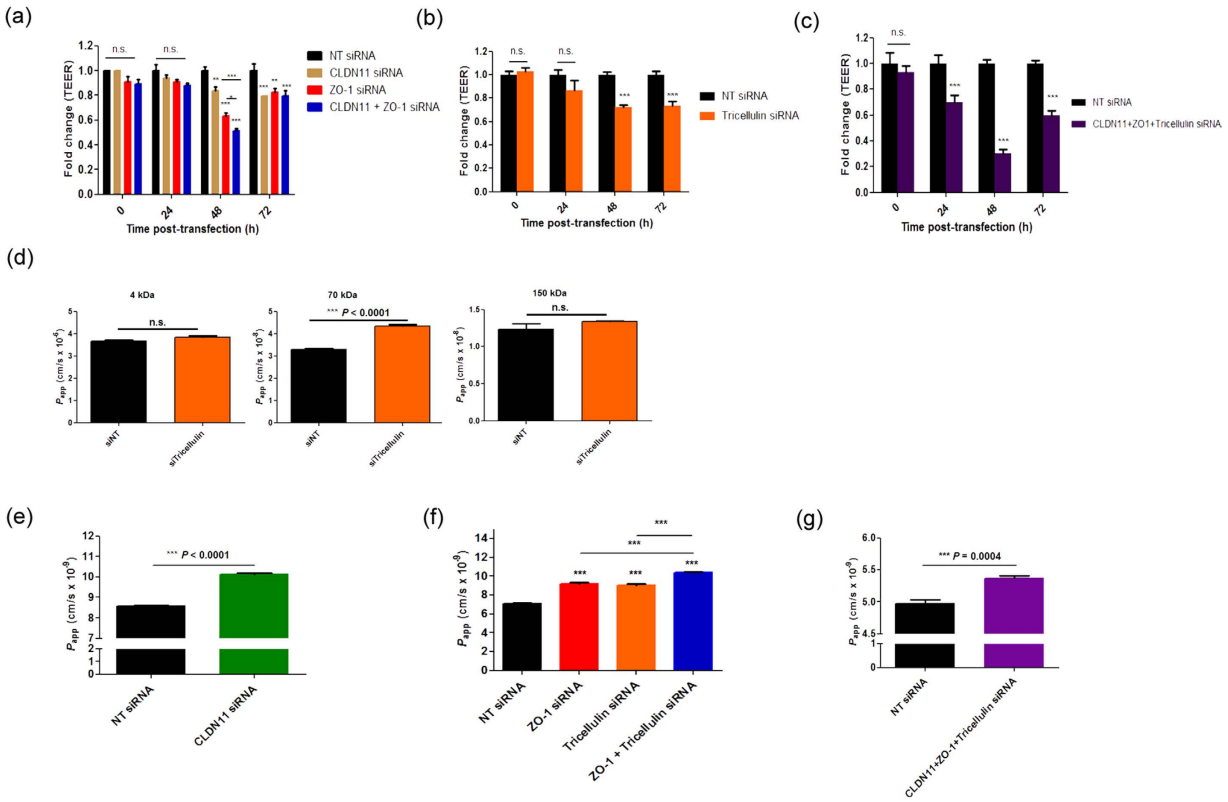

Figure 5. siRNA-mediated down-regulation of tight junction RNA transcripts modulates TEER and paracellular permeability in cultured SCEC monolayers. (**a**) Effect of siRNA-mediated knockdown of TJ RNA transcripts on TEER across human SCEC monolayers. 40 nM of siRNA targeting claudin-11, ZO-1, or in combination were transfected into human SCEC, and TEER was measured 24, 48 and 72 h post-transfection. $^{*}P < 0.05$, $^{**}P < 0.01$, $^{***}P < 0.001$, n.s. $P \geq 0.05$ (n = 3 separate cell transfection, two way analysis of variance (ANOVA) followed by Bonferroni's multiple comparison post-tests). Data are fold change ± s.e.m. (**b**) TEER measurements following treatment with tricellulin siRNAs in cultured SCEC monolayers (n = 5 separate cell transfections, two way ANOVA followed by Bonferroni's multiple comparison post-tests). $^{***}P < 0.0001$. Data are fold change ± s.e.m. (**c**) TEER measurements following treatment of SCEC monolayers with a combination of claudin-11, ZO-1 and tricellulin siRNAs (n = 7 separate cell transfections, two way ANOVA followed by Bonferroni's multiple comparison post-tests). $^{***}P < 0.001$. n.s. = $P > 0.05$. (**d**) Cultured SCEC monolayers demonstrate size selectivity. Apparent permeability co-efficient (P_{app}, cm/s) of 4, 70 and 150 kDa FITC dextrans was determined following treatment with siRNAs targeting tricellulin. ($^{***}p < 0.0001$; n = 3). n.s. = $P \geq 0.05$ (**e**,**f**,**g**) P_{app} of 70 kDa FITC-dextran through human SCEC monolayers following treatment with claudin-11, ZO-1 and tricellulin siRNAs, or in combination. NT = non-targeting. Data are mean ± s.e.m. Note the break in scale for P_{app} (**e**,**f**). (**e**) ***P < 0.0001, n = 6. (**f**) ($^{***}P < 0.0001$, n = 4). (**g**) ***P = 0.0004, n = 6. (unpaired Student's *t*-test for left and right bar graphs; one way ANOVA followed by Bonferroni's *post hoc* test for middle bar graphs).

eyes appeared similar. The inner wall was continuous without loss of cells or apparent cellular damage, and in both control and treated eyes there were no swollen cells that would indicate necrosis. There were also no cellular extensions and nuclear densifications or fragmentations that would indicate apoptosis.

To more clearly visualize cell membranes and junctions, sections were stained with UAR-EMS rather than uranyl acetate (see materials and methods). This staining allowed better visualization of the intercellular junctions and revealed that intercellular clefts between neighbouring SC cells were more often open in eyes treated with targeting siRNAs than in controls, indicating an absence or weakening of the TJ complexes. Open clefts exhibited a typical width of 10–20 nm without any contact between neighbouring cell membranes, while closed clefts exhibited a focal fusion between neighbouring cell membranes often surrounded by small cytoplasmic filaments (Fig. 6c,d). Quantification of intercellular junctions was performed by 2 independent observers, who examined TEM sections at 80,000x along the anterior-posterior extent of the inner wall from 4 regions of each eye (n = 6 treated and 5 control eyes; one control eye was removed as, for technical reasons, not all 4 regions could be evaluated). Each section contained between 10–30 cells, and each region was separated from another by at least several hundred microns, such that each region could be considered an independent sample. This quantification revealed that approximately 33% of intercellular junctions were open in eyes treated with targeting siRNA (Table 1). In contrast, only approximately 2% of intercellular junctions were open in contralateral eyes treated with non-targeting siRNA (Table 2), and this difference was statistically significant (p = 0.004, unpaired Student's

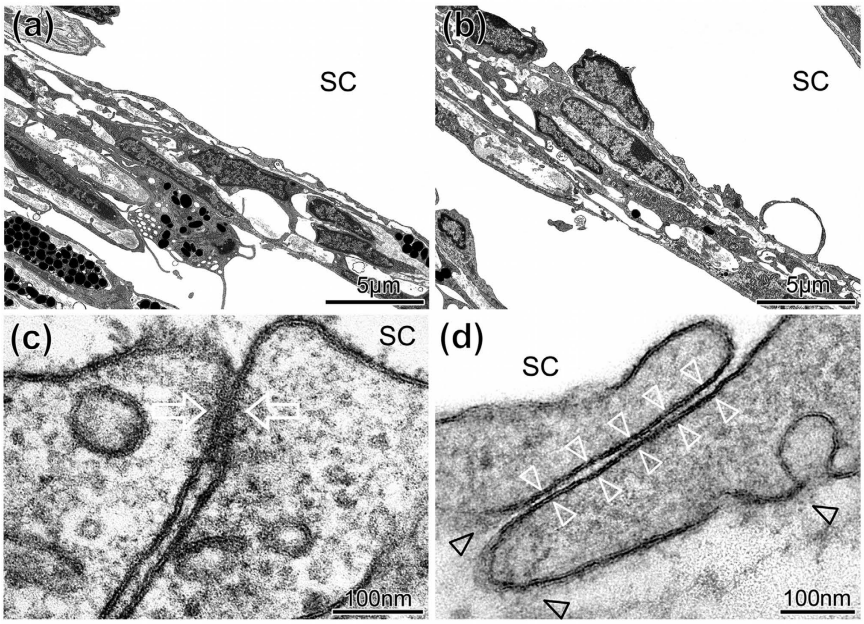

Figure 6. Transmission electron microscopic analysis of sagittal sections of the inner wall of SC following siRNA treatment. (**a**,**b**) Representative sagittal sections through the inner wall of Schlemm's canal (SC) and outer trabecular meshwork (TM) of a mouse eye treated with **(a)** non-targeting (NT) or **(b)** targeting (T) siRNA illustrating intact cells and an intact and continuous inner wall endothelium that appeared similar in both cases. The inner wall endothelium is connected to the underlying ECM so that no ballooning was visible. (**c**,**d**) High magnifications of sagittal sections through intercellular clefts along the inner wall endothelium of SC showing examples for junctions quantitatively evaluated as closed **(c)** with fusion between the neighbouring cell membranes (arrows) or open clefts **(d)** where the cell membranes of adjacent endothelial cells were clearly separated along the entire cleft length (white arrowheads). Despite the open clefts, adhesions to subendothelial matrix (black arrowheads) were preserved. The number of open intercellular clefts was quantified (see Tables 1 and 2).

	Region 1		Region 2		Region 3		Region 4		
Sample	N total	N open	N total	N open	N total	N open	N total	N open	% open
C4 NEP T	15	4	17	3	21	5	24	9	27%
C4 REP T	18	15	14	3	22	17	10	5	63%
C4 LEP T	9	5	26	1	18	9	12	3	28%
C5 LEP T	26	10	15	3	24	4	20	4	25%
C6 LEP T	25	11	31	11	15	4	18	2	31%
C6 NEP T	25	2	29	9	16	4	30	8	23%
								Average	33%
								SD	25%

Table 1. Quantification of total and open intercellular clefts along the inner wall in treated eyes that were immersion fixed immediately after death.

t-test). These data reveal that the siRNA treatment is opening intercellular clefts along the inner wall of SC *in vivo*, presumably by affecting TJs.

It is feasible that siRNA treatment may also have affected adherens or cell-matrix junctions that provide mechanical support between endothelial cells and to the subendothelial tissue. Indeed, TJs and adherens junctions are coupled, and disassembly of adherens junctions often leads to disassembly of TJ[30]. To determine whether siRNA had affected these other junctional types, we examined for disconnections between the inner wall and subendothelial tissue that typically leads to inner wall 'ballooning' as observed following treatment with Na_2-EDTA[31,32]. In none of the 4 regions examined per eye in either case, did we observe any ballooning of the inner wall (Fig. 6a,b). Even in areas with open intercellular clefts, the basal cell membranes of the endothelial cells were still attached to the underlying extracellular matrix (ECM) (Fig. 6d). This implies that the cell-matrix adhesions remained intact. We also examined for adhered platelets, which is a sign of inner wall damage, as platelets often seal endothelial gaps where ECM is exposed to the lumen of SC[31,32]. No adhering platelets were observed in any region of any eye.

Sample	Region 1		Region 2		Region 3		Region 4		% open
	N total	N open	N total	N open	N total	N open	N total	N open	
C4 NEP NT	8	0	22	0	17	2	28	0	3%
C4 REP NT	17	1	20	0	13	0	18	0	1%
C5 LEP NT	21	0	26	0	14	0	19	0	0%
C6 LEP NT	11	1	30	0	26	0	9	0	1%
C6 NEP NT	20	1	17	0	29	0	31	1	2%
								Average	2%
								SD	1%

Table 2. Quantification of total and open intercellular clefts along the inner wall in control eyes that were immersion fixed immediately after death.

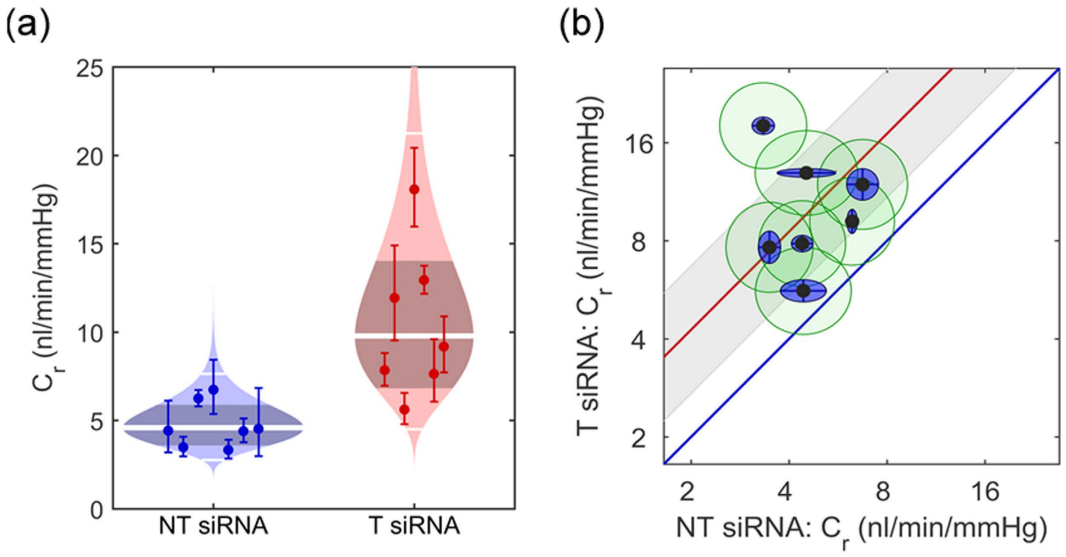

Figure 7. Effect of down-regulation of tight junction RNA transcripts on outflow facility *ex vivo*. (a) 'Cello' plots showing the individual values and statistical distribution of outflow facility at 8 mmHg (C_r) for eyes treated with either non-targeting (NT) siRNA or a combination of ZO-1 and tricellulin targeting (T) siRNA. Each individual point represents a single eye, with error bars showing the 95% confidence intervals on C_r arising from the regression analysis. For each condition, the predicted log-normal distribution is shown, with the thick central white band showing the geometric mean and the thinner white bands showing two geometric standard deviations from the mean. The shaded central region indicates the 95% confidence interval on the mean. **(b)** Paired facility plot: each data point represents one pair of eyes, with C_r for the treated T siRNA eye on the Y-axis and the C_r for contralateral control NT-siRNA eye on the X-axis. The red line shows the average difference between contralateral eyes, with its confidence interval in grey, whilst the blue line represents the case of identical facility between contralateral eyes, corresponding to no effect due to T siRNA. All data points are above the blue unity line, indicating that the facility was higher in the treated eyes compared to the controls; $n = 7$, $p = 0.006$. Inner blue ellipses show the 95% confidence intervals on C_r arising from the regression analysis, whilst the green outer ellipses show additional uncertainty due variability between contralateral eyes, estimated from 10 pairs of C57BL/6J eyes perfused only with glucose supplemented PBS[36].

Effect of down-regulation of tight junctions on outflow facility *ex vivo*. In order to evaluate whether down-regulation of TJs increases outflow facility, studies were performed in mouse eyes since the conventional outflow pathway of mice resembles that of human morphologically, physiologically and pharmacologically[33–35]. We targeted ZO-1 and tricellulin based on the IHC data obtained in Fig. 3a. Seven wild type C57BL/6J mice were intracamerally injected with a combination of 1 μg ZO-1 siRNA and 1 μg of tricellulin siRNA, and contralateral eyes were injected with 2 μg of NT siRNA. 48 h post-injection, all animals were sacrificed and enucleated eyes were perfused in pairs using the recently developed *iPerfusion*[36] system to measure outflow facility, calculated from the flow measured over multiple pressure steps (Supplementary Fig. S9). Outflow facility in the siRNA treated eyes was increased compared to eyes receiving NT siRNA (Fig. 7a). Figure 7b shows the paired facility data where the facility of the treated eye is plotted against that of the contralateral control eye. In all cases, the facility of the treated eye was elevated compared to control ($n = 7$ pairs), exhibiting an average facility increase of 113% (confidence interval [35, 234]%, $p = 0.0064$, facility values for each pair of eyes are provided in Supplementary Table S2). These data demonstrate that down-regulation of TJ components within the

conventional outflow pathway significantly increases conventional outflow facility in mouse eyes *ex vivo*. To investigate the long-term effect of TJ down-regulation, we perfused eyes from animals 8 weeks post-injection and we observed no difference in outflow facility between treated and control eyes (average facility increase of 9.2%, confidence interval [−14.22, 32.62]%, $p > 0.05$, $n = 4$ pairs, facility values for each pair of eyes are provided in Supplementary Table S2). This observation indicates that a single injection of siRNAs enables transient and reversible modulation of outflow facility in the anterior chamber of murine eyes.

Discussion

AH exiting the anterior chamber via the conventional outflow pathway passes through the tissues of the TM and into the SC lumen by crossing its endothelial barrier. Conceptually, loosening the TJs that bind endothelial cells could render the barrier more permeable resulting in reduced outflow resistance. However, this targeted approach has not been previously assessed in regard to AH outflow. The current study focused on identifying TJ components present in human, murine and non-human primate outflow tissues that might serve as plausible targets for siRNA-mediated down-regulation. A number of such targets were identified in primary cultures of human SCEC, disruption of which has previously been associated with altering endothelial cell permeability in other cell systems[37–39].

The TJ profile found in human SCEC identifies claudin-11 and tricellulin as SC specific TJ related proteins not present in TM cells, while ZO-1 has been found to be present in both SCEC and TM cells as previously reported[29,40]. Previous studies have also reported the identification of specific protein markers that are either exclusively expressed in the inner wall endothelium of SC, or differ appreciably in their expression from TM cells[14,28,41,42]. Owing to the high level of claudin-11 expression found in SCEC as compared to TM cells, this claudin-based TJ may also be used as a specific marker for identifying SC cells.

The association of both claudin-11 and tricellulin with SCEC is of significance because both TJs have been associated with maintenance of barrier function. Several studies on paracellular tightness have demonstrated that claudin-11 modulates paracellular cation permeability[39,43,44] and its knockdown increases TEER in human corpus cavernosum endothelial cells[45]. On the other hand, transcript knockdown studies have shown that the inhibition of tricellulin leads to instability of TJs[46], whereas tricellulin overexpression is associated with reduced permeability to macromolecules[47]. Accordingly, we observed that siRNA-mediated knockdown of selected TJ decreases transendothelial resistance and increases permeability to 70 kDa FD in cultured human SC cell monolayers. In particular, these effects were more profound when a combination of siRNAs was used, suggesting a synergistic effect in increasing paracellular permeability following down-regulation of a range of TJs.

Paracellular pathways have been well established to possess defined values of electrical conductance as well as charge and size selectivity[48]. For example, the junctional complexes comprising of tight and adherens junctions between cerebral endothelial cells enable the blood-brain barrier to regulate the entry of blood-borne molecules and preserve ionic homeostasis within the brain microenvironment[49]. Our size selectivity data indicate that SC endothelial barriers have restrictive properties to regulate paracellular passage, and direct alteration of TJ complex only allows the passage of dextrans of up to 70 kDa, representing a biologically relevant size comparable to albumin (66 kDa), which does not cross the paracellular route readily in unperturbed endothelial monolayers[50]. We have shown that TJ barriers are formed and localised along the endothelial cells of the inner wall of SC *in vivo*. In conjunction with *in vitro* permeability data, TJs in the inner wall endothelium of SC are identified as possibly playing a pivotal role in contributing to paracellular movement of AH and solutes across the endothelial layer. Similarly to human SCEC, non-human primates also express ZO-1, claudin-11 and tricellulin in the inner wall of SC. However, we did not detect claudin-11 expression in the mouse outflow pathway, which suggests differential expression patterns between species.

In order to prove the efficacy of the siRNA in an *in vivo* system, ZO-1 and tricellulin siRNA were injected into the anterior chambers of mice. We show that knockdown of transcripts encoding TJs in the conventional outflow pathway increases AH outflow facility in wild type mice, and that this effect is associated with the presence of an increased number of open intercellular clefts between SCEC. It is therefore reasonable to infer that opening of intercellular clefts is responsible for the increased outflow facility measured *ex vivo*. In contrast to studies using EDTA to disrupt cellular junctions along the inner wall[31,32], no eyes treated with siRNA exhibited signs of necrosis or apoptosis, and there were no platelets adhering to the inner wall. This indicates that the endothelial cell membranes remained intact and the subendothelial ECM was not exposed to the lumen of SC.

Our *in vivo* data also reinforce that the hydraulic conductivity of the inner wall endothelium of SC is maintained by the adhesive forces produced at the endothelial cell-cell junctions between TJ proteins[14,28]. It is therefore correct to propose that factors which change the adhesive properties of TJ proteins in the inner wall of SC may alter the existing behaviour of the outflow pathway. To illustrate this point, we have preliminary data demonstrating higher claudin-11 and ZO-1 expression in glaucomatous SCEC monolayers as compared to healthy controls (Supplementary Fig. S10a). In addition, cultured glaucomatous SCEC strains displayed higher TEER values than healthy strains (Supplementary Fig. S10b). The increase in TJ expression found in glaucomatous SCEC suggests that altered barrier function in the inner wall of SC may negatively impact on conventional outflow behaviour.

While conventional adeno-associated viruses (AAV) have been shown to be inefficient in transducing cells of the outflow tissues, self-complementary AAV have been reported to be effective in such transduction[51,52]. It is of note that AAV expressing inducible short hairpin RNAs (shRNA) targeting claudin-5, or a combination of claudin-5 and occludin have been used to transfect cerebral and retinal tissues, and that down-regulation of these TJ vascular endothelial cell components renders the blood-brain and inner blood-retina barriers reversibly permeable to compounds up to 1 kDa, or 5 kDa respectively[53,54]. Should it prove possible using this technique to periodically activate virus expressing shRNAs within SCEC using an inducible promoter, expression of such shRNA could in principle be used as a means of periodically increasing outflow facility in cases of POAG in which patients fail to achieve target IOP with conventional medications. Alternatively, episcleral delivery of

siRNA, where materials can be delivered non-invasively into the outflow tissues in a retrograde fashion as an outpatient procedure[55], might represent an attractive alternative, thus avoiding the necessity of introducing a viral vector into the anterior chamber to secure viral-mediated shRNA expression. To explore the feasibility of an episcleral delivery approach, we have successfully achieved delivery of biotin conjugated tracer molecules to the conventional outflow pathway via the episcleral route in mice. Taken together, results from this study support the concept that endothelial TJs of the inner wall of SC are an attractive target upon which to base future attempts to increase AH outflow in cases of ocular hypertension.

Materials and Methods

Cell Culture. Human SCEC and TM cells were isolated, cultured and characterised as previously described[56,57]. SCEC strains used in this study were SC65, SC68, SC73, SC76, SC77, SC82 and SC83. TM93 was used for RNA analysis, whereas TM120 and TM130 were used for protein analysis. All SCEC and TM cells were used between passages 2 and 6. SCEC were cultured in low glucose Dulbecco's modified Eagle medium (Gibco, Life Sciences) supplemented with 10% *Performance Plus* foetal bovine serum (FBS) (Gibco, Life Sciences), 1% Pen/Strep glutamine (Gibco, Life Sciences), in a 5% CO_2 incubator at 37 °C. TM cells underwent a differentiation step by plating at full confluency for one week in media containing 10% FBS, and changed over to media containing 1% FBS for an additional week prior to experimentation. Cultured cells were passaged with trypsin-EDTA (Gibco-BRL) to maintain exponential growth.

Human tight junction PCR array. The human TJ RT^2 Profiler PCR array (PAHS-143ZA, Qiagen) was used to profile the expression of 84 key genes encoding proteins that form selective barriers between epithelial and endothelial cells to regulate size selectivity, polarity, proliferation and differentiation. Total RNA was extracted from four different human SCEC strains (SC65, 68, 76 and 77) at passages 3 to 5 using RNEasy Mini Kit (Qiagen) according to manufacturer's protocol. Genomic DNA contamination was eliminated by DNase treatment. Total RNA was reverse-transcribed into cDNA using RT^2 First Strand Kit (Qiagen). The Threshold cycle (Ct) values of different passage numbers from each SCEC strain were determined and averaged using ABI Prism 7700 Sequence Detector. The mean normalised expression ($2^{-\Delta Ct}$) of genes encoding claudin and adhesion junctional proteins was determined and analysed using the online Qiagen RT^2 Profiler PCR Array Data Analysis software. Normalised gene expression was calculated by using the equation: $2^{-\Delta Ct} = 2^{-[Ct(\text{gene of interest}) - Ct(\text{Housekeeping genes})]}$. Normalisation was carried out with five housekeeping genes (*ACTB, B2M, GAPDH, HPRT1 and RPLP0*) included in the PCR array. The $2^{-\Delta\Delta CT} = 2^{-\Delta Ct\ \text{treated}}/2^{-\Delta Ct\ \text{control}}$ method was used to calculate fold changes for each gene as difference in gene expression[58].

Western Blot. Protein lysates were isolated from cultured cells in protein lysis buffer containing 1 M Tris pH 7.5, 1 M NaCl, 1% NP-40, 10% SDS, 1X protease inhibitor cocktail (Roche). The homogenate was centrifuged at 10,000 r.p.m. (IEC Micromax microcentrifuge, 851 rotor) at 4 °C for 20 min and the supernatant was stored at −80 °C until use. Protein concentration was determined by BCA Protein assay kit (Pierce, IL, USA) with bovine serum albumin (BSA) at 2 mg/ml as standards on 96-well plates according to the manufacturer's protocol. 30–50 μg of total protein was loaded in each lane. Protein samples were separated by electrophoresis on 7.5–10% SDS–PAGE under reducing conditions and electro-transferred to PVDF membranes. After blocking with 5% blotting grade blocker non-fat dry milk in TBS for 1 h at room temperature, membranes were incubated overnight at 4 °C with the following Rabbit polyclonal primary antibodies: anti-oligodendrocyte specific protein antibody (1:500; Abcam); anti-ZO-1 antibody (1:250; Invitrogen), anti-tricellulin C-terminal antibody (1:125; Invitrogen), anti-occludin antibody (1:500, Invitrogen) and anti-VE-cadherin antibody (1:1000; Abcam). Blots were washed with TBS and incubated with horse radish peroxidase-conjugated polyclonal rabbit IgG secondary antibody (Abcam). The blots were developed using enhanced chemiluminescent kit (Pierce Chemical Co.) and exposed to Fuji X-ray film. Each blot was stripped with Restore Western Blot Stripping Buffer (Pierce) and probed with rabbit polyclonal to β-actin or GAPDH (Abcam) as loading controls. Protein band intensities were quantified by scanning with a HP Scanjet Professional 10000 Mobile Scanner and analysed using *Image J* (Version 1.50c). The percentage reduction in band intensity was calculated relative to the control non-targeting siRNA, which was standardised to represent 100% and normalised against β-actin.

Immunocytochemistry. Human SCEC were grown on Lab-Tek II chamber slides and fixed in 4% paraformaldehyde (pH 7.4) for 20 min at room temperature and then washed with PBS for 15 min. Cell monolayers were blocked in PBS containing 5% normal goat serum and 0.1% Triton X-100 at room temperature for 20 min. Primary antibodies were diluted at 1:100 in blocking buffer and incubated overnight at 4 °C. Secondary antibodies diluted at 1:500 were then incubated for 2 h at room temperature in a humidity chamber. Following incubation, chamber slides were mounted with aqua-polymount (Polyscience) after nuclei-counterstaining with DAPI. Fluorescent images of SCEC monolayers were captured using a confocal microscope (Zeiss LSM 710), and processed using imaging software ZEN 2012.

Immunohistochemistry for frozen sections. Enucleated mouse eyes were fixed in 4% paraformaldehyde (pH 7.4) overnight at 4 °C on a rotating device. Posterior segments of the eye and the lens were removed and anterior segments were then washed with PBS for 15 min and sequentially submerged in 10, 20 and 30% sucrose. Dissected anterior segments were then suspended in specimen blocks with OCT solution (Tissue-Tek) and frozen in a bath of isopropanol submerged in liquid nitrogen. Frozen anterior segments were sectioned using a cryostat (Leica CM 1900) to 12 μm thickness. Sections were collected on Polysine® slides (Menzel-Glazer). To detect TJ proteins, sections were blocked for 20 min at room temperature in PBS containing 5% goat serum and 0.1% Triton-X, and incubated with the corresponding antibodies at 1:100 dilutions overnight at 4 °C in a humidity chamber. All sections were then washed three times in PBS and incubated with Cy-3 labelled anti-rabbit IgG

antibody at 1:500 (Abcam) for 2 h at room temperature in a humidity chamber. Following incubation, sections were washed with PBS and mounted with aqua-polymount (Polyscience) after nuclei-counterstaining with DAPI. Anterior segments were visualised using a confocal microscope (Zeiss LSM 710).

Immunohistochemistry for paraffin embedded sections. Paraffin sections of African green monkey (*Chlorocebus Sabeus*) anterior segments were rehydrated by immersion in the following solutions: twice for 2 min each in Histoclear solution; 100% ethanol for 1 min; 95% ethanol for 1 min; 70% ethanol for 1 min; deionised water for 1 min; washing twice for 5 min in PBS. For antigen retrieval, paraffin sections were heated to 95 °C for 10 min in citrate buffer (Sodium citrate, pH 6). Paraffin sections were then blocked and stained as described above.

siRNAs. All *in vivo* predesigned siRNAs used in this study were synthesised by Ambion and reconstituted as per manufacturer's protocol. siRNA identification numbers are as follows: human claudin-11 siRNA (ID number: s9925), human ZO-1 siRNA (ID number: s14156), human MARVELD2 siRNA (ID number: s45794), mouse ZO-1 siRNA (ID number: s75175), mouse MARVELD2 siRNA (ID number: ADCSU2H). Silencer Negative control siRNA (Ambion) was used as a non-targeting control in knockdown studies.

Cell viability assay. SCEC were grown to confluency on a 96-well plate. Cells were transfected with siRNA in quadruplicate using Lipofectamine RNAiMax reagent as outlined by the manufacturer (Life Technologies) at both 1 pmol/well (40 nM) and 5 pmol/well (200 nM). Cells were left for 48 hours, apart from a media change after 24 hours. CellTitre 96 AQueous One Solution Reagent (Promega) was thawed and mixed with culture medium at a 1:5 dilution. Cells were incubated with this mixture for a period of 2 hours, before transferring the media to a fresh 96-well plate. Absorbance of each well was recorded at 450 nm on a spectrophotometer (Multiskan FC, THermo Scientific). After blanking against wells with reagent and no cells, each treatment group was presented relative to a negative control containing no siRNA. A positive control was achieved by incorporating 1% SDS into the media-reagent mixture. A one-way ANOVA with a Tukey's post-test was performed on the data set.

Measurement of SCEC monolayer transendothelial electrical resistance (TEER). TEER was used as a measure of TJ integrity by the human SCEC monolayers as previously descrived[54]. In brief, human SCEC (1×10^4 cells per well) were grown to confluency on Costar HTS Transwell-polyester membrane inserts with a pore size of 0.4 μm. The volume of the apical side (inside of the membrane inserts) was 0.1 ml and that of the basal side (outside of the membrane inserts) was 0.6 ml. Confluent cells were then transfected in triplicates with 40 nM of claudin-11, ZO-1 and tricellulin siRNAs, or in combination, using Lipofectamine RNAiMax reagent as outlined by the manufacturer (Life Technologies). Non-targeting siRNA was used as a control. 48 h post-transfection, TEER values were determined using an EVOM resistance meter with Endohm Chamber (World Precision Instruments) and a Millicell-Electrical Resistance System. For measurement of TEER, both the apical and basolateral sides of the endothelial cells were bathed in fresh growth medium at 37 °C, and a current was passed across the monolayer with changes in electrical resistance, which was reported as $\Omega.cm^2$ after correcting for the surface area of the membrane (1.12 cm). Electrical resistance was measured in triplicate wells, and the inherent resistance of a blank transwell was subtracted from the values obtained for the endothelial cells.

Cell permeability assay using FITC-dextran. Human SCEC were prepared and treated using the same method for TEER measurement as described above. Transwell permeability assays were carried out as previously described[54]. In brief, 4 kDa, 70 kDa and 150 kDa fluorescein isothiocyanate (FITC)-conjugated dextran (FD) (Sigma) was applied at 1 mg/ml to the basal compartment of the transwells. Sampling aliquots of 0.1 ml were collected every 15 min for a total of 120 min from the apical side for fluorescence measurements and the same volume of culturing media was added to replace the medium removed. FITC fluorescence was determined using a spectrofluorometer (Optima Scientific) at an excitation wavelength of 485 nm and an emission wavelength of 520 nm. Relative fluorescence units (RFU) were converted to values of nanograms per millilitre using FITC-dextran standard curves, and were corrected for background fluorescence and serial dilutions over the course of the experiment. The apparent permeability co-efficient ($P_{app,}$ cm/s) for each treatment was calculated using the following equation:

$$P_{app} = (dM/dt)/(A \times C_0),$$

where dM/dt (μg/s) is the rate of appearance of FD on the apical side from 0 min to 120 min after application of FD. C_0 (μg/ml) is the initial FD concentration on the basal side, and A (cm^2) is the effective surface area of the insert. dM/dt is the slope calculated by plotting the cumulative amount of (M) versus time.

Animal Husbandry. The use of animals and injections carried out in this study were in accordance with the European Communities Regulations 2002 and 2005 and the Association for Research in Vision and Ophthalmology statement for the use of Animals in Ophthalmic and Vision Research, and was approved by the institutional Ethics Committee. In this case, all procedures carried out at Imperial College London and Trinity College Dublin were approved by the UK Home Office and by the Health Products Regulatory Authority of the Irish Medicines Board (project authorisation AE19136/P017) respectively. Male C57BL/6J mice (Charles River Laboratories, UK) of age 10 to 12 weeks were used. *Ex vivo* perfusions and intracameral injections were done under the UK Home Office Project at Imperial College London. Animals were brought into the animal facility one week prior injections for an acclimatisation period. Mice were housed in individually ventilated cages with 5 mice per cage. They were provided with food and water *ad libitum* and were under 12 h light/dark cycles (7 am to 7 pm) at 21 °C.

Intracameral injection. Adult C57BL/6J mice of 10 to 12 weeks of age were anaesthetised by intra-peritoneal injection of medetomidine hydrochloride (Domitor) and ketamine (0.66 and 66.6 mg/kg body weight, respectively). Pupils were dilated with 2.5% tropicamide and 2.5% phenylephrine eye drops. Glass micro-capillaries (outer diameter = 1 mm, inner diameter = 0.58 mm; World Precision Instruments) were pulled using a micropipette puller (Narishige PB-7). Under microscopic control, a pulled blunt-ended micro-glass needle (tip diameter ~100 μm) was first used to puncture the cornea to withdraw AH. Immediately after puncture, a pulled blunt-ended micro-glass needle attached to a 10 μl syringe (Hamilton, Bonaduz) was inserted through the puncture, and 1.5 μl of PBS containing 1 μg of ZO-1 siRNA and 1 μg of tricellulin siRNA was administered into the anterior chamber to give a final concentration of 16.84 μM. Contralateral eyes received an identical injection of 1.5 μl containing the same concentration of NT siRNA. Following surgery, a reversing agent (1.5 mg/kg body weight, atipamezole hydrochloride) was delivered by intra-peritoneal injection. Fusidic gel was applied topically to the eye as antibiotic and Vidisic gel was also applied topically as a moisturiser. Furthermore, 5 mg/kg enrofloxacin antimicrobial (Baytril; Bayer Healthcare) was injected subcutaneously.

Apoptosis markers staining. IHC was performed on perfused eyes 48 hours post injection with either targeting or non-targeting siRNA. Approximately 30–40 12 μm sections were each stained by TUNEL and complemented by cleaved caspase-3 staining as markers of apoptosis for representatives of targeting and non-targeting siRNA. Eyes were fixed and prepared for cryosectioning as described before. TUNEL staining was performed as per manufacturers protocol (*in situ* Cell Death Detection Kit, POD, Roche), for positive controls, slides treated with Dnase-1 for 10 minutes at room temperature after permeabilisation and prior to antibody labelling. Cleaved caspase-3 staining was performed as described before using cleaved caspase 3 marker antibody (#9661, Cell Signalling Technology), positive controls were obtained by perfusing wild type eyes *ex vivo* for 24 hours at 35 °C with 200 ng/ml of mouse IL-1B and 100 ng/ml of human TNF-α in DMEM to induce apoptosis.

Transmission electron microscopy (TEM). All eyes were immersion fixed in Karnovsky's solution initially and post-fixed in Ito's solution. The eyes were embedded in Epon and semi-thin sagittal sections were cut through the whole globe. Ultrathin sections of SC and TM were cut sagitally from one side of the eye first, and then another ultrathin section approximately 1mm deeper was cut. If possible, this section was taken from the other side of the eye. In the small mouse eye, this process could be repeated four times. In this way, different parts of the circumference of the eye were evaluated. Different staining methods were investigated to visualise cell membranes, and the best results were obtained using UAR-EMS (Science Services, Munich, Germany). In ultrathin sections of the entire anterior posterior length of the inner wall from all four regions of treated eyes and their controls, we investigated whether there was any ballooning of the inner wall endothelium, necrosis or apoptosis of endothelial cells or adherence of platelets to the inner wall endothelium. Intercellular gaps were counted at magnifications of 80.000x by two independent observers (ELD and CFK).

Outflow facility measurements. Mouse eyes were perfused *ex vivo* to measure outflow facility using the *iPerfusion* system[36]. Mice were culled by cervical dislocation and the eyes were enucleated within 10 min post mortem and stored in PBS at room temperature to await perfusion (~20 min). Both eyes were perfused simultaneously using two independent perfusion systems as described previously[36]. Briefly, each eye was affixed to a support using a small amount of cyanoacrylate glue and submerged in a PBS bath regulated at 35 °C. The eye was cannulated via the anterior chamber with a 33-gauge bevelled needle (NanoFil, #NF33BV-2, World Precision Instruments) under a stereomicroscope using a micromanipulator. The *iPerfusion* system comprises an automated pressure reservoir, a thermal flow sensor (SLG64-0075, Sensirion) and a wet-wet pressure transducer (PX409, Omegadyne) in order to apply a desired pressure, measure flow rate out of the system and measure the intraocular pressure respectively. The perfusate was DBG (PBS including divalent cations and 5.5 mM glucose), and was filtered through a 0.22 μm filter (VWR international) prior to use.

Following cannulation, eyes were perfused for 30 min at ~8 mmHg to allow the eye to acclimatise to the environment. Subsequently, nine discrete pressure steps were applied from 4.5 to 21 mmHg, while flow and pressure were recorded. Stability was defined programmatically, and data were averaged over 4 min at steady state. A non-linear model was fit to flow-pressure data to account for the pressure dependence of outflow facility in mouse eyes. This model was of the form $Q = C_r P (P/P_r)^{\beta}$. where Q and P and are the flow rate and pressure respectively, and C_r is the outflow facility at reference pressure P_r which is selected to be 8 mmHg (the approximate physiological pressure drop across the outflow pathway). The power law exponent β quantifies the non-linearity in the Q-P response and thus the pressure dependence of outflow facility. The data analysis methodology described previously[36] was applied in order to analyse the treatment effect, whilst accounting for measurement uncertainties and statistical significance was evaluated using the paired weighted t-test described therein.

Statistical analysis. For real-time PCR, TEER and paracellular permeability measurements, Student's t-tests and ANOVA with Bonferroni post-test were carried out using GraphPad Prism 5.0. For *ex vivo* perfusions, a paired weighted t-test was performed using MATLAB as described[36]. For open clefts quantification, an unpaired t-test was performed. Statistical significance was indicated by $p \leq 0.05$.

References

1. Bill, A. The aqueous humor drainage mechanism in the cynomolgus monkey (Macaca irus) with evidence for unconventional routes. *Invest Ophthalmol Vis Sci* **4,** 911–919 (1965).
2. Toris, C. B., Yablonski, M. E., Wang, Y. L. & Camras, C. B. Aqueous humor dynamics in the aging human eye. *Am J Ophthalmol* **127,** 407–412 (1999).
3. Bill, A. & Phillips, C. I. Uveoscleral drainage of aqueous humour in human eyes. *Exp Eye Res* **12,** 275–281 (1971).

4. Holmberg, A. The fine structure of the inner wall of Schlemm's canal. *AMA Arch Ophthalmol* **62,** 956–958 (1959).
5. Tripathi, R. C. Ultrastructure of Schlemm's canal in relation to aqueous outflow. *Exp Eye Res* **7,** 335–341 (1968).
6. Bill, A. & Svedbergh, B. Scanning electron microscopic studies of the trabecular meshwork and the canal of Schlemm–an attempt to localize the main resistance to outflow of aqueous humor in man. *Acta Ophthalmol (Copenh)* **50,** 295–320 (1972).
7. Grierson, I. & Lee, W. R. Pressure effects on flow channels in the lining endothelium of Schlemm's canal. A quantitative study by transmission electron microscopy. *Acta Ophthalmol* (*Copenh*) **56,** 935–952 (1978).
8. Epstein, D. L. & Rohen, J. W. Morphology of the trabecular meshwork and inner-wall endothelium after cationized ferritin perfusion in the monkey eye. *Invest Ophthalmol Vis Sci* **32,** 160–171 (1991).
9. Ethier, C. R., Coloma, F. M., Sit, A. J. & Johnson, M. Two pore types in the inner-wall endothelium of Schlemm's canal. *Invest Ophthalmol Vis Sci* **39,** 2041–2048 (1998).
10. Braakman, S. T., Read, A. T., Chan, D. W., Ethier, C. R. & Overby, D. R. Colocalization of outflow segmentation and pores along the inner wall of Schlemm's canal. *Exp Eye Res* **130,** 87–96 (2015).
11. Raviola, G. & Raviola, E. Paracellular route of aqueous outflow in the trabecular meshwork and canal of Schlemm. A freeze-fracture study of the endothelial junctions in the sclerocorneal angel of the macaque monkey eye. *Invest Ophthalmol Vis Sci* **21,** 52–72 (1981).
12. Bhatt, K., Gong, H. & Freddo, T. F. Freeze-fracture studies of interendothelial junctions in the angle of the human eye. *Invest Ophthalmol Vis Sci* **36,** 1379–1389 (1995).
13. Ye, W., Gong, H., Sit, A., Johnson, M. & Freddo, T. F. Interendothelial junctions in normal human Schlemm's canal respond to changes in pressure. *Invest Ophthalmol Vis Sci* **38,** 2460–2468 (1997).
14. Perkumas, K. M. & Stamer, W. D. Protein markers and differentiation in culture for Schlemm's canal endothelial cells. *Exp Eye Res* **96,** 82–87 (2012).
15. Braakman, S. T. *et al.* Biomechanical strain as a trigger for pore formation in Schlemm's canal endothelial cells. *Exp Eye Res* **127,** 224–235 (2014).
16. Braakman, S. T., Moore, J. E. Jr., Ethier, C. R. & Overby, D. R. Transport across Schlemm's canal endothelium and the blood-aqueous barrier. *Exp Eye Res* **146,** 17–21 (2015).
17. Stamer, W. D. *et al.* Biomechanics of Schlemm's canal endothelium and intraocular pressure reduction. *Prog Retin Eye Res* **44,** 86–98 (2015).
18. Grant, W. M. Clinical measurements of aqueous outflow. *Am J Ophthalmol* **34,** 1603–1605 (1951).
19. Johnson, M., Shapiro, A., Ethier, C. R. & Kamm, R. D. Modulation of outflow resistance by the pores of the inner wall endothelium. *Invest Ophthalmol Vis Sci* **33,** 1670–1675 (1992).
20. Lütjen-Drecoll, E. Structural factors influencing outflow facility and its changeability under drugs. A study in Macaca arctoides. *Invest Ophthalmol Vis Sci* **12,** 280–294 (1973).
21. Overby, D. R., Stamer, W. D. & Johnson, M. The changing paradigm of outflow resistance generation: towards synergistic models of the JCT and inner wall endothelium. *Exp Eye Res* **88,** 656–670 (2009).
22. Allingham, R. R. *et al.* The relationship between pore density and outflow facility in human eyes. *Invest Ophthalmol Vis Sci* **33,** 1661–1669 (1992).
23. Johnson, M. *et al.* The pore density in the inner wall endothelium of Schlemm's canal of glaucomatous eyes. *Invest Ophthalmol Vis Sci* **43,** 2950–2955 (2002).
24. Overby, D. R. *et al.* Altered mechanobiology of Schlemm's canal endothelial cells in glaucoma. *Proc Natl Acad Sci USA* **111,** 13876–13881 (2014).
25. Zhang, K., Zhang, L. & Weinreb, R. N. Ophthalmic drug discovery: novel targets and mechanisms for retinal diseases and glaucoma. *Nat Rev Drug Discov* **11,** 541–559 (2012).
26. Morita, K., Sasaki, H., Furuse, M. & Tsukita, S. Endothelial claudin: claudin-5/TMVCF constitutes tight junction strands in endothelial cells. *J Cell Biol* **147,** 185–194 (1999).
27. Campbell, M. *et al.* An experimental platform for systemic drug delivery to the retina. *Proc Natl Acad Sci USA* **106,** 17817–17822 (2009).
28. Heimark, R. L., Kaochar, S. & Stamer, W. D. Human Schlemm's canal cells express the endothelial adherens proteins, VE-cadherin and PECAM-1. *Curr Eye Res* **25,** 299–308 (2002).
29. Underwood, J. L. *et al.* Glucocorticoids regulate transendothelial fluid flow resistance and formation of intercellular junctions. *Am J Physiol* **277,** C330–342 (1999).
30. Gumbiner, B., Stevenson, B. & Grimaldi, A. The role of the cell adhesion molecule uvomorulin in the formation and maintenance of the epithelial junctional complex. *J Cell Biol* **107,** 1575–1587 (1988).
31. Bill, A., Lütjen-Drecoll, E. & Svedbergh, B. Effects of intracameral Na2EDTA and EGTA on aqueous outflow routes in the monkey eye. *Invest Ophthalmol Vis Sci* **19,** 492–504 (1980).
32. Hamanaka, T. & Bill, A. Morphological and functional effects of Na2EDTA on the outflow routes for aqueous humor in monkeys. *Exp Eye Res* **44,** 171–190 (1987).
33. Bàràny, E. H. Simultaneous measurement of changing intraocular pressure and outflow facility in the vervet monkey by constant pressure infusion. *Invest Ophthalmol Vis Sci* **3,** 135–143 (1964).
34. Overby, D. R. *et al.* The structure of the trabecular meshwork, its connections to the ciliary muscle, and the effect of pilocarpine on outflow facility in mice. *Invest Ophthalmol Vis Sci* **55,** 3727–3736 (2014).
35. Li, G. *et al.* Pilocarpine-induced dilation of Schlemm's canal and prevention of lumen collapse at elevated intraocular pressures in living mice visualized by OCT. *Invest Ophthalmol Vis Sci* **55,** 3737–3746 (2014).
36. Sherwood, J. M., Reina-Torres, E., Bertrand, J. A., Rowe, B. & Overby, D. R. Measurement of outflow facility using iPerfusion. *Plos One* **11,** e0150694 (2016).
37. Van Itallie, C. M., Fanning, A. S., Bridges, A. & Anderson, J. M. ZO-1 stabilizes the tight junction solute barrier through coupling to the perijunctional cytoskeleton. *Mol Biol Cell* **20,** 3930–3940 (2009).
38. Ikenouchi, J., Sasaki, H., Tsukita, S., Furuse, M. & Tsukita, S. Loss of occludin affects tricellular localization of tricellulin. *Mol Biol Cell* **19,** 4687–4693 (2008).
39. Gow, A. *et al.* CNS myelin and sertoli cell tight junction strands are absent in Osp/claudin-11 null mice. *Cell* **99,** 649–659 (1999).
40. Alvarado, J. A., Betanzos, A., Franse-Carman, L., Chen, J. & Gonzalez-Mariscal, L. Endothelia of Schlemm's canal and trabecular meshwork: distinct molecular, functional, and anatomic features. *Am J Physiol Cell Physiol* **286,** C621–634 (2004).
41. Park, D. Y. *et al.* Lymphatic regulator PROX1 determines Schlemm canal integrity and identity. *J Clin Invest* (2014).
42. Kizhatil, K., Ryan, M., Marchant, J. K., Henrich, S. & John, S. W. Schlemm's canal is a unique vessel with a combination of blood vascular and lymphatic phenotypes that forms by a novel developmental process. *PLoS Biol* **12,** e1001912 (2014).
43. Van Itallie, C., Rahner, C. & Anderson, J. M. Regulated expression of claudin-4 decreases paracellular conductance through a selective decrease in sodium permeability. *J Clin Invest* **107,** 1319–1327 (2001).
44. Morita, K., Sasaki, H., Fujimoto, K., Furuse, M. & Tsukita, S. Claudin-11/OSP-based tight junctions of myelin sheaths in brain and Sertoli cells in testis. *J Cell Biol* **145,** 579–588 (1999).
45. Wessells, H. *et al.* Transcriptional profiling of human cavernosal endothelial cells reveals distinctive cell adhesion phenotype and role for claudin 11 in vascular barrier function. *Physiol Genomics* **39,** 100–108 (2009).
46. Ikenouchi, J. *et al.* Tricellulin constitutes a novel barrier at tricellular contacts of epithelial cells. *J Cell Biol* **171,** 939–945 (2005).

47. Krug, S. M. *et al.* Tricellulin forms a barrier to macromolecules in tricellular tight junctions without affecting ion permeability. *Mol Biol Cell* **20,** 3713–3724 (2009).
48. Bazzoni, G. Endothelial tight junctions: permeable barriers of the vessel wall. *Thromb Haemost* **95,** 36–42 (2006).
49. Stamatovic, S. M., Keep, R. F. & Andjelkovic, A. V. Brain endothelial cell-cell junctions: how to "open" the blood brain barrier. *Curr Neuropharmacol* **6,** 179–192 (2008).
50. Johnstone, M. A. In *Becker-Shaffer's Diagnosis and Therapy of the Glaucomas* (8th Edition) (eds Marc F. Lieberman & Michael V. Drake) 25–46 (Mosby, 2009).
51. Buie, L. K. *et al.* Self-complementary AAV virus (scAAV) safe and long-term gene transfer in the trabecular meshwork of living rats and monkeys. *Invest Ophthalmol Vis Sci* **51,** 236–248 (2010).
52. Bogner, B. *et al.* Capsid mutated adeno-associated virus delivered to the anterior chamber results in efficient transduction of trabecular meshwork in mouse and rat. *Plos One* **10,** e0128759 (2015).
53. Campbell, M. *et al.* Systemic low-molecular weight drug delivery to pre-selected neuronal regions. *EMBO Mol Med* **3,** 235–245 (2011).
54. Keaney, J. *et al.* Autoregulated paracellular clearance of amyloid-beta across the blood-brain barrier. *Sci Adv* **1,** e1500472 (2015).
55. Morrison, J. C. *et al.* A rat model of chronic pressure-induced optic nerve damage. *Exp Eye Res* **64,** 85–96 (1997).
56. Stamer, W. D., Roberts, B. C., Howell, D. N. & Epstein, D. L. Isolation, culture, and characterization of endothelial cells from Schlemm's canal. *Invest Ophthalmol Vis Sci* **39,** 1804–1812 (1998).
57. Stamer, W. D., Seftor, R. E., Williams, S. K., Samaha, H. A. & Snyder, R. W. Isolation and culture of human trabecular meshwork cells by extracellular matrix digestion. *Curr Eye Res* **14,** 611–617 (1995).
58. Schmittgen, T. D. & Livak, K. J. Analyzing real-time PCR data by the comparative C(T) method. *Nat Protoc* **3,** 1101–1108 (2008).

Acknowledgements

Work at the Ocular Genetics Unit at the University of Dublin, Trinity College, was supported by the European Research Council ERC-2012-AdG. The Unit also receives support from Science Foundation Ireland. Work at Duke University was supported by grants from the US National Institutes of Health (EY022359 and EY019696) and at Imperial College London by Fight for Sight UK (Ref 1385), the US National Institutes of Health (EY022359 and EY019696), and the UK Engineering and Physical Sciences Research Council (EP/J010499/1). We would like to thank C. Woods and C. Murray for animal husbandry. We thank Elke Kretshmar, Hong Nguyen and Britta Bäckermann for their technical assistance with TEM, Jörg Pekarsky for preparing the schematic drawing and Marco Gößwein for preparing the final version of Figure 1.

Author Contributions

All authors reviewed the manuscript. L.C.S.T. performed PCR arrays, RNAi knockdown, gene expression analysis in SCEC, IHC, TEER and P*app* measurements, and wrote the main manuscript text; E.R.-T. performed mouse intracameral injections, iPerfusion, gene expression analysis in TM cells and contributed to manuscript preparation; J.M.S. contributed to experimental design, performed statistical analysis for iPerfusion and contributed to manuscript preparation; P.C. performed RNAi knockdown, mouse intracameral injection and assisted with iPerfusion; D.C. performed mouse IHC and protein inhibition analysis in mouse; E.L.-D. performed TEM; C.F.-K. performed TEM; K.P. provided SCEC lines; M.M.H. performed gene sequencing and contributed to siRNA design; A.-S.K. assisted with PCR array analysis and contributed to manuscript preparation; J.O'C assisted with iPerfusion and performed cell viability experiments; J.J.C. provided non-human primate anterior segment paraffin sections; A.T.R. contributed to the interpretation of physiological data and statistical analysis, and provided revisions to the manuscript; C.R.E. contributed to the interpretation of physiological data and statistical analysis, and provided revisions to the manuscript; C.O'B. contributed to manuscript preparation; M.L. contributed to manuscript preparation; M.C. contributed to manuscript preparation; W.D.S. conceived the concept and assisted with experimental design, provided cell lines and contributed to manuscript preparation; D.R.O. assisted with experimental design, iPerfusion and contributed to manuscript preparation; P.H. conceived the concept and contributed to experimental design and writing of the manuscript.

Additional Information

Supplementary information accompanies this paper at http://www.nature.com/srep

Competing financial interests: The authors declare no competing financial interests.

How to cite this article: Tam, L. C. S. *et al.* Enhancement of Outflow Facility in the Murine Eye by Targeting Selected Tight-Junctions of Schlemm's Canal Endothelia. *Sci. Rep.* **7**, 40717; doi: 10.1038/srep40717 (2017).

Publisher's note: Springer Nature remains neutral with regard to jurisdictional claims in published maps and institutional affiliations.

This work is licensed under a Creative Commons Attribution 4.0 International License. The images or other third party material in this article are included in the article's Creative Commons license, unless indicated otherwise in the credit line; if the material is not included under the Creative Commons license, users will need to obtain permission from the license holder to reproduce the material. To view a copy of this license, visit http://creativecommons.org/licenses/by/4.0/

© The Author(s) 2017

Human Molecular Genetics, 2017, Vol. 26, No. 7 1230–1246

doi: 10.1093/hmg/ddx028
Advance Access Publication Date: 1 February 2017
Original Article

ORIGINAL ARTICLE

Therapeutic potential of AAV-mediated MMP-3 secretion from corneal endothelium in treating glaucoma

Jeffrey O'Callaghan[1,*], Darragh. E. Crosbie[1], Paul. S. Cassidy[1], Joseph M. Sherwood[2], Cassandra Flügel-Koch[3], Elke Lütjen-Drecoll[3], Marian M. Humphries[1], Ester Reina-Torres[1], Deborah Wallace[4], Anna-Sophia Kiang[1], Matthew Campbell[1], W. Daniel Stamer[5], Darryl R. Overby[2], Colm O'Brien[6], Lawrence C. S. Tam[1,*,†] and Peter Humphries[1,*,†]

[1]Ocular Genetics Unit, Smurfit Institute of Genetics, University of Dublin, Trinity College, Dublin, D2, Ireland, [2]Department of Bioengineering, Imperial College London, London, SW7 2BX, UK, [3]Department of Anatomy II, University of Erlangen-Nürnberg, D-91054 Erlangen, Germany, [4]Clinical Research Centre, UCD School of Medicine and Medical Science, University College Dublin, Belfield, Dublin 4, Ireland, [5]Departments of Ophthalmology and Biomedical Engineering, Duke University, Durham, NC, USA and [6]Department of Ophthalmology, Mater Misericordiae University Hospital, Dublin, D7, Ireland

*To whom correspondence should be addressed: Tel: 353 1 896 2164, 353 1 896 1547; Fax: 353 1 679 8558; E-mail: ocallaje@tcd.ie (J.O.), lawrenct@tcd.ie (L.C.S.T.), pete.humphries@tcd.ie (P.H.)

Abstract

Intraocular pressure (IOP) is maintained as a result of the balance between production of aqueous humour (AH) by the ciliary processes and hydrodynamic resistance to its outflow through the conventional outflow pathway comprising the trabecular meshwork (TM) and Schlemm's canal (SC). Elevated IOP, which can be caused by increased resistance to AH outflow, is a major risk factor for open-angle glaucoma. Matrix metalloproteinases (MMPs) contribute to conventional aqueous outflow homeostasis in their capacity to remodel extracellular matrices, which has a direct impact on aqueous outflow resistance and IOP. We observed decreased MMP-3 activity in human glaucomatous AH compared to age-matched normotensive control AH. Treatment with glaucomatous AH resulted in significantly increased transendothelial resistance of SC endothelial and TM cell monolayers and reduced monolayer permeability when compared to control AH, or supplemented treatment with exogenous MMP-3.

Intracameral inoculation of AAV-2/9 containing a CMV-driven MMP-3 gene (AAV-MMP-3) into wild type mice resulted in efficient transduction of corneal endothelium and an increase in aqueous concentration and activity of MMP-3. Most importantly, AAV-mediated expression of MMP-3 increased outflow facility and decreased IOP, and controlled expression using an inducible promoter activated by topical administration of doxycycline achieved the same effect. Ultrastructural analysis of MMP-3 treated matrices by transmission electron microscopy revealed remodelling and degradation of core extracellular

†These authors contributed equally to this work.

Received: December 9, 2016. **Revised:** January 17, 2017. **Accepted:** January 18, 2017

© The Author 2017. Published by Oxford University Press.
This is an Open Access article distributed under the terms of the Creative Commons Attribution Non-Commercial License (http://creativecommons.org/licenses/by-nc/4.0/), which permits non-commercial re-use, distribution, and reproduction in any medium, provided the original work is properly cited. For commercial re-use, please contact journals.permissions@oup.com

matrix components. These results indicate that periodic induction, via use of an eye drop, of AAV-mediated secretion of MMP-3 into AH could have therapeutic potential for those cases of glaucoma that are sub-optimally responsive to conventional pressure-reducing medications.

Introduction

The eye is pressurised by a balance in the production of aqueous humour (AH) by the ciliary processes and resistance to its drainage through the trabecular meshwork (TM) and Schlemm's canal (SC). Located at the apex of the iridocorneal angle, SC is a flattened circular vessel with an average meridional diameter of 233 μm in humans (1). AH exits the lumen of SC into collector channels and drains into the episcleral veins that are visible on the surface of the sclera. Precise regulation of aqueous inflow together with outflow resistance is critical in maintaining an average intraocular pressure (IOP) of approximately 16 mmHg in a normal functioning eye (2). In cases of primary open-angle glaucoma (POAG), so-called because the iridocorneal angle remains open without noticeable physical obstruction, resistance to AH drainage through the TM and SC is increased by mechanisms that have yet to be fully elucidated, resulting in elevated IOP (3). This, in turn, results in deformation of the lamina cribrosa—the tissue that structurally supports the optic nerve head—(often referred to as 'cupping' of the optic nerve head), damaging retinal ganglion cell axons, leading to ganglion cell degeneration and irreversible blindness.

Lowering IOP remains the only effective treatment for POAG. Topical pressure reducing medications either increase the rate of aqueous outflow through the conventional or unconventional pathway, or reduce aqueous production (3). The U.S. spends $1.9 billion per annum to treat glaucoma, 38–52% of such costs being related to topical pressure reducing medications (4). However, such medications often do not reduce IOP to the desired target pressure and may induce side effects in certain patients. Such patients may then undergo surgical interventions, which have associated risks and complications. Hence, there remains an unmet clinical need for improved methods of disease treatment.

Functional studies have provided evidence that the generation of aqueous outflow resistance is most significant in the juxtacanalicular tissue (JCT—the outer layer of the TM) and inner wall endothelium of SC (5,6). In particular, the extracellular matrix (ECM) composition in the JCT region has been shown to influence outflow patterns and resistance generation (6–11). Competitive disruption or inhibition of integrin-ECM linkages that attach the cell to the ECM, or inhibition of ECM receptors have been associated with increases in endothelial monolayer permeability and transendothelial transport (12–15). This implicates features that are relevant to SC endothelial cells (SCEC) and their supporting basement membrane, such as integrin-ECM interactions, along with other inter-endothelial junctions that govern cell shape, in the control of endothelial paracellular permeability (16). TM cells play an integral role in modulating the ECM of the JCT to preserve AH flow pathways via continual and signal-initiated ECM remodelling (17). The ECM in the JCT region is comprised of a heterogeneous group of fibrous and matrical materials including collagen type IV, proteoglycans, laminin and fibronectin, all of which provide tensile strength and support to surrounding cells. The cribriform plexus, a structure composed of elastic fibres, connects the inner wall endothelium and the ciliary muscle, allowing for JCT expansion in response to IOP elevation (18). ECM reconditioning of these matrix networks can thus induce changes in the actin cytoskeleton through integrin-ECM linkages, enabling F-actin or alpha-smooth muscle actin (α-SMA) to act as markers for active ECM remodelling (19–21). ECM turnover in the conventional outflow pathway is regulated by a family of zinc-dependent endopeptidases, the matrix metalloproteinases (MMPs). These secreted proteases are responsible for the degradation of ECM proteins and cell proliferation, and are thus key components in ECM remodelling and outflow tissue homeostasis (22). MMPs are secreted as inactive protein precursors and are activated when cleaved by extracellular proteinases and other MMPs (23). Levels of MMPs, along with TIMPs (Tissue Inhibitors of Metalloproteinases), have been shown to differ in glaucomatous AH and TM tissue as compared to those from normotensive individuals (24,25). Imbalance in MMP/TIMP ratios, and reduced MMP enzymatic activity, has been correlated with the accumulation of ECM materials in the TM that ultimately leads to an increase in outflow resistance (26,27). Therefore, reduction in ECM turnover within the TM and JCT region as a result of an imbalanced latent-to-activated MMP ratio can be a contributing factor to increased outflow resistance, as observed in glaucoma. It is therefore evident that increasing ECM turnover in outflow tissues may have therapeutic significance by reducing outflow resistance. Here, we set out to develop a gene-based therapy for the delivery of MMP targeting the conventional outflow tissues, with the primary aim of reducing both outflow resistance and IOP. Introduction of MMPs into the anterior chamber of the eye has previously been shown to increase outflow facility in organ-perfused cultures, indicating their therapeutic potential (28–31). Of the many classes of MMPs, MMP-3 (stromelysin-1) presents itself as an attractive candidate for targeting the ECM of outflow tissues. MMP-3 possesses a vast proteolytic target profile including type IV collagen, fibronectin, laminin, elastin, and proteoglycans, all of which are present in the meshwork and JCT regions of the outflow tissues, making this MMP of particular interest (32–36). In addition, MMP-3 can also activate other MMPs, including MMP-1 and MMP-9 (23,37–39), further assisting in the remodelling of ECM components (40–42).

Efficient gene delivery into the anterior segment of the eye is feasible through the use of adenoviral and adeno-associated viral (AAV) vectors. In particular, self-complementary AAV vectors have been shown to have such capability (43–46). Owing to the fact that MMP-3 is a secretory enzyme synthesised in the endoplasmic reticulum, transduction of tissues of the anterior segment with AAV expressing MMP-3 will result in the secretion of the protein into the AH. This will subsequently enable MMP-3 to be delivered into outflow tissues via conventional aqueous flow, potentially facilitating targeted degradation of ECM components and thus increasing aqueous outflow. In this regard, we observed highly efficient transduction of corneal endothelial cells following a single intracameral inoculation of AAV-2/9 expressing MMP-3, and both levels and activity of MMP-3 were significantly elevated in mouse AH following such inoculation. Importantly, AAV-mediated expression of MMP-3 in corneal endothelium, either from a CMV-, or doxycycline-inducible promoter, resulted in a marked increase in outflow facility and reduction in IOP. These observations correlated with structural alterations in the ECM of the outflow tissues, suggesting a mechanism of action for MMP-3 in modulating outflow resistance.

Results

Effects of glaucomatous aqueous humour on SC endothelial and TM cell monolayers

We treated cultured human SCEC monolayers with human glaucomatous (POAG) or control (cataract) AH for 24 h, and quantified levels of total secreted and activated MMP-3 in culture media. This was achieved by performing an ELISA and FRET assay, to monitor the degree of cleavage of an MMP-3 specific substrate, on cell media 24 h post-treatment. We did not observe a significant increase in the level of total (latent and active forms) secreted MMP-3 in culture media following treatment with POAG aqueous, with an increase of 0.15 [−0.35, 0.66] ng/ml (mean [95% confidence interval (CI)]) ($P = 0.45$, $n = 3$, Fig. 1A) over controls. However, activity assays indicated that the MMP-3 secreted in response to POAG aqueous had less enzymatic activity than that of cataract control AH, with an average change of −0.15 [−0.28, −0.02] mU/ml ($P = 0.024$, $n = 9$ cataract, $n = 7$ POAG, Fig. 1B). These observations corroborate results obtained involving other members of the MMP family in POAG aqueous (24) in that the amount of secreted MMP may remain relatively unchanged but its proteolytic activity is reduced.

Effects of glaucomatous AH on the permeability of SCEC and human TM (HTM) monolayers were determined by trans-endothelial electrical resistance (TEER) and FITC-dextran flux assays. Treatment of cultured SCEC monolayers with POAG AH resulted in increased TEER by an average of 102% after 24-h treatment compared to control AH (−7%), displaying an average absolute increase of 19.82 [15.82, 23.81] $\Omega.cm^2$ ($P < 0.0001$, $n = 6$ cataract, $n = 12$ POAG, Fig. 1C). Similarly, HTM responded with an increase of 9.79 [5.55, 14.05] $\Omega.cm^2$ in response to glaucomatous AH, ($P = 0.0002$, $n = 8$, Fig. 1D). Glaucomatous AH also reduced paracellular flux, as measured by permeability co-efficient (P_{app}), to dextran of 70 kDa as compared to cataract controls, with a mean difference of 0.14 [0.05, 0.22] cm/s $\times 10^{-8}$ ($P = 0.009$, $n = 3$ cataract, $n = 3$ POAG, Fig. 1E). A reduction in HTM permeability was also observed with a mean difference of 0.17 [0.09, 0.23] cm/s $\times 10^{-9}$ ($P = 0.005$, $n = 8$ cataract, $n = 7$ POAG, Fig. 1F).

Treatment of outflow cell monolayers with recombinant human MMP-3 increases permeability with concomitant reductions in TEER

In contrast to the negative effects of glaucomatous AH on SCEC and HTM permeability and resistance, we observed that treatment of cultured monolayers with 10 ng/ml of active recombinant human MMP-3 reduced TEER values on average by 5.62 [2.92, 8.32] $\Omega.cm^2$ greater than inactivated MMP-3 controls over the course of 24 h for SCEC ($P < 0.0001$, $n = 8$, Fig. 2A) and by 4.29 [0.11, 8.48] $\Omega.cm^2$ for HTM ($P = 0.0137$, $n = 8$, Fig. 2B) respectively. Permeability assays complemented these data as increases in paracellular flux of 70 kDa FITC-dextran by 0.14 [0.12, 0.18] cm/s $\times 10^{-9}$ ($P < 0.0001$, $n = 8$, Fig. 2C) were observed in SCEC, and 0.04 [0.01, 0.06] cm/s $\times 10^{-9}$ ($P < 0.01$, $n = 8$, Fig. 2D) in HTM monolayers when comparing treatments of MMP-3 to its inactivated counterpart control: TIMP-1 incubated with MMP-3. To rule out cytotoxicity as a reason for the observed changes in paracellular permeability, a cell viability assay was undertaken. Based on data shown in Figure 2E, for concentrations below 36 ng/ml MMP-3, the average SCEC cell viability for $n = 3$ will exceed 85%. Greater tolerability was observed in HTM cases, retaining an average viability of at least 85% for MMP-3 concentrations up to 151 ng/ml ($n = 3$, Fig. 2F).

Treatment of SCEC and HTM monolayers with active recombinant human MMP-3 induces remodelling and degradation of ECM components

In order to attribute increases in permeability to the ECM remodelling effects associated with MMP-3, SCEC and HTM monolayers were both treated as above with 10 mg/ml MMP-3 for 24 h. Following treatment, we observed changes in the staining pattern and intensity of a number of ECM proteins by immunocytochemistry. Specific collagen IV staining was localised to perinuclear areas and cytoplasm in both SCEC and HTM cells (Fig. 3A and B). In particular, we observed a decrease in the staining intensity around perinuclear areas in treated cells as compared to controls. A-SMA fibres facilitating cell-cell contacts in SCEC localised specifically to the cytoplasm and cytoskeleton, and MMP-3 treatment led to an attenuation of fibre bundles with thinning of intercellular connections (Fig. 3C). Fluorescent images of F-actin in HTM monolayers also revealed constricted actin bundles and a reduced tendency for bundle crossovers (Fig. 3D). Immunofluorescence staining of laminin in SCEC and HTM cells showed diminished cytoplasmic localisation and reduced network complexity and multiplicity in MMP-3 treated cells as compared to control staining intensity of laminin (Fig. 3E and F). To visualise fibronectin clearly without cellular interference, decellularisation was performed after MMP-3 treatment to isolate the ECM scaffold from the cell monolayer. Fluorescent images show significant perturbation of fibronectin network in treated cells as opposed to the linear cellular organisation observed in control cells (asterisk, Fig. 3G and H). To quantitatively demonstrate remodelling of these proteins, western blot analysis was performed on both cell lysate and media fractions of SC and HTM cell monolayers (Supplementary Material, Fig. S1). Specific bands were observed at 300 kDa for collagen IV, 42 kDa for α-SMA, 220 kDa for laminin and 290 kDa for fibronectin. A significant reduction of collagen IV ($P = 0.01$, $P = 0.01$) α-SMA ($P = 0.04$, $P = 0.04$) and laminin ($P = 0.04$, $P = 0.03$) were observed in SC and HTM whole cell lysate samples respectively ($n = 4$ for all cases). Collectively, these data clearly illustrate that MMP-3 mediates remodelling of ECM components in both SCEC and HTM cell monolayers.

Intracameral inoculation of AAV-2/9 expressing a CMV-driven MMP-3 gene efficiently transduces corneal endothelium and results in elevated levels of MMP-3 in aqueous humour

AAV-mediated transduction of corneal endothelium could, in principle, serve as an efficient means of expressing and secreting MMP-3 into AH. The advantage of such an approach is that the natural flow dynamics of AH will allow transportation of secreted MMP-3 towards the outflow tissues (Fig. 4A). We evaluated the efficiency of a number of AAV serotypes with either single stranded or self-complementary genomes to deliver MMP-3 to the outflow tissues. 2μl of viral particles (2×10^{12} vector genomes/ml) of each serotype, expressing a CMV-driven eGFP reporter gene (Fig. 4B) were intracamerally inoculated into wild type C57BL/6 mice and eyes examined via fluorescent microscopy at 3 weeks post-inoculation. Extensive expression of the reporter gene was observed in the corneal endothelium of eyes injected with non-self-complementary AAV-2/9 (Fig. 4C top), with no fluorescence being detectable in the outflow tissues themselves using this construct. Hence, the eGFP cDNA from AAV-2/9 was exchanged with murine MMP-3 cDNA to generate AAV-MMP-3, and similar inoculation resulted in MMP-3 expression that was prominently detected in the corneal

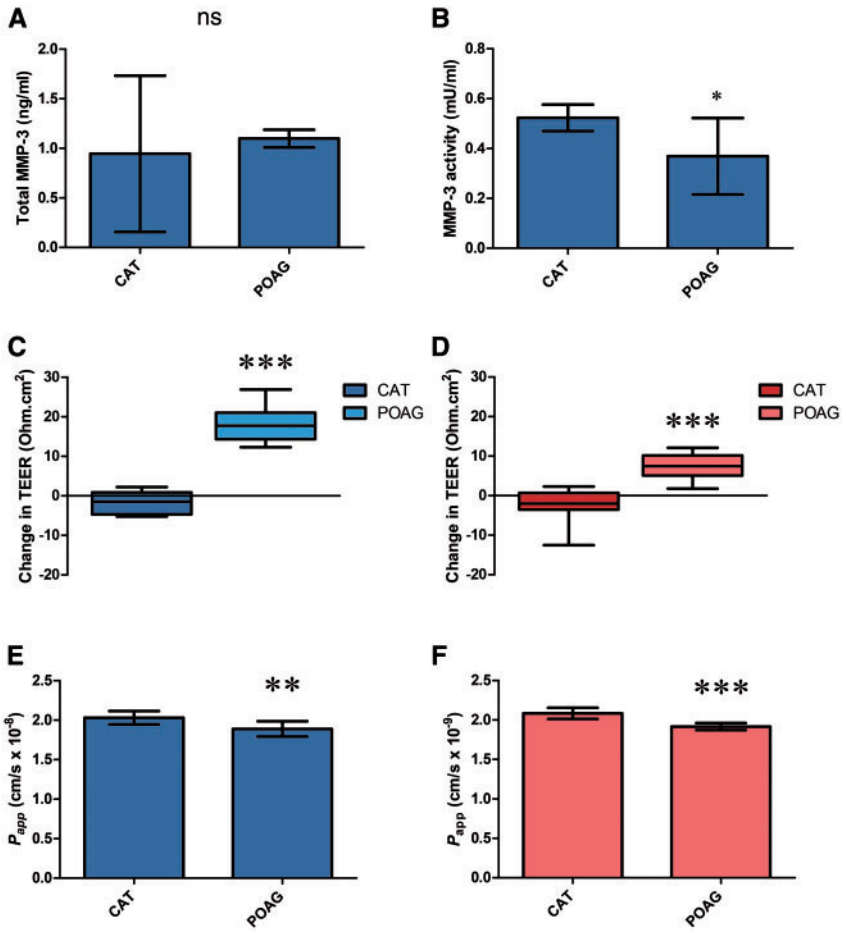

Figure 1. MMP-3 concentration in glaucomatous AH and the resulting effect on SCEC and HTM monolayers. (**A**) MMP-3 concentrations in the media of SCEC monolayers treated with either cataract (control) or POAG human AH showed no significant difference after 24 h. (**B**) POAG aqueous-treated SC media samples from (A) were found to have an average change in MMP-3 proteolytic activity of -0.15 [−0.28, −0.02] mU/ml compared to control media. (**C**) Addition of POAG aqueous humour onto SC monolayers resulted in an average increase in TEER of 102% compared to controls. (**D**) Treatment of HTM cells with human aqueous also increased TEER value. (**E,F**) SCEC and HTM subjected to AH were tested for cellular permeability using a FITC-Dextran flux assay respectively. Decreased permeability to a 70 kDa dextran was observed in response to POAG rather than cataract AH. Graphs show mean with 95% CI error bars. CAT = cataract, POAG = primary open-angle glaucoma. Figures A-F were analysed with a Student's *t*-test. NS = non-significant. Symbols *, ** and *** denote *P* values of < 0.05, < 0.01 and < 0.001, respectively.

endothelium and not in null controls (Fig. 4C, bottom). No significant difference in central corneal thickness was detected following AAV inoculation between treated (116.7 [112.5, 120.9] μm) and control eyes (116.4 [113.6, 119.1] μm) ($n = 4$, Supplementary Material, Fig. S2). Corneas also appeared clear with no signs of cataracts upon visual inspection.

The level of total MMP-3 in the AH of twelve inoculated animals was quantified using enzyme-linked immunosorbent assay (ELISA), and we observed a significant average increase in total MMP-3 protein of 56%, 1.37 [0.89, 1.84] ng/ml as compared to 0.87 [0.59, 1.12] ng/ml for control AAV ($P = 0.016$, $n = 12$, Fig. 4D). The activity of AAV-mediated production of MMP-3 was also assessed using FRET, and a significant increase in activity of 34 [6.86, 61.14] % was observed, on average, in AAV-MMP-3 treated eyes compared to contralateral controls ($P = 0.0164$, $n = 17$, Fig. 4E).

Intracameral inoculation of AAV-2/9 expressing an MMP-3 gene increases outflow facility and reduces IOP in murine eyes

In order to determine the effect of AAV-mediated expression of MMP-3 from the corneal endothelium on aqueous outflow, the conventional outflow facility was measured using the recently developed *iPerfusion* system designed specifically to measure conventional outflow facility in mice (47). Wild type mice were intracamerally injected with $1x10^{11}$ vector genomes of AAV-MMP-3, and contralateral eyes received the same quantity of AAV-Null. Four weeks post-inoculation, eyes were enucleated and perfused in pairs over incrementing steps in applied pressure. A representative flow-pressure plot provided in Supplementary Material, Figure S3A describes the relationship between flow rate (Q) at each pressure (P) step in both AAV-MMP-3 (red) and AAV-Null (blue) eyes. Furthermore, the relative percentage difference in facility within each data pair is depicted in Supplementary Material, Figure S3B (left). The resulting facility data presented in Figure 5A and B clearly illustrate that control eyes have an average facility of 8.44 [6.14, 11.60] nl/min/mmHg with treated eyes having an average facility of 11.73 [8.05, 17.08] nl/min/mmHg. There is, therefore, an average increase in outflow facility of 39 [19, 63] % in pairs, between treated eyes and their contralateral controls ($P = 0.002$, $n = 8$ pairs).

As the major pathology in POAG is IOP elevation, and an increased outflow facility was observed, tonometric IOP

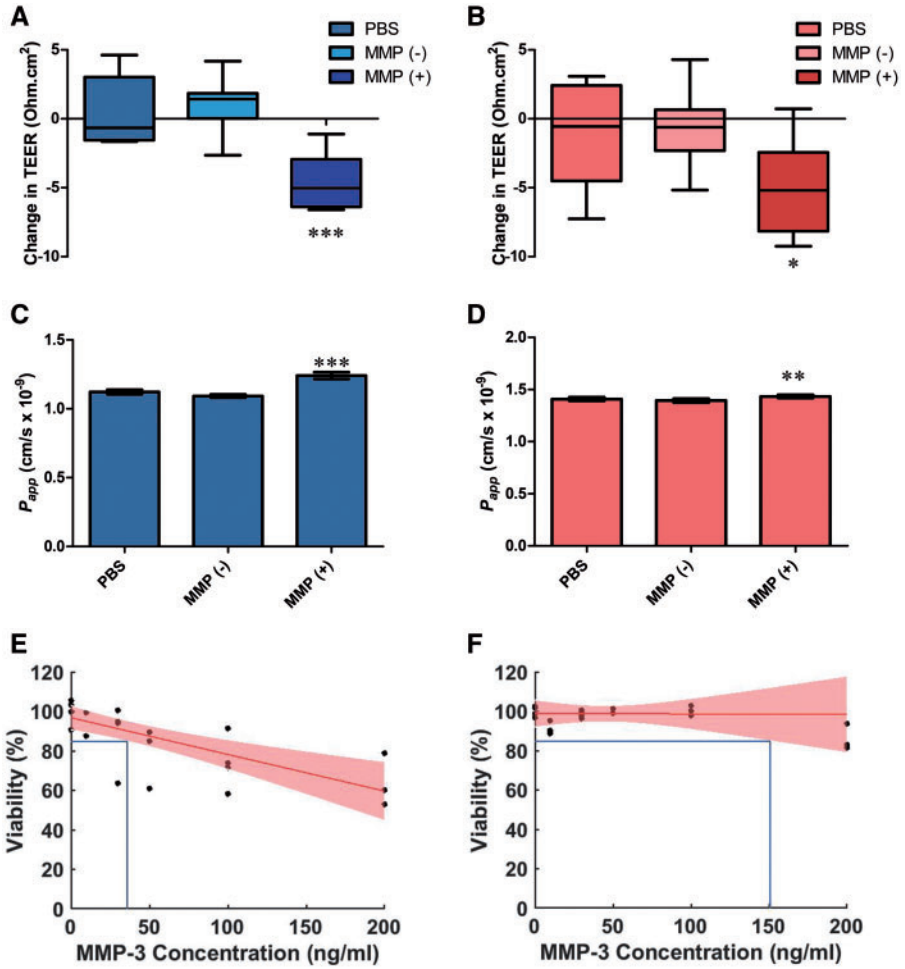

Figure 2. Effect of recombinant human MMP-3 on paracellular permeability in HTM and SCEC cell monolayers. SCEC and HTM cells were treated with 10 ng/ml recombinant MMP-3 for 24 h, using PBS and inactivated MMP-3 (incubation with TIMP-1, MMP(−)) as vehicle and negative controls respectively. (**A**) SCEC and (**B**) HTM both show reductions in TEER values after treatment of 4.6 [2.9, 6.2] and 5 [2.2, 7.8] Ohms.cm^2 respectively. Permeability to a 70 kDa dextran was increased in treated cells (MMP (+)) in both (**C**) SCEC and (**D**) HTM. (**E**) An average viability of 85% was expected for SCEC with MMP-3 concentrations up to 36 ng/ml. (**F**) 85% viability is retained on average in HTM cells at concentrations up to 151 ng/ml MMP-3. A, C and E in blue represent SCEC data, whereas B, D and F in red represent HTM data.

measurements were taken both immediately before (pre), and four weeks after (post) intracameral injection of AAV-2/9 expressing MMP-3 or a null vector in the case of the control. Differences between pre- and post-injection IOP were calculated using the non-parametric Wilcoxon matched-pairs signed rank test. Eyes treated with AAV-Null had no significant change in IOP -0.5 ± 2.9 mmHg (median ± median absolute deviation (MAD), $P = 0.61$, $n = 7$, Wilcoxon signed-rank test with a theoretical median IOP change of 0) after treatment. In comparison, when treated with AAV-MMP-3, median IOP significantly decreased by 3.0 ± 2.9 mmHg ($P = 0.022$, $n = 7$, Fig. 5C). The IOP difference in AAV-MMP-3 treated eyes was significantly greater than the IOP difference in the contralateral AAV-Null treated eyes by 2.5 ± 0.7 mmHg ($P = 0.034$, $n = 7$, Fig. 5C).

Controlled periodic activation of MMP-3

To incorporate a control mechanism for the secretion of MMP-3 from corneal endothelium, we first introduced AAV-2/9 expressing eGFP under the control of a tetracycline-inducible promoter into the anterior chambers of both eyes of wild type mice. After 3 weeks, mice were treated with a regime of one drop of 0.2% doxycycline (a tetracycline derivative) two times per day (approx. 8 h between each application) for 10–16 days in one eye only. PBS was administered onto the contralateral eye as a control. As illustrated in Supplementary Material, Figure S4, extensive expression of the reporter gene was observed only in the corneal endothelium, and no expression was observed in the contralateral control. Following this, we replaced the reporter cDNA with murine MMP-3 cDNA and the resulting AAV (Induc. AAV-MMP-3) was injected into the anterior chambers of animals at $1x10^{11}$ viral genomes per eye. Using the inducible eGFP virus (Induc. AAV-eGFP) as a contralateral control, expression was induced by administering doxycycline (as above) to both eyes. Contralateral eyes were perfused as above, the control group exhibiting an average facility of 8.30 [5.75, 11.26] nl/min/mmHg and the MMP-3 treatment group resulting in a facility of 14.01 [11.09, 17.72] nl/min/mmHg. Paired, these eyes exhibit an average increase in outflow facility of 68 [24, 128] % ($P = 0.004$, $n = 11$, Fig. 5D and E). The relative difference in facility within individual pairs is presented in Supplementary Material, Figure S3B (right). This observation strongly supports the concept that MMP-3 expression could be induced in a controlled and reversible manner, with periodic IOP measurements utilised to guide the induction of expression.

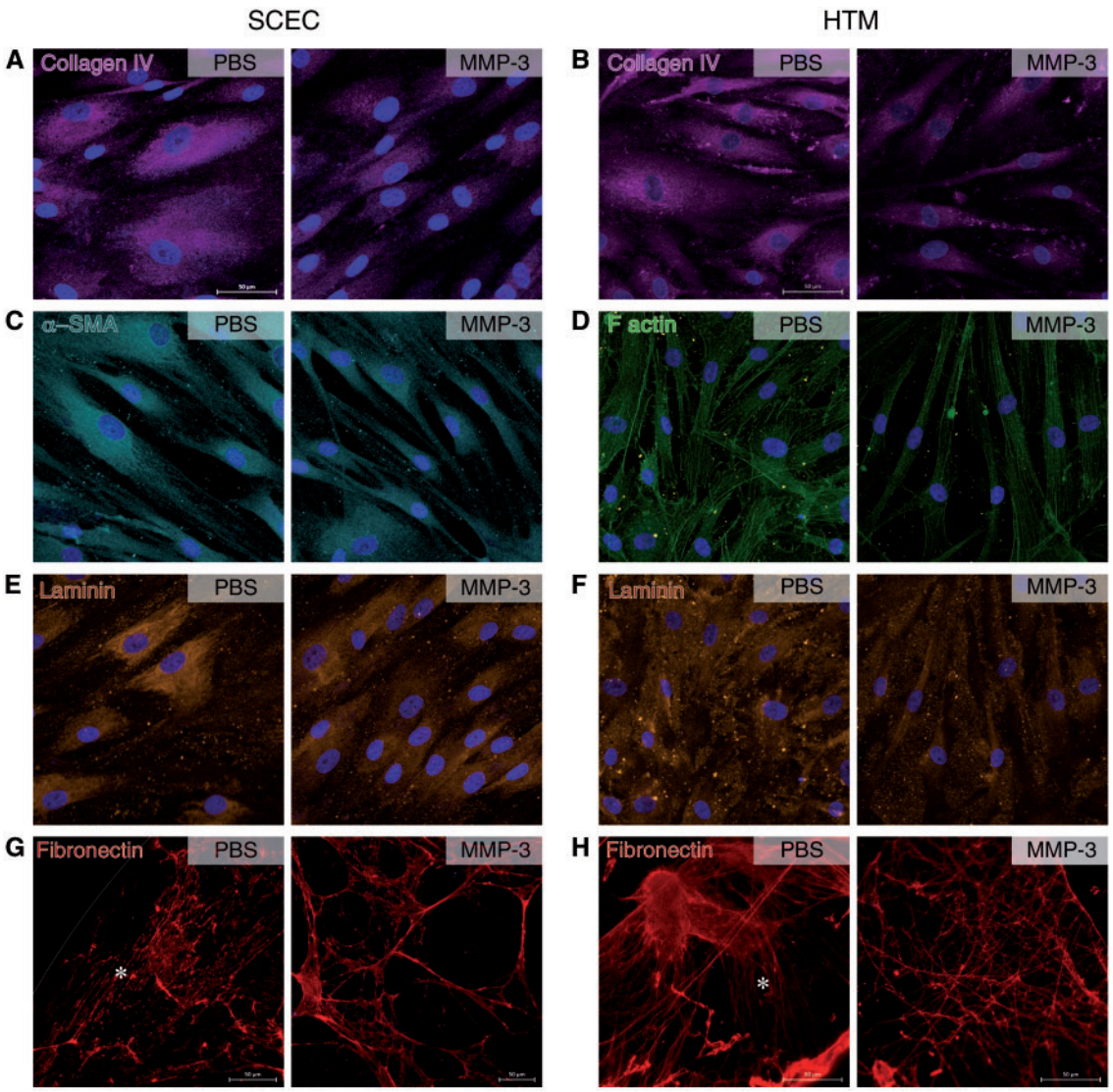

Figure 3. Remodelling of ECM components in SCEC and HTM cell monolayers. Immunocytochemistry shows various remodelling artefacts on core ECM components in SCEC and HTM cells in response to MMP-3 treatment. (**A,B**) Collagen IV appears to have reduced intensity in both cell types after treatment. Collagen IV is concentrated around cells in controls but shows reduced spread after treatment, fibrils barely protruding past the cell nuclei. (**C**) Alpha smooth muscle fibres extend the width of the cell towards a neighbouring cell. Treated samples show that these fibre bundles have constricted, leading to multiple thin connections between cells. (**D**) HTM F-actin staining depicts a slight thinning of filament bundles and a reduction of filament branching post MMP-3 treatment. (**E,F**) Laminin expression exhibits a modest reduction in staining intensity in both cell types, and a reduction in network complexity in TM cells. (**G,H**) Fibronectin was visualised after decellularisation, depicting linear and organised strands in PBS controls, as denoted by an asterisk. Treatment groups lacked a linear network, and instead showed a disjointed, porous network. Scale bars represent 50 μm. Left column pairs = SCEC, right column pairs = HTM.

Ultrastructural analysis of AAV-MMP-3 treated eyes

In order to evaluate whether the AAV-MMP-3 treatment affects the morphology of the eye and the TM including the inner wall of SC, ultrastructural investigation was performed in four pairs of mouse eyes. Corneas appeared translucent and healthy on visual inspection during enucleation. Semi-thin sections clearly demonstrated that there were no signs of an inflammatory reaction, either in the TM or in the cornea, uvea or retina (Fig. 6A and B). Ultrastructural analysis of control eyes revealed normal outflow structural morphology, cell-matrix attachments and cell-cell connections between the SC and TM. The inner wall endothelial cells formed foot-like connections with subendothelial TM cells, as well as connections to underlying elastic fibres and discontinuous basement membrane (Fig. 6C). However, in some regions of treated eyes, especially those with a prominent SC lumen and scleral spur-like structure typical of the nasal quadrant (48), there appeared to be more optically empty space directly underlying the inner wall endothelium of SC, compared to AAV-Null controls (Fig. 6D). In these optically empty spaces, foot-like extensions of the inner wall to the sub-endothelial layer were absent or disconnected from the subendothelial cells or elastic fibres (Fig. 6D and E). Occasionally, we observed an accumulation of ECM clumps beneath the inner wall that were not observed within the controls (Fig. 6F) and may represent remnants of digested material.

We quantified the optically empty length directly underlying the inner wall of SC. In control eyes, the percent optically empty length in any one region ranged from 19 to 49% with an average of 37%. In the treated eyes, the equivalent range was

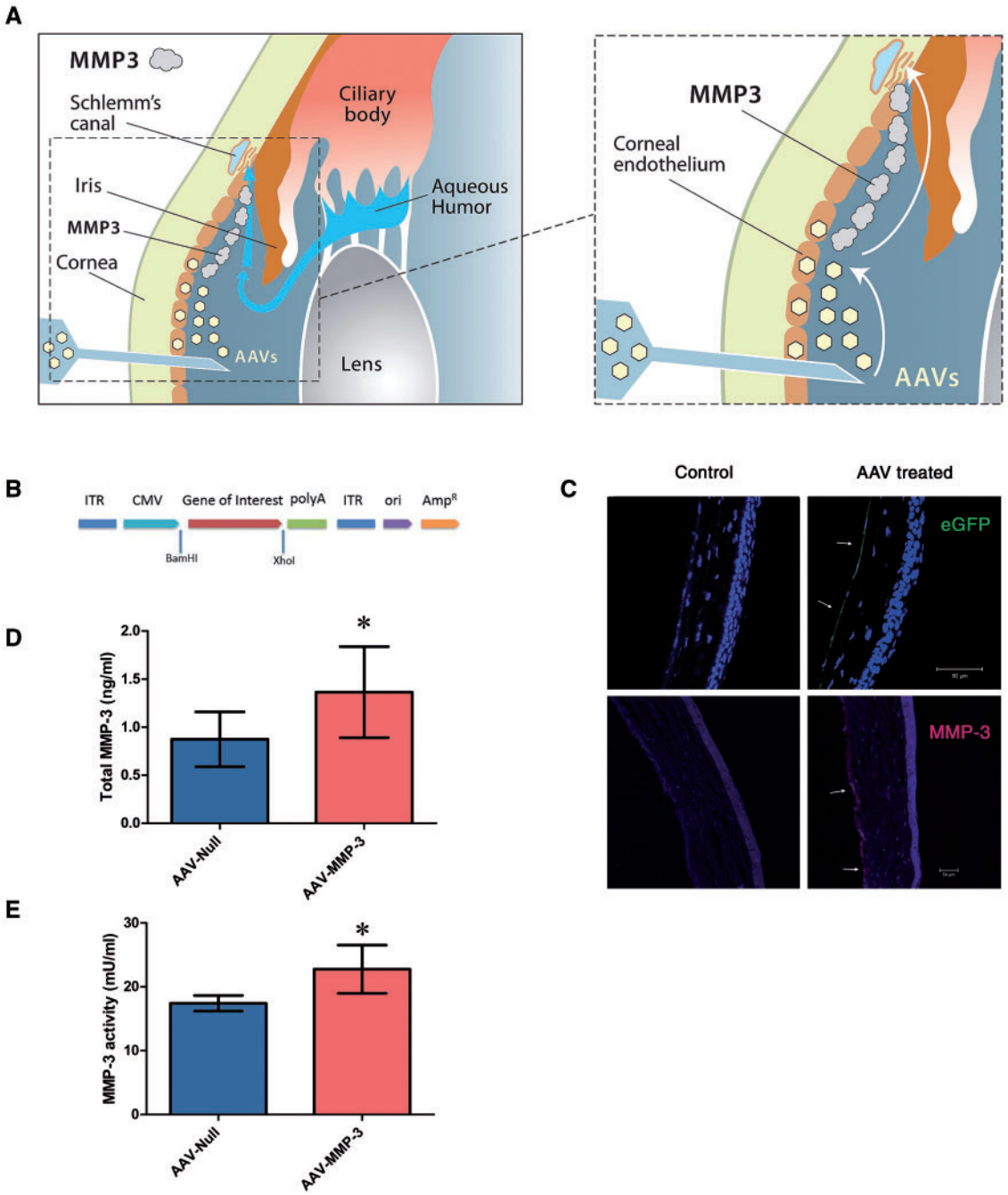

Figure 4. AAV-2/9 mediated MMP-3 expression in the corneal endothelium. (**A**) Diagrams illustrating the therapeutic concept addressed in this study. AAV-2/9 transduces the corneal endothelium upon intracameral inoculation (left). MMP-3 molecules are secreted into the AH from this location and are transported toward the outflow tissue by the natural flow of the aqueous (right). (**B**) A schematic diagram of the AAV-2/9 vector used for the expression of either eGFP or MMP-3. Murine MMP-3 cDNA was sub-cloned into the pAAV-MCS plasmid and constitutively driven by a CMV promoter (AAV-MMP-3). (**C**) Immunohistochemistry images of corneas from WT murine eyes intracamerally inoculated with AAV-2/9 expressing eGFP. AAV virus containing a CMV promoter demonstrates transduction and expression at the corneal endothelium (marked with arrows). Using the AAV-MMP-3 virus, MMP-3 was detected at the corneal endothelium in treated eyes only, denoted by arrows. (**D**) ELISA was performed on murine AH 4 weeks post-injection of virus. MMP-3 concentrations had increased by an average of 0.49 [0.11, 0.87] ng/ml in AAV-MMP-3 treated eyes (paired Student's *t*-test). (**E**) Aqueous MMP-3 activity was significantly increased by an average of 5.34 [1.12, 9.57] mU in AAV-MMP-3 treated eyes. Scale bars represent 50 μm. Asterisk symbol denotes a *P* value of < 0.05.

39–76% with an average of 59% (Fig. 6G). The differences between control and experimental eyes for each pair ranged from 16 to 26%, which corresponded to a statistically significant increase in the proportion of open space underlying the inner wall with AAV-MMP-3 relative to AAV-Null ($P = 0.002$, $n = 4$; paired Student's *t*-test). These data indicate that reduced ECM material in the TM and along the inner wall of SC is associated with AAV-MMP-3 treatment and may explain the enhanced outflow facility and IOP reduction. Furthermore, these morphological changes, because they were absent from controls, could not be attributed to an inflammatory or lytic response to AAV alone.

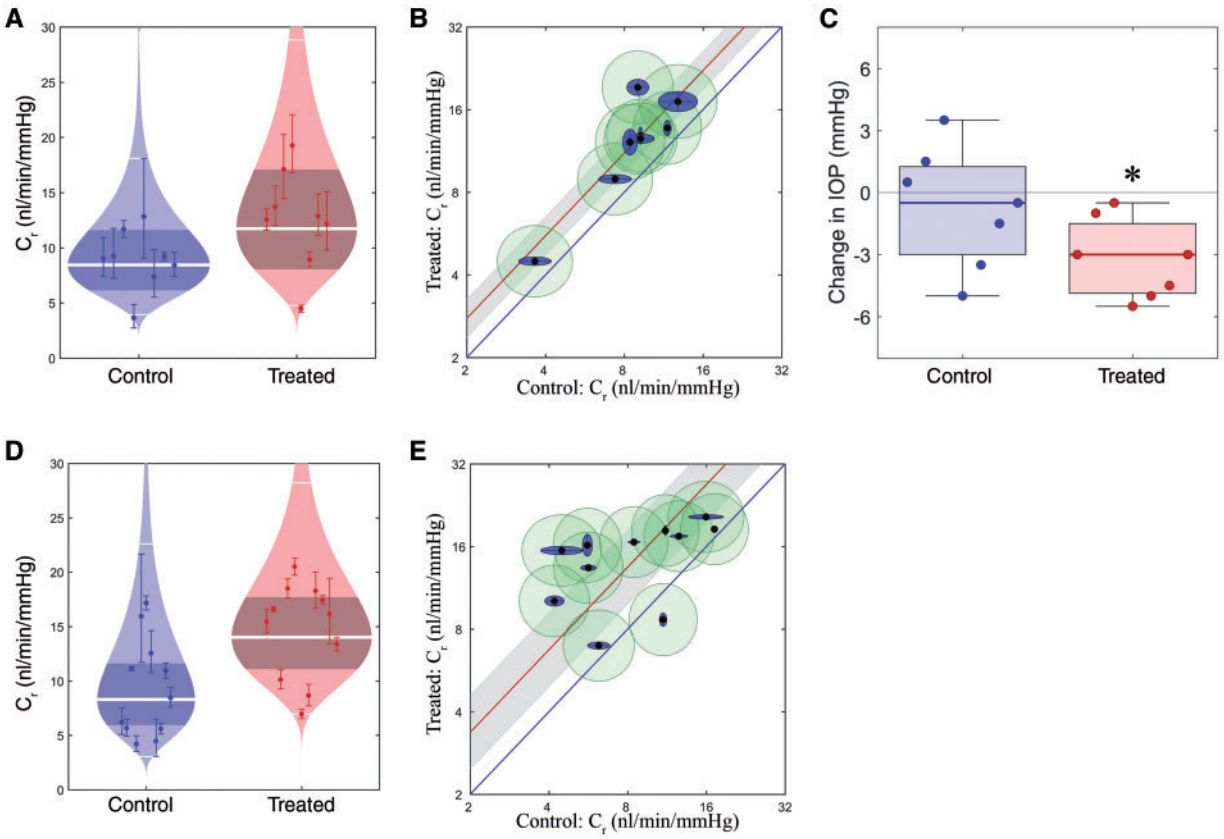

Figure 5. Effect of ECM remodelling on outflow facility and IOP. (**A**) 'Cello' plot depicting individual outflow facility values for eyes at 8 mmHg (Cr) and statistical distribution of both control (AAV-Null) and experimental (AAV-MMP-3) groups. Each point represents a single eye with 95% CI on C_r. Log normal distribution is shown, with the central white band showing the geometric mean and the thinner white bands showing two geometric standard deviations from the mean. The shaded region represents the 95% CI on the mean. (**B**) Paired outflow facility plot. Each inner point represents an eye pair, with log-transformed facilities of the control eye plotted on the x axis, and treated eye on the y axis. Outer blue and green ellipses show uncertainties generated from fitting the data to a model, intra-individual and cannulation variability respectively. Average increase is denoted by the red line, enclosed by a grey 95% CI, indicating significantly increased facility (does not overlap the blue unity line). (**C**) Box plots showing the change in IOP in treated and control eyes. Boxes show interquartile range and error bars represent the 5th and 95th percentiles. A significant reduction in IOP is observed in AAV-MMP-3 treated eyes (Wilcoxon signed-rank test). (**D-E**) Cello and paired facility plots for inducible AAV data sets.

Discussion

Matrix metalloproteinases are key regulators in the remodelling of extracellular matrices in the JCT region of the TM. Dysregulation of MMP expression and loss of MMP/TIMP homeostasis in glaucomatous AH have been associated with abnormal fibrillary ECM accumulation in the JCT region of POAG eyes (49–53). Furthermore, perfusion of anterior segments with purified MMPs increased outflow facility, while the use of metalloproteinase inhibitors (TIMP, minocycline) reduced outflow rates (30). Consistent with these findings, upregulation of MMPs following clinical laser treatment has been associated with the ocular hypotensive effect of trabeculoplasty (54,55). It is therefore apparent that the reduction in ECM turnover within the outflow tissues contributes to increased outflow resistance, and strategies specifically targeting outflow ECM may be effective in reducing outflow resistance. In this study, we focused on the development of a gene-based therapy for the delivery of MMP-3 into outflow tissues to facilitate aqueous outflow and reduce IOP.

It has been reported that the activity of a range of regulatory cytokines and growth factors found in AH directly impacts permeability in the outflow tissue, and many of these are known to be dysregulated in POAG AH (56,57). In particular, cytokines such as IL-1, TGF and TNF are known to influence the expression and secretion of ECM modulators, including MMPs in outflow tissues (58–60). It was therefore of interest to assess how POAG AH may affect the MMP-3 secretion and their relative activity in outflow cell culture systems.

We performed permeability assays with AH-treated SCEC and HTM monolayers to demonstrate that dysregulated MMP's in POAG AH influence monolayer permeability via modified ECM remodelling. (12,61). SCEC monolayers showed decreased permeability *in vitro* in response to glaucomatous AH, and this decrease was associated with a reduction in extracellular MMP-3 activity. HTM cells exhibited similar reductions in permeability. In contrast, treatment of cell monolayers exclusively with recombinant MMP-3 elevated monolayer permeability in comparison to controls, suggesting that MMP-3 could correct the permeability lowering effects of POAG aqueous. Because MMP-3 has previously been associated with apoptotic behaviour in Chinese hamster ovary cells and osteoclasts (62,63), we evaluated the effect of a wide concentration range of MMP-3 on SCEC and HTM viability. This way, we confirm that increases in paracellular permeability were not related to an MMP-3 cytotoxic effect, but rather its proteolytic activities, which these data support. More importantly, even lower concentrations of MMP-3 were detected *in vivo* in murine AH after AAV-mediated MMP-3 secretion (1.37 [0.89, 1.84] ng/ml, Fig. 4D) than those used in *in vitro* experiments. Collectively, these results indicate that a

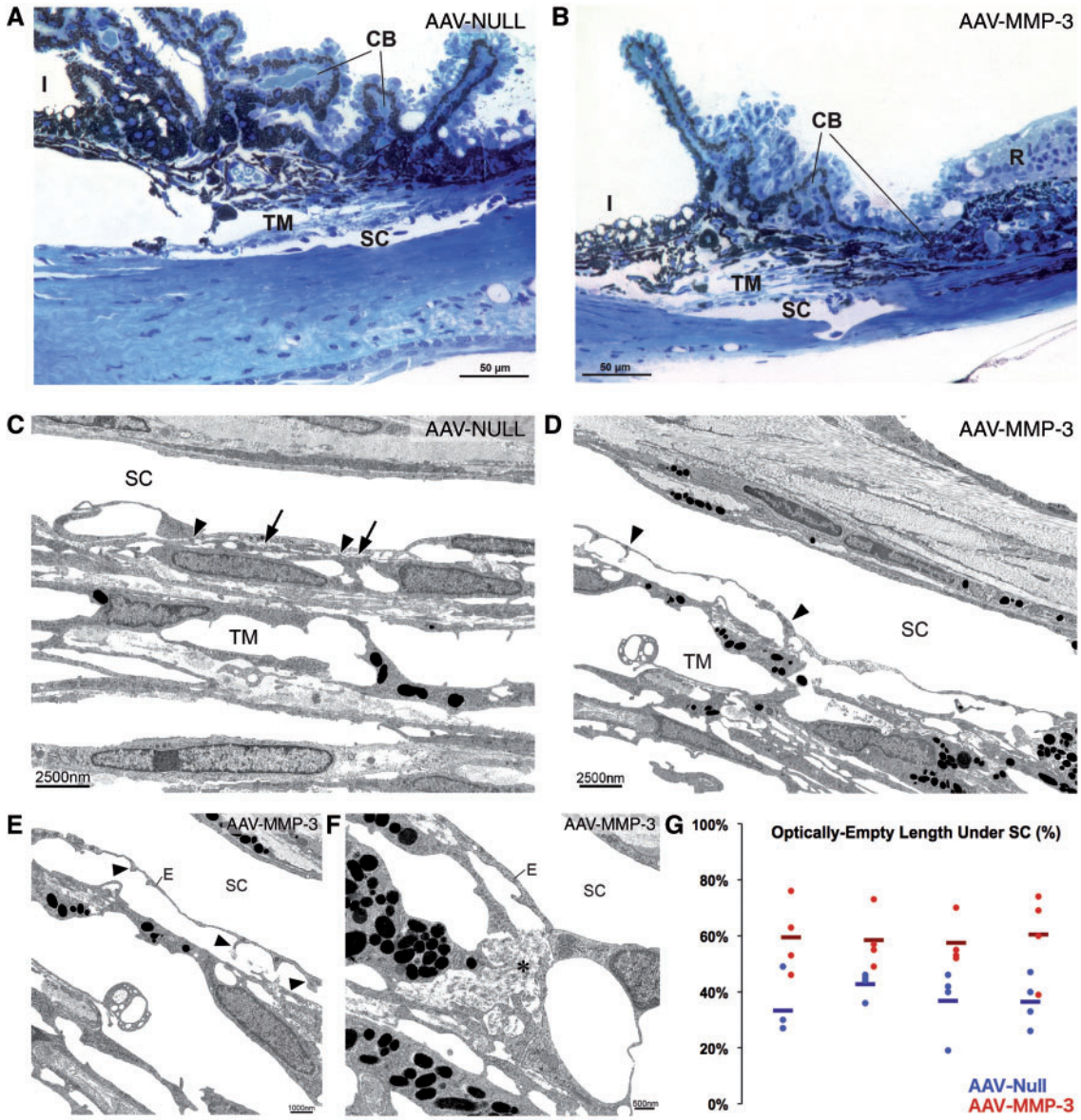

Figure 6. Transmission electron microscopy (TEM) analysis of ECM remodelling in outflow tissues. Semi-thin sections of the iridocorneal angle in mouse eyes treated with either (**A**) AAV-Null or (**B**) AAV-MMP-3. AAV-MMP-3 treated eyes show greater inter-trabecular spaces in outer trabecular meshwork (TM) than controls. Scale bar denotes 50 μm. (**C,D**) Transmission electron micrograph of the inner wall of Schlemm's Canal (SC) and the outer TM. (C) Control eye illustrating normal attachment between foot-like extensions of the inner wall endothelium and subendothelial cells (arrowheads), as well as with the discontinuous basement-membrane material underlying the inner wall endothelium (arrows). (D) Representative TEM image of an MMP-3 treated eye showing a disconnection of the inner wall endothelium from the subendothelial cells and the ECM (arrowheads). The widened subendothelial region lacks basement-membrane material and other ECM components. (**E,F**) Higher magnification of the inner wall of a treated eye. (E) Foot-like extensions of the inner wall endothelium (E) have disconnected from the subendothelial cells and the ECM (arrowheads), and the lack of ECM in this region is shown. (F) In other regions of treated eyes, clumps of presumably degraded ECM-material are localised underneath the inner wall of SC (asterisk). Such clumps of ECM are not present in controls. Scale bars are denoted on each image. CB = ciliary body, I = iris, R = retina. (**G**). Morphometric measurements of the optically empty space immediately underlying SC from four regions of contralateral eyes treated with AAV-MMP-3 (red data points) or AAV-Null (blue data points). Bars indicate average values for each eye. Contralateral eyes are presented immediately next to one another.

plausible target for MMP-3 activity is likely to be the ECM of TM and the inner wall endothelium of SC. This further contributes to the body of evidence demonstrating that the molecular pathological effects of glaucomatous AH are due, in part, to dysregulations of MMP-mediated remodelling and that induced elevations in MMP-3 expression in outflow tissues will have an enhancing effect on increasing aqueous outflow.

Previously, perfusion of explants of human anterior segments with a mixture of MMP-3, -2, -9 has been shown to result in an increase in outflow facility to 160% of baseline level (30). It has also been demonstrated that increases in IOP lead to an up-regulation of MMP-2, -3 and -14 through mechanical stretching of the TM and a reduction in TIMP2 (31,64–68). Such observations support the concept that controlled expression of MMPs within the anterior chamber holds therapeutic potential in regard to facilitating aqueous outflow. The inner wall endothelium of SC along with its basement membrane and JCT modulate the resistance to outflow. The interconnections between all components responsible for the outflow resistance generation is essential to maintain the homeostasis of outflow

drainage (11). Thus, targeting the ECM for remodelling in the JCT region using MMPs may effectively increase permeability of surrounding cells, thus increasing AH outflow rate and lowering IOP.

Owing to the fact that MMP-3 is a secretory enzyme, transduction of the corneal endothelium with AAV-MMP-3 will result in the secretion and delivery of the protein to the outflow tissues by following the natural flow of AH in the anterior chamber. *Ex vivo* studies in human corneas or corneal fibroblasts have demonstrated the potential and efficiency of delivering AAV to this tissue type (69,70). Successful transfection of different layers in the rabbit cornea by recombinant AAV further supports the potential of recombinant/exogenous protein delivery from corneal cells (71). Thus, it is likely that secreted MMP-3, expressed by corneal endothelia, will be directed toward the outflow tissue and activated with the aid of existing endogenous MMP-3 after which it will then be available for remodelling a range of ECM components. Attaining exclusive AAV expression in the cornea was obtained by using a single stranded AAV-2/9, as although single stranded AAV may enter other cells such as the TM, self-complementary viruses are required for sufficient DNA replication, and hence transduction of these cells (72).

The current data provide a direct proof of concept that AAV-mediated expression of MMP-3 from corneal endothelium decreases IOP with a concomitant increase in the rate of AH outflow through the drainage channels *ex vivo*. A number of parameters will require further refinement in order to address the translational feasibility of this approach. Although significant elevations in transient MMP-3 were found in murine AH post-treatment with AAV-MMP-3, these were well within tolerable limits as defined by our *in vitro* experiments (Fig. 2E and F). These MMP-3 elevations in AH (Fig. 4D), along with visually translucent corneas of normal thickness (Supplementary Material, Fig. S2), suggests that MMP-3 is preferentially secreted apically into the AH. MMP-3 expressed in the corneal endothelial cell layer is in the inactive form, which requires secretion for cleavage-induced activation, and is therefore unlikely to induce remodelling or damage to the endothelium itself. Activation is likely to occur in the AH after secretion, or extracellularly within the outflow tissues in the presence of other proteases. The observed elevation in aqueous MMP-3 activity indicates that activation at least begins in the AH (Fig. 4E). However, sustained expression of MMP-3, as would occur following permanent transfection of cells of the anterior chamber, could result in off-target proteolysis over time. A potentially more effective approach will be to employ an inducible promoter to drive MMP-3 expression on a periodic basis once the virus has been introduced into the anterior segment tissues of the eye. It is of note that the use of glucocorticoid-inducible promoters has been explored in this regard in adenoviral and AAV delivery systems to express MMP-1 in tissues of the TM (46). However, the use of a steroid response promoter may not be ideally suited from a therapeutic standpoint in humans, as activation of the promoter would require continuous exposure to steroid components, which can lead to abnormal IOP elevation (73–75). Glucocorticoids have also been shown to influence gene expression, which may play a pathogenic role in developing hypertension (76). Hence, we explored the effectiveness of a tetracycline-inducible system to express MMP-3 from the corneal endothelia, which allows for controllable and reversible activation by topically applied eye drops. We noted that activation of AAV for over 10 days was sufficient to significantly increase outflow facility *ex vivo* in mice and suggest that incorporation of other tetracycline derivatives may further enhance the effectiveness of the promoter and hence MMP-3 production. Our observed increase in facility of 68 [24, 128] % rivals that of conventional prostaglandin analogues which are in current use to treat glaucoma, noted to have an increase of 56 [−4, 154] % in the case of PDA205, also using the iPerfusion system (47).

To date, in studies utilising MMPs for increasing outflow or reducing IOP little emphasis has been given to the mechanism of action. Here, we show that MMP-3-mediated remodelling of specific ECM components is likely responsible for increased outflow, and hence, decreased IOP. Reductions in intensity and distribution of core ECM materials including collagen IV and laminin were observed *in vitro*, along with the disorganisation of the fibronectin meshwork and constrictions in the actin skeleton. These modifications suggest the development of a porous nature within the ECM of these monolayers. Semi-quantitation via western blot analysis coincides with these results, showing significant reductions in collagen IV, α-SMA and laminin proteins in the cell lysate fraction, where ECM proteins are likely to reside as no significant changes were displayed in media samples. It is reasonable to assume that these extracellular changes contribute to the observed alterations in electrical resistance and paracellular flux. Ultrastructural analysis of AAV-MMP-3 treated mouse eyes also showed reductions in ECM material at the sub-endothelial/JCT region, including areas of degraded ECM and widened inter-trabecular spaces. Upon quantification, these areas optically lacking ECM material were found to be consistently increased in response to MMP-3 both between regions of the anterior chamber and between treated eyes. Tight junctions remained intact after incubation with AAV-MMP-3 (Supplementary Material, Fig. S5), contrary to previous studies which have shown tight junction degradation by MMPs (77,78); validating that MMP-3 may primarily augment cell monolayer permeability via other mechanisms such as alteration of ECM components. These data indicate that a reduction in ECM material in the TM and inner wall of SC is responsible for the enhancement of outflow facility and consequently lowering of IOP in the treated eyes. The data also show that the reduction in ECM is not due to an inflammatory response that secondarily induces lytic enzymes in the treated eyes but most likely to the induction of MMP-3 through the treatment directly.

We show here for the first time that a topical eye drop regime can control the expression of a gene therapy vector utilised to reduce outflow resistance and IOP through ECM remodelling. The current approach may hold substantial potential as an effective human therapy should long-term safety and efficacy prove successful in non-human primates.

Materials and Methods

Cell culture

Human SCEC were isolated, cultured and fully characterised according to previous protocols (79–81). Briefly, cells were isolated from the SC lumen of human donor eyes using a cannulation technique. Isolated cells were tested for positive expression of VE-cadherin and fibulin-2, but absence of myocilin induction upon treatment with 100 nM dexamethasone for 5 days. Confluent cells displayed a characteristic linear fusiform morphology, were contact inhibited and generated a net transendothelial electrical resistance (TEER) greater than 10 $\Omega.cm^2$. TEER values were confirmed again prior to MMP-3 treatments. SCEC strains used were SC82 and SC83 between passages 2 and 7. Dulbecco's modified eagle medium (Gibco, Life Sciences) 1%

Pen/Strep/glutamine (Gibco, Life Sciences) and 10% foetal bovine serum (FBS) performance plus (Gibco, Life Sciences) was used as culture media in a 5% CO_2 incubator at 37 °C. Cells were passaged with trypsin-EDTA (Gibco-BRL) and seeded into 12 well or 24 well transwell plates (Costar, Corning). Human trabecular meshwork (HTM) cells were isolated and fully characterised according to the procedures described in (82–85). TM tissue is removed from human donor eyes using a blunt dissection technique, and TM cells are dissociated from the tissue using a collagenase digestion protocol as previously described (82). Isolated cells are characterised by their dramatic induction of myocilin protein following treatment with dexamethasone (100 nM) for 5 days as detailed before (79). HTM123 and HTM134 cells were cultured similar to SCEC's and matured for one week in 1% FBS media prior to treatment.

Human AH samples (detailed below) were added 1:10 to fresh media for cellular treatment for use with TEER and permeability assays as described below.

Recombinant human active MMP-3 (ab96555, Abcam) was added to cell media at a concentration of 10 ng/ml for TEER, permeability assays, western blotting and immunocytochemistry as described below. Inactivated MMP-3 controls were achieved by incubating active MMP-3 (10 ng/ml) with recombinant human active TIMP-1 (100 ng/ml, ab82104, Abcam) in cell media for 1 h prior to treatment.

Animals

Animals and procedures used in this study were carried out in accordance with regulations set out by The Health Products Regulatory Authority (HPRA), responsible for the correct implementation of EU directive 2010/63/EU. 8–11-week-old male and female C57BL/6 mice were used in all experimentation outlined in this study. Animals were bred and housed in specific-pathogen-free environments in the University of Dublin, Trinity College and all injections and IOP measurements complied with the HPRA project authorisation number AE19136/P017.

Patient aqueous humour samples

Human aqueous was obtained from the Mater Misericordiae Hospital, Dublin, Ireland. Upon informed consent, AH samples were collected from both POAG and control patients undergoing routine cataract surgery. The criteria for POAG was defined as the presence of glaucomatous optic disc cupping with associated visual field loss in an eye with a gonioscopically open anterior drainage channel, with an intraocular pressure > 21 mmHg (86). The samples were taken immediately prior to corneal incision at the start of the procedure using a method described previously (87). Human AH collection conformed to the WMA Declaration of Helsinki and was approved by the Mater Misericordiae University Hospital Research Ethics Committee.

TEER measurement

Electrical resistance values were used as a representative of the integrity of the endothelial cell-cell junctions. Cells grown on Costar transwell-polyester membrane inserts with a pore size of 0.4 μm were treated with 10 ng/ml MMP-3 as described above. TEER readings were measured before and 24 h after treatment. An electrical probe (Millicell ERS-2 Voltohmmeter, Millipore) was placed into both the apical and basal chambers of the transwells and a current was passed through the monolayers, reported as a resistance in $\Omega.cm^2$. A correction was applied for the surface area of the membrane (0.33 cm^2) and for the electrical resistance of the membrane (blank transwell).

Permeability assessment by FITC-dextran flux

The extent of monolayer permeability was assessed by the basal to apical movement of a tracer molecule through the monolayer. Measures of permeability were taken 24h after treatment immediately after TEER values, keeping experimental set-up identical to that of TEER readings. The permeability protocol was repeated as described in (88). A 70 kDa fluorescein isothiocyanate (FITC)-conjugated dextran (Sigma) was added to the basal compartment of the transwell. Fresh medium was applied to the apical chamber and aliquots of 100 μl were taken every 15 min for a total of 120 min, replacing with fresh media. Sample aliquots were analysed for FITC fluorescence (FLUOstar OPTIMA, BMG Labtech) at an excitation wavelength of 492 nm and emission wavelength of 520 nm. Relative fluorescent units (RFU) were converted to their corresponding concentrations by interpolating from a known standard curve. Corrections were made for background fluorescence and the serial dilutions generated over the experiments time course. P_{app} values were calculated representing the apparent permeability coefficient for control (PBS) and treatment (10 ng/ml MMP-3). This was achieved via the following equation:

$$P_{app}(cm/s) = (dM/dT)/(A \times C_0),$$

Where dM/dT is the rate of appearance of FITC-dextran (FD) (μg/s) in the apical chamber from 0 to 120 min after the introduction of FD into the basal chamber. A is the effective surface area of the insert (cm^2) and C_0 is the initial concentration of FD in the basal chamber.

Cell viability

Cultured cells were treated with increasing concentrations of recombinant human MMP-3 (ab96555, Abcam) from 0 to 200 ng/ml. Cell viability was assessed 24 h post-treatment with MMP-3 using a CellTitre 96® AQueous One Solution Cell Proliferation Assay (Promega). Cell media was aspirated and a 1 in 6 dilution of the supplied reagent in media was added to the cell surface. Cells were incubated at 37 °C for 1 h and the media/reagent was transferred to a 96-well plate for reading by spectrophotometry (Multiskan FC, Thermo Scientific) at 450 nm. Standard *in vitro* viability calculations fail to consider sample size and the biological significance of the data. Hence, a modified approach was taken to determine at which concentration SCEC's show a reduced tolerability to MMP-3. This was defined at an average of 85% viability over three cell samples. This conservative value ensures that a cell population would remain viable and still be able to proliferate. Anything lower should be regarded as MMP-3 intolerability i.e. reduced cell proliferation or cell death. Control samples (0 ng/ml MMP-3) were normalised to 100% viability and a linear model fitted to the normalised data. The MMP-3 concentration at which cells had an average of 85% viability was interpolated from the lower 95% confidence bound from this linear model. This value represents the concentration of MMP-3 at which the average of three cell samples would have a 97.5% chance of retaining a greater to or equal than 85% viability.

Immunocytochemistry (cell monolayers)

Immunocytochemistry was performed to visualise changes in ECM composition in response to MMP-3. Human SCEC and HTM were grown on chamber slides (Lab-Tek II) and fixed in 4% paraformaldehyde (pH 7.4) for 20 min at room temperature and then washed with PBS for 15 min. Cell monolayers were blocked in PBS containing 5% normal goat serum (10658654, Fischer Scientific) and 0.1% Triton X-100 (T8787, Sigma) at room temperature for 30 min. Primary antibodies of collagen IV (ab6586, Abcam), α-SMA (ab5694, Abcam), laminin (ab11575, Abcam) and F-actin (A12379, ThermoFisher Scientific) were diluted at 1:100 in blocking buffer and incubated overnight at 4 °C. Secondary antibodies (ab6939, Abcam) were diluted at 1:500 in blocking buffer and then incubated for 2 h at room temperature. Following incubation, chamber slides were mounted with aqua-polymount (Polyscience) after nuclei-counterstaining with DAPI. Fluorescent images of SCEC monolayers were captured using a confocal microscope (Zeiss LSM 710), and processed using imaging software ZEN 2012.

For clear fibronectin (ab23750, Abcam) staining, cells were grown on cover slips and subsequently decellularised, leaving only the ECM material. Round cover slips (15 mm Diameter, Sparks Lab Supplies) were silanised before cell seeding to enhance binding to ECM products. This was achieved by initially immersing slips in 1% acid alcohol (1% concentrated HCL, 70% ethanol, 29% dH_2O) for 30 mins. Slips were washed in running water for 5 min, immersed in dH_2O twice for 5 min, immersed in 95% ethanol twice for 5 min and let air dry for 15 min. Cover slips were then immersed in 2% APES (3-aminopropyl triethoxysilane (A3648, Sigma) in acetone (Fisher Chemical)) for 1 min. Slips were again washed twice in dH_2O for 1 min and dried overnight at 37 °C. Cells were grown to confluency on these cover slips and, following treatment, were decellularised. This was achieved by consecutive washes in Hank's Balanced Salt Solution (HBSS), 20 mM ammonium hydroxide (Sigma) with 0.05% Triton X-100, and finally HBSS again. Matrices were fixed and stained as described above with chamber slides.

Western blotting

Cells were treated with 10 ng/ml MMP-3 for 24 h in serum-free media. Media supernatants were aspirated and mixed 1:6 with StrataClean resin (Agilent). After centrifugation, the supernatant was removed and the pellet was resuspended in NP-40 lysis buffer containing 50 mM Tris pH 7.5, 150 mM NaCL, 1% NP-40, 10% SDS, 1X protease inhibitor (Roche). Cells were lysed using NP-40 lysis buffer for protein collection. Samples were centrifuged at 10,000 rpm for 15 min (IEC Micromax microcentrifuge) and supernatant was retained. Protein samples were loaded onto a 10% SDS-PAGE gel at 30–50μg per well. Proteins were separated by electrophoresis over the course of 150 min at constant voltage (120 V) under reducing conditions and subsequently electro-transferred onto methanol-activated PVDF membranes at constant voltage (12 V). Gels intended for use with Collagen IV antibodies were run under native conditions. Membranes were blocked for 1 h at room temperature in 5% non-fat dry milk and incubated overnight at 4 °C with a rabbit primary antibodies to collagen IV, α-SMA, laminin and fibronectin as previously stated at concentrations of 1 in 1000 but 1 in 500 for laminin. Membrane blots were washed 3x5 min in TBS and incubated at room temperature for 2 h with horse radish peroxidase-conjugated anti-rabbit secondary antibody (Abcam). Blots were again washed and treated with a chemiluminescent substrate (WesternBright ECL, Advansta) and developed on a blot scanner (C-DiGit, LI-COR). The membranes containing cell lysate samples were re-probed with GAPDH antibody (ab9485, Abcam) for loading control normalisation. Media samples were normalised against their total protein concentration as determined by a spectrophotometer (ND-1000, NanoDrop). A total of four replicate blots were quantified for each cell lysate sample antibody, and 2–3 replicates for a media sample. Band images were quantified using Image J software. Fold change in band intensity was represented in comparison to vehicle control treatments of PBS.

AAV

AAV-2/9 containing the enhanced green fluorescent protein (eGFP) reporter gene (Vector Biolabs) was initially used to assess viral transduction and expression in the anterior chambers of wild type mice (C57/BL6). Murine MMP-3 cDNA was incorporated into Bam HI/Xhol sites of the pAAV-MCS vector (Cell Biolabs Inc) for constitutive expression of MMP-3. A null virus was used as contralateral control using the same capsid and vector. The inducible vector was designed by cloning MMP-3 cDNA into a pSingle-tTS (Clontech) vector. This vector was then digested with BsrBI and BsrGI and the fragment containing the inducible system and MMP-3 cDNA was ligated into the Not1 site of expression vector pAAV-MCS, to incorporate left and right AAV inverted terminal repeats (L-IRT and R-ITR). AAV-2/9 was generated using a triple transfection system in a stable HEK-293 cell line (Vector Biolabs). For animals injected with the inducible virus, after a 3-week incubation period, 0.2% doxycycline (D9891, Sigma) in PBS was administered twice daily to the eye for 10–16 days to induce viral expression. A similar inducible virus expressing eGFP was used as a control in the inducible study.

Intracameral injection

Animals were anaesthetised by intra-peritoneal injection of ketamine (Vetalar V, Zoetis) and domitor (SedaStart, Animalcare) (66.6 and 0.66 mg/kg, respectively). Pupils were dilated using one drop of tropicamide and phenylephrine (Bausch & Lomb) on each eye. 2 μl of virus at a stock titre of $5x10^{13}$ vector genomes per ml was initially back-filled into a glass needle (ID1.0 mm, WPI) attached via tubing (ID-1.02 mm, OD-1.98 mm, Smiths) to a syringe pump (PHD Ultra, Harvard Apparatus). An additional 1 μl of air was then withdrawn into the needle. Animals were injected intracamerally just above the limbus. Viral solution was infused at a rate of 1.5 μl/min for a total of 3 μl to include the air bubble. Contralateral eyes received an equal volume and titre of either AAV-MMP-3 or AAV-Null. The air bubble prevented the reflux of virus/aqueous back through the injection site when the needle was removed. Fucidic gel (Fucithalmic Vet, Dechra) was applied topically following injection as an antibiotic agent. To counter anaesthetic, Antisedan (atipamezole hydrochloride, SedaStop, Animalcare) was intra-peritoneally injected (8.33 mg/kg) and a carbomer based moisturising gel (Vidisic, Bausch & Lomb) was applied during recovery to prevent corneal dehydration.

Immunohistochemistry (mouse eyes)

Eyes were enucleated 4 weeks post-injection of virus and fixed in 4% paraformaldehyde overnight at 4 °C. The posterior

segment was removed by dissection and anterior segments were washed in PBS and placed in a sucrose gradient of incrementing sucrose concentrations containing 10%, 20% and finally 30% sucrose in PBS. Anterior segments were frozen in O.C.T compound (VWR Chemicals) in an isopropanol bath immersed in liquid nitrogen and cryosectioned (CM 1900, Leica Microsystems) at 12 μm thick sections. Sections were gathered onto charged Polysine® slides (Menzel-Gläser) and blocked for 1 h with 5% normal goat serum (10658654, Fischer Scientific) and 0.1% Triton X-100 in PBS. Slides were incubated overnight at 4 °C in a humidity chamber with a 1:100 dilution of primary antibody. Antibodies used were MMP-3 (ab52915, Abcam) and GFP (Cell Signalling). Sections were washed three times in PBS for 5 min and incubated with a Cy-3 conjugated anti-rabbit IgG antibody (ab6936, Abcam) at a 1:500 dilution for 2 h at 37 °C in a humidity chamber. Slides were washed as before and counter stained with DAPI for 30 s. Slides were mounted using Aquamount (Hs-106, National Diagnostics) with coverslips (Deckgläser) and visualised using a confocal microscope (Zeiss LSM 710).

Total MMP-3 quantification

MMP-3 concentration was quantified using enzyme-linked immunosorbent assay (ELISA) kits for both human SC monolayers (DMP300, R&D Systems) and murine aqueous (RAB0368-1KT, Sigma) according to the manufacturer's protocol. SC monolayers were cultured and treated with a 1 in 10 dilution of human cataract and POAG AH, a method previously described (87). Media was taken from the monolayers 24 h post-treatment and assayed for total MMP-3.

To measure the secretion of MMP-3 by AAV-2/9 into the AH, animals were inoculated with virus as described previously via intracameral injection. Four weeks post-injection, the animals were sacrificed and AH was collected. This was achieved by the cannulation of the cornea with a pulled glass needle (1B100-6, WPI) and gentle pressing of the eye until it was deflated. Aqueous was expelled from the needle (approximately 5 μl) by the attachment of a 25ml syringe connected via barb fitting and tubing (Smiths Medical) and a gradual push of the syringe plunger. Aqueous was assayed using the previously mentioned ELISA kit.

MMP-3 activity assay (FRET)

Enzymatic activity of secreted MMP-3 was quantified using fluorescence resonance energy transfer (FRET). A fluorescent peptide consisting of a donor/acceptor pair remains quenched in its intact state. This peptide contains binding sites specific to MMP-3. Once cleavage occurs through MMP-3 mediated proteolysis, fluorescence is recovered by the transfer of energy from the donor to the acceptor, resulting in an increase in the acceptor's emission intensity. Cleavage of substrate, and therefore fluorescence, was monitored on a FLUOstar OPTIMA (BMG Labtech) over the course of 2.5 h at 37 °C, to allow ample time for substrate cleavage. Media samples were collected from treated SC monolayers and combined with a 1:100 dilution of an MMP-3 specific substrate (ab112148, Abcam). Levels of active MMP-3 were interpolated from a standard curve defined by ELISA. For murine aqueous MMP-3 activity, aqueous was retrieved four weeks post-injection of AAV-MMP-3 or AAV-Null as described above. Aqueous samples were processed through an activity kit (abe3730, Source Bioscience), selected for its high sensitivity and specificity, according to the manufacturer's protocol.

Enzymatic activity was calculated as described in MMP-3 activity Assay Kit's (ab118972, Abcam) protocol:

$$\text{MMP}-3\ \text{Activity}\ (\text{nmol/min/ml}) = \frac{B\ \times\ \textit{Dilution Factor}}{(T2-T1)\ \times\ V},$$

Where B is the level of MMP-3 interpolated from the standard curve, T1 is the time (min) of the initial reading, T2 is the time (min) of the second reading and V is the sample volume (ml) added to the reaction well. The units 'nmol/min/ml' are equivalent to 'mU/ml'.

Measurement of outflow facility

Animals were sacrificed for outflow facility measurement 4 weeks after injection of virus. Eyes were enucleated for *ex vivo* perfusion using the *iPerfusion*™ system as described in (47). Contralateral eyes were perfused simultaneously using two independent but identical iPerfusion systems. Each system comprises an automated pressure reservoir, a thermal flow sensor (SLG64-0075, Sensiron) and a wet-wet differential pressure transducer (PX409, Omegadyne), in order to apply a desired pressure, measure flow rate out of the system and measure the intraocular pressure respectively. Enucleated eyes were secured to a pedestal using a small amount of cyanoacrylate glue in a PBS bath regulated at 35 °C. Perfusate was prepared (PBS including divalent cations and 5.5mM glucose) and filtered (0.2 μm, GVS Filter Technology) before use. Eyes were cannulated using a bevelled needle (NF33BV NanoFil™, World Precision Instruments) with the aid of a stereomicroscope and micromanipulator (World Precision Instruments). Eyes were perfused for 30 min at a pressure of ∼8 mmHg in order to acclimatise to the environment. Incrementing pressure steps were applied from 4.5 to 21 mmHg, while recording flow rate and pressure. Flow (Q) and pressure (P) were averaged over 4 min of steady data, and a power law model of the form

$$Q = C_r\left(\frac{P}{P_r}\right)^{\beta} P$$

was fit to the data using weighted power law regression, yielding values of C_r, the reference facility at reference pressure $P_r = 8$ mmHg (corresponding to the physiological pressure drop across the outflow pathway), and β, a nonlinearity parameter characterising the pressure-dependent increase in facility observed in mouse eyes (47).

IOP

IOP measurements were performed by rebound tonometry (TonoLab, Icare) both prior to intracameral injection and 4 weeks post-injection. Readings, which were the average IOP values after five tonometric events, were taken 10 min after the intraperitoneal administration of mild general anaesthetic (53.28 mg/kg ketamine and 0.528 mg/kg domitor). Two readings were taken for one eye, then the other. This was repeated for a total of four readings per eye. Due to a minimum reading of 7 mmHg by the tonometer, a non-parametric approach was taken in the analysis of the readings. The median IOP was

calculated for each eye, and MAD (median absolute deviation) values were used as a measure of dispersion. For comparing median values in a paired population, the Wilcoxon matched-pairs signed-rank test was employed to test for changes in IOP pre- and post-injection, and also for changes between contralateral eyes.

Analysis of central corneal thickness

Enucleated mouse eyes transduced with AAV-MMP-3 or its contralateral control, AAV-Null, were fixed overnight in 4% PFA and washed in PBS. Posterior segments were removed by dissection under the microscope and anterior segments were embedded in medium (Tissue-Tek OCT Compound). Serial sectioning was performed on each eye and five frozen sections (12 μm) were transferred to a Polysine slide (Thermo Scientific) for staining with DAPI and mounted with aqua-polymount (Polyscience). Corneal sections were judged to be central by qualitatively taking the same distance from both iridocorneal angles. For quantitation, we measured the corneal thickness of sections on five consecutive slides by light and confocal microscopy (Zeiss LSM 710). A total of 25 measurements were taken from each eye to represent mean central corneal thickness (μm) using the NIH ImageJ software.

Transmission electron microscopy

Ultrastructural investigation was performed by transmission electron microscopy (TEM) in four pairs of mouse eyes. One eye of each pair was injected with AAV-Null, the other with AAV-MMP-3, as described above. Four weeks after injection, the eyes were enucleated and immersion fixed in Karnovsky's fixative (2.5% PFA, 0.1M cacodylate, 2.25% glutaraldehyde and dH_2O) for 1 h. Eyes were then removed from fixative and the cornea pierced using a 30-gauge needle (BD Microlance 3, Becton Dickinson). Eyes were placed back into fixative overnight at 4 °C, washed 3x10 min, stored in 0.1M cacodylate and sent to Erlangen.

Here the eyes were cut meridionally through the centre of the pupil, the lens carefully removed, and the two halves of each eye embedded in Epon. Semi-thin sagittal and then ultrathin sections of Schlemm's canal (SC) and trabecular meshwork (TM) were cut from one end of each half, and then the other approximately 0.2–0.3 mm deeper. The location of the superficial and deeper cut ends was alternated for the second half of the eye such that all four regions examined were at least 0.2–0.3 mm distant from one another. The ultrathin sections contained the entire anterior posterior length of the inner wall and the TM.

In four regions of each eye, we measured the length of optically empty space immediately underlying the inner wall endothelium of SC (Supplementary Material, Fig. S6). We also measured the inner wall length in contact with ECM, including basement membrane material, elastic fibres, or amorphous material. The optically empty length divided by the total length (optically empty + ECM lengths) was calculated and defined as the percentage of optically empty length for that region. All measurements were performed at 10,000x magnification, with each region including approximately 100 individual lengths of ECM or optically empty space. The measurements were performed by the two authors: ELD and CFK.

Statistical analysis

For TEER values, activity units (mU/ml) and concentrations (ng/ml), statistical differences were analysed by using unpaired two-tailed Student's *t*-tests. Differences in P_{app} values (cm/s) were determined by a one way ANOVA with Tukey's correction for multiple comparisons, where appropriate. ELISA standard curve concentrations were log-transformed and absorbance values were fitted to a sigmoidal dose response curve with variable slope for interpolation. Fold change of western blot data was log-transformed and investigated for significance using a one-sample *t*-test against a theoretical mean of 0. To measure MMP-3 concentration and activity in the AH of wild type (WT) mice, a paired two-tailed *t*-test was carried out for contralateral samples. Outflow facility was analysed using a weighted paired *t*-test performed in MATLAB as described in (47), incorporating both system and biological uncertainties. For IOP data, median values were obtained to reflect the non-parametric nature of the tonometer, and the Wilcoxon matched-pairs signed rank test was used to compare changes in paired populations. For morphology, the distribution of values representing the percent optically empty length was first examined using a Shapiro-Wilk and Anderson-Darling tests to detect for deviations from a normal distribution. The percent optically empty length between contralateral eyes was then analysed using a paired Student's *t*-test. Statistical significance was inferred when $P < 0.05$ in all experimentation. Results were depicted as 'mean, [95% Confidence Intervals]' unless otherwise stated in the results section.

Supplementary Material

Supplementary Material is available at *HMG* online.

Acknowledgements

We wish to acknowledge Caroline Woods and Charles Murray for animal husbandry. We would also like to thank Elke Kretzschmar, Britta Bäckermann and Andrea Eichnorn for preparing the semi-and ultrathin sections and Marco Gößwein for his assistance in finalizing the TEM images for publication.

Conflict of Interest statement. None declared.

Funding

Research at the Ocular Genetics Unit at the University of Dublin, Trinity College was supported by the European Research Council [ERC-2012-AdG 322656-Oculus]. We also acknowledge an equipment grant from Science Foundation Ireland in support of this project [12/ERC/B2539]. Research at Imperial College London was supported by the US National Institutes of Health (EY022359 and EY019696), the UK Engineering and Physical Sciences Research Council (EP/J010499/1), and Fight for Sight UK (Ref 1385). Work at Duke University was also supported by the US National Institutes of Health (EY022359). Funding to pay the Open Access publication charges for this article was provided by the European Research Council.

References

1. Yan, X., Li, M., Chen, Z., Zhu, Y., Song, Y. and Zhang, H. (2016) Schlemm's Canal and Trabecular Meshwork in Eyes with Primary Open Angle Glaucoma: A Comparative Study Using High-Frequency Ultrasound Biomicroscopy. *PLoS One*, **11**, e0145824.

2. Lanza, M., Iaccarino, S., Mele, L., Carnevale, U.A., Irregolare, C., Lanza, A., Femiano, F. and Bifani, M. (2016) Intraocular pressure evaluation in healthy eyes and diseased ones using contact and non contact devices. *Cont. Lens. Anterior. Eye*, **39**, 154–159.
3. Grant, W.M. (1951) Clinical measurements of aqueous outflow. *Am. J. Ophthalmol.*, **34**, 1603–1605.
4. Rylander, N.R. and Vold, S.D. (2008) Cost analysis of glaucoma medications. *Am. J. Ophthalmol.*, **145**, 106–113.
5. Hamanaka, T. and Bill, A. (1988) Effects of alpha-chymotrypsin on the outflow routes for aqueous humor. *Exp. Eye Res.*, **46**, 323–341.
6. Johnson, M. (2006) 'What controls aqueous humour outflow resistance?' *Exp. Eye Res.*, **82**, 545–557.
7. Tanihara, H., Inatani, M., Koga, T., Yano, T. and Kimura, A. (2002) Proteoglycans in the eye. *Cornea*, **21**, 62–69.
8. Floyd, B.B., Cleveland, P.H. and Worthen, D.M. (1985) Fibronectin in human trabecular drainage channels. *Invest. Ophthalmol. Vis. Sci.*, **26**, 797–804.
9. Keller, K.E., Bradley, J.M., Vranka, J.A. and Acott, T.S. (2011) Segmental versican expression in the trabecular meshwork and involvement in outflow facility. *Invest. Ophthalmol. Vis. Sci.*, **52**, 5049–5057.
10. Swaminathan, S.S., Oh, D.J., Kang, M.H., Ren, R., Jin, R., Gong, H. and Rhee, D.J. (2013) Secreted protein acidic and rich in cysteine (SPARC)-null mice exhibit more uniform outflow. *Invest. Ophthalmol. Vis. Sci.*, **54**, 2035–2047.
11. Overby, D.R., Stamer, W.D. and Johnson, M. (2009) The changing paradigm of outflow resistance generation: towards synergistic models of the JCT and inner wall endothelium. *Exp. Eye Res.*, **88**, 656–670.
12. Curtis, T.M., McKeown-Longo, P.J., Vincent, P.A., Homan, S.M., Wheatley, E.M. and Saba, T.M. (1995) Fibronectin attenuates increased endothelial monolayer permeability after RGD peptide, anti-alpha 5 beta 1, or TNF-alpha exposure. *Am. J. Physiol.*, **269**, 248–260.
13. Stickel, S.K. and Wang, Y.L. (1988) Synthetic peptide GRGDS induces dissociation of alpha-actinin and vinculin from the sites of focal contacts. *J. Cell Biol.*, **107**, 1231–1239.
14. Lampugnani, M.G., Resnati, M., Dejana, E. and Marchisio, P.C. (1991) The role of integrins in the maintenance of endothelial monolayer integrity. *J. Cell Biol.*, **112**, 479–490.
15. Wu, M.H., Ustinova, E. and Granger, H.J. (2001) Integrin binding to fibronectin and vitronectin maintains the barrier function of isolated porcine coronary venules. *J. Physiol.*, **532**, 785–791.
16. Mehta, D. and Malik, A.B. (2006) Signaling mechanisms regulating endothelial permeability. *Physiol. Rev.*, **86**, 279–367.
17. Keller, K.E. and Acott, T.S. (2013) The Juxtacanalicular Region of Ocular Trabecular Meshwork: A Tissue with a Unique Extracellular Matrix and Specialized Function. *J. Ocul. Biol. Dis. Infor.*, **1**, 3.
18. Rohen, J.W., Futa, R. and Lutjen-Drecoll, E. (1981) The fine structure of the cribriform meshwork in normal and glaucomatous eyes as seen in tangential sections. *Invest. Ophthalmol. Vis. Sci.*, **21**, 574–585.
19. Faralli, J.A., Schwinn, M.K., Gonzalez, J.M., Jr., Filla, M.S. and Peters, D.M. (2009) Functional properties of fibronectin in the trabecular meshwork. *Exp. Eye Res.*, **88**, 689–693.
20. Tamm, E.R., Siegner, A., Baur, A. and Lutjen-Drecoll, E. (1996) Transforming growth factor-beta 1 induces alpha-smooth muscle-actin expression in cultured human and monkey trabecular meshwork. *Exp. Eye Res.*, **62**, 389–397.
21. Schlunck, G., Han, H., Wecker, T., Kampik, D., Meyer-ter-Vehn, T. and Grehn, F. (2008) Substrate rigidity modulates cell matrix interactions and protein expression in human trabecular meshwork cells. *Invest. Ophthalmol. Vis. Sci.*, **49**, 262–269.
22. Acott, T.S., Kelley, M.J., Keller, K.E., Vranka, J.A., Abu-Hassan, D.W., Li, X., Aga, M. and Bradley, J.M. (2014) Intraocular pressure homeostasis: maintaining balance in a high-pressure environment. *J. Ocul. Pharmacol. Ther.*, **30**, 94–101.
23. Nagase, H., Suzuki, K., Enghild, J.J. and Salvesen, G. (1991) Stepwise activation mechanisms of the precursors of matrix metalloproteinases 1 (tissue collagenase) and 3 (stromelysin). *Biomed. Biochim. Acta*, **50**, 749–754.
24. Schlotzer-Schrehardt, U., Lommatzsch, J., Kuchle, M., Konstas, A.G. and Naumann, G.O. (2003) Matrix metalloproteinases and their inhibitors in aqueous humor of patients with pseudoexfoliation syndrome/glaucoma and primary open-angle glaucoma. *Invest. Ophthalmol. Vis. Sci.*, **44**, 1117–1125.
25. Ronkko, S., Rekonen, P., Kaarniranta, K., Puustjarvi, T., Terasvirta, M. and Uusitalo, H. (2007) Matrix metalloproteinases and their inhibitors in the chamber angle of normal eyes and patients with primary open-angle glaucoma and exfoliation glaucoma. *Graefes Arch. Clin. Exp. Ophthalmol.*, **245**, 697–704.
26. Tektas, O.Y. and Lutjen-Drecoll, E. (2009) Structural changes of the trabecular meshwork in different kinds of glaucoma. *Exp. Eye Res.*, **88**, 769–775.
27. Overby, D.R., Bertrand, J., Tektas, O.Y., Boussommier-Calleja, A., Schicht, M., Ethier, C.R., Woodward, D.F., Stamer, W.D. and Lutjen-Drecoll, E. (2014) Ultrastructural changes associated with dexamethasone-induced ocular hypertension in mice. *Invest. Ophthalmol. Vis. Sci.*, **55**, 4922–4933.
28. Pang, I.H., Fleenor, D.L., Hellberg, P.E., Stropki, K., McCartney, M.D. and Clark, A.F. (2003) Aqueous outflow-enhancing effect of tert-butylhydroquinone: involvement of AP-1 activation and MMP-3 expression. *Invest. Ophthalmol. Vis. Sci.*, **44**, 3502–3510.
29. Webb, J.G., Husain, S., Yates, P.W. and Crosson, C.E. (2006) Kinin modulation of conventional outflow facility in the bovine eye. *J. Ocul. Pharmacol. Ther.*, **22**, 310–316.
30. Bradley, J.M., Vranka, J., Colvis, C.M., Conger, D.M., Alexander, J.P., Fisk, A.S., Samples, J.R. and Acott, T.S. (1998) Effect of matrix metalloproteinases activity on outflow in perfused human organ culture. *Invest. Ophthalmol. Vis. Sci.*, **39**, 2649–2658.
31. De Groef, L., Van Hove, I., Dekeyster, E., Stalmans, I. and Moons, L. (2013) MMPs in the trabecular meshwork: promising targets for future glaucoma therapies?. *Invest. Ophthalmol. Vis. Sci.*, **54**, 7756–7763.
32. Rehnberg, M., Ammitzboll, T. and Tengroth, B. (1987) Collagen distribution in the lamina cribrosa and the trabecular meshwork of the human eye. *Br. J. Ophthalmol.*, **71**, 886–892.
33. Medina-Ortiz, W.E., Belmares, R., Neubauer, S., Wordinger, R.J. and Clark, A.F. (2013) Cellular fibronectin expression in human trabecular meshwork and induction by transforming growth factor-beta2. *Invest. Ophthalmol. Vis. Sci.*, **54**, 6779–6788.
34. Hann, C.R., Springett, M.J., Wang, X. and Johnson, D.H. (2001) Ultrastructural localization of collagen IV, fibronectin, and laminin in the trabecular meshwork of normal and glaucomatous eyes. *Ophthalmic Res.*, **33**, 314–324.

35. Umihira, J., Nagata, S., Nohara, M., Hanai, T., Usuda, N. and Segawa, K. (1994) Localization of elastin in the normal and glaucomatous human trabecular meshwork. *Invest. Ophthalmol. Vis. Sci.*, **35**, 486–494.
36. Wirtz, M.K., Bradley, J.M., Xu, H., Domreis, J., Nobis, C.A., Truesdale, A.T., Samples, J.R., Van Buskirk, E.M. and Acott, T.S. (1997) Proteoglycan expression by human trabecular meshworks. *Curr. Eye Res.*, **16**, 412–421.
37. Murphy, G., Cockett, M.I., Stephens, P.E., Smith, B.J. and Docherty, A.J. (1987) Stromelysin is an activator of procollagenase. A study with natural and recombinant enzymes. *Biochem. J.*, **248**, 265–268.
38. Lijnen, H.R., Silence, J., Van Hoef, B. and Collen, D. (1998) Stromelysin-1 (MMP-3)-independent gelatinase expression and activation in mice. *Blood*, **91**, 2045–2053.
39. Ogata, Y., Enghild, J.J. and Nagase, H. (1992) Matrix metalloproteinase 3 (stromelysin) activates the precursor for the human matrix metalloproteinase 9. *J. Biol. Chem.*, **267**, 3581–3584.
40. Yang, Y., Estrada, E.Y., Thompson, J.F., Liu, W. and Rosenberg, G.A. (2007) Matrix metalloproteinase-mediated disruption of tight junction proteins in cerebral vessels is reversed by synthetic matrix metalloproteinase inhibitor in focal ischemia in rat. *J. Cereb. Blood Flow Metab.*, **27**, 697–709.
41. Yamada, H., Yoneda, M., Inaguma, S., Watanabe, D., Banno, S., Yoshikawa, K., Mizutani, K., Iwaki, M. and Zako, M. (2013) Infliximab counteracts tumor necrosis factor-alpha-enhanced induction of matrix metalloproteinases that degrade claudin and occludin in non-pigmented ciliary epithelium. *Biochem. Pharmacol.*, **85**, 1770–1782.
42. Rajashekhar, G., Shivanna, M., Kompella, U.B., Wang, Y. and Srinivas, S.P. (2014) Role of MMP-9 in the breakdown of barrier integrity of the corneal endothelium in response to TNF-alpha. *Exp. Eye Res.*, **122**, 77–85.
43. Buie, L.K., Rasmussen, C.A., Porterfield, E.C., Ramgolam, V.S., Choi, V.W., Markovic-Plese, S., Samulski, R.J., Kaufman, P.L. and Borras, T. (2010) Self-complementary AAV virus (scAAV) safe and long-term gene transfer in the trabecular meshwork of living rats and monkeys. *Invest. Ophthalmol. Vis. Sci.*, **51**, 236–248.
44. Bogner, B., Boye, S.L., Min, S.H., Peterson, J.J., Ruan, Q., Zhang, Z., Reitsamer, H.A., Hauswirth, W.W. and Boye, S.E. (2015) Capsid Mutated Adeno-Associated Virus Delivered to the Anterior Chamber Results in Efficient Transduction of Trabecular Meshwork in Mouse and Rat. *PLoS One*, **10**, e0128759.
45. Gerometta, R., Spiga, M.G., Borras, T. and Candia, O.A. (2010) Treatment of sheep steroid-induced ocular hypertension with a glucocorticoid-inducible MMP1 gene therapy virus. *Invest. Ophthalmol. Vis. Sci.*, **51**, 3042–3048.
46. Borras, T., Buie, L.K. and Spiga, M.G. (2016) Inducible scAAV2.GRE.MMP1 lowers IOP long-term in a large animal model for steroid-induced glaucoma gene therapy. *Gene Ther.*, **23**, 438–449.
47. Sherwood, J.M., Reina-Torres, E., Bertrand, J.A., Rowe, B. and Overby, D.R. (2016) Measurement of Outflow Facility Using iPerfusion. *PLoS One*, **11**, e0150694.
48. Overby, D.R., Bertrand, J., Schicht, M., Paulsen, F., Stamer, W.D. and Lutjen-Drecoll, E. (2014) The structure of the trabecular meshwork, its connections to the ciliary muscle, and the effect of pilocarpine on outflow facility in mice. *Invest. Ophthalmol. Vis. Sci.*, **55**, 3727–3736.
49. Nga, A.D., Yap, S.L., Samsudin, A., Abdul-Rahman, P.S., Hashim, O.H. and Mimiwati, Z. (2014) Matrix metalloproteinases and tissue inhibitors of metalloproteinases in the aqueous humour of patients with primary angle closure glaucoma - a quantitative study. *BMC Ophthalmol.*, **14**, 33.
50. Ashworth Briggs, E.L., Toh, T., Eri, R., Hewitt, A.W. and Cook, A.L. (2015) TIMP1, TIMP2, and TIMP4 are increased in aqueous humor from primary open angle glaucoma patients. *Mol. Vis.*, **21**, 1162–1172.
51. Badier-Commander, C., Verbeuren, T., Lebard, C., Michel, J.B. and Jacob, M.P. (2000) Increased TIMP/MMP ratio in varicose veins: a possible explanation for extracellular matrix accumulation. *J. Pathol.*, **192**, 105–112.
52. Lutjen-Drecoll, E., Shimizu, T., Rohrbach, M. and Rohen, J.W. (1986) Quantitative analysis of 'plaque material' between ciliary muscle tips in normal- and glaucomatous eyes. *Exp. Eye Res.*, **42**, 457–465.
53. Rohen, J.W., Lutjen-Drecoll, E., Flugel, C., Meyer, M. and Grierson, I. (1993) Ultrastructure of the trabecular meshwork in untreated cases of primary open-angle glaucoma (POAG). *Exp. Eye Res.*, **56**, 683–692.
54. Parshley, D.E., Bradley, J.M., Samples, J.R., Van Buskirk, E.M. and Acott, T.S. (1995) Early changes in matrix metalloproteinases and inhibitors after in vitro laser treatment to the trabecular meshwork. *Curr. Eye Res.*, **14**, 537–544.
55. Parshley, D.E., Bradley, J.M., Fisk, A., Hadaegh, A., Samples, J.R., Van Buskirk, E.M. and Acott, T.S. (1996) Laser trabeculoplasty induces stromelysin expression by trabecular juxtacanalicular cells. *Invest. Ophthalmol. Vis. Sci.*, **37**, 795–804.
56. Takai, Y., Tanito, M. and Ohira, A. (2012) Multiplex cytokine analysis of aqueous humor in eyes with primary open-angle glaucoma, exfoliation glaucoma, and cataract. *Invest. Ophthalmol. Vis. Sci.*, **53**, 241–247.
57. Chua, J., Vania, M., Cheung, C.M., Ang, M., Chee, S.P., Yang, H., Li, J. and Wong, T.T. (2012) Expression profile of inflammatory cytokines in aqueous from glaucomatous eyes. *Mol. Vis.*, **18**, 431–438.
58. Kelley, M.J., Rose, A.Y., Song, K., Chen, Y., Bradley, J.M., Rookhuizen, D. and Acott, T.S. (2007) Synergism of TNF and IL-1 in the induction of matrix metalloproteinase-3 in trabecular meshwork. *Invest. Ophthalmol. Vis. Sci.*, **48**, 2634–2643.
59. Bradley, J.M., Anderssohn, A.M., Colvis, C.M., Parshley, D.E., Zhu, X.H., Ruddat, M.S., Samples, J.R. and Acott, T.S. (2000) Mediation of laser trabeculoplasty-induced matrix metalloproteinase expression by IL-1beta and TNFalpha. *Invest. Ophthalmol. Vis. Sci.*, **41**, 422–430.
60. Alexander, J.P., Samples, J.R. and Acott, T.S. (1998) Growth factor and cytokine modulation of trabecular meshwork matrix metalloproteinase and TIMP expression. *Curr. Eye Res.*, **17**, 276–285.
61. Partridge, C.A., Jeffrey, J.J. and Malik, A.B. (1993) A 96-kDa gelatinase induced by TNF-alpha contributes to increased microvascular endothelial permeability. *Am. J. Physiol.*, **265**, 438–447.
62. Si-Tayeb, K., Monvoisin, A., Mazzocco, C., Lepreux, S., Decossas, M., Cubel, G., Taras, D., Blanc, J.F., Robinson, D.R. and Rosenbaum, J. (2006) Matrix metalloproteinase 3 is present in the cell nucleus and is involved in apoptosis. *Am. J. Pathol.*, **169**, 1390–1401.
63. Garcia, A.J., Tom, C., Guemes, M., Polanco, G., Mayorga, M.E., Wend, K., Miranda-Carboni, G.A. and Krum, S.A. (2013) ERalpha signaling regulates MMP3 expression to induce FasL cleavage and osteoclast apoptosis. *J. Bone Miner. Res.*, **28**, 283–290.

64. Bradley, J.M., Kelley, M.J., Rose, A. and Acott, T.S. (2003) Signaling pathways used in trabecular matrix metalloproteinase response to mechanical stretch. *Invest. Ophthalmol. Vis. Sci.*, **44**, 5174–5181.
65. Bradley, J.M., Kelley, M.J., Zhu, X., Anderssohn, A.M., Alexander, J.P. and Acott, T.S. (2001) Effects of mechanical stretching on trabecular matrix metalloproteinases. *Invest. Ophthalmol. Vis. Sci.*, **42**, 1505–1513.
66. Gonzalez, P., Epstein, D.L. and Borras, T. (2000) Genes upregulated in the human trabecular meshwork in response to elevated intraocular pressure. *Invest. Ophthalmol. Vis. Sci.*, **41**, 352–361.
67. Luna, C., Li, G., Liton, P.B., Epstein, D.L. and Gonzalez, P. (2009) Alterations in gene expression induced by cyclic mechanical stress in trabecular meshwork cells. *Mol. Vis.*, **15**, 534–544.
68. Vittitow, J. and Borras, T. (2004) Genes expressed in the human trabecular meshwork during pressure-induced homeostatic response. *J. Cell. Physiol.*, **201**, 126–137.
69. Lai, L., Lin, K., Foulks, G., Ma, L., Xiao, X. and Chen, K. (2005) Highly efficient ex vivo gene delivery into human corneal endothelial cells by recombinant adeno-associated virus. *Curr. Eye Res.*, **30**, 213–219.
70. Sharma, A., Ghosh, A., Hansen, E.T., Newman, J.M. and Mohan, R.R. (2010) Transduction efficiency of AAV 2/6, 2/8 and 2/9 vectors for delivering genes in human corneal fibroblasts. *Brain Res. Bull.*, **81**, 273–278.
71. Liu, J., Saghizadeh, M., Tuli, S.S., Kramerov, A.A., Lewin, A.S., Bloom, D.C., Hauswirth, W.W., Castro, M.G., Schultz, G.S. and Ljubimov, A.V. (2008) Different tropism of adenoviruses and adeno-associated viruses to corneal cells: implications for corneal gene therapy. *Mol. Vis.*, **14**, 2087–2096.
72. Borras, T., Xue, W., Choi, V.W., Bartlett, J.S., Li, G., Samulski, R.J. and Chisolm, S.S. (2006) Mechanisms of AAV transduction in glaucoma-associated human trabecular meshwork cells. *J. Gene Med.*, **8**, 589–602.
73. Herschler, J. (1976) Increased intraocular pressure induced by repository corticosteroids. *Am. J. Ophthalmol.*, **82**, 90–93.
74. Mandapati, J.S. and Metta, A.K. (2011) Intraocular pressure variation in patients on long-term corticosteroids. *Indian Dermatol. Online J.*, **2**, 67–69.
75. Pleyer, U., Ursell, P.G. and Rama, P. (2013) Intraocular pressure effects of common topical steroids for post-cataract inflammation: are they all the same? *Opthalmol. Ther.*, **2**, 55–72.
76. Clark, A.F., Steely, H.T., Dickerson, J.E., Jr., English-Wright, S., Stropki, K., McCartney, M.D., Jacobson, N., Shepard, A.R., Clark, J.I., Matsushima, H., *et al.* (2001) Glucocorticoid induction of the glaucoma gene MYOC in human and monkey trabecular meshwork cells and tissues. *Invest. Ophthalmol. Vis. Sci.*, **42**, 1769–1780.
77. Gurney, K.J., Estrada, E.Y. and Rosenberg, G.A. (2006) Blood-brain barrier disruption by stromelysin-1 facilitates neutrophil infiltration in neuroinflammation. *Neurobiol. Dis.*, **23**, 87–96.
78. Vermeer, P.D., Denker, J., Estin, M., Moninger, T.O., Keshavjee, S., Karp, P., Kline, J.N. and Zabner, J. (2009) MMP9 modulates tight junction integrity and cell viability in human airway epithelia. *Am. J. Physiol. Lung Cell Mol. Physiol.*, **296**, 751–762.
79. Stamer, W.D., Roberts, B.C., Howell, D.N. and Epstein, D.L. (1998) Isolation, culture, and characterization of endothelial cells from Schlemm's canal. *Invest. Ophthalmol. Vis. Sci.*, **39**, 1804–1812.
80. Perkumas, K.M. and Stamer, W.D. (2012) Protein markers and differentiation in culture for Schlemm's canal endothelial cells. *Exp. Eye Res.*, **96**, 82–87.
81. Heimark, R.L., Kaochar, S. and Stamer, W.D. (2002) Human Schlemm's canal cells express the endothelial adherens proteins, VE-cadherin and PECAM-1. *Curr. Eye Res.*, **25**, 299–308.
82. Stamer, W.D., Seftor, R.E., Williams, S.K., Samaha, H.A. and Snyder, R.W. (1995) Isolation and culture of human trabecular meshwork cells by extracellular matrix digestion. *Curr. Eye Res.*, **14**, 611–617.
83. Stamer, W.D., Seftor, R.E., Snyder, R.W. and Regan, J.W. (1995) Cultured human trabecular meshwork cells express aquaporin-1 water channels. *Curr. Eye Res.*, **14**, 1095–1100.
84. Stamer, W.D., Huang, Y., Seftor, R.E., Svensson, S.S., Snyder, R.W. and Regan, J.W. (1996) Cultured human trabecular meshwork cells express functional alpha 2A adrenergic receptors. *Invest. Ophthalmol. Vis. Sci.*, **37**, 2426–2433.
85. Stamer, W.D. and Clark, A.F. (2016) The many faces of the trabecular meshwork cell. *Exp. Eye Res*, in press.
86. Siah, W.F., Loughman, J. and O'Brien, C. (2015) Lower Macular Pigment Optical Density in Foveal-Involved Glaucoma. *Ophthalmology*, **122**, 2029–2037.
87. Wallace, D.M., Clark, A.F., Lipson, K.E., Andrews, D., Crean, J.K. and O'Brien, C.J. (2013) Anti-connective tissue growth factor antibody treatment reduces extracellular matrix production in trabecular meshwork and lamina cribrosa cells. *Invest. Ophthalmol. Vis. Sci.*, **54**, 7836–7848.
88. Keaney, J., Walsh, D.M., O'Malley, T., Hudson, N., Crosbie, D.E., Loftus, T., Sheehan, F., McDaid, J., Humphries, M.M., Callanan, J.J., *et al.* (2015) Autoregulated paracellular clearance of amyloid-beta across the blood-brain barrier. *Sci. Adv.*, **1**, e1500472.

Manipulating ocular endothelial tight junctions: applications in treatment of retinal disease pathology and ocular hypertension

Matthew Campbell[1*], Paul S. Cassidy[1], Jeffrey O' Callaghan[1], Darragh E. Crosbie[1] and Pete Humphries[1*]

Affiliation
[1]Smurfit Institute of Genetics, Lincoln Place Gate, Trinity College, University of Dublin, Dublin 2, Ireland.

* To whom correspondence should be addressed
Pete Humphries
Phone: **353 1 8961547**
Fax: **353 1 8963848**
Email: pete.humphries@tcd.ie

Abstract
Protein levels of endothelial tight-junctions of the inner retinal microvasculature, together with those of Schlemm's canal, can be readily manipulated by RNA interference (RNAi), resulting in the paracellular clefts between such cells to be reversibly modulated. This facilitates access to the retina of systemically-deliverable low molecular weight, potentially therapeutic compounds, while also allowing potentially toxic material, for example, soluble Amyloid-β1-40, to be removed from the retina into the peripheral circulation. The technique has also been shown to be highly effective in alleviation of pathological cerebral oedema and we speculate that it may therefore have similar utility in the oedematous retina. Additionally, by manipulating endothelial tight-junctions of Schlemm's canal, inflow of aqueous humour from the trabecular meshwork into the Canal can be radically enhanced, suggesting a novel avenue for control of intraocular pressure. Here, we review the technology underlying this approach together with specific examples of clinical targets that are, or could be, amenable to this novel form of genetic intervention.

Key words; Tight junctions, RNAi, blood-retina barrier (BRB), Schlemm's canal, endothelium. Retinal degeneration.

Contents:
1. **Introduction**
2. **Structure and organization of endothelial tight junctions of cerebral and inner retinal vasculatures**
3. **Structure and organization of Schlemm's canal endothelial tight junctions**
4. **Induction of inner retinal microvessel permeability: validation of the concept as a potentially therapeutic modality**
5. **Site-specific modulation of the iBRB**
6. **On the potential therapeutic utility of manipulation of iBRB permeability**
   6.1. Enhancing macular pigment access to retina
   6.2. Alleviation of retinal oedema
   6.3. Enhancing clearance of soluble Amyloid ß1-40 from glaucomatous retinas.
   6.4. Targeting oxidative stress
   6.5. Targeting unique IRD molecular pathologies

7. **Targeting Schlemm's canal endothelial tight junctions: a novel process for enhancement of aqueous outflow through the conventional outflow pathway**
8. **Future prospects**

1. Introduction

Endothelial cells lining the cerebral and inner retinal micro-vasculatures, together with those of the Canal of Schlemm, possess tight-junctions. In the brain and retina, tight junctions form an exceedingly tight seal, with very low rates of fluid-phase transcytosis. Such junctions, constituting the blood-brain and inner blood-retina barriers (BBB/iBRB), prevent potentially noxious materials, including for example, low molecular weight blood-borne enzymes, anaphylatoxins, antibodies etc., from entering and damaging neurological tissues [1, 2, 3, 4, 5]. Additionally, in the anterior segment of the eye, Schlemm's Canal (SC) constitutes part of the conventional aqueous humour outflow pathway, aqueous produced by the ciliary body passing into the anterior chamber of the eye and then into the trabecular meshwork, from where it filters into the canal across its endothelial barrier [6]. While weaker and less well characterised than their counterparts of the inner retinal vessels, the tight junctions of canal endothelia are dynamically responsive to fluctuations in intraocular pressure (see Fig 1 and 2) [7]. Since it is well proven and within our capabilities to artificially modulate levels of transcript encoding tight-junctions, a means exists to enhance the permeability of the inner retinal vessels and the Canal for potentially therapeutic purposes.

Here, we provide an overview of the structure of tight junctions and of how levels of transcripts encoding tight junction components can be reversibly modulated both in retinal and SC endothelial cells. We provide examples of how low molecular weight compounds can be systemically delivered to the retina in its 'barrier modulated' state, and speculate on those degenerative retinal conditions in which oedema accumulates in the presence of an essentially intact iBRB and which could, in principle, be targeted using this approach. In the context of glaucoma, up to six percent of cases of open-angle disease are bilaterally sub-optimally responsive to standard topically-applied pressure-reducing medications [8] and for the most commonly used prostaglandin analogue, Latanoprost, between 25-50% of patients do not achieve greater than a 20% reduction in intraocular pressure [9, 10]. These topical formulations act largely by inhibiting aqueous secretion by the ciliary body or to increase aqueous outflow through the unconventional drainage pathway. Down regulation of SC endothelial tight junctions has been shown to increase aqueous humour outflow in experimental animal model systems [11] and could form the basis of a radical therapeutic approach targeting the major aqueous humour outflow system of the eye.

2. Structure and organization of endothelial tight junctions of cerebral and inner retinal vasculatures

Tight junctions (TJs), are essentially contact points between the plasma membranes of adjacent cells, or indeed the point where one endothelial cell contacts itself in a microvessel. TJs are located at the apical periphery of the plasma membrane, and each TJ is paired to and associates with another TJ on the membrane of the adjacent cell. TJs have numerous functions and can act as sites for vesicle targeting, proliferation, transcription signals, mediating cell polarity. Given their molecular complexity, TJs

also act as a physical barrier to limit paracellular diffusion of solutes across the BBB/iBRB and indeed the endothelium of Schlemm's canal.

Typically, each TJ consists of at least three different types of protein; 1) occludin, 2) junction adhesion molecule (JAM) family of proteins, and 3) claudin proteins [12]. However, the TJ itself can consist of over 40 individual proteins between support proteins, structural proteins, transport proteins, and other more unique proteins such as tricellulin, a homologue of occludin that concentrates when three cells come together [13]. In addition, the actin cytoskeleton of the cell is critical for TJ formation, as actin strands bind the PDZ-domain containing scaffolding proteins ZO-1, ZO-2, ZO-3, MAGI-1, PatJ, PALS1 and MUPP1, which can subsequently bind to the TJ proteins that can mediate extracellular interaction with adjacent TJ proteins.

During the assembly stage of the TJ, the proteins Par3, Par6 and aPKC are critical and the TJ is also important for the function of the basolateral-located adherens junctions, which are largely cadherin based junctions. Indeed, the protein VE-cadherin can act as a mediator of intracellular signalling via its interaction with phosphatidylinositol-3-OH kinase or other growth factor receptors. For example, VE-cadherin has been shown to interact directly with β-catenin, which can subsequently regulate cellular homeostasis or responses to cellular stress [14]. Paracellular transport of molecules from blood to retina or across the Schlemm's canal endothelium is exclusively passive, driven predominantly by concentration gradients [15].

The molecular composition and indeed the overt permeability of TJs varies considerably amongst different tissue types. For example, some tissues display variable electrical conductance, charge selectivity, non-charged solute permeability, and size selectivity, and this is reflected to a large degree on the density of claudin proteins present in their TJs. Importantly, TJs are distinguished from adherens junctions (AJs) in that they are located at the apical periphery of the contact point of endothelial cells, with AJs expressed below them. Additionally, AJs have a different molecular composition, being enriched with cadherins, catenins and nectin amongst others.

Structurally claudins are integral membrane proteins with four transmembrane domains and two extracellular and one intracellular loop. In the first extracellular loop claudins have a common WGLWCC motif, and they also possess a C-terminus PDZ domain. This region binds to the PDZ domains of the TJ support proteins, such as ZO-1, ZO-2, ZO-3 [16] and MUPP-1 [17]. The C-terminus tail, is also the region which confers stability to claudins, and swapping the C-terminus tails has been found to coincide with a reversal of protein half-lives [18].

Various post-translational modifications have also been implicated in claudin function. For example, phosphorylation has been shown to increase claudin1-4 permeability to chloride ions [19], and loss of palmitoylation sites on claudin-14 results in reduced localization of the protein to the membrane [20].

Some claudins, such as claudin-1, are widely expressed [15], whereas other claudin proteins are expressed only in certain cell types or during embryonic development [21]. This, suggests that claudins play various roles not necessarily limited to the TJs.

Various studies expressing combinations of different claudins in Madin-Darby canine kidney (MDCK) cells found that over-expression of claudin-7 increased paracellular permeability to cations, while reducing it to anions. Additionally, over-expression of claudin-4, -8 and -14 reduced permeability to cations but not anions, while over-expression of claudin-2 decreased barrier integrity without reducing the number of TJ strands [12, 22].

The finding that claudin-14 reduces permeability to cations aligns with its abundant *in vivo* expression in the outer hair cells of the cochlea in the ear. Here TJs function to separate the K^+-rich endolymph and Na^--rich perilymph, a separation essential for optimal hearing. The importance of claudin-14 for this role is observed in the deafness observed in mice and humans with claudin-14 mutations [12]. Claudin-11-null mice also exhibit deafness, and this is due to a similar role of claudin-11 in maintaining the endocochlear potential in the ear [23].

Indeed, mutations in the claudin-16 gene, expressed in the thick ascending limb of the nephron, cause Mg^{2+} reabsorption in humans and cattle, resulting in deficiency of the ion. Claudin-16 contains a number of negatively charged residues in its first extracellular loop, which appear to electrostatically interact with soluble ions, enabling or inhibiting their passage [24]. Detailed in Table 1, are some key properties of the claudins listed in this section.

Table 1

Gene	Protein Name	Chromosome	Tissue expression (protein)
CLDN1	claudin 1	3q28	Heart, brain, lung, liver testis
CLDN2	claudin 2	Xq22.3	Liver, kidney
CLDN3	claudin 3	7q11.23	Lung, liver, kidney, testis
CLDN4	claudin 4	7q11.23	Lung, kidney
CLDN5	claudin 5	22q11.21	Brain, heart, lung, liver, kidney, testis, endothelial cells in general
CLDN6	claudin 6	16p13.3	Embryonic tissues
CLDN7	claudin 7	17p13.1	Lung, kidney, testis
CLDN8	claudin 8	21q22.11	Lung, liver, kidney, testis
CLDN10	claudin 10	13q32.1	Liver
CLDN11	claudin 11	3q26.2	Brain, testis
CLDN14	claudin 14	21q22.13	Liver, kidney, ear
CLDN16	claudin 16	3q28	Kidney

As well as mediating selective ion transport across the paracellular pathway, claudins also play a central role in determining the maximum size of molecules that diffuse across an endothelial cell layer. Claudin-1 knockout mice, for example, die within one day of birth due to excessive water loss across the skin. Additionally, mutations in claudin-1 are associated in humans with ichthyosis – a condition manifested by skin dehydration [25]. These observed phenotypes in humans and other animals lacking claudin proteins demonstrate their importance in regulating TJ function and in controlling passive paracellular diffusion of materials across the TJ. Claudins are distinguished from other tight junction proteins such as occludin in that their extracellular domains have a certain degree of homology and mediate size selectivity and ion flux across the various barriers. Occludin appears to have a more regulatory role at the tight junction.

3. Structure and organization of Schlemm's canal endothelial tight junctions

The endothelial tight junctions of Schlemm's Canal differ from those seen in vascular endothelia in several ways. Early studies using electron microscopy showed electron dense junctions present between endothelial cells of Schlemm's Canal similar to those seen in vascular endothelia [26]. Subsequent freeze fracture studies showed that Schlemm's Canal endothelial cells TJs were composed of parallel junctional strands

with minimal branching which did not form complex bi-dimensional networks. The lack of branching between TJ strands in SC endothelial cells leads to the formation of channels between junction strands that are continuous from the juxtacanalicular tissue to the SC lumen. These channels were identified as a potential paracellular route for AH outflow in to the SC lumen through intercellular clefts in the SC inner wall endothelium [27, 28]. Early tracer studies using cationised ferritin showed staining of cell membranes lining channels between tight junctions in the SC inner wall endothelium, showing therefore that these channels represented a paracellular pathway across the SC inner wall. Further, these channels were of greater size and number in eyes that were fixed at elevated pressure, [29]. Additionally, endothelial tight junctions in perfused human donor eyes were shown by freeze fracture to exist in single and double stranded forms at the majority of TJs, with a minority of TJs having three or more junctional strands. The complexity of these junctions was shown to be responsive to applied pressure in the eye, with the number of junctional strands decreasing as perfusion pressure increased, [7]. The above features are in contrast to TJs of the inner retinal vascular endothelium, which are composed of complex networks of multiple TJ strands, and do not exhibit dynamic regulation in response to pressure, with no changes to TJ strand structure in response to perfusion pressure [30, 31].

Schlemm's canal endothelial cells also differ from inner retinal vascular endothelial cells in that they have remarkably high hydraulic conductivity, with Schlemm's canal having a hydraulic conductivity of 4000-9000$\times 10^{-11}$ cm^2 sec/g, significantly higher than other ocular barriers, and possibly one of the highest hydraulic conductivities of all body vessel linings [32]. The inner wall endothelium of SC is also permeable to higher molecular weight tracer molecules than other endothelial cells of the eye, with labelled ferritin, 450kDa, staining the interior of paracellular pores, while the inner blood-retinal barrier (iBRB) excludes molecules as small as 500 Da [29, 33]. It must be noted that these differences in endothelial permeability cannot be solely apportioned to differences in TJ structure and organization as, in addition to TJ mediated paracellular pores between cells, SCECs possess giant vacuoles containing large intracellular pores. These intracellular pores have an average pore size of approximately 1 μm in diameter, with pores greater than 3 μm reported (see Fig 3 for an overview of the differences in iBRB and SC endothelia) [34].

Human SC endothelial cells have differing TJ protein expression profiles than is seen other endothelial cells. For example, at the iBRB, ZO-1, occludin and claudin-5 are instrumental in maintaining barrier function, with claudin-5 being particularly important in controlling paracellular permeability [5, 35]. Contrastingly, recent studies have shown a more simplistic TJ composition in human SC endothelial cells, with claudin-11 and ZO-1 being the major TJ proteins present, and claudin-5 and occludin being expressed at low levels only [11].

4. Induction of inner retinal microvessel permeability: validation of the concept as a potentially therapeutic modality

In the original experimental approach [33, 36] targeting both the BBB and iBRB simultaneously, 20 μg of siRNA targeting Claudin-5 was hydrodynamically injected into the tail veins of mice in a volume of 10% of the body weight of the animal, a procedure that was well tolerated given the overtly high volumes. Using this approach, maximum suppression of claudin-5 was observed approximately 48 hours

after each tail injection, levels of claudin-5 returning to normal by 72 hours post inoculation. During this period, both the BBB and iBRB became permeable to the perfused nuclear stain, Hoechst H33342 (molecular weight, 563Da). In cryosections of the retina, staining of the inner nuclear layer (INL) was evident 24 hours post-siRNA injection, while staining of the outer nuclear layer (ONL) became evident at 48 hours. However, 72 hours after siRNA inoculation, no staining could be detected in any of the nuclear layers (Fig 4). Under the same conditions, systemically administered FITC-labelled dextran, FD-4 (MW 4,400Da), showed no evidence of being able to access any of the nuclear layers of the retina, these data indicating that down-regulation of claudin-5 facilitates a transient and size-selective enhancement of permeability at the iBRB to compounds of at least 563 Da, but not to those of higher molecular weight. In subsequent studies [4], tail injections were undertaken with siRNA complexed with a clinically enabled polyethylene imine (PEI) carrier, *in vivo*-JetPEI (Polyplus Transfection). 20 micrograms of claudin-5 siRNA injected in a volume of 0.4 ml with this carrier was shown to be as effective as the hydrodynamic approach in down-regulation of claudin-5. While these initial experiments validated barrier modulation technology as an enabling system for enhancing drug delivery to neural tissues, it was unable to selectively target the retina while leaving the BBB intact.

5. Site-specific modulation of the iBRB

In order to selectively target the retina, claudin-5 shRNA was incorporated into an AAV-2/9 vector, inducible by doxycycline [3]. A single once off sub-retinal injection of this vector was required, provision of doxycycline in drinking water (2mg/ml) being used to induce claudin-5 shRNA expression (viral constructs are now available that are capable of accessing the retina following intravitreal inoculation and there is no reason not to assume that such constructs will act in a similar manner, providing they have tropism for vascular endothelia). The efficacy of this system was initially validated in a light-induced murine model of apoptotic photoreceptor degeneration, in which it has been firmly established that death of photoreceptor cells is calpain-dependent [37]. N-Acetyl-L-leucyle-L-methioninal; calpain inhibitor II (ALLM), molecular weight 401Da is a potent calpain inhibitor. Albino mice given doxycycline in drinking water, were treated IP with 20mg/kg ALLM followed by exposure to 7,900 lux of white light. After 24 hours, photoreceptor cell death was assessed by TUNEL staining of retinal cryosections. As illustrated in Figure 5, photoreceptor cell viability was extensively preserved in animals systemically treated with the drug which, under conditions where permeability of the iBRB had not been modulated, could not gain sufficiently effective access to the retina to provide therapeutic benefit.

Validating this approach, a murine model of the exudative form of age-related macular degeneration (AMD) was also used [3]. Wild type C57BL/6J mice were sub-retinally inoculated in one eye with an AAV-2/9 expressing claudin-5 shRNA and the other eye with an AAV-2/9 expressing a non-targeting shRNA as control. Animals were administered doxycycline (2 mg/kg) for 3 weeks prior to induction of laser burns to the RPE/Bruch's membrane, inducing localised expression of vascular endothelial growth factor (VEGF) and choroidal neovascularisation (CNV) at the site of laser burns. During an interval of 14 days subsequent to laser treatment, mice were administered two systemic (IP) doses either of 17-AAG (30 mg/kg), or sunitinib malate (20 mg/kg), both well characterised and potent inhibitors of VEGFR-2. As shown in Figure 6, animals having received a claudin-5 targeting vector showed

highly significant suppression of CNV compared to the contralateral eye receiving a non-targeting vector.

It is of interest also to note that endothelial tight junctions at the iBRB can be further manipulated in order to increase barrier permeability beyond that achievable using claudin-5 alone. In this regard, Keaney et al (2015) [38], demonstrated that co-suppression of transcripts encoding claudin-5 and occludin rendered the iBRB reversibly permeable to systemically administered compounds up to approximately 4 kDa in molecular weight. While manipulating permeability to this extent runs the risk of admission into the retina (or brain) of potentially damaging low molecular weight materials such as anaphylatoxins, or low molecular weight enzymes, no observable negative physiological consequences of such modulation were noted. The possible therapeutic implications of this observation will be considered later in this review.

6 On the potential therapeutic utility of manipulation of iBRB permeability

6.1 Experimentally enhancing macular pigment (MP) access to retina

The macular pigments, lutein, zeaxanthin and mesozeaxanthin, act protectively within the retina, acting as filters for short wavelength blue light and also as scavengers of reactive oxygen species [39]. Potentially beneficial effects of dietary supplementation have been investigated in a number of scenarios, including for example, inherited retinal degenerations, specifically retinitis pigmentosa and Usher syndrome [40] and in patients with AMD [41, 42]. In the study by Aleman et al (2001) [40], there was a trend toward more severe progression of disease in those patients who had lower retinal MP levels. In the study by Ma et al (2012) [41], abnormalities in central retinal function in early AMD were reported to be improved and in the study reported by Liu (2015) [42], a meta-analysis of 1176 AMD patients, both visual acuity and contrast sensitivity were found to improve with supplementation. However, it is well recognised that not all on supplementation show increases in MP density within the retina, a probable reflection of variability in carotenoid transporter efficiency(40, 43, 44)

While mice do not possess a macula, they nevertheless could represent a highly cost efficient avenue for study of the physiological effects of MPs in normal and degenerating retinas. However, wild type mice do not accumulate these carotenoids within retinal tissues even when supplemented in their diet. Recent studies however, have shown that mice with targeted disruptions of β-carotene oxygenases 1 and 2 (*Bco2-/-* in particular) are able to accumulate MPs within the retina [45]. However, a very large amount of carotenoid ~ 2.6mg per mouse per day, equivalent to an average human dose of about 635 mg per day, was required to achieve measurable levels of MP within these retinas. Controlled modulation of the permeability of the iBRB of *Bco2-/-* mice, would enable very much smaller systemic doses of MP to be required in order to achieve elevated MP levels within retinal tissues. Given the fact that lutein and zeaxanthin have molecular weights (569Da), well below the cut off for systemic delivery following transient down regulation of claudin-5, *Bco2-/-* mice would likely be rendered a more versatile and useful model for studies of the physiological or protective efffects of MPs within the retina. The same system could be used to experimentally enhance MP uptake in primates.

6.2 Alleviation of retinal oedema

Previous studies from this laboratory [4] have shown that siRNA-mediated down regulation of claudin-5 is highly effective in reducing pathological cerebral oedema in a murine model of traumatic brain injury (TBI). In this model, a small ultra-cold probe is placed for a short period of time onto the skulls of anaesthetised animals. This induces a focal necrotic cerebral lesion and breakdown of the BBB, with extensive extravasation of fluid from the cerebral capillaries into the parenchyma of the brain. The barrier then reforms, pathological oedema remaining within penumbral region of the brain, adjacent to the injury site. [It is of interest to note that TBI accounts for about 1% of all adult mortality worldwide and cerebral oedema induced by out-of-hospital cardiac arrest is similarly prevalent. Treatments involving injection of the osmotic diuretic, mannitol, are archaic and inefficient if oedema persists beyond 24 h. This treatment paradigm has hardly changed in over 80 years]. In the current approach, claudin-5 siRNA complexed with the carrier agent *in-vivoJetPEI* was systemically administered. The transiently modulated BBB allowed efficient fluid drainage from the brain, reducing lesion volumes and improving cognitive function (Fig 7).

It is of interest to note in the above context, that a number of well- defined retinal conditions are characterized by a build-up of intra-retinal oedema and could be targetable using this approach. In general, retinal edema as a co-morbidity of a range of retinal conditions will involve vasogenic edema as the initial insult, *i.e.*, edema derived from a vascular source, with extravasation of fluid from blood to neural tissues. Vasogenic edema will lead to acute pressure changes within neural tissue and will lead to eventual cytotoxic edema, where cells within the penumbral region of injury/damage will gradually decline. Bearing in mind that the retina is simply an extension of the central nervous system (CNS), we speculate that in such conditions, it may be possible to counterbalance fluid exudation into retinal tissues, by enhancing fluid resorption into the inner retinal vasculature by manipulating iBRB permeability. While this may appear counter-intuitive, the approach is now validated in murine models of TBI, where BBB breakdown is a hallmark pathology. The same will apply to retinal oedematous conditions, where penumbral regions are at risk of perpetuating neural damage. Such conditions include, *inter alia,* Non-arteritic Anterior Ischaemic Opthic Neuropathy (NAION), characterised by axoplasmic flow stasis and extracellular oedema at the optic nerve head and X-linked Juvenile Retinoschisis, in which fluid-filled cavities develop as the retina splits, cavities largely forming in the outer/inner plexiform and inner nuclear layers of the retina (fundus images of these conditions, clearly revealing the presence of retinal oedema are shown in Figure 8). NAION is caused by reduced blood flow in the posterior ciliary artery, which causes ischaemia in the anterior part of the optic nerve head, resulting in a vasogenic oedema and axoplasmic flow stasis in ganglion cell axons, causing them to swell and become damaged [46]. It is a major cause of visual handicap in older people, with approximately 6,000 cases per year in US (the prevalence is higher in diabetics). 25% of patients experience NAION in contralateral eye within five years of developing the disease and loss of vision is often permanent. Most importantly, there are no effective treatments [47]. Animal models of NAION are controversial. However, given the impelling data that exist on efficient clearance of oedema from the brain, we suggest that claudin-5 suppression within the inner retinal endothelial vasculature could represent a plausible means of alleviation of optic nerve head swelling. In this regard, we tested the efficacy of intravitreal inoculation of GLP grade claudin-5 siRNA in the Vervet (African Green) monkey. Tissues at the optic nerve head were dissected and subjected to RT-PCR analysis. Clearly, claudin-5 levels can be reduced using this

approach (see Figure 9). In the current context it is of note that intravitreal inoculation is widely accepted in routine ophthalmic practice (some patients have now received several hundred intravitreal injections of Lucentis). Moreover, therapy could readily be packaged as lyophilized compound, reconstituted and administered in outpatient facilities and readout of efficacy over days/weeks following therapy would be rapid, using standard clinical techniques (fluorescein angiography, visual acuity, OCT, ERG).

X-linked juvenile retinoschisis, caused by recessive mutations within the RS1 (Retinoschisin) gene, is characterized by splitting of the retina, particularly in the region of the macula, largely occurring in the OPL, INL and IPL layers [48, 49, 50]. Retinoschisin is an extracellular matrix (ECM) protein secreted from a number of retinal cell types including photoreceptors, bipolar, amacrine and ganglion cells, and binding strongly to the membranes of photoreceptors and bipolar cells, stabilizing retinal cellular architecture [51, 52]. AAV-mediated therapeutic intervention involving either CMV or endogenous promoter-driven expression of the RS1 gene, has now progressed from murine models [53, 54, 55, 56] into clinical evaluation (Clinicaltrials.gov.NCT02416622; NCT0231787). It is also of note that regression of retinal cysts in one patient with juvenile XL retinoschisis was induced by oral administration (500 mg/day over four days) of the carbonic anhydrase inhibitor, acetozolmide [57]. The latter is used as a topical medication for open angle glaucoma and acts by enhancing aqueous outflow through the uveoscleral route. However, it also enhances the pumping activity of the RPE enabling excess fluid accumulating in intra-retinal cysts to be transported into the choroidal circulation. In view of the fact that the inner retinal microvessels innervate the layers of the retina in which schisis most frequently occurs, we speculate that modulation of the permeability of the inner retinal vessels may assist in facilitating fluid clearance from the large cysts that occur within these retinal layers. In this regard, it is noteworthy that intravitreal inoculation is an accepted mode of delivery of siRNA, the following trials serving as an indication: QPI-1007 (Quark): siRNA targeting caspase-2 for suppression of apoptosis in NAAION; AGN211745 (siRNA/Allergan): siRNA targets VEGFR1 (AMD); Bevasiranib (Opko Health): siRNA targets VEGF (diabetic macular oedema); PF-04523655 (Quark): siRNA targets RTP801/REDD1 apoptotic stress response gene; ALY040012 (Sylentis): siRNA targeting ocular hypertension. (Bevasiranib was initially withdrawn from trial owing to lack of efficiency in suppressing VEGF activity. Note however, that in the scenario described above, only partial knockdown of claudin-5 transcript is required to enhance iBRB permeability). This approach could also be envisaged as an adjunct to AAV-mediated therapeutic intervention, where AAV expressing an inducible claudin-5 shRNA is used in conjunction with gene replacement.

6.3 Enhancing clearance of soluble Amyloid ß1-40 from glaucomatous retinas.

Evidence has accumulated over a number of years to suggest a pathological role for amyloid-β (Aβ) in degenerative retinopathies, including AMD and glaucoma. Co-localization of Aβ and drusen in post-mortem human AMD eyes has been observed in a number of studies, including those reported by Dentchev (2003), Anderson (2004) and Johnson (2002) [58, 59, 60], such studies suggesting Aβ as a putative activator of complement cascades. Further evidence for a pathological role for Aβ in AMD was reported by Ding et al (2011) and Liu (2015) [61, 62]. In the former study, systemic anti-Aβ antibody treatment of APOE4 mice, fed on a high fat diet to induce AMD-like retinal symptoms, resulted in an alleviation of disease pathology, while in the

latter, sub-retinal inoculation of Aβ into wild type mice produced pathological changes in RPE and photoreceptors. In optic nerve head post mortem tissue from individuals with glaucoma, Gupta et al (2016) [63] detected elevated levels of soluble Aβ, which has also been detected in aqueous humor from up to 40 % of patients with glaucoma [64].

These, and many other studies, strongly suggest that suppression of Aβ accumulation within retinal tissues may be protective in AMD, glaucoma and possibly in inherited retinal degenerations. In this regard, our own studies [38] have shown that siRNA-mediated down regulation of endothelial tight junction transcripts encoding claudin-5 together with occludin, allowed paracellular transport of a soluble Aβ1-40 monomer (MW 4.3kDa), modified with proline at position 19 and not prone to aggregation into higher molecular weight structures, to readily diffuse across brain endothelial cell monolayers *in vitro*. However, a dityrosine cross-linked Aβ1-40 dimer (MW 8.6 kDa) did not diffuse in such a manner, these data demonstrating that the paracellular spaces between brain endothelial cells can be widened sufficiently by down regulation of two tight junction components to allow soluble Aβ1-40 dimers to diffuse across them. These observations were confirmed *in vivo* in wild type mice and in a murine AD model (Tg2576) expressing a mutated form of APP, where it was shown that tail vein co-inoculation of claudin-5 and occludin siRNAs rendered the BBB reversibly permeable to biotinylated dextran of 3kD but not of 10kD. Periodic intravenous inoculation of claudin-5 and occludin siRNAs every 21 days into AD mice for a period of 9 months resulted during this period in a significant induction of movement of soluble Aβ1-40 from brain tissue into the peripheral circulation. Furthermore, in a murine model of pseudoexfoliative glaucoma, the DBA/2J mouse, in which Aβ1-40 was clearly detectable in retinal sections, a single intravenous injection of claudin-5 and occludin siRNAs resulted in retina:plasma ratios of Aβ1-40 being significantly reduced (Figure 10).

These data raise the distinct possibility for an avenue of clearance of neurotoxic Aβ1-40 from retinal tissues as a means of protecting against ganglion cell death in glaucoma. It will be of interest in this context to assess such an approach in additional models more accurately resembling the primary open-angle form of glaucoma, for example in transgenic mice expressing a C437H mutation within the human myocilin gene, a model mimicking primary open angle glaucoma in which there is an intracellular accumulation of ECM material within cells of the Trabecular meshwork, and a decrease in secretion of MMPs, favouring an extracellular accumulation of ECM materials, these animals classically displaying elevations in IOP and reduced outflow facility, with concomitant demise of retinal ganglion cells [65].

6.4 Targeting oxidative stress

The brain and retina account for approx. 20% of the body's oxygen consumption, which generates appreciable levels of reactive oxygen species and peroxides, contributing to neurological and retinal degeneration [66]. For example, oxygen free radicals interact with membrane phospholipids generating MDA (malondialdehyde; HOCH=CH-CHO, or $C_3H_4O_2$). This compound is pro-inflammatory, and has been recently shown [67] to be normally sequestered by complement factor H (CFH). CFH is an inhibitor of the alternative complement pathway and a mutation, His402Tyr within the SCR-7 domain of the protein was the first to be strongly associated with AMD. The risk variant, CC has been shown to have a very much lower affinity for MDA than the non-risk variant TT. People with AMD who are heterozygous for the normal and risk variants have a compromised ability to bind MDA, presumably

increasing the risk of disease progression. The Authors conclude: 'We report the identification of CFH as a hitherto unrecognized innate defence protein against MDA, which is a ubiquitously generated pro-inflammatory product of lipid peroxidation'. Reactive oxygen species are also similarly important in contributing to disease pathology in IRDs and in diabetic retinopathy [68].

Mitochondria are a major site of generation of oxygen free radicals in the retina. A recently developed oxygen free radical scavenger, XJB -5-131 (4- hydroxy-2,2,6,6-tetramethyl piperidine-1-oxyl nitroxide chemically linked to a mitochondrial targeting peptide, Leu-D-Phe-Pro-Val-Orn), enables the systemically-administered drug to become localized in the membranes of the mitochondria and it has been shown to be protective against neurological degeneration in a murine model of Huntington's disease [69]. While this drug, with a molecular weight of 959 Da, can access the brain in the Huntington model, it's systemic access to the retina could be radically enhanced (with concomitant reduction in systemic dosage) by periodic manipulation of iBRB permeability, possibly representing a approach to slowing disease progression in a manner independent of primary mutations in IRDs or other retinopathies.

6.5 Targeting unique IRD molecular pathologies

With over 260 genes having so far been identified in IRDs, with 70 in retinitis pigmentosa, the molecular pathologies associated with these conditions are clearly of immense diversity, genes encoding proteins, or enzymes involved in transport processes, protein deglutamylation, membrane trafficking, ciliogenesis, calcium-sensitive chloride channels, proteins with protective function against apoptosis/oxidative stress, retinal neurotransmission, photoreceptor morphogenesis, fatty acid and steroid metabolism, extracellular proteins of the retina, retinal adhesion proteins, phagocytosis of rod outer segments, transcription factors and activators, semaphorins, protein ubiquitination, actin binding proteins, pre-mRNA processing, the rate-limiting step of the alternative pathway of guanine nucleotide biosynthesis, and about every gene encoding proteins or enzymes of the visual transduction and retinoid cycles, and indeed many more [70]. In some cases, molecular pathologies specific to only one, or a limited number of genetic subtypes of disease may offer opportunities to target such uniqueness by systemic drug treatment.

The RP10 form of RP is arguably one of these, accounting for at least 5% of autosomal dominant cases of RP (perhaps 25-30,000 cases world-wide). It is an early onset, aggressive retinopathy, symptoms manifesting within the first decade. The disease is caused by mutations within the inosine monophosphate dehydrogenase 1 (IMPDH1) gene [71, 72, 73], which, together with IMPDH2, are the rate-limiting enzymes of *de novo* guanine nucleotide biosynthesis. While each enzyme performs the same role in converting IMP to XMP, which is then converted to GMP, levels of expression between tissues vary considerably, the predominant enzyme within the murine retina being IMPDH1 [73]. IMPDH1-/- mice (hence having little or no IMPDH activity because of minimal expression of IMPDH2) have only a very slow deterioration in retinal function, the outer nuclear layer (ONL) of these animals remaining largely intact [73]. Since both IMPDH1 and IMPDH2 are minimally expressed in these retinas, retinal function appears to be maintained with a sufficient supply of guanine nucleotides generated by the salvage pathway of guanine nucleotide biosynthesis. Mutations identified in RP10, occur within the CBS domain of the IMPDH1 enzyme, a binding site for GDP/GTP inhibition, indicating that mutations within the IMPDH1 gene result in constitutive activation of the enzyme,

disturbing guanine nucleotide pools within the retina and thus causing loss of photoreceptor function [74]. Interestingly however, OCT imaging (unpublished data) of severely affected individuals reveals a remarkably intact outer nuclear retinal layer, indicating that while visual function is lost, photoreceptors appear to remain viable (Fig 11), thus providing a potentially very robust window of opportunity for therapeutic intervention. These data suggest that suppression of IMPDH in dominant RP10 could result in a restoration of visual function. A number of FDA-approved IMPDH inhibitors (inhibiting both IMPDH1 and 2) are available, including CellCept, Mizorbine and VX-497 and these have been used as effective immunosuppressive agents (B and T lymphocytes are highly dependent upon the alternative, rather than the salvage pathway of guanine nucleotide biosynthesis). The concept of repositioning such agents as orally-available therapeutics for an IRD, delivery of which could be enhanced (thus reducing systemic dosage) by manipulating ocular endothelial tight junctions is a provocative but potentially realistic concept, dependent on long term tolerability. Given the ease with which systemically-deliverable compounds can access the retina (Fig 3), tolerable doses may be achievable.

The gene encoding Bestrophin, a calcium-gated chloride channel located in the basolateral region of RPE cells, is mutated in the ciliopathy, autosomal recessive bestrophinopathy [75]. Mutated proteins have been shown to mis-localise and end up in proteasomes in the cytoplasm and are degraded [76]. These authors have shown in vitro that proteasomal inhibitors, Bortezomib and 4-phenylbutyrate (4PBA), both approved proteasomal inhibitors, effectively restore the location of mutant bestrophins to the RPE and restore Cl- conductance of the channels in vitro. The Authors comment: “The functional rescue achieved with 4PBA is significant because it suggests that this drug, which is already approved for long-term use in infants and adults, might represent a promising therapy for the treatment of ARB and other bestrophinopathies resulting from missense mutations in BEST1”. Again, the degree of enhancement of systemic drug uptake by claudin-5 modulated iBRB could render such compounds (MW 4-PBA 186Da; MW Bortezomib 384Da) systemically tolerable over prolonged periods.

7. Targeting Schlemm’s canal endothelial tight junctions: a novel process for enhancement of aqueous outflow through the conventional outflow pathway.

Glaucoma in its various forms represents the second most common blinding disease on a global basis after cataract, elevations in IOP being the greatest risk factor [77, 78, 79]. Aqueous humour leaves the eye through the so-called conventional and un-conventional outflow pathways located close together in the periphery of the anterior chamber, at the apex of the narrow angle formed between the iris and the cornea. The conventional outflow pathway comprises the trabecular meshwork, which, as the name suggests, is an interlaced structure of cells embedded in a pressure-responsive ECM through which aqueous flows into the Canal of Schlemm both through paracellular gaps or through cellular pores in the canal’s endothelial lining. While a number of genes have been firmly associated with open-angle glaucoma susceptibility, a robust understanding of the molecular pathology of the disease remains to be determined. It should be highlighted, that a balance in the production of matrix metalloproteinases (MMPs) and their tissue inhibitors within the trabecular meshwork is a significant factor in the maintenance of physiological IOP at between 12-22 mmHg [80]. From the canal, fluid flows through collector channels and eventually into the episcleral veins. Some aqueous also leaves the eye through the bundles of the ciliary muscles – the so-called un-conventional or uveoscleral route.

Interestingly, currently used topical medications (including prostaglandin analogues, carbonic anhydrase inhibitors and ß-blockers) either slow up aqueous production by the ciliary body, or enhance its clearance via the uveoscleral route, none of these formulations directly and primarily targeting the conventional pathway. Since an appreciable number of those with open angle disease do not respond adequately to currently available pressure-reducing drugs, a large amount of research in recent years has gone into the development of medicines capable of enhancing aqueous outflow through the conventional route. These include Rho kinase inhibitors [81, 82], adenosine receptor agonists [83, 84], marine macrolides [85], prostanoid receptor agonists [86] and AAV-mediated gene therapies involving enhanced MMP expression to remodel the ECM within the Trabecular meshwork [87, 88, 89, 90].

The bulk of outflow resistance in the conventional pathway is generated within the juxtacanalicular tissues and the endothelial cells of the canal itself. Aqueous enters Schlemm's canal either through the formation of intra-endothelial fluid-filled vacuoles (so called 'giant' vacuoles) or through the paracellular route, where it passes through pores left between the endothelial tight junctions. Less is known of the nature of the tight junctions joining SC endothelia than those of the cerebral and inner retinal vasculatures. Interestingly claudin-5, a major component of the tight junctions of the cerebral and inner retinal vascular endothelia, is absent from human SC endothelial cells [11]. However, as outlined earlier, ZO-1, tricellulin and claudin-11 are prominently expressed TJ proteins. In order to explore the hypothesis that down-regulation of SC endothelial TJs might result in an increase in the permeability of the canal, Tam *et al.* (2017) [11] intracamerally injected siRNA validated against tricellulin and ZO-1 into wild type mice. Injected material followed the natural flow of aqueous through the trabecular meshwork and into the canal's endothelial cells. As illustrated in Fig 12, transmission electron microscopy revealed reversible opening of the paracellular clefts between endothelial cells as a result of such down-regulation. This was accompanied by a significant elevation in outflow facility in treated eyes *ex vivo*.

In translational terms, a major factor to be considered in this approach is the mode of siRNA delivery. Recent reports have indicated that siRNA can be effectively delivered to the eye in the form of topical drops to the cornea. However, in this approach, while the siRNA (SYL040012, targeting the β2-adrenoceptor) was able to efficiently access the ciliary body which was the primary site of action, little siRNA was found in the aqueous humour using this technique [91, 92]. While periodic intracameral injection of siRNA as indicated by IOP is a realistic option, an alternative and less invasive procedure would involve retrograde introduction of siRNA into Schlemm's canal via the episcleral veins and a device facilitating this approach has been manufactured (Retroject Inc, NC). An alternative would be the use of AAV as a delivery vehicle for shRNAs. While single stranded AAV particles will not transfect tissues of the trabecular meshwork, self-complementary AAV have been reported to do so with high efficiency [93]. However, it is unclear from this work as to whether AAV directly transfects SC endothelial cells. If this can be demonstrated, an AAV expressing shRNAs under the control of a promoter inducible by a topical eye drop could in principle be used. In this regard, it is of interest to note in a recently reported experimental system, that AAV transfecting the corneal endothelium can be activated to express MMP3 via the use of doxycycline applied to the cornea, the enzyme then being secreted from the corneal endothelia in to the TM, where re-modelling of the ECM resulted in increased outflow facility and decreased IOP in wild type mice [90]. Since an inducing agent will travel with the natural flow of

aqueous toward Schlemm's canal, there is reason to believe that AAVs transfecting SC endothelia could be periodically activated using such a procedure. A combinatorial AAV-mediated approach, targeting ECM remodelling together with incrementing SC permeability, is a realistic possibility based on observations to date.

8. Future prospects

Retinal endothelial barrier modulation technologies are, in principle, deployable in a stand-alone sense, or in combination with gene and other molecular therapeutic approaches. There is a significant need for a therapy for one of the more common idiopathic retinopathies, NAION, which is currently incurable and can lead to irreversible blindness. Clearance of oedema from the optic nerve head by intravitreal injection of siRNA targeting claudin-5 could well be effective in this scenario. It is also of note that as yet there are no medicines available for the most common (non-exudative) form of AMD, and yet, clearance of Aß, or drug-mediated suppression of oxidative stress within the retina, could have utility in slowing down disease progression in this, and indeed other forms of retinal degeneration including glaucoma. It will also be of interest to assess the efficacies of gene therapy for XL-retinoschisis *vis-à-vis* direct facilitation of fluid egress from intraretinal cysts, perhaps the two approaches, each using AAV could be used in a combinatorial sense. Repositioning approved drugs for use as therapies in early stage IRDs where the iBRB is essentially intact, is an interesting possibility, several scenarios having been outlined, including the possibility of IMPDH1 suppression in the RP10 form of RP and the use of proteasome inhibitors for at least one form of bestrophinopathy, but there will be many other examples based on the very extensive range of molecular pathologies that are involved, low molecular weight drug-mediated inhibition of protein mis-folding for example, being one. Improved treatment regimens for open-angle glaucoma continue to be a priority. As outlined, much research is currently being directed toward the development of topical formulations targeting the major (conventional) outflow pathway. The fact that siRNA could periodically be delivered in a retrograde fashion into Schlemm's canal endothelia through the episcleral veins, obviating a requirement for intracameral inoculation, is an interesting concept which, in principle, could be deployed as an outpatient procedure. In summary, we suggest that direct manipulation of permeability of both the inner retinal microvasculature and the Canal of Schlemm, may have significant potential clinical utility.

Acknowledgement

We thank Blanca Garcia Sandoval and Carmen Ayuso for provision of unpublished OCT images of RP10; Matthew Lawrence for provision of dissected primate tissues from the optic nerve head and David Keegan for OCT and fundus images of NAION and XL-retinoschisis. Research on modulation of permeability at the blood-brain and inner blood-retina barriers has been supported by grants from the Wellcome Trust, Science Foundation Ireland, the Health Research Board of Ireland, Enterprise Ireland, Bright Focus Foundation and the US Department of Defense. Studies on enhancement of aqueous outflow by modulation of permeability at SC endothelia is supported by the European Research Council (ERC-2012-AdG 322656-Oculus). Primate studies on claudin-5 suppression were supported by the St. Kitt's Medical Research Foundation.

References

1. Hawkins BT, Davis TP. The blood-brain barrier/neurovascular unit in health and disease. Pharmacol Rev. 2005;57:173-85.
2. Abbott NJ, Patabendige AA, Dolman DE, Yusof SR, Begley DJ. Structure and function of the blood-brain barrier. Neurobiol Dis. 2010;37:13-25.
3. Campbell M, Humphries MM, Kiang AS, Nguyen AT, Gobbo OL, Tam LC, Suzuki M, Hanrahan F, Ozaki E, Farrar GJ, Kenna PF, Humphries P. Systemic low-molecular weight drug delivery to pre-selected neuronal regions. EMBO Mol Med. 2011;3:235-45.
4. Campbell M, Hanrahan F, Gobbo OL, Kelly ME, Kiang AS, Humphries MM, Nguyen AT, Ozaki E, Keaney J, Blau CW, Kerskens CM, Cahalan SD, Callanan JJ, Wallace E, Grant GA, Doherty CP, Humphries P. Targeted suppression of claudin-5 decreases cerebral oedema and improves cognitive outcome following traumatic brain injury. Nat Commun. 2012;3:849.
5. Campbell M, Humphries P. The blood-retina barrier: tight junctions and barrier modulation. Adv Exp Med Biol. 2012;763:70-84.
6. Stamer WD, Clark AF. The many faces of the trabecular meshwork cell. Exp Eye Res. 2017;158:112-23.
7. Ye W, Gong H, Sit A, Johnson M, Freddo TF. Interendothelial junctions in normal human Schlemm's canal respond to changes in pressure. Invest Ophthalmol Vis Sci. 1997;38:2460-8.
8. Kass MA, Heuer DK, Higginbotham EJ, Johnson CA, Keltner JL, Miller JP, Parrish RK, 2nd, Wilson MR, Gordon MO. The Ocular Hypertension Treatment Study: a randomized trial determines that topical ocular hypotensive medication delays or prevents the onset of primary open-angle glaucoma. Arch Ophthalmol. 2002;120:701-13; discussion 829-30.
9. Scherer WJ. A retrospective review of non-responders to latanoprost. J Ocul Pharmacol Ther. 2002;18:287-91.
10. Noecker RS, Dirks MS, Choplin NT, Bernstein P, Batoosingh AL, Whitcup SM, Bimatoprost/Latanoprost Study G. A six-month randomized clinical trial comparing the intraocular pressure-lowering efficacy of bimatoprost and latanoprost in patients with ocular hypertension or glaucoma. Am J Ophthalmol. 2003;135:55-63.
11. Tam LC, Reina-Torres E, Sherwood JM, Cassidy PS, Crosbie DE, Lutjen-Drecoll E, Flugel-Koch C, Perkumas K, Humphries MM, Kiang AS, O'Callaghan J, Callanan JJ, Read AT, Ethier CR, O'Brien C, Lawrence M, Campbell M, Stamer WD, Overby DR, Humphries P. Enhancement of Outflow Facility in the Murine Eye by Targeting Selected Tight-Junctions of Schlemm's Canal Endothelia. Sci Rep. 2017;7:40717.
12. Ben-Yosef T, Belyantseva IA, Saunders TL, Hughes ED, Kawamoto K, Van Itallie CM, Beyer LA, Halsey K, Gardner DJ, Wilcox ER, Rasmussen J, Anderson JM, Dolan DF, Forge A, Raphael Y, Camper SA, Friedman TB. Claudin 14 knockout mice, a model for autosomal recessive deafness DFNB29, are deaf due to cochlear hair cell degeneration. Hum Mol Genet. 2003;12:2049-61. Epub 2003/08/13.
13. Anderson JM, Van Itallie CM. Tight junctions. Curr Biol. 2008;18:R941-3.

14. Taddei A, Giampietro C, Conti A, Orsenigo F, Breviario F, Pirazzoli V, Potente M, Daly C, Dimmeler S, Dejana E. Endothelial adherens junctions control tight junctions by VE-cadherin-mediated upregulation of claudin-5. Nat Cell Biol. 2008;10:923-34.
15. Van Itallie CM, Anderson JM. The molecular physiology of tight junction pores. Physiology (Bethesda). 2004;19:331-8.
16. Itoh M, Furuse M, Morita K, Kubota K, Saitou M, Tsukita S. Direct binding of three tight junction-associated MAGUKs, ZO-1, ZO-2, and ZO-3, with the COOH termini of claudins. J Cell Biol. 1999;147:1351-63.
17. Hamazaki Y, Itoh M, Sasaki H, Furuse M, Tsukita S. Multi-PDZ domain protein 1 (MUPP1) is concentrated at tight junctions through its possible interaction with claudin-1 and junctional adhesion molecule. J Biol Chem. 2002;277:455-61.
18. Van Itallie CM, Colegio OR, Anderson JM. The cytoplasmic tails of claudins can influence tight junction barrier properties through effects on protein stability. J Membr Biol. 2004;199:29-38. Epub 2004/09/16.
19. Yamauchi K, Rai T, Kobayashi K, Sohara E, Suzuki T, Itoh T, Suda S, Hayama A, Sasaki S, Uchida S. Disease-causing mutant WNK4 increases paracellular chloride permeability and phosphorylates claudins. Proc Natl Acad Sci U S A. 2004;101:4690-4.
20. Van Itallie CM, Gambling TM, Carson JL, Anderson JM. Palmitoylation of claudins is required for efficient tight-junction localization. J Cell Sci. 2005;118:1427-36. Epub 2005/03/17.
21. Turksen K, Troy TC. Claudin-6: a novel tight junction molecule is developmentally regulated in mouse embryonic epithelium. Dev Dyn. 2001;222:292-300.
22. Furuse M, Tsukita S. Claudins in occluding junctions of humans and flies. Trends Cell Biol. 2006;16:181-8.
23. Kitajiri S, Miyamoto T, Mineharu A, Sonoda N, Furuse K, Hata M, Sasaki H, Mori Y, Kubota T, Ito J, Furuse M, Tsukita S. Compartmentalization established by claudin-11-based tight junctions in stria vascularis is required for hearing through generation of endocochlear potential. J Cell Sci. 2004;117:5087-96.
24. Simon DB, Lu Y, Choate KA, Velazquez H, Al-Sabban E, Praga M, Casari G, Bettinelli A, Colussi G, Rodriguez-Soriano J, McCredie D, Milford D, Sanjad S, Lifton RP. Paracellin-1, a renal tight junction protein required for paracellular Mg2+ resorption. Science. 1999;285:103-6.
25. Hadj-Rabia S, Baala L, Vabres P, Hamel-Teillac D, Jacquemin E, Fabre M, Lyonnet S, De Prost Y, Munnich A, Hadchouel M, Smahi A. Claudin-1 gene mutations in neonatal sclerosing cholangitis associated with ichthyosis: a tight junction disease. Gastroenterology. 2004;127:1386-90.
26. Vegge T. The fine structure of the trabeculum cribriforme and the inner wall of Schlemm's canal in the normal human eye. Z Zellforsch Mikrosk Anat. 1967;77:267-81.
27. Raviola G, Raviola E. Paracellular route of aqueous outflow in the trabecular meshwork and canal of Schlemm. A freeze-fracture study of the endothelial junctions in the sclerocorneal angel of the macaque monkey eye. Invest Ophthalmol Vis Sci. 1981;21:52-72.

28. Bhatt K, Gong H, Freddo TF. Freeze-fracture studies of interendothelial junctions in the angle of the human eye. Invest Ophthalmol Vis Sci. 1995;36:1379-89.
29. Epstein DL, Rohen JW. Morphology of the trabecular meshwork and inner-wall endothelium after cationized ferritin perfusion in the monkey eye. Invest Ophthalmol Vis Sci. 1991;32:160-71.
30. Fujimoto K. Freeze-fracture replica electron microscopy combined with SDS digestion for cytochemical labeling of integral membrane proteins. Application to the immunogold labeling of intercellular junctional complexes. J Cell Sci. 1995;108 (Pt 11):3443-9.
31. Schneeberger EE, Karnovsky MJ. Substructure of intercellular junctions in freeze-fractured alveolar-capillary membranes of mouse lung. Circ Res. 1976;38:404-11.
32. Johnson M. 'What controls aqueous humour outflow resistance?'. Exp Eye Res. 2006;82:545-57.
33. Campbell M, Nguyen AT, Kiang AS, Tam LC, Gobbo OL, Kerskens C, Ni Dhubhghaill S, Humphries MM, Farrar GJ, Kenna PF, Humphries P. An experimental platform for systemic drug delivery to the retina. Proc Natl Acad Sci U S A. 2009;106:17817-22.
34. Sit AJ, Coloma FM, Ethier CR, Johnson M. Factors affecting the pores of the inner wall endothelium of Schlemm's canal. Invest Ophthalmol Vis Sci. 1997;38:1517-25.
35. Morita K, Sasaki H, Furuse M, Tsukita S. Endothelial claudin: claudin-5/TMVCF constitutes tight junction strands in endothelial cells. J Cell Biol. 1999;147:185-94.
36. Campbell M, Kiang AS, Kenna PF, Kerskens C, Blau C, O'Dwyer L, Tivnan A, Kelly JA, Brankin B, Farrar GJ, Humphries P. RNAi-mediated reversible opening of the blood-brain barrier. J Gene Med. 2008;10:930-47.
37. Perche O, Doly M, Ranchon-Cole I. Caspase-dependent apoptosis in light-induced retinal degeneration. Invest Ophthalmol Vis Sci. 2007;48:2753-9.
38. Keaney J, Walsh DM, O'Malley T, Hudson N, Crosbie DE, Loftus T, Sheehan F, McDaid J, Humphries MM, Callanan JJ, Brett FM, Farrell MA, Humphries P, Campbell M. Autoregulated paracellular clearance of amyloid-beta across the blood-brain barrier. Sci Adv. 2015;1:e1500472.
39. Whitehead AJ, Mares JA, Danis RP. Macular pigment: a review of current knowledge. Arch Ophthalmol. 2006;124:1038-45.
40. Aleman TS, Duncan JL, Bieber ML, de Castro E, Marks DA, Gardner LM, Steinberg JD, Cideciyan AV, Maguire MG, Jacobson SG. Macular pigment and lutein supplementation in retinitis pigmentosa and Usher syndrome. Invest Ophthalmol Vis Sci. 2001;42:1873-81.
41. Ma L, Dou HL, Huang YM, Lu XR, Xu XR, Qian F, Zou ZY, Pang HL, Dong PC, Xiao X, Wang X, Sun TT, Lin XM. Improvement of retinal function in early age-related macular degeneration after lutein and zeaxanthin supplementation: a randomized, double-masked, placebo-controlled trial. Am J Ophthalmol. 2012;154:625-34 e1.
42. Liu R, Wang T, Zhang B, Qin L, Wu C, Li Q, Ma L. Lutein and zeaxanthin supplementation and association with visual function in age-related macular degeneration. Invest Ophthalmol Vis Sci. 2014;56:252-8.

43. Hammond BR, Jr., Johnson EJ, Russell RM, Krinsky NI, Yeum KJ, Edwards RB, Snodderly DM. Dietary modification of human macular pigment density. Invest Ophthalmol Vis Sci. 1997;38:1795-801.
44. Johnson EJ, Hammond BR, Yeum KJ, Qin J, Wang XD, Castaneda C, Snodderly DM, Russell RM. Relation among serum and tissue concentrations of lutein and zeaxanthin and macular pigment density. Am J Clin Nutr. 2000;71:1555-62.
45. Li B, Vachali PP, Shen Z, Gorusupudi A, Nelson K, Besch BM, Bartschi A, Longo S, Mattinson T, Shihab S, Polyakov NE, Suntsova LP, Dushkin AV, Bernstein PS. Retinal accumulation of zeaxanthin, lutein, and beta-carotene in mice deficient in carotenoid cleavage enzymes. Exp Eye Res. 2017;159:123-31.
46. Hayreh SS. Ischemic optic neuropathies - where are we now? Graefes Arch Clin Exp Ophthalmol. 2013;251:1873-84.
47. Hayreh SS. Ocular vascular occlusive disorders: natural history of visual outcome. Prog Retin Eye Res. 2014;41:1-25.
48. Gerth C, Zawadzki RJ, Werner JS, Heon E. Retinal morphological changes of patients with X-linked retinoschisis evaluated by Fourier-domain optical coherence tomography. Arch Ophthalmol. 2008;126:807-11.
49. Yu J, Ni Y, Keane PA, Jiang C, Wang W, Xu G. Foveomacular schisis in juvenile X-linked retinoschisis: an optical coherence tomography study. Am J Ophthalmol. 2010;149:973-8 e2.
50. Gregori NZ, Berrocal AM, Gregori G, Murray TG, Knighton RW, Flynn HW, Jr., Dubovy S, Puliafito CA, Rosenfeld PJ. Macular spectral-domain optical coherence tomography in patients with X linked retinoschisis. Br J Ophthalmol. 2009;93:373-8.
51. Vijayasarathy C, Ziccardi L, Sieving PA. Biology of retinoschisin. Adv Exp Med Biol. 2012;723:513-8.
52. Molday RS, Kellner U, Weber BH. X-linked juvenile retinoschisis: clinical diagnosis, genetic analysis, and molecular mechanisms. Prog Retin Eye Res. 2012;31:195-212.
53. Zeng Y, Takada Y, Kjellstrom S, Hiriyanna K, Tanikawa A, Wawrousek E, Smaoui N, Caruso R, Bush RA, Sieving PA. RS-1 Gene Delivery to an Adult Rs1h Knockout Mouse Model Restores ERG b-Wave with Reversal of the Electronegative Waveform of X-Linked Retinoschisis. Invest Ophthalmol Vis Sci. 2004;45:3279-85.
54. Bush RA, Zeng Y, Colosi P, Kjellstrom S, Hiriyanna S, Vijayasarathy C, Santos M, Li J, Wu Z, Sieving PA. Preclinical Dose-Escalation Study of Intravitreal AAV-RS1 Gene Therapy in a Mouse Model of X-linked Retinoschisis: Dose-Dependent Expression and Improved Retinal Structure and Function. Hum Gene Ther. 2016;27:376-89.
55. Byrne LC, Ozturk BE, Lee T, Fortuny C, Visel M, Dalkara D, Schaffer DV, Flannery JG. Retinoschisin gene therapy in photoreceptors, Muller glia or all retinal cells in the Rs1h-/- mouse. Gene Ther. 2014;21:585-92.
56. Dalkara D, Byrne LC, Klimczak RR, Visel M, Yin L, Merigan WH, Flannery JG, Schaffer DV. In vivo-directed evolution of a new adeno-associated virus for therapeutic outer retinal gene delivery from the vitreous. Sci Transl Med. 2013;5:189ra76.

57. Zhang L, Reyes R, Lee W, Chen CL, Chan L, Sujirakul T, Chang S, Tsang SH. Rapid resolution of retinoschisis with acetazolamide. Doc Ophthalmol. 2015;131:63-70.
58. Dentchev T, Milam AH, Lee VM, Trojanowski JQ, Dunaief JL. Amyloid-beta is found in drusen from some age-related macular degeneration retinas, but not in drusen from normal retinas. Mol Vis. 2003;9:184-90.
59. Anderson DH, Talaga KC, Rivest AJ, Barron E, Hageman GS, Johnson LV. Characterization of beta amyloid assemblies in drusen: the deposits associated with aging and age-related macular degeneration. Exp Eye Res. 2004;78:243-56.
60. Johnson LV, Leitner WP, Rivest AJ, Staples MK, Radeke MJ, Anderson DH. The Alzheimer's A beta -peptide is deposited at sites of complement activation in pathologic deposits associated with aging and age-related macular degeneration. Proc Natl Acad Sci U S A. 2002;99:11830-5.
61. Ding JD, Johnson LV, Herrmann R, Farsiu S, Smith SG, Groelle M, Mace BE, Sullivan P, Jamison JA, Kelly U, Harrabi O, Bollini SS, Dilley J, Kobayashi D, Kuang B, Li W, Pons J, Lin JC, Bowes Rickman C. Anti-amyloid therapy protects against retinal pigmented epithelium damage and vision loss in a model of age-related macular degeneration. Proc Natl Acad Sci U S A. 2011;108:E279-87.
62. Liu C, Cao L, Yang S, Xu L, Liu P, Wang F, Xu D. Subretinal injection of amyloid-beta peptide accelerates RPE cell senescence and retinal degeneration. Int J Mol Med. 2015;35:169-76.
63. Gupta V, Gupta VB, Chitranshi N, Gangoda S, Vander Wall R, Abbasi M, Golzan M, Dheer Y, Shah T, Avolio A, Chung R, Martins R, Graham S. One protein, multiple pathologies: multifaceted involvement of amyloid beta in neurodegenerative disorders of the brain and retina. Cell Mol Life Sci. 2016;73:4279-97.
64. Janciauskiene S, Krakau T. Alzheimer's peptide: a possible link between glaucoma, exfoliation syndrome and Alzheimer's disease. Acta Ophthalmol Scand. 2001;79:328-9.
65. Zode GS, Kuehn MH, Nishimura DY, Searby CC, Mohan K, Grozdanic SD, Bugge K, Anderson MG, Clark AF, Stone EM, Sheffield VC. Reduction of ER stress via a chemical chaperone prevents disease phenotypes in a mouse model of primary open angle glaucoma. J Clin Invest. 2011;121:3542-53.
66. Ott M, Gogvadze V, Orrenius S, Zhivotovsky B. Mitochondria, oxidative stress and cell death. Apoptosis. 2007;12:913-22.
67. Weismann D, Hartvigsen K, Lauer N, Bennett KL, Scholl HP, Charbel Issa P, Cano M, Brandstatter H, Tsimikas S, Skerka C, Superti-Furga G, Handa JT, Zipfel PF, Witztum JL, Binder CJ. Complement factor H binds malondialdehyde epitopes and protects from oxidative stress. Nature. 2011;478:76-81.
68. Kiang AS, Humphries MM, Campbell M, Humphries P. Antioxidant therapy for retinal disease. Adv Exp Med Biol. 2014;801:783-9.
69. Xun Z, Rivera-Sanchez S, Ayala-Pena S, Lim J, Budworth H, Skoda EM, Robbins PD, Niedernhofer LJ, Wipf P, McMurray CT. Targeting of XJB-5-131 to mitochondria suppresses oxidative DNA damage and motor decline in a mouse model of Huntington's disease. Cell Rep. 2012;2:1137-42.
70. Jane Farrar G, Carrigan M, Dockery A, Millington Ward S, Palfi A, Chadderton N, Humphries M, Kiang AS, Kenna PF, Humphries P. Toward an elucidation of the molecular genetics of inherited retinal degenerations. Hum Mol Genet. 2017.

71. Jordan SA, Farrar GJ, Kenna P, Humphries MM, Sheils DM, Kumar-Singh R, Sharp EM, Soriano N, Ayuso C, Benitez J, et al. Localization of an autosomal dominant retinitis pigmentosa gene to chromosome 7q. Nat Genet. 1993;4:54-8.
72. Kennan A, Aherne A, Palfi A, Humphries M, McKee A, Stitt A, Simpson DA, Demtroder K, Orntoft T, Ayuso C, Kenna PF, Farrar GJ, Humphries P. Identification of an IMPDH1 mutation in autosomal dominant retinitis pigmentosa (RP10) revealed following comparative microarray analysis of transcripts derived from retinas of wild-type and Rho(-/-) mice. Hum Mol Genet. 2002;11:547-57.
73. Aherne A, Kennan A, Kenna PF, McNally N, Lloyd DG, Alberts IL, Kiang AS, Humphries MM, Ayuso C, Engel PC, Gu JJ, Mitchell BS, Farrar GJ, Humphries P. On the molecular pathology of neurodegeneration in IMPDH1-based retinitis pigmentosa. Hum Mol Genet. 2004;13:641-50.
74. Buey RM, Ledesma-Amaro R, Velazquez-Campoy A, Balsera M, Chagoyen M, de Pereda JM, Revuelta JL. Guanine nucleotide binding to the Bateman domain mediates the allosteric inhibition of eukaryotic IMP dehydrogenases. Nat Commun. 2015;6:8923.
75. Johnson AA, Guziewicz KE, Lee CJ, Kalathur RC, Pulido JS, Marmorstein LY, Marmorstein AD. Bestrophin 1 and retinal disease. Prog Retin Eye Res. 2017;58:45-69.
76. Uggenti C, Briant K, Streit AK, Thomson S, Koay YH, Baines RA, Swanton E, Manson FD. Restoration of mutant bestrophin-1 expression, localisation and function in a polarised epithelial cell model. Dis Model Mech. 2016;9:1317-28.
77. Quigley HA, Broman AT. The number of people with glaucoma worldwide in 2010 and 2020. Br J Ophthalmol. 2006;90:262-7.
78. Tham YC, Li X, Wong TY, Quigley HA, Aung T, Cheng CY. Global prevalence of glaucoma and projections of glaucoma burden through 2040: a systematic review and meta-analysis. Ophthalmology. 2014;121:2081-90.
79. Actis AG, Versino E, Brogliatti B, Rolle T. Risk Factors for Primary Open Angle Glaucoma (POAG) Progression: A Study Ruled in Torino. Open Ophthalmol J. 2016;10:129-39.
80. De Groef L, Van Hove I, Dekeyster E, Stalmans I, Moons L. MMPs in the trabecular meshwork: promising targets for future glaucoma therapies? Invest Ophthalmol Vis Sci. 2013;54:7756-63.
81. Li G, Mukherjee D, Navarro I, Ashpole NE, Sherwood JM, Chang J, Overby DR, Yuan F, Gonzalez P, Kopczynski CC, Farsiu S, Stamer WD. Visualization of conventional outflow tissue responses to netarsudil in living mouse eyes. Eur J Pharmacol. 2016;787:20-31.
82. Ren R, Li G, Le TD, Kopczynski C, Stamer WD, Gong H. Netarsudil Increases Outflow Facility in Human Eyes Through Multiple Mechanisms. Invest Ophthalmol Vis Sci. 2016;57:6197-209.
83. Laties A, Rich CC, Stoltz R, Humbert V, Brickman C, McVicar W, Baumgartner RA. A Randomized Phase 1 Dose Escalation Study to Evaluate Safety, Tolerability, and Pharmacokinetics of Trabodenoson in Healthy Adult Volunteers. J Ocul Pharmacol Ther. 2016;32:548-54.
84. Myers JS, Sall KN, DuBiner H, Slomowitz N, McVicar W, Rich CC, Baumgartner RA. A Dose-Escalation Study to Evaluate the Safety, Tolerability, Pharmacokinetics, and Efficacy of 2 and 4 Weeks of Twice-Daily Ocular

Trabodenoson in Adults with Ocular Hypertension or Primary Open-Angle Glaucoma. J Ocul Pharmacol Ther. 2016;32:555-62.
85. Ethier CR, Read AT, Chan DW. Effects of latrunculin-B on outflow facility and trabecular meshwork structure in human eyes. Invest Ophthalmol Vis Sci. 2006;47:1991-8.
86. Kalouche G, Beguier F, Bakria M, Melik-Parsadaniantz S, Leriche C, Debeir T, Rostene W, Baudouin C, Vige X. Activation of Prostaglandin FP and EP2 Receptors Differently Modulates Myofibroblast Transition in a Model of Adult Primary Human Trabecular Meshwork Cells. Invest Ophthalmol Vis Sci. 2016;57:1816-25.
87. Spiga MG, Borras T. Development of a gene therapy virus with a glucocorticoid-inducible MMP1 for the treatment of steroid glaucoma. Invest Ophthalmol Vis Sci. 2010;51:3029-41.
88. Gerometta R, Spiga MG, Borras T, Candia OA. Treatment of sheep steroid-induced ocular hypertension with a glucocorticoid-inducible MMP1 gene therapy virus. Invest Ophthalmol Vis Sci. 2010;51:3042-8.
89. Borras T, Buie LK, Spiga MG. Inducible scAAV2.GRE.MMP1 lowers IOP long-term in a large animal model for steroid-induced glaucoma gene therapy. Gene Ther. 2016;23:438-49.
90. O'Callaghan J, Crosbie DE, Cassidy PS, Sherwood JM, Flugel-Koch C, Lutjen-Drecoll E, Humphries MM, Reina-Torres E, Wallace D, Kiang AS, Campbell M, Stamer WD, Overby DR, O'Brien C, Tam LCS, Humphries P. Therapeutic potential of AAV-mediated MMP-3 secretion from corneal endothelium in treating glaucoma. Hum Mol Genet. 2017;26:1230-46.
91. Martinez T, Gonzalez MV, Roehl I, Wright N, Paneda C, Jimenez AI. In vitro and in vivo efficacy of SYL040012, a novel siRNA compound for treatment of glaucoma. Mol Ther. 2014;22:81-91.
92. Moreno-Montanes J, Sadaba B, Ruz V, Gomez-Guiu A, Zarranz J, Gonzalez MV, Paneda C, Jimenez AI. Phase I clinical trial of SYL040012, a small interfering RNA targeting beta-adrenergic receptor 2, for lowering intraocular pressure. Mol Ther. 2014;22:226-32.
93. Buie LK, Rasmussen CA, Porterfield EC, Ramgolam VS, Choi VW, Markovic-Plese S, Samulski RJ, Kaufman PL, Borras T. Self-complementary AAV virus (scAAV) safe and long-term gene transfer in the trabecular meshwork of living rats and monkeys. Invest Ophthalmol Vis Sci. 2010;51:236-48.

Figure Legends

Figure 1: Aqueous humour is secreted by the ciliary body and moves through the pupil, around the iris. A pressure gradient directs it toward the SC lumen, where most aqueous egresses (red arrow). This is termed the conventional pathway (C). The unconventional pathway (UC) involves the removal of aqueous through the fibres of the ciliary body into the supraciliary and suprachoroidal spaces.

Figure 2: a) Structure of the neurovascular unit of the inner blood retina barrier (iBRB) comprising endothelial cells (EC), pericytes (P) and atrocyte foot processes (A). The contacting point of an iBRB EC is where the tight junction (TJ) is formed. Neurons (N) and microglia (M) are located on the retina aspect of the iBRB. **b)** Schlemm's canal endothelial cells contain TJs but also manifest giant vacuoles to allow for aqueous humour movement (see arrows for directionality of flow) into Schlemm's canal via the trabecular meshwork (TM).

Figure 3: a) Molecular architecture of the Schlemm's canal endothelial cells shows an enrichment of claudin-11 and claudin-12 at the tight junction. **b)** Tight junctions of endothelial cells associated with the inner blood retina barrier (iBRB) show an enrichment of claudin-5 and occludin at the tight junction.

Figure 4: Extravasation of Hoechst H33342 from the retinal microvessels was manifested by distinct staining of nuclei in the inner nuclear layer (INL) and outer nuclear layer (ONL) 48 hours post delivery of claudin-5 siRNA when compared to control groups.

Figure 5: (a) Albino BalB/c mice were inoculated sub-retinally with either the NT AAV-2/9 in their left eye or the CLDN5 AAV-2/9 in their right eye. Significant protection of photoreceptor cells was observed in the right eyes (CLDN5 AAV-2/9) of mice compared to the left eyes (NT AAV-2/9) (***P = 0.0006). (b) TUNEL positive cells were shown to be consistently localized in large numbers to the outer nuclear layer (ONL) of NT AAV-2/9 injected retinas compared to CLDN5 AAV-2/9 injected retinas. Outer plexiform layer (OPL), inner nuclear layer (INL), inner plexiform layer (IPL), ganglion cell layer (GCL). (c) Extensive cleavage of the calpain substrate α-fodrin was observed in mice receiving the NT AAV compared to mice receiving the CLDN5 AAV with ALLM prior to light ablation.

Figure 6: (a) Albino BalB/c mice were inoculated sub-retinally with either the NT AAV-2/9 in their left eye or the CLDN5 AAV-2/9 in their right eye. Significant protection of photoreceptor cells was observed in the right eyes (CLDN5 AAV-2/9) of mice compared to the left eyes (NT AAV-2/9) (***P = 0.0006). (b) TUNEL positive cells were shown to be consistently localised in large numbers to the outer nuclear layer (ONL) of NT AAV-2/9 injected retinas compared to CLDN5 AAV-2/9 injected retinas. Outer plexiform layer (OPL), inner nuclear layer (INL), inner plexiform layer (IPL), ganglion cell layer (GCL). (c) Extensive cleavage of the calpain substrate α-fodrin was observed in mice receiving the NT AAV compared to mice receiving the CLDN5 AAV with ALLM prior to light ablation.

Figure 7: Three-Dimensional volumetric rendering of MRI data showed lesion volume in red (pseudocolor) with NT siRNA injected mice in the left column and

claudin-5 siRNA injected mice in the right column. **a)** NT siRNA and claudin-5 siRNA 24 h post injury. **b)** 48 h post injury**. c)** 72 h post injury.

Figure 8: **a)** and **b)** Optical coherence tomography (OCT) analysis of X-linked retinoschisis. **c)** and **d)** OCT analysis of non-arteritic ischemic optic neuropathy (NAION)

Figure 9: Claudin-5 suppression in the vasculature associated with the optic nerve head in african green monkeys 48 hours post injection of claudin-5 siRNA

Figure 10: Aβ in retinas of 8-month old siRNA-treated DBA/2J mice. **a)** Aβ immunostaining in the ganglion cell layer of wild-type (WT) and DBA/2J mouse retinas (ONL: outer nuclear layer, INL: inner nuclear layer, GCL: ganglion cell layer. Scale bar = 50 μm). **b)** Western blot analysis of claudin-5 and occludin in retinas of DBA/2J mice following systemic administration of non-targeting (NT) or claudin-5 and occludin (C/O) siRNAs. **c)** Retina/plasma ratios of Aβ(1-40) (pg/g soluble retina Aβ(1-40) to pg/ml plasma Aβ(1-40)) in DBA/2J mice after a single round of siRNA administration (unpaired Student's *t*-test, n = 12 animals per experimental group, **P* = 0.045. Data are means ± s.e.m.).

Figure 11: Preserved outer nuclear layer (ONL) in a patient with the RP10 form of retinitis pigmentosa.

Figure 12: Representative sagittal sections through the inner wall of Schlemm's canal (SC) and outer trabecular meshwork (TM) of a mouse eye treated with **(a)** non-targeting (NT) or **(b)** targeting (T) siRNA illustrating intact cells and an intact and continuous inner wall endothelium that appeared similar in both cases. The inner wall endothelium is connected to the underlying ECM so that no ballooning was visible. (**c**, **d**) High magnifications of sagittal sections through intercellular clefts along the inner wall endothelium of SC showing examples for junctions quantitatively evaluated as closed **(c)** with fusion between the neighbouring cell membranes (arrows) or open clefts **(d)** where the cell membranes of adjacent endothelial cells were clearly separated along the entire cleft length (white arrowheads). Despite the open clefts, adhesions to sub-endothelial matrix (black arrowheads) were preserved.

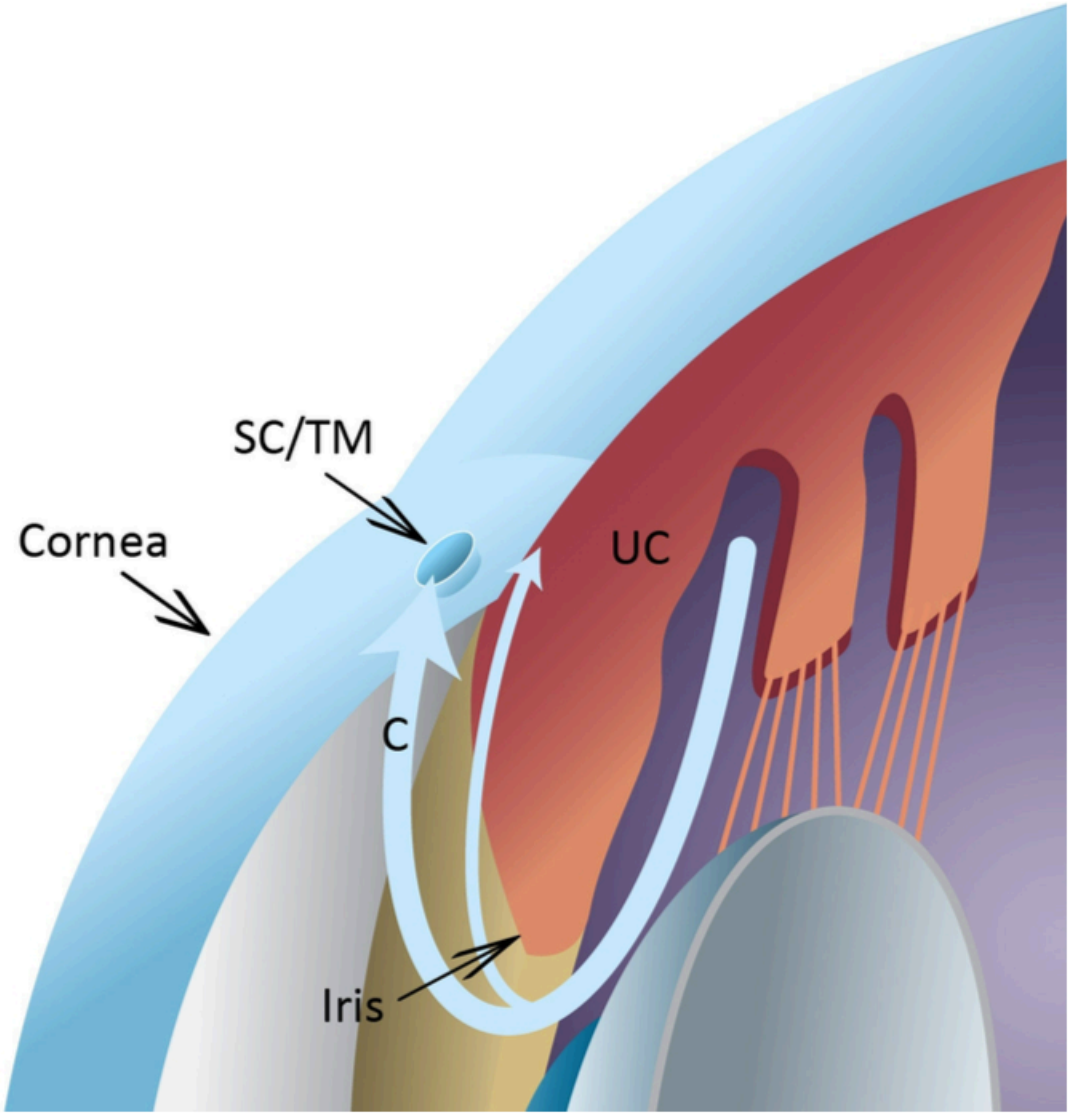
SC/TM
Cornea
UC
C
Iris

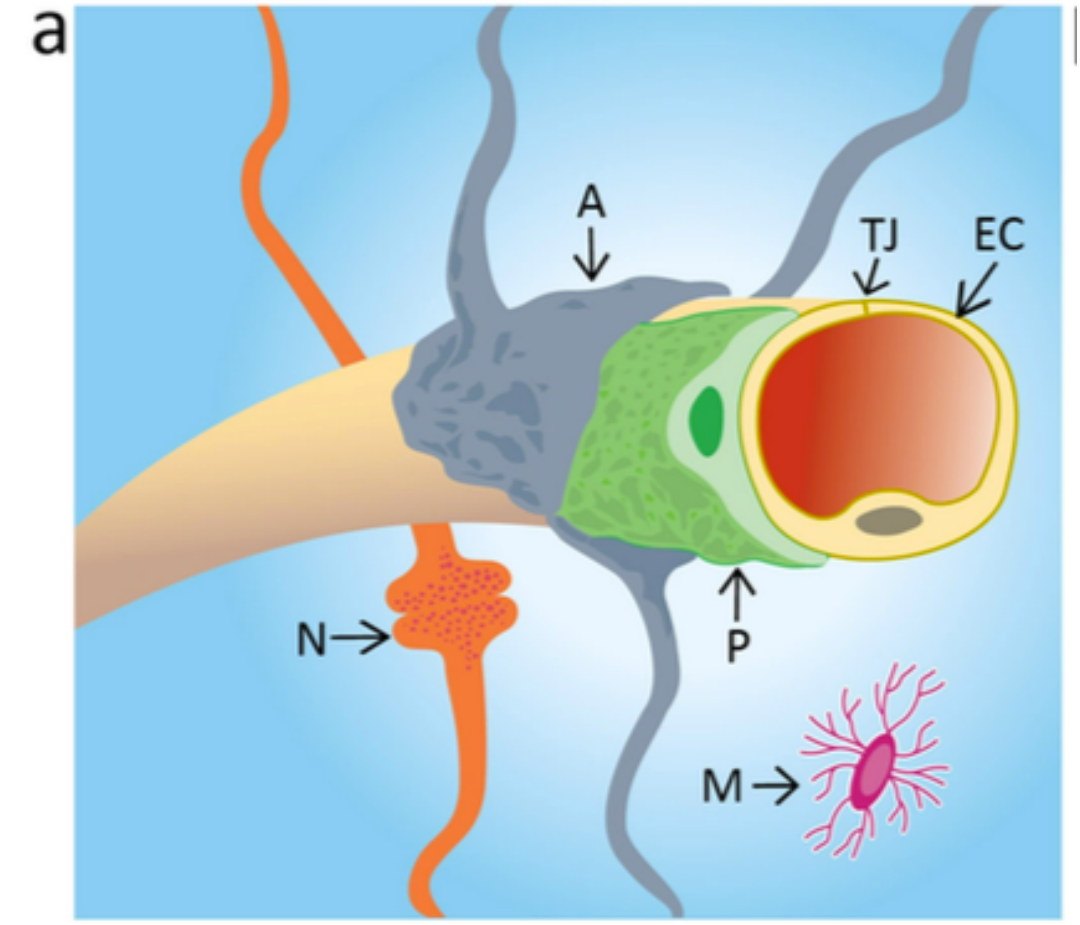
a
A
TJ
EC
N
P
M

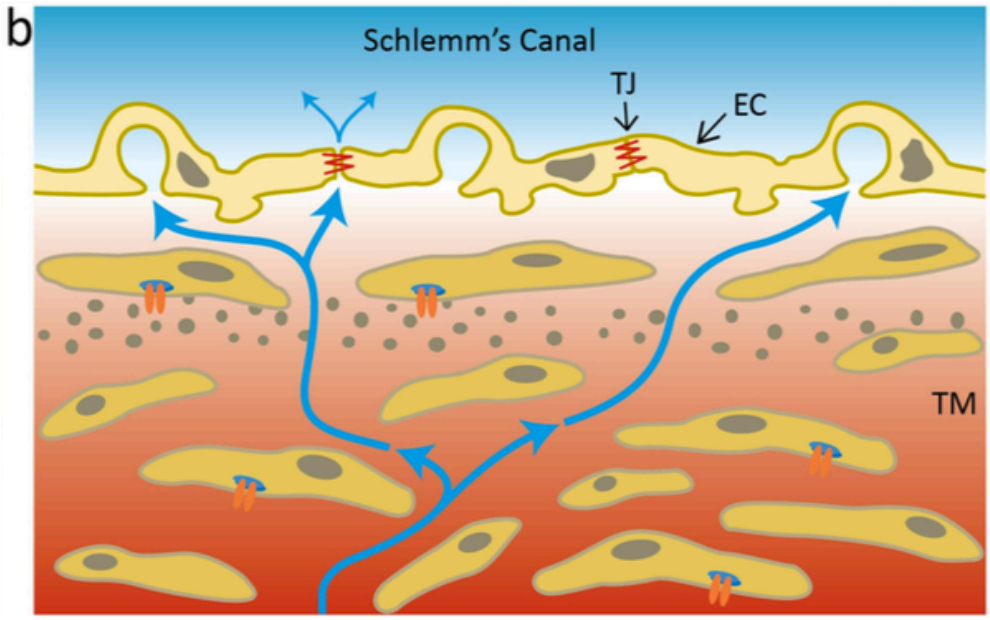
b
Schlemm's Canal
TJ
EC
TM

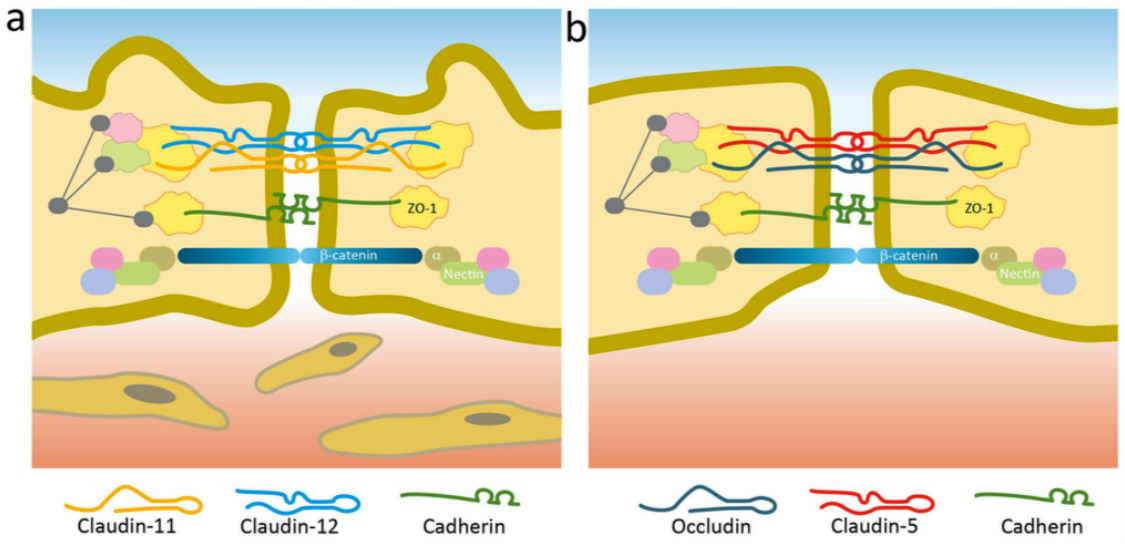
a
b
ZO-1
β-catenin
α
Nectin
Claudin-11
Claudin-12
Cadherin
Occludin
Claudin-5
Cadherin

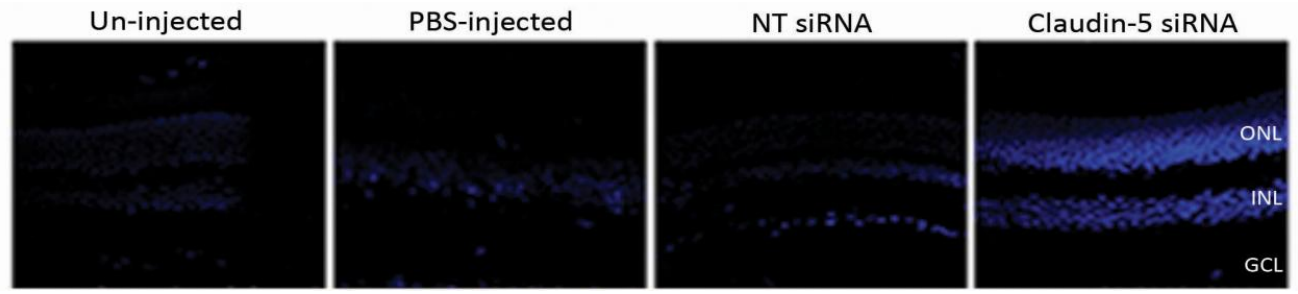
Un-injected
PBS-injected
NT siRNA
Claudin-5 siRNA
ONL
INL
GCL

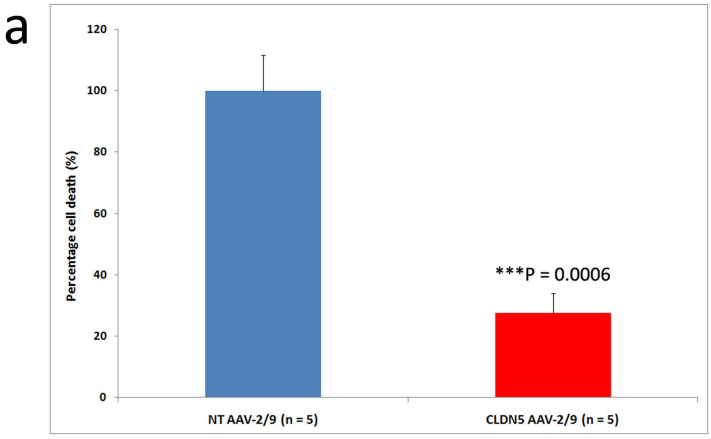
a
Percentage cell death (%)
120
100
80
60
40
20
0
***P = 0.0006
NT AAV-2/9 (n = 5)
CLDN5 AAV-2/9 (n = 5)

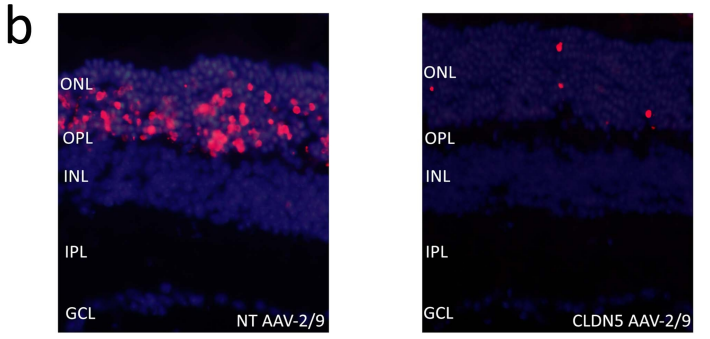
b
ONL
OPL
INL
IPL
GCL
NT AAV-2/9
ONL
OPL
INL
IPL
GCL
CLDN5 AAV-2/9

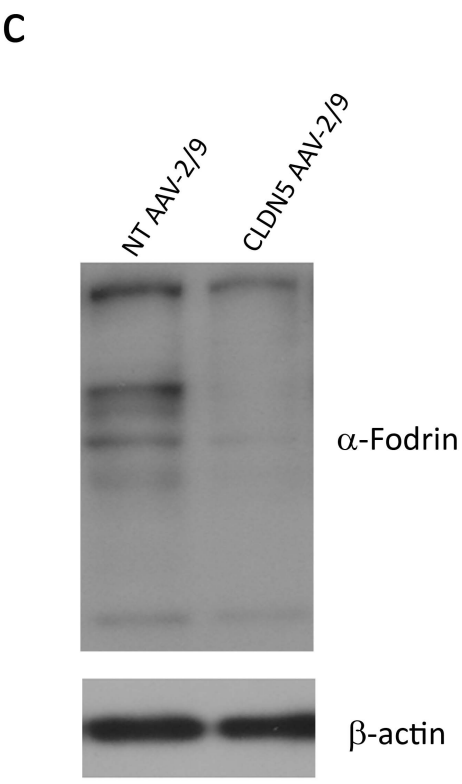
c
NT AAV-2/9
CLDN5 AAV-2/9
α-Fodrin
β-actin

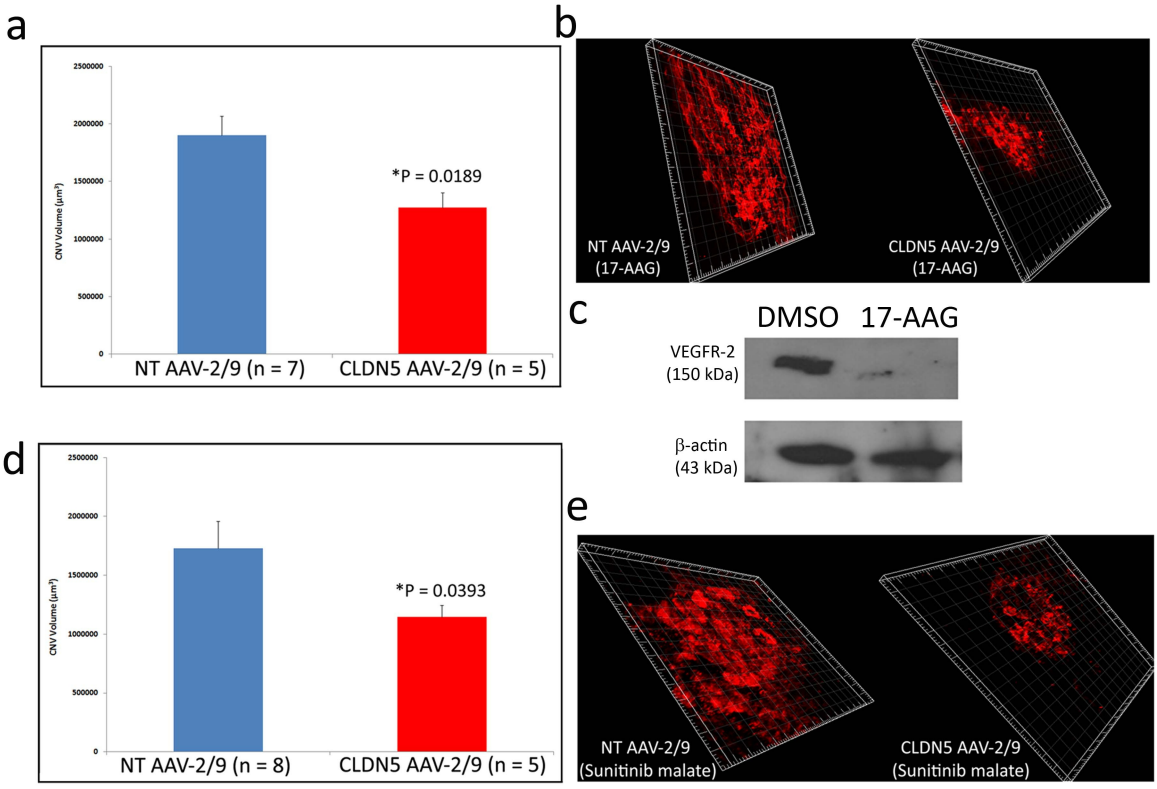
a
2500000
2000000
1500000
1000000
500000
0
CNV Volume (μm³)
*P = 0.0189
NT AAV-2/9 (n = 7)
CLDN5 AAV-2/9 (n = 5)
b
NT AAV-2/9
(17-AAG)
CLDN5 AAV-2/9
(17-AAG)
c
DMSO
17-AAG
VEGFR-2
(150 kDa)
β-actin
(43 kDa)
d
2500000
2000000
1500000
1000000
500000
0
CNV Volume (μm³)
*P = 0.0393
NT AAV-2/9 (n = 8)
CLDN5 AAV-2/9 (n = 5)
e
NT AAV-2/9
(Sunitinib malate)
CLDN5 AAV-2/9
(Sunitinib malate)

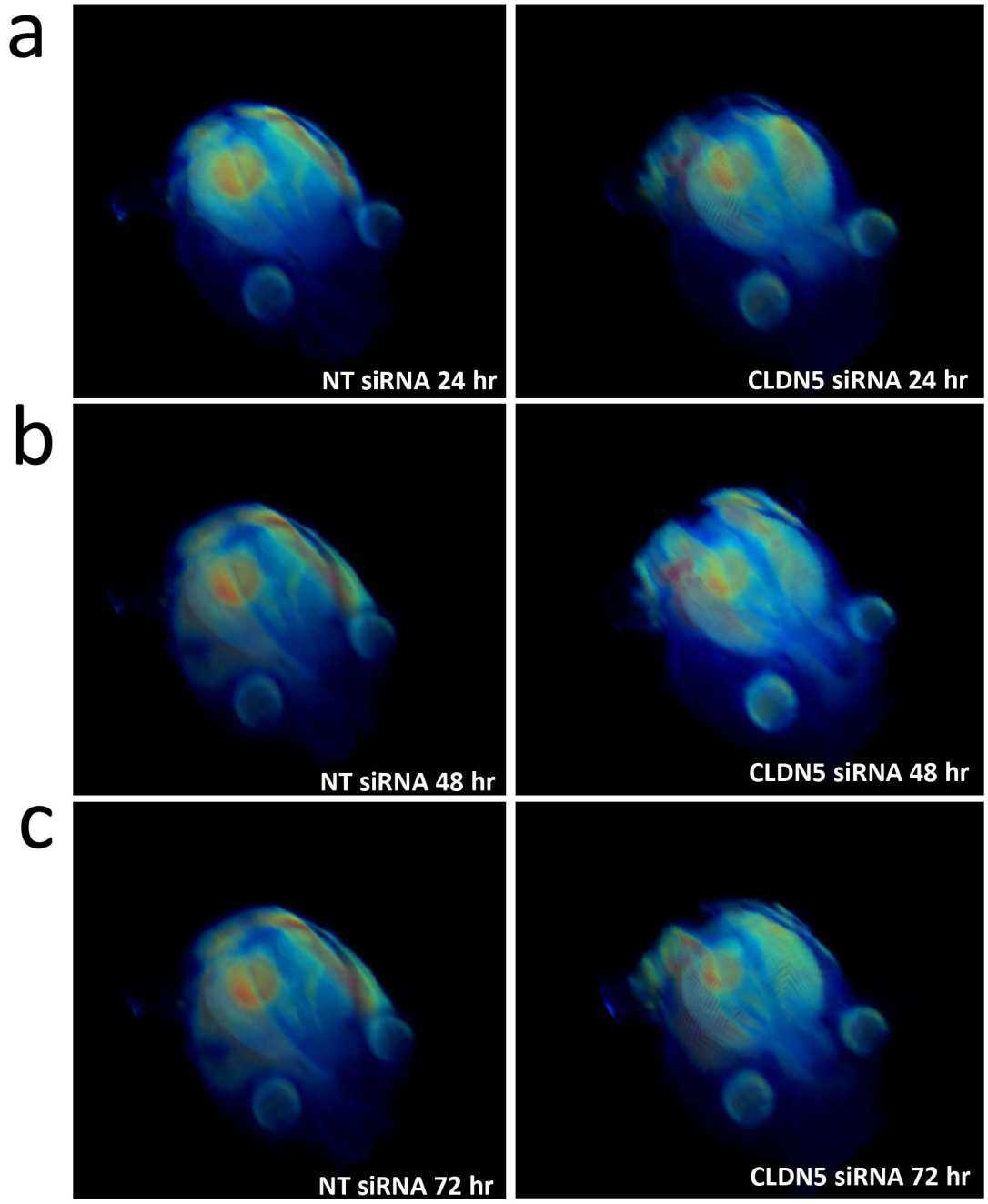
a
NT siRNA 24 hr
CLDN5 siRNA 24 hr
b
NT siRNA 48 hr
CLDN5 siRNA 48 hr
c
NT siRNA 72 hr
CLDN5 siRNA 72 hr

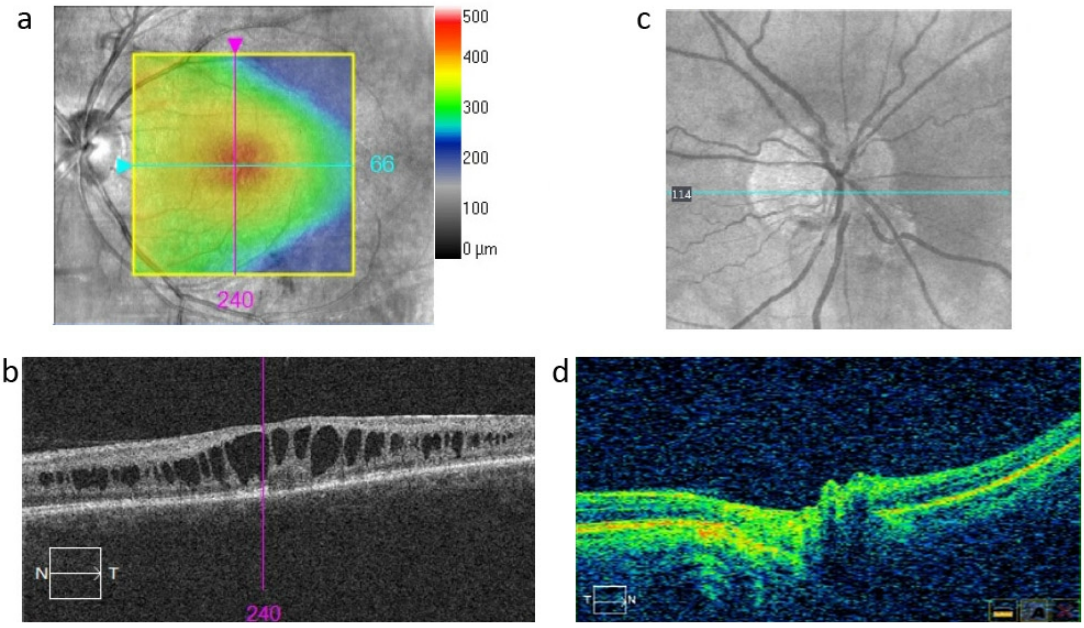
a
500
400
300
200
100
0 µm
66
240
c
114
b
N
T
240
d
T
N

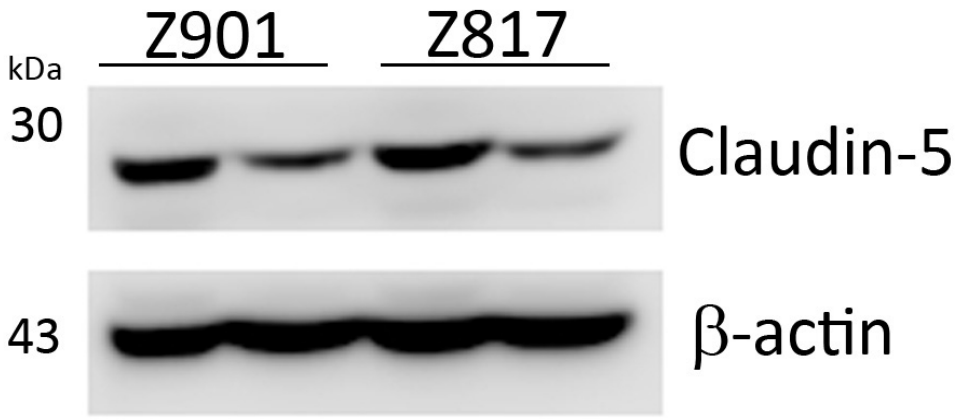
Z901
Z817
kDa
30
Claudin-5
43
β-actin

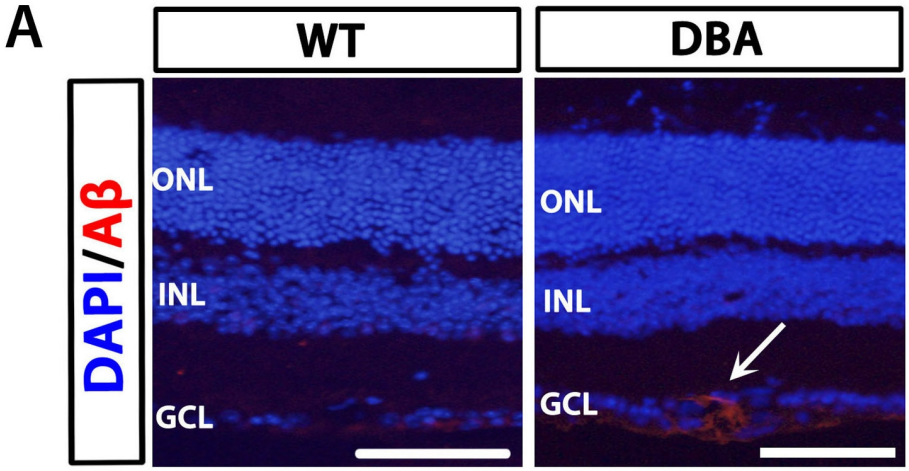
A
WT
DBA
DAPI/Aβ
ONL
INL
GCL
ONL
INL
GCL

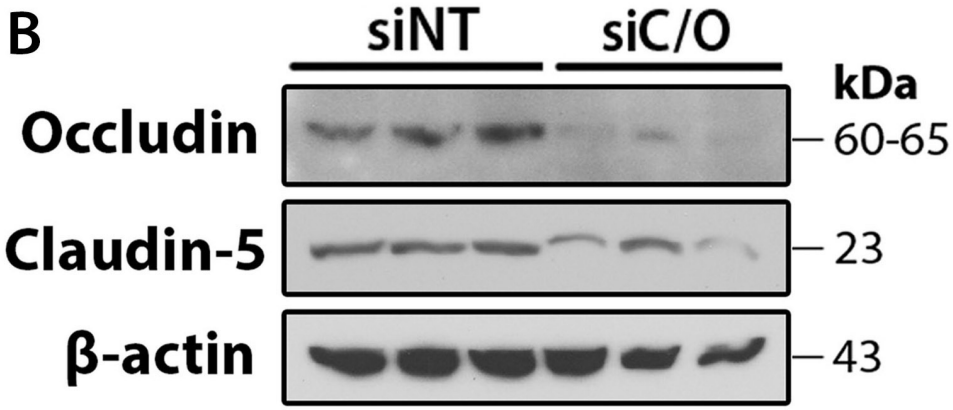
B
siNT
siC/O
kDa
Occludin
60-65
Claudin-5
23
β-actin
43

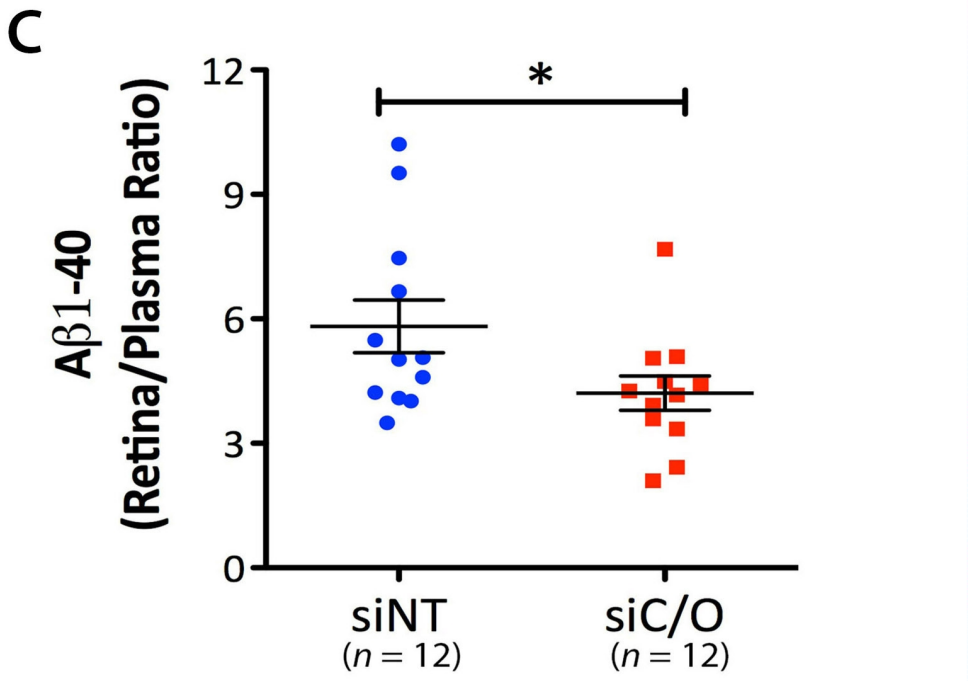
C
Aβ1-40
(Retina/Plasma Ratio)
12
9
6
3
0
*
siNT
(n = 12)
siC/O
(n = 12)

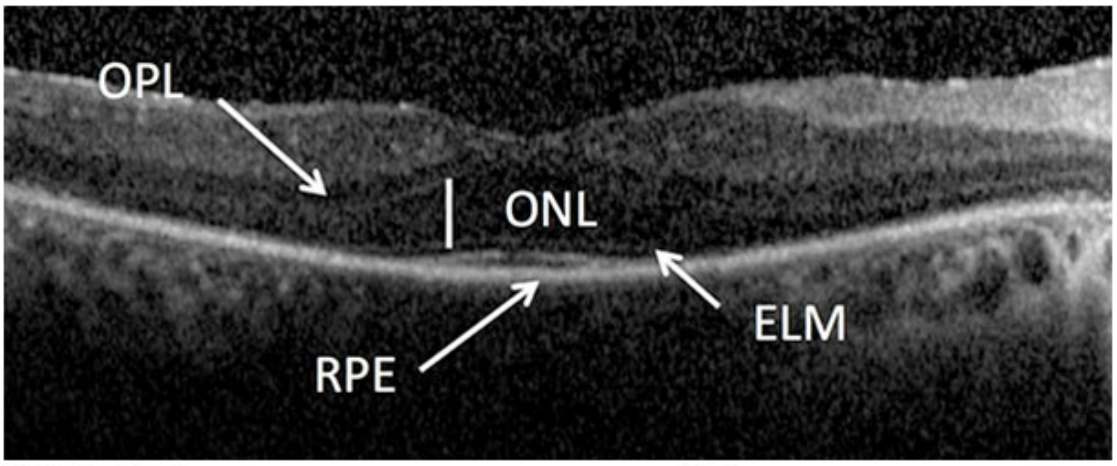
OPL
ONL
ELM
RPE

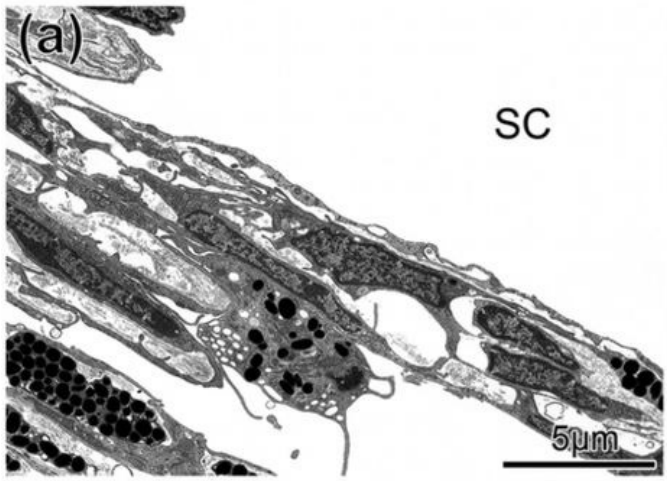
(a)
SC
5μm

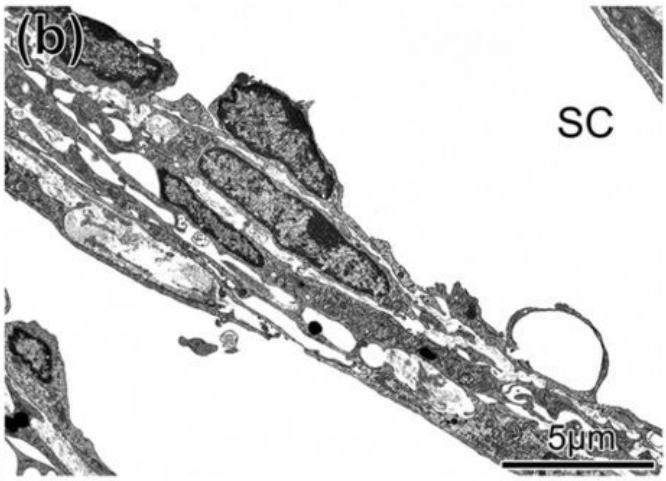
(b)
SC
5μm

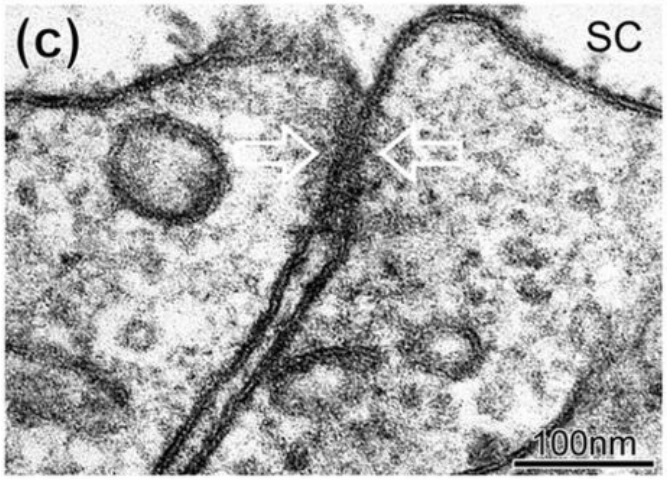
(c)
SC
100nm

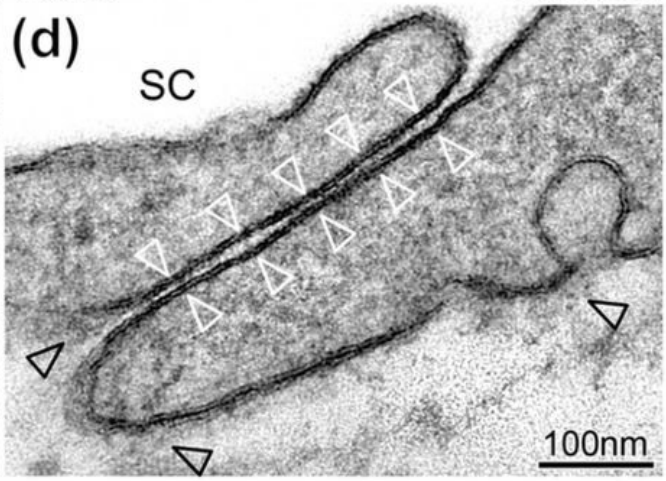
(d)
SC
100nm

Open-angle Glaucoma: Therapeutically Targeting the Extracellular Matrix of the Conventional Outflow Pathway

Jeffrey O'Callaghan[1], BA, Paul S. Cassidy[1], BA, and Pete Humphries[1], PhD

[1]Ocular Genetics Unit, Smurfit Institute of Genetics, University of Dublin, Trinity College, Dublin, D2, Ireland

To whom correspondence should be addressed: Tel: 353 1 896 2164, 353 1 896 1547; E-mail: ocallaje@tcd.ie, pete.humphries@tcd.ie

ORCiD for Jeffrey O'Callaghan: orcid.org/0000-0001-8818-4331

ORCiD for Paul S. Cassidy: orcid.org/0000-0003-1454-0318

Open-angle Glaucoma: Therapeutically Targeting the Extracellular Matrix of the Conventional Outflow Pathway

Abstract

Introduction:

Ocular hypertension in open-angle glaucoma is caused by a reduced rate of removal of aqueous humour (AH) from the eye, with the majority of AH draining from the anterior chamber through the conventional outflow pathway, comprising the trabecular meshwork (TM) and Schlemm's Canal. Resistance to outflow is generated, in part, by the extracellular matrix (ECM) of the outflow tissues. Current pressure-lowering topical medications largely suppress AH production, or enhance its clearance through the unconventional pathway. However, therapies targeting the ECM of the conventional pathway in order to decrease intraocular pressure have become a recent focus of attention.

Areas covered:

We discuss the role of ECM of the TM in outflow homeostasis and its relevance as a target for glaucoma therapy, including progress in development of topical eye formulations, together with gene therapy approaches based on inducible, virally-mediated expression of matrix metalloproteinases to enhance aqueous outflow.

Expert opinion:

There remains a need for improved glaucoma medications that more specifically act upon sites causative to glaucoma pathogenesis. Emerging strategies targeting the ECM of the conventional outflow pathway, or associated components of the cytoskeleton of TM cells, involving new pharmacological formulations or genetically-based therapies, are promising avenues of future glaucoma treatment.

1.1 Introduction

Glaucoma encompasses a range of eye disorders including pigmentary-, secondary-, and normal-tension forms of disease, however the most prevalent are primary open-angle (POAG) and primary angle-closure glaucomas (PACG). POAG represents greater than 74% of all glaucoma cases [1]. In this form, the narrow angle between the cornea and iris leading to the conventional outflow tissues remains open, while the conventional outflow tissues themselves, the trabecular meshwork (TM) and Schlemm's canal (SC), retain only partial AH drainage function. In contrast, while these outflow tissues remain functional in PACG, flow of AH through them becomes physically blocked by the apposition of the iris against the cornea, often due to deformity of the iris. Thus, in both forms of disease, AH drainage becomes restricted, leading to increased intraocular pressure (IOP). Ocular hypertension is recognised as the major disease risk factor for vision loss in glaucoma, along with age, lifestyle, and gender [2, 3]. As a result of elevations in IOP, the optic nerve head degenerates, visibly recognisable as receding, or 'cupping', of the optic disc. This in turn places stress on the axons

of the ganglion cells of the retina, ultimately resulting in a progressive loss of the visual fields. The disease, if left untreated, often leads to a complete loss of vision.

Glaucoma, in its various forms, is one of the most common causes of visual handicap in the world, rivalling cataract and infection. Glaucoma currently affects an estimated 70 million people, with projections showing an increase to 76-79 million people in 2020 and nearly 120 million by 2040 [1, 3]. Worldwide, approximately 10% of those suffering from glaucoma are bilaterally blind [1, 4], with fewer than 50% of patients in developed countries being aware of having the disease until visual fields become significantly reduced [5].

1.2 Genes associated with POAG

POAG is a classically multifactorial disease in that, while there are familial tendencies, the vast majority of cases are of adult onset and are not inherited in a Mendelian sense. However, rare hereditary forms of disease do exist that segregate in families in an autosomal dominant fashion, and through genetic linkage studies, genes involved in such forms of disease were localised and characterised. Recent association studies have also highlighted an array of genes with moderate correlation to POAG [6].

The first gene to be identified through genetic linkage encoded a TM glucocorticoid response protein (TIGR), now known as myocilin. Most ocular tissues produce myocilin, but it is only secreted by some, including the TM [7, 8]. Myocilin interacts with ECM components including fibronectin, laminin and decorin [9, 10], however the function of such interactions remain unknown. Current evidence suggests that mutant myocilin protein misfolds and aggregates in cells of the TM, rather than being secreted [11], leading to endoplasmic reticulum (ER) stress and dysfunction of TM cells. In TM cells expressing a dominant human Myocilin (Tyr437His) mutation there is an intracellular build-up of ECM components and a decrease in secretion of matrix metalloproteinases [12]. Transgenic animals expressing this mutation exhibit elevated IOP and reduced outflow facility, characteristic of glaucoma [12, 13].

The second gene to be mapped in POAG using genetic linkage studies encoded Optic neuropathy-inducing protein, or optineurin. The gene is expressed in the TM, non-pigmented ciliary epithelium, retina, brain and in other tissues [14]. Optineurin may play a neuroprotective role against TNF-α mediated cytolysis, and translocates to the membrane in response to oxidative stress [14, 15, 16]. Most commonly associated with normal tension glaucoma, optineurin mutations have also been linked to POAG [17]. Together, mutations within the optineurin and myocilin genes have been encountered in up to 5% of adult-onset cases of POAG [18].

In regard to adult-onset disease, genome-wide association studies (GWAS) have implicated caveolins CAV1 and CAV2 in POAG. These proteins appear to affect the organization of collagen matrix fibres in lung tissue [19, 20] and fibronectin, collagens and α-SMA in murine mammary tumours [21], all of which are perturbed during fibrosis. Reduced expression of caveolins in glaucomatous tissues may be indicative of a pathological role for caveolins in

POAG, such as their role in suppressing TGF-β2 transcription, a known inducer of ECM expression [22, 23]. Interestingly, it has recently been shown that lack of caveolae in the TM of mice results in ocular hypertension, with cells of the outflow tissues having a greater susceptibility to rupture through mechanical stress, indicating a possible genetic and functional link to glaucoma [24]. GWAS have resulted in the elucidation of additional glaucomatous or IOP-related susceptibility loci. Primary candidate genes related to both IOP and POAG include TMCO1, ABCA1 and GAS7 [25, 26, 27]. Their contributions to the pathogenesis of glaucoma are still unclear, however basic functionalities have been established. TMCO1 encodes a transmembrane protein that functions as a calcium channel in response to excess calcium levels in the endoplasmic reticulum [28]. ABCA1 belongs to a family of transporters and functions as a cholesterol efflux pump, and GAS7 may promote maturation and differentiation of neurons. Proteins encoded by these genes have been shown to be expressed in human ocular tissues [27].

While some of these high-penetrance glaucoma-causing genes are known to encode proteins that interact with ECM components, no genetic variants in ECM genes have as yet been significantly linked to POAG. There are, however, several genetic variants within the collagen genes that are significantly associated with glaucomatous endophenotypes such as maximum vertical cup-disc ratio, increased optic disc cup area and altered central corneal thickness [29, 30, 31, 32]. Other mutations within fibrillin 1, latent-transforming growth factor beta-binding protein 2 and versican genes have been associated with glaucoma in humans [33, 34, 35, 36, 37]. These proteins constitute large ECM fibrils that have roles in cell adhesion within the matrix. Mutations in genes involved in the remodelling of the ECM, such as the ADAMTS proteins, members of the matrix metalloproteinase (MMP) family, are associated with increased vertical cup-disc ratio and reduced central corneal thickness [29, 31, 38]. Collectively, these data support the concept that genetic variations affecting ECM homeostasis may be related to the development of glaucomatous endophenotypes.

2. The ECM as a therapeutic target

2.1 ECM composition within the outflow tissues

The ECM of the conventional outflow tissues not only provides structural support, but is also involved in the regulation of a variety of cellular processes and functions. ECM within this region is comprised of a heterogenous group of fibrous and matrical materials, including proteoglycans, collagens, fibronectin, laminin, elastin and others, all of which contribute to its dynamic and complex function. The juxtacanalicular (JCT) region, adjoining the inner-most layer of the TM and the inner wall of the SC comprises cells resting on a basement membrane, surrounded by an amorphous ECM dispersed with open spaces, allowing aqueous egress [39, 40]. The SC itself is a unique vessel in that it incorporates both blood and lymphatic endothelial cell phenotypes [41]. It is a continuous endothelial layer on a discontinuous basement membrane that facilitates flow in the basal to apical direction, differing from other vessels [42]. It is also distinct from other vessels in its ability to form giant vacuoles under high

pressure and its unique tight junction profile including claudin-11 [43]. These features have allowed for new therapeutic opportunities to arise, such as the use of the VEGF family in outflow facility modulation [44, 45]. The basement membrane is a fibrous layer of ECM material separating the endothelium from underlying connective tissues. It is discontinuous around the canal circumference tethering SC cells against large pressure gradients. As with other vascular endothelia, the basement membrane incorporates a lattice of collagen IV and laminin-511 along with collagen I, dystroglycans and other laminin chains. Although these components are found throughout the ECM of the JCT, they are critical to basement function, in particular, the heterotrimer of laminin subunits with arms containing binding sites for SC cell surface receptors, integrins and proteoglycans [46]. Co-localisation studies show an overlap of laminin-511 and the integrin α6, expressed at the SC endothelial periphery and not the TM, indicating that this focal adhesion complex is involved in basement membrane-endothelial adhesion [47].

The ECM is formed by complex proteinaceous meshworks in the extracellular spaces throughout the JCT, which are regularly remodelled to retain porosity. Collagen fibers are irregularly orientated within the matrix of the JCT, which may provide an explanation as to why JCT cells are stationary while other cells in regularly orientated collagen matrices are migratory [39]. Fibronectin is a major ECM component, with the protein organising into interwoven repeating chains that form extensible fibrils involved in the contractility of the TM in response to IOP. Alternative splicing of fibronectin occurs in the TM, and POAG patients are more likely to express key exons that promote assembly of fibronectin matrices which may decrease outflow facility [48]. Elastin is one of the core elements of the JCT, with elastin fibres forming the cribriform plexus, which runs tangential to the inner wall endothelium joining the basement material of the SC with the ciliary muscles. Elastin and its associated proteins react to muscle tension and thus induce widening or contraction of the SC lumen [49]. The binding of ECM to cell membranes is facilitated by integrin-ECM interactions at sites referred to as focal adhesions [50]. Transmembrane integrin subunits interact with the Arg-Gly-Asp domains of ECM proteins, while the cytoplasmic domain connects to actin-binding proteins [51, 52, 53]. Interaction between these proteins and the actin cytoskeleton reflect the importance of focal adhesions in regulating cellular function and response to environmental cues. In conjunction with integrins, inter-endothelial junctions maintain endothelial cell-cell adhesion, regulating paracellular transport channels. These features are summarised in Figure 1.

The TM expresses MMP-2, tenascin-C and α-SMA at consistently high levels, normally only expressed highly in cells undergoing remodelling, suggesting a constant remodelling process at the TM to maintain open flow channels [46]. TGF-β2 is a cytokine with an important regulatory role at the TM, inducing the expression of collagens, α-SMA, fibronectin, PAI-1 among others. TGF-β2 signalling is mediated by elastic microfibrils, specifically the fibrillin component that confers ECM elasticity, which is critical to sequestration and activation of TGF-β2 complexes [54]. Induction of ECM cross-linking by TGF-β2 bears similarities to the cross linking observed in glaucomatous tissues, and may be a contributing factor to disease

pathogenesis. Matricellular proteins are those described as non-structural glycoproteins enabling communication between the cell and the surrounding ECM such as CTGF, SPARC, tenascin-C, thrombospondin and others. These proteins are upregulated in response to TGF-β signalling, the levels of which are upregulated in POAG AH, and are associated with fibrosis and ECM deposition [55].

The ECM of glaucomatous tissues bears similarities to fibrotic tissue, in particular, excessive accumulation of ECM components such as α-SMA, progressing to a hardening or scarring of connective tissues [56, 57]. The ECM at the glaucomatous JCT displays some hallmarks of fibrosis in the form of sheath-derived plaques, i.e. an increase in elastic fibril sheath size due to increased adherence of fibrils and other ECM components to the sheath, particularly in the ageing TM [39, 58].

2.2 ECM in outflow resistance

AH secreted from the ciliary body moves from the posterior chamber through the pupil and into the anterior chamber. From here it crosses the TM, its movement being facilitated by a pressure gradient, and is then directed towards the SC lumen. This pathway, known as the conventional outflow pathway, accounts for up to 90% of human aqueous drainage, especially in the elderly [59, 60, 61]. AH can also leave the eye through the unconventional pathway, where it flows between the ciliary muscle bundles into the supraciliary and suprachoroidal space (Figure 2). AH enters the SC either transcellularly, through pores in giant vacuoles formed in the endothelial cells lining the inner wall of the canal, or paracellularly, through the spaces between SC cells regulated by the inter-endothelial junctions [62, 63, 64]. AH then exits the lumen through collector channels into aqueous veins that discharge into the episcleral venous circulation. At lower IOP, the cross sectional area of the SC lumen is too large to generate any significant outflow resistance. While canal collapse is seen to occur at high IOP, the resistance increase generated by lumen narrowing is not nearly as high as that observed in glaucomatous eyes. This indicates that although canal collapse could worsen the glaucomatous condition, it cannot be causative of it [65]. Regions of high flow are concentrated at collector channels, however as is the case with the SC lumen, collector channels should not contribute significantly to resistance as their relatively large diameters suggests that resistance is again negligible [66, 67]. After trabeculotomy 25% of outflow resistance remains, implicating the collector channels, however such remaining resistance is not thought to be relevant to glaucoma as trabeculotomy also eliminates the elevated resistance observed in glaucoma [68, 69]. This indicates that in glaucoma, the site of increased outflow resistance lies proximal to the collector channels, ruling out distal outflow pathway tissues as potential therapeutic targets [65, 68, 70]. It is generally accepted that the majority of outflow resistance is generated at the JCT [42, 66], in particular, at the ECM of the JCT [34, 71, 72, 73]. Porous spaces within the ECM of this region allow AH to reach the endothelial lining of SC, however proteoglycans, glycosaminoglycans and other large ECM constituents can fill these spaces further increasing resistance to AH outflow [42, 74, 75, 76, 77]. Obstruction of AH flow through ECM components reducing ECM porosity is more likely in

aged and glaucomatous tissue [75]. AH funnels from the full expanse of the TM/JCT to discrete pores in SC endothelium, leading to generation of outflow resistance through a bottleneck effect. As ECM accumulates, the extracellular space close to SCEC becomes more tortuous, leading to increased outflow resistance [42]. The effect that this ECM has on outflow resistance alone is difficult to measure, however recent developments in measuring and modelling of perfusion data may lead to more accurate estimations of outflow facility [78].

In general, changes in ECM composition and turnover in the TM play an important role in outflow resistance, including dynamic reactions to environmental cues, such as mechanosensation of IOP [46, 79].

2.3 Modulation of ECM turnover

Homeostatic ECM turnover plays an important role in the regulation of outflow resistance, turnover being triggered, for example, by stretch or distortion of TM cells, often as a result of elevated IOP [80]. JCT cells constitutively express a range of ECM proteins, with exposure to environmental stresses, synthetic agents, or laser trabeculoplasty surgeries invoking alterations in ECM gene expression profiles [81, 82, 83, 84]. High gene expression levels are a reflection of the fact that regular ECM turnover, facilitated by proteinases that target ECM components, is essential to homeostasis [82]. Homeostatic proteinases include zinc-dependant proteinases - classical matrix metalloproteinases (MMP's), adamalysins (ADAM and ADAMTS proteins), and other proteinases involved in plasminogen activation [85]. The MMP group of proteinases is secreted extracellularly in their inactive form, and require further processing for activation [86, 87]. MMPs are constitutively expressed throughout the TM, expression profiles responding to various stimuli [88, 89, 90]. Tight regulation of proteinase expression within the ECM is required for effective control of outflow resistance. To this end, tissue inhibitors of metalloproteinases (TIMPs) are expressed in a manner similar to that of MMPs, while the ratios of MMP:TIMP determine the extent of ECM modulation [58, 91]. Such ratios tend to be imbalanced in POAG [92, 93, 94, 95], and may be indicative of dysfunctional ECM turnover. MMP proteins are often upregulated in glaucomatous AH, however the activity of these proteins is reduced in comparison to cataract controls, likely reflective of MMP:TIMP imbalance [92, 96, 97, 98]. Perfusion of ocular tissues with MMPs or MMP-activating compounds results in increased outflow facility, possibly the most convincing demonstration of ECM involvement in regulating outflow resistance [99, 100, 101, 102]. Furthermore, recent studies on ECM characteristics, such as stiffness resulting from crosslinking, or caveolin-mediated matrix endocytosis, also highlight ECM influence on outflow facility [103, 104].

ADAMs proteins have a similar domain structure to those of classic MMPs and also associate with ECM proteins and integrins [105]. As a result of MMP-related proteolysis, ECM remodelling can induce changes at the sites of focal (cell-matrix) adhesions. Disruption or inhibition of integrin-ECM linkages binding cells to the ECM, or ECM receptor inhibition has been associated with increases in endothelial permeability and transendothelial transport [52,

106, 107, 108]. ECM remodelling at focal adhesions alters migration of fibres within the actin cytoskeleton, allowing F-actin and α-actin to act as indicators of ECM turnover [48, 109, 110]. It is also worthy of note that ECM proteinases affect inter-endothelial SC junctions, providing an additional avenue for modulation of outflow resistance. [43, 111, 112, 113].

Newly emerging treatments, detailed below, have a greater focus on the conventional pathway, representing the major site of outflow resistance, often with direct or indirect effects on the ECM. This more targeted approach to glaucoma treatment will hopefully allow for the development of a new class of drugs that may prove to be more efficacious in arresting disease progression.

3. Traditional topical medications in the management of glaucoma

The primary standard of care for patients with open angle glaucoma involves topically-administered eye drops, surgery, or both, with the annual cost of such interventions in the US having recently been estimated to amount to $1.9 billion, 38-52% of which is related to topical pressure reducing medications [114]. Glaucoma management involves either reducing AH production at the ciliary body, or increasing AH outflow. A recent meta-analysis has confirmed that prostaglandin analogues are the most effective in lowering IOP, a reflection of the fact that these compounds are the most commonly prescribed eye-drop [115]. Significant increases in unconventional outflow [116], and to a lesser extent, conventional outflow [117, 118], are observed with such analogues. Prostaglandins are endogenously expressed in many tissues and throughout the anterior chamber [119], such expression being influenced by bioactive molecules, laser treatments, mechanical stress, or glucocorticoids, indicating their importance in homeostasis [120]. Extensive studies have demonstrated prostaglandin-related decreases in TM cell contractility and outflow resistance of organ-cultured anterior segments [121, 122, 123]. The overall mechanisms through which prostaglandins enhance AH outflow remain to be fully elucidated, however it is widely accepted that remodelling of the ECM plays a part [124, 125, 126, 127], and it is of note that upregulation in MMP expression, through activation of prostaglandin receptors, may be involved [89, 128]. However, the unique receptor profile for each analogue may induce ECM modulation via different cascade pathways. One EP4 receptor agonist in particular has been shown to induce an increase in conventional outflow facility specifically [129]. Comparisons have been made between the effects of laser treatment and prostaglandins in SC monolayer permeability. Cells treated by laser, media conditioned from lasered cells, or prostaglandins all show a reduction in levels of tight junctions and a concomitant increase in cell conductivity [130]. Modulation of SC permeability by prostaglandins further indicates an effect on enhancement of outflow through the conventional pathway.

Second line medications include carbonic anhydrase inhibitors and ß-blockers, however the latter may have potentially dangerous off-target side effects. ß-blockers inhibit either ß1-, or both ß1- and ß2-adrenoceptors [131]. Since these receptors are abundantly expressed in the ciliary processes, this may result in an excess of noradrenaline, which may, in turn, induce

vasoconstriction and decreases in blood supply to the ciliary body, aiding in the reduction of AH production [132]. Alpha2-adrenergic receptor agonists work in a similar way, but are not often used as topical medications owing to their side effects. These agents cause an initial decrease in aqueous production, and an increase in unconventional outflow after chronic exposure, likely due to elevated prostaglandin expression [133, 134]. Carbonic anhydrase inhibitors also decrease AH production through chemical inhibition of bicarbonate formation [135].

Cholinergic drugs represent third line medications that have seen a reduction in clinical use in recent years, primarily due to the frequency with which they need to be instilled (3-4 times per day). These drugs increase conventional outflow and decrease IOP [136, 137] by inducing ciliary muscle contraction, increasing SC lumen area, in turn allowing for increased aqueous fluid transport across SC endothelial cells [138]. As previously mentioned, elastin fibres are responsible for the connection of the ciliary body to SC and associated muscle contractions. The ciliary muscles express cholinergic nerve terminals facilitating contraction, and it is presumed that the muscle is pulled back again by a recoil of the elastin net [137, 139].

It is important to emphasise that these widely-used topical medications predominantly target unconventional outflow and mostly only influence the conventional pathway by means of secondary or indirect responses. It is of interest to note however, that administration of alpha/ß-blockers, alpha1-blockers, alpha2-agonist- and prostaglandin derivatives all upregulate MMPs and downregulate TIMPs, in contrast to the effects of ß-blockers, suggesting at least some role in ECM modulation for these anti-glaucoma drugs [140].

It should be noted that for the most commonly used prostaglandin analogues, between 25 and 50% of patients are sub-optimally responsive, commonly defined as not achieving more than a 20% reduction in IOP [141, 142]. Consequently, there continues to be a need for improved treatment methods, particularly targeting the conventional pathway.

4. Emerging medications

4.1 New classes of drug

A collective objective in developing new formulations is to increase conventional outflow via targeting of the JCT or cytoskeleton of cells of the outflow tissues. Rho kinase inhibitors, marine macrolides, adenosine- and prostanoid-receptor agonists together with siRNA formulations are all currently under evaluation. Arguably, the most advanced of these are rho kinase (ROCK) inhibitors that have already been approved for use in Japan and have completed phase III trials in the US. IOP decrease in response to ROCK inhibitors is associated with enhanced outflow facility caused by expansion of the TM, JCT and episcleral veins and increases in SC cross-sectional area [143, 144]. Studies using a rho kinase inhibitor in conjunction with a norepinephrine transport inhibitor demonstrated similar results, but with the advantage of a dual mechanism of action that also decreases AH production [145]. Rho

family GTPases are seen to be elevated in glaucomatous optic nerve heads, activating effector kinases to polymerize actin fibers and regulate smooth muscle contraction [146, 147, 148, 149]. Decreases in myosin light chain phosphorylation were observed in ROCK inhibitor-treated TM tissue, suggesting that outflow enhancement was facilitated by actomyosin cytoskeletal disorganisation at the JCT/inner wall assembly [150, 151]. ROCK effectors also indirectly stabilize filamentous actin, reducing cell migration and interact with actin-binding proteins. Depolymerisation of filaments by ROCK inhibitors may further widen the empty spaces in the JCT and increase SC vacuoles, thereby increasing outflow facility [152, 153]. Similarly, Rho GTPase inhibition via expression of exoenzyme C3 transferase has been shown to disrupt actin bundles in human TM cells, correlating with increased outflow facility in primates. Focal adhesions, as visualised through vinculin staining (involved in integrin-actin binding) were distinctly reduced, as was ß-catenin, indicating a loss of intercellular junctions, reflected in the decrease in cellularity [154].

Marine macrolides, isolated from aquatic sponges, have antifungal, cytotoxic and antiproliferative properties. Interactions of these compounds with actin are similar to those of the ROCK inhibitors. Macrolides have established functions in: 1) severing polymeric actin (F-actin) and stabilising dimeric actin, disrupting the cytoskeleton (swinholide A); 2) sequestering actin monomers (G-actin) preventing their use in polymerisation, thus disrupting filament organisation as is the case with latrunculin-B; 3) competing for actin binding to induce and stabilise its polymerisation (jasplakinolide) [155, 156, 157, 158]. Macrolides have been shown to increase aqueous outflow facility in primate eyes, with the greatest focus appearing to have been placed on latrunculin-B. [155, 159, 160, 161]. Topical administration of latrunculin-B is sufficient to increase aqueous outflow facility and lower IOP [160], while in treated eyes, noticeable changes have been observed in the JCT region, including increased intercellular space and dilated SC, but with normal and intact corneoscleral regions [162]. Inter-endothelial junctions of primate SC endothelia appeared intact, although there was a loss of ordered alignment and integrity in actin filaments. Similar studies in human eyes have shown some focal SC inner wall separation from the ECM of the JCT [161]. Increased central corneal thickness and transient increase of corneal endothelium permeability was observed in one study, raising questions of safety issues in using macrolides in the anterior chamber [163]. Phase I trials have been conducted however, and have reported few clinically significant adverse effects [164].

Adenosine receptor agonists have been shown to increase conventional outflow and lower IOP, with a similar mechanism to those of cholinergic agonists. A_3 agonists reduce AH flow by inhibiting chloride ion channels in ciliary epithelial cells [165]. An A_1 agonist in phase III trials has demonstrated favourable toxicity profiles, possible neuroprotective effects, and efficacious IOP lowering [166]. Receptor activation has also been shown to induce the secretion of MMPs, particularly MMP-2, probably the cause of reduced outflow resistance [167, 168]. Increases in facility were negated by the addition of an MMP inhibitor, implicating

ECM remodelling along with cell volume shrinkage as mediators of outflow enhancement [169, 170].

Developments on prostanoid receptors have yielded agonists specific to individual receptor subtypes. Further understanding of the mechanism of action of the prostaglandin pathway has resulted in the development of drugs that include nitric oxide-donating prostaglandin F2-analogues, which strongly increase fluid drainage across both pathways. Relaxation of TM cells as a result of a reduction of actin stress fibres and vinculin localisation at focal adhesions was observed using such analogues [171]. Interest is increasing in the development of EP_2 and EP_4 receptor agonists for the treatment of POAG, with one such EP_2 agonist having been shown to reduce IOP by increasing both unconventional and conventional flow, facilitated by the relaxation of SC and by decrease in contractility and collagen deposition at the TM [172, 173, 174]. These effects are similar to those of traditional FP receptor agonists, however these, in contrast, may increase TM contractility. Furthermore, selective EP_4 agonists have also been shown to be efficacious in treatment of POAG. Both SC and TM cells express EP_4 receptors, and hypertension lowering effects are believed to be primarily localised to the conventional pathway [129, 175]. EP_4 receptors alone induce expression of early growth response factor-1, mediated by extracellular signal-regulated kinases [176], while these kinases are also known to influence MMP expression [177]. These observations illustrate the unique modes of action of prostanoid receptors, and the potential that these drugs can be tailored to have greater specificity and efficacy.

A number of siRNA therapies are in clinical trial for glaucoma, some functioning in a similar manner to that of ß-blockers, inhibiting the B2-adrenergic receptors at the ciliary body, thereby reducing AH production. Tolerability and safety profiles indicate that siRNA was only present in ocular tissues, providing a possible alternative form of therapy for patients that may have asthma or congestive heart failure where the use of traditional, nonselective beta blockers is limited [178, 179]. It is also interesting to note that a recent study in rodents using siRNA targeting the tight junctions of the SC reported increased outflow facility corresponding to additional open clefts, indicating increased paracellular transport [43].

Since patient compliance is a major issue, the development of longer-lasting medications could provide great benefit to patients. Strategies for enhanced delivery include drug re-formulation into nanocapsules or nanospheres, reducing the amount of preservatives (which may illicit side effects [180]), or modulation of solution viscosity by incorporation of polymers, collagen shields, gels or liposomes. Such engineering allows greater cell-specificity and retention of stability. Slow release implants are also in development, including those designed for sustained release of prostaglandin by an implant introduced into the eye via intracameral injection. Other devices include plugs or rings to deliver traditionally topical medications into the puntum or conjunctival fornices respectively [181, 182]. A summary of traditional and emerging formulations is provided in table 1.

4.2 On the development of genetic therapies

Adenoviral (AV), Herpes simplex (HSV), Lentiviral and Adeno-associated viral (AAV) vectors have all been used in targeting experimental gene therapies to the Trabecular meshwork. There have also been a limited number of early reports on the use of HSV vectors in transfection of the TM, however, limited reporter gene expression and significant inflammatory responses were observed [183, 184]. Long-term expression in TM cells and in rodents has been achieved with lentivirus following a single intracameral inoculation [185, 186]. The first demonstration of efficient lentiviral transduction in primates reported well tolerated, extensive viral expression with a mild inflammatory response [187]. In early AV studies, gene expression was obtained in TM cells of mice for up to 14 days following intracameral inoculation of a replication-deficient AV vector expressing a LacZ gene [188]. In practice however, the feasibility of using AV as a gene therapy vector is extremely limited owing to its immunogenicity and the non-sustainability of viral expression, however AV has been a useful vector in demonstrating proof of principle of gene therapy strategies [189, 190, 191]. In this regard, an AV system in which MMP-1 expression could be activated by a glucocorticoid-responsive promoter has been developed. Corticosteroid treatments can result in elevations in IOP in a significant number of individuals, thus steroid induced expression of MMP-1 within the TM will result in a reduction in collagen type I, potentially preventing an increase in IOP [192]. This approach was subsequently extended to sheep, where steroid-induced expression of MMP-1 resulted in a decrease in IOP [193], and later deployed in a scAAV system more appropriate to human intervention [194].

AAVs are the most widely used gene therapy vector systems in use today. AAV is an innate human virus, integrated into the human genome on chromosome 19, and will only replicate in the presence of AV helper functions. It is minimally immunogenic even when used in high doses [195, 196]. Moreover, AAV has been used extensively in human trials of gene therapy for retinopathies, particularly for Leber congenital amaurosis and retinitis pigmentosa. Conventional AAVs have a single stranded DNA genome, which requires second strand synthesis by host DNA polymerases. By incorporating a second self-complementary DNA strand into these vectors (scAAV), these viruses have been shown to be significantly more efficient in transducing target cells, with the disadvantage of a reduction in the size of their DNA handling capacity [197]. While standard AAV constructs transfect but do not appear to be expressed in cells of the conventional outflow pathway, highly efficient expression has been demonstrated via the use of scAAV [198]. Rapid and widespread transfection of the TM has been demonstrated following intracameral inoculation of GFP-expressing scAAV2 constructs in both rats and non-human primates, with expression lasting in rats for greater than 3.5 months and in monkeys for at least 2.35 years.

In the case of glucocorticoid inducible expression of MMP-1 previously mentioned, IOP was successfully reduced in sheep following intracameral inoculation of the AAV virus, with no localized or systemic negative effects [194]. This study was the first in which the feasibility of a gene therapy approach for steroid induced IOP was demonstrated with a virus that could be deployed as a human therapy. The feasibility of controlled AAV-mediated expression of

MMPs was further investigated in recent studies [98] in which a conventional AAV2/9 vector expressing a doxycycline-inducible MMP-3 gene was intracamerally inoculated into wild type mice, with extensive transfection of the corneal endothelia being observed. As MMP-3 is a secretory protein, its expression in corneal endothelial cells resulted in secretion of the protease into the AH, where it traversed the anterior chamber with the natural flow of AH toward the outflow tissues. Here the pro-peptide was initially cleaved by non-specific proteases, allowing for further cleavage by MMP's, including other MMP-3 molecules themselves. ECM proteolysis ensued, reducing collagen and laminin contents, constriction of actin filaments and disorganisation of fibronectin networks, resulting in elevated outflow facility and a reduction in IOP. Few adverse reactions were observed in the anterior chamber using this method, while ECM components were visibly modulated and greater intercellular spaces observed. Given the safety profile of AAV and its wide use in ocular gene therapy, having progressed through Phase III trials for Leber congenital amaurosis and Leber hereditary optic neuropathy [199, 200], AAV systems in which MMP expression can be periodically induced as indicated by IOP hold substantial promise as gene medicines.

5. Conclusion

The ECM is a dynamic structure capable of enhancing outflow resistance at the JCT region of the conventional outflow tissues. Normal responses to elevated IOP allow this structure to expand and alter its configuration to facilitate increased outflow facility, thus alleviating ocular hypertension. In open-angle glaucoma however, hypertension remains through as of yet incompletely elucidated mechanisms. As lowering IOP remains the primary treatment for patients with this disease, medications and surgeries aim to do so via a variety of biological and mechanical interventions. New strategies in development target the conventional outflow pathway more specifically, many of which employ remodelling of the ECM. Re-organisation of matrix components using MMPs, inhibition of focal adhesions, depolymerisation of the actin cytoskeleton and deterioration of inter-endothelial junctions are such examples that provide a means by which AH outflow facility can be increased, ultimately leading to a reduction in IOP. Novel targeting approaches, together with advanced delivery systems and combination therapies, may assist in improving patient compliance, long term cost, chronic reductions in IOP, and ultimately a reduction in vision loss.

6. Expert opinion

That the bulk of AH outflow is through the conventional pathway and that most of the medications in current clinical use do not primarily target this pathway will be a matter of intrigue to most non-specialists. However, while many of the new formulations in development target pathological disease processes which are primarily located in the anterior part of the eye, death of the retina's output sensory neurons, the ganglion cells, is the final determinant of vision loss caused by elevated IOP. It is therefore not unreasonable to speculate that combinatorial therapies, simultaneously targeting outflow together with

ganglion cell survival, may prove more highly efficacious than attempting to lower IOP singularly. Mediators of the cytoskeleton, focal adhesions, intercellular junctions and ECM can all alter the architecture of the outflow tissues, including alterations in cell geometry, contractility, and migration, among other functions, leading to changes in outflow resistance. However, it remains to be determined whether such morphological changes are transient, and whether treated tissues will remain in their remodelled state if treatment is discontinued. To date, the underlying mechanisms by which current first line medications act remain to be fully elucidated, although significant steps have been made in recent years. Emerging knowledge has led to the development of new formulations showing greater efficacy and safety than conventional medications, with many of these are currently in clinical trial. Many drugs, both old and new, target the conventional outflow pathway, in particular the ECM and cytoskeletal structures, but this is often secondary or indirect to their primary mode of action. Remodelling of the ECM has been shown to influence outflow resistance greatly, giving strength to the hypothesis that the ECM at the JCT contributes substantially to outflow resistance. Perfusion with compounds that activate matrix modulators, such as MMPs, or even traditional medications, have been shown to increase outflow facility with simultaneous elevations in MMP expression. It is not surprising however, that perfusion with purified MMP's alone significantly alters conventional outflow, in both its morphology and AH dynamics. Recent developments have demonstrated the efficacy of introducing MMP-1 and MMP-3 genes into the anterior chamber via AAVs. Implementing proteases directly modulating the ECM reduces the potential for unwanted off-target and downstream adversities in comparison to activators or inducers of such proteases, however MMPs themselves also have downstream signalling cascades, thus selection of specific proteases is important and further development may see an even more specific use of metalloproteinases. For example, MMP-1 was chosen for glucocorticoid-induced expression as it is a well-documented MMP with a large target profile. MMP-3 was chosen for doxycycline eye-drop expression in the cornea due to its secretory domain, its ability to auto activate and activate other MMPs, and for its target profile being similar to that of the composition of the ECM at the JCT. Similar selection must be undertaken for other drugs in development. ECM modulation by metalloproteinases should in theory be effective in targeting secondary glaucoma, including pseudoexfoliative, pigmentary and uveitic glaucoma, which involve physical blockage of drainage channels. AAV used as a vector for gene delivery has an excellent safety and tolerability profile. External inducers of viral expression are avenues in themselves, response elements currently ranging from glucocorticoid responsive promoters to tetracycline responsive promoters. The tetracycline-inducible systems have been widely used in AAV expression, however with them comes their own limitations including leaky promoters and potential toxicity of the inducer. In this regard it is of note that doxycycline is commonly used as an antibiotic and is also approved for inhibition of select MMP expression. Alternative tetracycline derivatives could prove more efficacious, or the design of unique inducible elements may generate new means of controlling expression in disease states. Such

therapies are still in proof of concept stages however, and pre-clinical functional validation and safety in non-human primates will be required.

There is clearly an unmet need for novel glaucoma therapeutics which sufficiently demonstrate a long term reduction of IOP with minimal side effects. Further elucidation of the exact mechanisms of open angle glaucoma, and its treatments, may lead to medications that directly target the causative site, arresting disease progress and restoring function to existing tissues.

Article highlights

- Glaucoma, a multifactorial disease, affects approximately 70 million people today. Several genetic components have been identified, with some variations indicating a link to ECM homeostasis.
- The ECM has a significant influence on the regulation of outflow resistance in the eye, and thus presents itself as an attractive therapeutic target.
- Commercially available medications do not significantly lower IOP over long periods of time, and often have indirect effects on the ECM.
- Medications in development have a greater focus on ECM modulation including cytoskeletal disorganisation, decreased cellular contractility and enhanced ECM turnover via MMPs, which are associated with improved efficacy.
- Recent gene therapy advancements allow for induced secretion of MMPs into the anterior chamber, resulting in significant decreases in IOP and increases in outflow facility.

Keywords

MMP, Extracellular Matrix, ECM, Glaucoma, Outflow Facility, Treatment, Prostaglandin, AAV

Funding

Glaucoma research at the Ocular Genetics Unit is supported by the European Research

Council under grant ERC-2012-AdG 322656-Oculus and an equipment grant from Science

Foundation Ireland under grant [12/ERC/B2539].

Declaration of Interest

The authors have no conflicting interests to declare.

References

Papers of particular interest are identified using asterisk symbols (* = of interest, ** = of considerable interest).

1. Quigley HA, Broman AT. The number of people with glaucoma worldwide in 2010 and 2020. Br J Ophthalmol. 2006;90:262-7
2. Actis AG, Versino E, Brogliatti B, et al. Risk Factors for Primary Open Angle Glaucoma (POAG) Progression: A Study Ruled in Torino. Open Ophthalmol J. 2016;10:129-39
3. Tham YC, Li X, Wong TY, et al. Global prevalence of glaucoma and projections of glaucoma burden through 2040: a systematic review and meta-analysis. Ophthalmology. 2014;121:2081-90
4. Quigley HA. Number of people with glaucoma worldwide. Br J Ophthalmol. 1996;80:389-93
5. Sommer A, Tielsch JM, Katz J, et al. Relationship between intraocular pressure and primary open angle glaucoma among white and black Americans. The Baltimore Eye Survey. Arch Ophthalmol. 1991;109:1090-5
6. Abu-Amero K, Kondkar AA, Chalam KV. An Updated Review on the Genetics of Primary Open Angle Glaucoma. Int J Mol Sci. 2015;16:28886-911
7. Hardy KM, Hoffman EA, Gonzalez P, et al. Extracellular trafficking of myocilin in human trabecular meshwork cells. J Biol Chem. 2005;280:28917-26
8. Hoffman EA, Perkumas KM, Highstrom LM, et al. Regulation of myocilin-associated exosome release from human trabecular meshwork cells. Invest Ophthalmol Vis Sci. 2009;50:1313-8
9. Peters DM, Herbert K, Biddick B, et al. Myocilin binding to Hep II domain of fibronectin inhibits cell spreading and incorporation of paxillin into focal adhesions. Exp Cell Res. 2005;303:218-28
10. Ueda J, Wentz-Hunter K, Yue BY. Distribution of myocilin and extracellular matrix components in the juxtacanalicular tissue of human eyes. Invest Ophthalmol Vis Sci. 2002;43:1068-76
11. Jacobson N, Andrews M, Shepard AR, et al. Non-secretion of mutant proteins of the glaucoma gene myocilin in cultured trabecular meshwork cells and in aqueous humor. Hum Mol Genet. 2001;10:117-25
12. Kasetti RB, Phan TN, Millar JC, et al. Expression of Mutant Myocilin Induces Abnormal Intracellular Accumulation of Selected Extracellular Matrix Proteins in the Trabecular Meshwork. Invest Ophthalmol Vis Sci. 2016;57:6058-69
13. Zode GS, Kuehn MH, Nishimura DY, et al. Reduction of ER stress via a chemical chaperone prevents disease phenotypes in a mouse model of primary open angle glaucoma. J Clin Invest. 2011;121:3542-53
14. Rezaie T, Child A, Hitchings R, et al. Adult-onset primary open-angle glaucoma caused by mutations in optineurin. Science. 2002;295:1077-9
15. De Marco N, Buono M, Troise F, et al. Optineurin increases cell survival and translocates to the nucleus in a Rab8-dependent manner upon an apoptotic stimulus. J Biol Chem. 2006;281:16147-56
16. Gemenetzi M, Yang Y, Lotery AJ. Current concepts on primary open-angle glaucoma genetics: a contribution to disease pathophysiology and future treatment. Eye (Lond). 2012;26:355-69
17. Fuse N, Takahashi K, Akiyama H, et al. Molecular genetic analysis of optineurin gene for primary open-angle and normal tension glaucoma in the Japanese population. J Glaucoma. 2004;13:299-303
18. Fingert JH. Primary open-angle glaucoma genes. Eye (Lond). 2011;25:587-95
19. Tourkina E, Gooz P, Pannu J, et al. Opposing effects of protein kinase Calpha and protein kinase Cepsilon on collagen expression by human lung fibroblasts are mediated via MEK/ERK and caveolin-1 signaling. J Biol Chem. 2005;280:13879-87
20. Del Galdo F, Lisanti MP, Jimenez SA. Caveolin-1, transforming growth factor-beta receptor internalization, and the pathogenesis of systemic sclerosis. Curr Opin Rheumatol. 2008;20:713-9
21. Thompson C, Rahim S, Arnold J, et al. Loss of caveolin-1 alters extracellular matrix protein expression and ductal architecture in murine mammary glands. PLoS One. 2017;12:e0172067
22. Surgucheva I, Surguchov A. Expression of caveolin in trabecular meshwork cells and its possible implication in pathogenesis of primary open angle glaucoma. Mol Vis. 2011;17:2878-88
23. Razani B, Zhang XL, Bitzer M, et al. Caveolin-1 regulates transforming growth factor (TGF)-beta/SMAD signaling through an interaction with the TGF-beta type I receptor. J Biol Chem. 2001;276:6727-38
24. Elliott MH, Ashpole NE, Gu X, et al. Caveolin-1 modulates intraocular pressure: implications for caveolae mechanoprotection in glaucoma. Sci Rep. 2016;6:37127
25. Ozel AB, Moroi SE, Reed DM, et al. Genome-wide association study and meta-analysis of intraocular pressure. Hum Genet. 2014;133:41-57
26. Burdon KP, Macgregor S, Hewitt AW, et al. Genome-wide association study identifies susceptibility loci for open angle glaucoma at TMCO1 and CDKN2B-AS1. Nat Genet. 2011;43:574-8
27. Hysi PG, Cheng CY, Springelkamp H, et al. Genome-wide analysis of multi-ancestry cohorts identifies new loci influencing intraocular pressure and susceptibility to glaucoma. Nat Genet. 2014;46:1126-30
28. Wang QC, Zheng Q, Tan H, et al. TMCO1 Is an ER Ca(2+) Load-Activated Ca(2+) Channel. Cell. 2016;165:1454-66
29. Lu Y, Vitart V, Burdon KP, et al. Genome-wide association analyses identify multiple loci associated with central corneal thickness and keratoconus. Nat Genet. 2013;45:155-63
30. Springelkamp H, Hohn R, Mishra A, et al. Meta-analysis of genome-wide association studies identifies novel loci that influence cupping and the glaucomatous process. Nat Commun. 2014;5:4883
31. Iglesias AI, Springelkamp H, Ramdas WD, et al. Genes, pathways, and animal models in primary open-angle glaucoma. Eye (Lond). 2015;29:1285-98
32. Springelkamp H, Mishra A, Hysi PG, et al. Meta-analysis of Genome-Wide Association Studies Identifies Novel Loci Associated With Optic Disc Morphology. Genet Epidemiol. 2015;39:207-16

33. Kloeckener-Gruissem B, Bartholdi D, Abdou MT, et al. Identification of the genetic defect in the original Wagner syndrome family. Mol Vis. 2006;12:350-5
34. Keller KE, Bradley JM, Vranka JA, et al. Segmental versican expression in the trabecular meshwork and involvement in outflow facility. Invest Ophthalmol Vis Sci. 2011;52:5049-57
35. Jelodari-Mamaghani S, Haji-Seyed-Javadi R, Suri F, et al. Contribution of the latent transforming growth factor-beta binding protein 2 gene to etiology of primary open angle glaucoma and pseudoexfoliation syndrome. Mol Vis. 2013;19:333-47
36. Kuchtey J, Chang TC, Panagis L, et al. Marfan syndrome caused by a novel FBN1 mutation with associated pigmentary glaucoma. Am J Med Genet A. 2013;161A:880-3
37. Kuchtey J, Kuchtey RW. The microfibril hypothesis of glaucoma: implications for treatment of elevated intraocular pressure. J Ocul Pharmacol Ther. 2014;30:170-80
38. Morales J, Al-Sharif L, Khalil DS, et al. Homozygous mutations in ADAMTS10 and ADAMTS17 cause lenticular myopia, ectopia lentis, glaucoma, spherophakia, and short stature. Am J Hum Genet. 2009;85:558-68
39. Keller KE, Acott TS. The Juxtacanalicular Region of Ocular Trabecular Meshwork: A Tissue with a Unique Extracellular Matrix and Specialized Function. Journal of Ocular Biology, Diseases, and Informatics. 2013;1:3
* A comprehensive review of the JCT
40. Fuchshofer R, Welge-Lussen U, Lutjen-Drecoll E, et al. Biochemical and morphological analysis of basement membrane component expression in corneoscleral and cribriform human trabecular meshwork cells. Invest Ophthalmol Vis Sci. 2006;47:794-801
41. Kizhatil K, Ryan M, Marchant JK, et al. Schlemm's canal is a unique vessel with a combination of blood vascular and lymphatic phenotypes that forms by a novel developmental process. PLoS Biol. 2014;12:e1001912
42. Overby DR, Stamer WD, Johnson M. The changing paradigm of outflow resistance generation: towards synergistic models of the JCT and inner wall endothelium. Exp Eye Res. 2009;88:656-70
** An important paper exploring the sites of resistance generation in the outflow tissue, and the ECM molecules that might be involved.
43. Tam LC, Reina-Torres E, Sherwood JM, et al. Enhancement of Outflow Facility in the Murine Eye by Targeting Selected Tight-Junctions of Schlemm's Canal Endothelia. Sci Rep. 2017;7:40717
44. Reina-Torres E, Wen JC, Liu KC, et al. VEGF as a Paracrine Regulator of Conventional Outflow Facility. Invest Ophthalmol Vis Sci. 2017;58:1899-908
45. Aspelund A, Tammela T, Antila S, et al. The Schlemm's canal is a VEGF-C/VEGFR-3-responsive lymphatic-like vessel. J Clin Invest. 2014;124:3975-86
46. Vranka JA, Kelley MJ, Acott TS, et al. Extracellular matrix in the trabecular meshwork: intraocular pressure regulation and dysregulation in glaucoma. Exp Eye Res. 2015;133:112-25
47. VanderWyst SS, Perkumas KM, Read AT, et al. Structural basement membrane components and corresponding integrins in Schlemm's canal endothelia. Mol Vis. 2011;17:199-209
48. Faralli JA, Schwinn MK, Gonzalez JM, Jr., et al. Functional properties of fibronectin in the trabecular meshwork. Exp Eye Res. 2009;88:689-93
49. Rohen JW, Futa R, Lutjen-Drecoll E. The fine structure of the cribriform meshwork in normal and glaucomatous eyes as seen in tangential sections. Invest Ophthalmol Vis Sci. 1981;21:574-85
50. Burridge K, Fath K, Kelly T, et al. Focal adhesions: transmembrane junctions between the extracellular matrix and the cytoskeleton. Annu Rev Cell Biol. 1988;4:487-525
51. Cheng YF, Kramer RH. Human microvascular endothelial cells express integrin-related complexes that mediate adhesion to the extracellular matrix. J Cell Physiol. 1989;139:275-86
52. Lampugnani MG, Resnati M, Dejana E, et al. The role of integrins in the maintenance of endothelial monolayer integrity. J Cell Biol. 1991;112:479-90
53. Geiger B, Bershadsky A, Pankov R, et al. Transmembrane crosstalk between the extracellular matrix--cytoskeleton crosstalk. Nat Rev Mol Cell Biol. 2001;2:793-805
54. Han H, Wecker T, Grehn F, et al. Elasticity-dependent modulation of TGF-beta responses in human trabecular meshwork cells. Invest Ophthalmol Vis Sci. 2011;52:2889-96
55. Wallace DM, Murphy-Ullrich JE, Downs JC, et al. The role of matricellular proteins in glaucoma. Matrix Biol. 2014;37:174-82
56. Mutsaers SE, Bishop JE, McGrouther G, et al. Mechanisms of tissue repair: from wound healing to fibrosis. Int J Biochem Cell Biol. 1997;29:5-17
57. Wight TN, Potter-Perigo S. The extracellular matrix: an active or passive player in fibrosis? Am J Physiol Gastrointest Liver Physiol. 2011;301:G950-5
58. Tektas OY, Lutjen-Drecoll E. Structural changes of the trabecular meshwork in different kinds of glaucoma. Exp Eye Res. 2009;88:769-75
* A comparison of the TM in different types of glaucoma using electron microscopy
59. Alm A, Nilsson SF. Uveoscleral outflow--a review. Exp Eye Res. 2009;88:760-8
60. Stamer WD. The cell and molecular biology of glaucoma: mechanisms in the conventional outflow pathway. Invest Ophthalmol Vis Sci. 2012;53:2470-2
61. Goel M, Picciani RG, Lee RK, et al. Aqueous humor dynamics: a review. Open Ophthalmol J. 2010;4:52-9
62. Bill A, Svedbergh B. Scanning electron microscopic studies of the trabecular meshwork and the canal of Schlemm--an attempt to localize the main resistance to outflow of aqueous humor in man. Acta Ophthalmol (Copenh). 1972;50:295-320
63. Inomata H, Bill A, Smelser GK. Aqueous humor pathways through the trabecular meshwork and into Schlemm's canal in the cynomolgus monkey (Macaca irus). An electron microscopic study. Am J Ophthalmol. 1972;73:760-89
64. Johnstone MA, Grant WG. Pressure-dependent changes in structures of the aqueous outflow system of human and monkey eyes. Am J Ophthalmol. 1973;75:365-83
65. Johnson MC, Kamm RD. The role of Schlemm's canal in aqueous outflow from the human eye. Invest Ophthalmol Vis Sci. 1983;24:320-5
66. Johnson M. 'What controls aqueous humour outflow resistance?'. Exp Eye Res. 2006;82:545-57
67. Rosenquist R, Epstein D, Melamed S, et al. Outflow resistance of enucleated human eyes at two different perfusion pressures and different extents of trabeculotomy. Curr Eye Res. 1989;8:1233-40
68. Grant WM. Experimental aqueous perfusion in enucleated human eyes. Arch Ophthalmol. 1963;69:783-801
69. Wise JB, Witter SL. Argon laser therapy for open-angle glaucoma. A pilot study. Arch Ophthalmol. 1979;97:319-22

70. Swaminathan SS, Oh DJ, Kang MH, et al. Aqueous outflow: segmental and distal flow. J Cataract Refract Surg. 2014;40:1263-72
71. Tanihara H, Inatani M, Koga T, et al. Proteoglycans in the eye. Cornea. 2002;21:62-9
72. Floyd BB, Cleveland PH, Worthen DM. Fibronectin in human trabecular drainage channels. Invest Ophthalmol Vis Sci. 1985;26:797-804
73. Swaminathan SS, Oh DJ, Kang MH, et al. Secreted protein acidic and rich in cysteine (SPARC)-null mice exhibit more uniform outflow. Invest Ophthalmol Vis Sci. 2013;54:2035-47
74. Keller KE, Bradley JM, Kelley MJ, et al. Effects of modifiers of glycosaminoglycan biosynthesis on outflow facility in perfusion culture. Invest Ophthalmol Vis Sci. 2008;49:2495-505
75. Gong H, Freddo TF, Johnson M. Age-related changes of sulfated proteoglycans in the normal human trabecular meshwork. Exp Eye Res. 1992;55:691-709
76. Berggren L, Vrabec F. Demonstration of a coating substance in the trabecular meshwork of the eye and its decrease after perfusion experiments with different kinds of hyaluronidase. Am J Ophthalmol. 1957;44:200-8
77. Francois J. Corticosteroid glaucoma. Ann Ophthalmol. 1977;9:1075-80
78. Sherwood JM, Reina-Torres E, Bertrand JA, et al. Measurement of Outflow Facility Using iPerfusion. PLoS One. 2016;11:e0150694
79. Vranka JA, Acott TS. Pressure-induced expression changes in segmental flow regions of the human trabecular meshwork. Exp Eye Res. 2016
* This review describes the importance of the ECM at the TM in the homeostatic regulation of intraocular pressure
80. Bradley JM, Kelley MJ, Zhu X, et al. Effects of mechanical stretching on trabecular matrix metalloproteinases. Invest Ophthalmol Vis Sci. 2001;42:1505-13
* This article describes how changes in the ECM induce responses in nearby cells, influencing the turnover rates of ECM. This feedback mechanism is fundamental to homeostatic regulation.
81. Zhao X, Ramsey KE, Stephan DA, et al. Gene and protein expression changes in human trabecular meshwork cells treated with transforming growth factor-beta. Invest Ophthalmol Vis Sci. 2004;45:4023-34
82. Vittal V, Rose A, Gregory KE, et al. Changes in gene expression by trabecular meshwork cells in response to mechanical stretching. Invest Ophthalmol Vis Sci. 2005;46:2857-68
83. Lo WR, Rowlette LL, Caballero M, et al. Tissue differential microarray analysis of dexamethasone induction reveals potential mechanisms of steroid glaucoma. Invest Ophthalmol Vis Sci. 2003;44:473-85
84. Izzotti A, Longobardi M, Cartiglia C, et al. Trabecular meshwork gene expression after selective laser trabeculoplasty. PLoS One. 2011;6:e20110
85. Keller KE, Aga M, Bradley JM, et al. Extracellular matrix turnover and outflow resistance. Exp Eye Res. 2009;88:676-82
86. Nagase H, Suzuki K, Enghild JJ, et al. Stepwise activation mechanisms of the precursors of matrix metalloproteinases 1 (tissue collagenase) and 3 (stromelysin). Biomedica biochimica acta. 1991;50:749-54
* A detailed description of the mechanisms required to activate MMPs.
87. Chakraborti S, Mandal M, Das S, et al. Regulation of matrix metalloproteinases: an overview. Mol Cell Biochem. 2003;253:269-85
88. Alexander JP, Samples JR, Van Buskirk EM, et al. Expression of matrix metalloproteinases and inhibitor by human trabecular meshwork. Invest Ophthalmol Vis Sci. 1991;32:172-80
89. Oh DJ, Martin JL, Williams AJ, et al. Effect of latanoprost on the expression of matrix metalloproteinases and their tissue inhibitors in human trabecular meshwork cells. Invest Ophthalmol Vis Sci. 2006;47:3887-95
* An indication that MMP expression can be influenced by topical administration of medications.
90. Kelley MJ, Rose AY, Song K, et al. Synergism of TNF and IL-1 in the induction of matrix metalloproteinase-3 in trabecular meshwork. Invest Ophthalmol Vis Sci. 2007;48:2634-43
91. Overby DR, Bertrand J, Tektas OY, et al. Ultrastructural changes associated with dexamethasone-induced ocular hypertension in mice. Invest Ophthalmol Vis Sci. 2014;55:4922-33
92. Schlotzer-Schrehardt U, Lommatzsch J, Kuchle M, et al. Matrix metalloproteinases and their inhibitors in aqueous humor of patients with pseudoexfoliation syndrome/glaucoma and primary open-angle glaucoma. Invest Ophthalmol Vis Sci. 2003;44:1117-25
93. Ronkko S, Rekonen P, Kaarniranta K, et al. Matrix metalloproteinases and their inhibitors in the chamber angle of normal eyes and patients with primary open-angle glaucoma and exfoliation glaucoma. Graefe's archive for clinical and experimental ophthalmology = Albrecht von Graefes Archiv fur klinische und experimentelle Ophthalmologie. 2007;245:697-704
94. Fountoulakis N, Labiris G, Aristeidou A, et al. Tissue inhibitor of metalloproteinase 4 in aqueous humor of patients with primary open angle glaucoma, pseudoexfoliation syndrome and pseudoexfoliative glaucoma and its role in proteolysis imbalance. BMC Ophthalmol. 2013;13:69
95. Ashworth Briggs EL, Toh T, Eri R, et al. TIMP1, TIMP2, and TIMP4 are increased in aqueous humor from primary open angle glaucoma patients. Mol Vis. 2015;21:1162-72
96. Weinstein WL, Dietrich UM, Sapienza JS, et al. Identification of ocular matrix metalloproteinases present within the aqueous humor and iridocorneal drainage angle tissue of normal and glaucomatous canine eyes. Veterinary ophthalmology. 2007;10 Suppl 1:108-16
97. Maatta M, Tervahartiala T, Vesti E, et al. Levels and activation of matrix metalloproteinases in aqueous humor are elevated in uveitis-related secondary glaucoma. J Glaucoma. 2006;15:229-37
98. O'Callaghan J, Crosbie DE, Cassidy PS, et al. Therapeutic potential of AAV-mediated MMP-3 secretion from corneal endothelium in treating glaucoma. Hum Mol Genet. 2017
** This article demonstrated that virally expressed MMP-3 could be induced via eye drop to increase ooutflow facility and reduce IOP.
99. Bradley JM, Vranka J, Colvis CM, et al. Effect of matrix metalloproteinases activity on outflow in perfused human organ culture. Invest Ophthalmol Vis Sci. 1998;39:2649-58
100. Pang IH, Fleenor DL, Hellberg PE, et al. Aqueous outflow-enhancing effect of tert-butylhydroquinone: involvement of AP-1 activation and MMP-3 expression. Invest Ophthalmol Vis Sci. 2003;44:3502-10
101. Webb JG, Husain S, Yates PW, et al. Kinin modulation of conventional outflow facility in the bovine eye. J Ocul Pharmacol Ther. 2006;22:310-6
102. De Groef L, Van Hove I, Dekeyster E, et al. MMPs in the trabecular meshwork: promising targets for future glaucoma therapies? Invest Ophthalmol Vis Sci. 2013;54:7756-63

103. Aga M, Bradley JM, Wanchu R, et al. Differential effects of caveolin-1 and -2 knockdown on aqueous outflow and altered extracellular matrix turnover in caveolin-silenced trabecular meshwork cells. Invest Ophthalmol Vis Sci. 2014;55:5497-509
104. Yang YF, Sun YY, Acott TS, et al. Effects of induction and inhibition of matrix cross-linking on remodeling of the aqueous outflow resistance by ocular trabecular meshwork cells. Sci Rep. 2016;6:30505
105. Huovila AP, Turner AJ, Pelto-Huikko M, et al. Shedding light on ADAM metalloproteinases. Trends Biochem Sci. 2005;30:413-22
106. Stickel SK, Wang YL. Synthetic peptide GRGDS induces dissociation of alpha-actinin and vinculin from the sites of focal contacts. J Cell Biol. 1988;107:1231-9
107. Curtis TM, McKeown-Longo PJ, Vincent PA, et al. Fibronectin attenuates increased endothelial monolayer permeability after RGD peptide, anti-alpha 5 beta 1, or TNF-alpha exposure. Am J Physiol. 1995;269:248-60
108. Wu MH, Ustinova E, Granger HJ. Integrin binding to fibronectin and vitronectin maintains the barrier function of isolated porcine coronary venules. J Physiol. 2001;532:785-91
109. Tamm ER, Siegner A, Baur A, et al. Transforming growth factor-beta 1 induces alpha-smooth muscle-actin expression in cultured human and monkey trabecular meshwork. Exp Eye Res. 1996;62:389-97
110. Schlunck G, Han H, Wecker T, et al. Substrate rigidity modulates cell matrix interactions and protein expression in human trabecular meshwork cells. Invest Ophthalmol Vis Sci. 2008;49:262-9
111. Yang Y, Estrada EY, Thompson JF, et al. Matrix metalloproteinase-mediated disruption of tight junction proteins in cerebral vessels is reversed by synthetic matrix metalloproteinase inhibitor in focal ischemia in rat. Journal of cerebral blood flow and metabolism : official journal of the International Society of Cerebral Blood Flow and Metabolism. 2007;27:697-709
112. Vermeer PD, Denker J, Estin M, et al. MMP9 modulates tight junction integrity and cell viability in human airway epithelia. Am J Physiol Lung Cell Mol Physiol. 2009;296:751-62
113. Yamada H, Yoneda M, Inaguma S, et al. Infliximab counteracts tumor necrosis factor-alpha-enhanced induction of matrix metalloproteinases that degrade claudin and occludin in non-pigmented ciliary epithelium. Biochem Pharmacol. 2013;85:1770-82
114. Rylander NR, Vold SD. Cost analysis of glaucoma medications. Am J Ophthalmol. 2008;145:106-13
115. Li T, Lindsley K, Rouse B, et al. Comparative Effectiveness of First-Line Medications for Primary Open-Angle Glaucoma: A Systematic Review and Network Meta-analysis. Ophthalmology. 2016;123:129-40
116. Mastropasqua R, Fasanella V, Pedrotti E, et al. Trans-conjunctival aqueous humor outflow in glaucomatous patients treated with prostaglandin analogues: an in vivo confocal microscopy study. Graefe's archive for clinical and experimental ophthalmology = Albrecht von Graefes Archiv fur klinische und experimentelle Ophthalmologie. 2014;252:1469-76
117. Toris CB, Gabelt BT, Kaufman PL. Update on the mechanism of action of topical prostaglandins for intraocular pressure reduction. Surv Ophthalmol. 2008;53 Suppl1:S107-20
* This paper shows that prostaglandins can affect the conventional outflow pathway, not only the unconventional.
118. Richter M, Krauss AH, Woodward DF, et al. Morphological changes in the anterior eye segment after long-term treatment with different receptor selective prostaglandin agonists and a prostamide. Invest Ophthalmol Vis Sci. 2003;44:4419-26
119. Goh Y, Urade Y, Fujimoto N, et al. Content and formation of prostaglandins and distribution of prostaglandin-related enzyme activities in the rat ocular system. Biochim Biophys Acta. 1987;921:302-11
120. Wan Z, Woodward DF, Stamer WD. Endogenous Bioactive Lipids and the Regulation of Conventional Outflow Facility. Expert Rev Ophthalmol. 2008;3:457-70
121. Bahler CK, Howell KG, Hann CR, et al. Prostaglandins increase trabecular meshwork outflow facility in cultured human anterior segments. Am J Ophthalmol. 2008;145:114-9
122. Wan Z, Woodward DF, Cornell CL, et al. Bimatoprost, prostamide activity, and conventional drainage. Invest Ophthalmol Vis Sci. 2007;48:4107-15
123. Thieme H, Schimmat C, Munzer G, et al. Endothelin antagonism: effects of FP receptor agonists prostaglandin F2alpha and fluprostenol on trabecular meshwork contractility. Invest Ophthalmol Vis Sci. 2006;47:938-45
124. Weinreb RN, Toris CB, Gabelt BT, et al. Effects of prostaglandins on the aqueous humor outflow pathways. Surv Ophthalmol. 2002;47 Suppl 1:S53-64
125. Schachtschabel U, Lindsey JD, Weinreb RN. The mechanism of action of prostaglandins on uveoscleral outflow. Curr Opin Ophthalmol. 2000;11:112-5
126. Ocklind A. Effect of latanoprost on the extracellular matrix of the ciliary muscle. A study on cultured cells and tissue sections. Exp Eye Res. 1998;67:179-91
127. Sagara T, Gaton DD, Lindsey JD, et al. Topical prostaglandin F2alpha treatment reduces collagen types I, III, and IV in the monkey uveoscleral outflow pathway. Arch Ophthalmol. 1999;117:794-801
128. Weinreb RN, Kashiwagi K, Kashiwagi F, et al. Prostaglandins increase matrix metalloproteinase release from human ciliary smooth muscle cells. Invest Ophthalmol Vis Sci. 1997;38:2772-80
129. Woodward DF, Nilsson SF, Toris CB, et al. Prostanoid EP4 receptor stimulation produces ocular hypotension by a mechanism that does not appear to involve uveoscleral outflow. Invest Ophthalmol Vis Sci. 2009;50:3320-8
130. Alvarado JA, Iguchi R, Martinez J, et al. Similar effects of selective laser trabeculoplasty and prostaglandin analogs on the permeability of cultured Schlemm canal cells. Am J Ophthalmol. 2010;150:254-64
131. Brooks AM, Gillies WE. Ocular beta-blockers in glaucoma management. Clinical pharmacological aspects. Drugs Aging. 1992;2:208-21
132. Trope GE, Clark B. Beta adrenergic receptors in pigmented ciliary processes. Br J Ophthalmol. 1982;66:788-92
133. Camras CB, Podos SM. The role of endogenous prostaglandins in clinically-used and investigational glaucoma therapy. Prog Clin Biol Res. 1989;312:459-75
134. Toris CB, Camras CB, Yablonski ME. Acute versus chronic effects of brimonidine on aqueous humor dynamics in ocular hypertensive patients. Am J Ophthalmol. 1999;128:8-14
135. Beidoe G, Mousa SA. Current primary open-angle glaucoma treatments and future directions. Clin Ophthalmol. 2012;6:1699-707
136. Avila MY, Carre DA, Stone RA, et al. Reliable measurement of mouse intraocular pressure by a servo-null micropipette system. Invest Ophthalmol Vis Sci. 2001;42:1841-6
137. Overby DR, Bertrand J, Schicht M, et al. The structure of the trabecular meshwork, its connections to the ciliary muscle, and the effect of pilocarpine on outflow facility in mice. Invest Ophthalmol Vis Sci. 2014;55:3727-36

138. Li G, Farsiu S, Chiu SJ, et al. Pilocarpine-induced dilation of Schlemm's canal and prevention of lumen collapse at elevated intraocular pressures in living mice visualized by OCT. Invest Ophthalmol Vis Sci. 2014;55:3737-46
139. Selbach JM, Gottanka J, Wittmann M, et al. Efferent and afferent innervation of primate trabecular meshwork and scleral spur. Invest Ophthalmol Vis Sci. 2000;41:2184-91
140. Ito T, Ohguro H, Mamiya K, et al. Effects of antiglaucoma drops on MMP and TIMP balance in conjunctival and subconjunctival tissue. Invest Ophthalmol Vis Sci. 2006;47:823-30
141. Scherer WJ. A retrospective review of non-responders to latanoprost. J Ocul Pharmacol Ther. 2002;18:287-91
142. Noecker RS, Dirks MS, Choplin NT, et al. A six-month randomized clinical trial comparing the intraocular pressure-lowering efficacy of bimatoprost and latanoprost in patients with ocular hypertension or glaucoma. Am J Ophthalmol. 2003;135:55-63
143. Li G, Mukherjee D, Navarro I, et al. Visualization of conventional outflow tissue responses to netarsudil in living mouse eyes. Eur J Pharmacol. 2016;787:20-31
144. Ren R, Li G, Le TD, et al. Netarsudil Increases Outflow Facility in Human Eyes Through Multiple Mechanisms. Invest Ophthalmol Vis Sci. 2016;57:6197-209
145. Wang RF, Williamson JE, Kopczynski C, et al. Effect of 0.04% AR-13324, a ROCK, and norepinephrine transporter inhibitor, on aqueous humor dynamics in normotensive monkey eyes. J Glaucoma. 2015;24:51-4
146. Fukata Y, Amano M, Kaibuchi K. Rho-Rho-kinase pathway in smooth muscle contraction and cytoskeletal reorganization of non-muscle cells. Trends Pharmacol Sci. 2001;22:32-9
147. Goldhagen B, Proia AD, Epstein DL, et al. Elevated levels of RhoA in the optic nerve head of human eyes with glaucoma. J Glaucoma. 2012;21:530-8
148. Rao VP, Epstein DL. Rho GTPase/Rho kinase inhibition as a novel target for the treatment of glaucoma. BioDrugs. 2007;21:167-77
149. Wettschureck N, Offermanns S. Rho/Rho-kinase mediated signaling in physiology and pathophysiology. J Mol Med (Berl). 2002;80:629-38
150. Rao PV, Deng PF, Kumar J, et al. Modulation of aqueous humor outflow facility by the Rho kinase-specific inhibitor Y-27632. Invest Ophthalmol Vis Sci. 2001;42:1029-37
151. Lu Z, Overby DR, Scott PA, et al. The mechanism of increasing outflow facility by rho-kinase inhibition with Y-27632 in bovine eyes. Exp Eye Res. 2008;86:271-81
152. Wang SK, Chang RT. An emerging treatment option for glaucoma: Rho kinase inhibitors. Clin Ophthalmol. 2014;8:883-90
153. Riento K, Ridley AJ. Rocks: multifunctional kinases in cell behaviour. Nat Rev Mol Cell Biol. 2003;4:446-56
154. Liu X, Hu Y, Filla MS, et al. The effect of C3 transgene expression on actin and cellular adhesions in cultured human trabecular meshwork cells and on outflow facility in organ cultured monkey eyes. Mol Vis. 2005;11:1112-21
155. Tian B, Kiland JA, Kaufman PL. Effects of the marine macrolides swinholide A and jasplakinolide on outflow facility in monkeys. Invest Ophthalmol Vis Sci. 2001;42:3187-92
156. Bubb MR, Spector I, Bershadsky AD, et al. Swinholide A is a microfilament disrupting marine toxin that stabilizes actin dimers and severs actin filaments. J Biol Chem. 1995;270:3463-6
157. Coue M, Brenner SL, Spector I, et al. Inhibition of actin polymerization by latrunculin A. FEBS Lett. 1987;213:316-8
158. Bubb MR, Senderowicz AM, Sausville EA, et al. Jasplakinolide, a cytotoxic natural product, induces actin polymerization and competitively inhibits the binding of phalloidin to F-actin. J Biol Chem. 1994;269:14869-71
159. Peterson JA, Tian B, Geiger B, et al. Effect of latrunculin-B on outflow facility in monkeys. Exp Eye Res. 2000;70:307-13
160. Okka M, Tian B, Kaufman PL. Effect of low-dose latrunculin B on anterior segment physiologic features in the monkey eye. Arch Ophthalmol. 2004;122:1482-8
161. Ethier CR, Read AT, Chan DW. Effects of latrunculin-B on outflow facility and trabecular meshwork structure in human eyes. Invest Ophthalmol Vis Sci. 2006;47:1991-8
162. Sabanay I, Tian B, Gabelt BT, et al. Latrunculin B effects on trabecular meshwork and corneal endothelial morphology in monkeys. Exp Eye Res. 2006;82:236-46
163. Peterson JA, Tian B, McLaren JW, et al. Latrunculins' effects on intraocular pressure, aqueous humor flow, and corneal endothelium. Invest Ophthalmol Vis Sci. 2000;41:1749-58
164. Rasmussen CA, Kaufman PL, Ritch R, et al. Latrunculin B Reduces Intraocular Pressure in Human Ocular Hypertension and Primary Open-Angle Glaucoma. Transl Vis Sci Technol. 2014;3:1
165. Mitchell CH, Peterson-Yantorno K, Carre DA, et al. A3 adenosine receptors regulate Cl- channels of nonpigmented ciliary epithelial cells. Am J Physiol. 1999;276:C659-66
166. Laties A, Rich CC, Stoltz R, et al. A Randomized Phase 1 Dose Escalation Study to Evaluate Safety, Tolerability, and Pharmacokinetics of Trabodenoson in Healthy Adult Volunteers. J Ocul Pharmacol Ther. 2016;32:548-54
167. Zhong Y, Yang Z, Huang WC, et al. Adenosine, adenosine receptors and glaucoma: an updated overview. Biochim Biophys Acta. 2013;1830:2882-90
168. Shearer TW, Crosson CE. Adenosine A1 receptor modulation of MMP-2 secretion by trabecular meshwork cells. Invest Ophthalmol Vis Sci. 2002;43:3016-20
169. Crosson CE, Sloan CF, Yates PW. Modulation of conventional outflow facility by the adenosine A1 agonist N6-cyclohexyladenosine. Invest Ophthalmol Vis Sci. 2005;46:3795-9
170. Chen J, Runyan SA, Robinson MR. Novel ocular antihypertensive compounds in clinical trials. Clin Ophthalmol. 2011;5:667-77
171. Cavet ME, Vollmer TR, Harrington KL, et al. Regulation of Endothelin-1-Induced Trabecular Meshwork Cell Contractility by Latanoprostene Bunod. Invest Ophthalmol Vis Sci. 2015;56:4108-16
172. Kalouche G, Beguier F, Bakria M, et al. Activation of Prostaglandin FP and EP2 Receptors Differently Modulates Myofibroblast Transition in a Model of Adult Primary Human Trabecular Meshwork Cells. Invest Ophthalmol Vis Sci. 2016;57:1816-25
173. Nilsson SF, Drecoll E, Lutjen-Drecoll E, et al. The prostanoid EP2 receptor agonist butaprost increases uveoscleral outflow in the cynomolgus monkey. Invest Ophthalmol Vis Sci. 2006;47:4042-9
174. Wang JW, Woodward DF, Stamer WD. Differential effects of prostaglandin E2-sensitive receptors on contractility of human ocular cells that regulate conventional outflow. Invest Ophthalmol Vis Sci. 2013;54:4782-90
175. Millard LH, Woodward DF, Stamer WD. The role of the prostaglandin EP4 receptor in the regulation of human outflow facility. Invest Ophthalmol Vis Sci. 2011;52:3506-13

176. Fujino H, Xu W, Regan JW. Prostaglandin E2 induced functional expression of early growth response factor-1 by EP4, but not EP2, prostanoid receptors via the phosphatidylinositol 3-kinase and extracellular signal-regulated kinases. J Biol Chem. 2003;278:12151-6
177. Zhong J, Gencay MM, Bubendorf L, et al. ERK1/2 and p38 MAP kinase control MMP-2, MT1-MMP, and TIMP action and affect cell migration: a comparison between mesothelioma and mesothelial cells. J Cell Physiol. 2006;207:540-52
178. Martinez T, Jimenez AI, Paneda C. Short-interference RNAs: becoming medicines. EXCLI J. 2015;14:714-46
179. Moreno-Montanes J, Sadaba B, Ruz V, et al. Phase I clinical trial of SYL040012, a small interfering RNA targeting beta-adrenergic receptor 2, for lowering intraocular pressure. Mol Ther. 2014;22:226-32
180. Datta S, Baudouin C, Brignole-Baudouin F, et al. The Eye Drop Preservative Benzalkonium Chloride Potently Induces Mitochondrial Dysfunction and Preferentially Affects LHON Mutant Cells. Invest Ophthalmol Vis Sci. 2017;58:2406-12
181. Schehlein EM, Novack GD, Robin AL. New classes of glaucoma medications. Curr Opin Ophthalmol. 2017;28:161-8
182. Rasmussen CA, Kaufman PL. Exciting directions in glaucoma. Can J Ophthalmol. 2014;49:534-43
183. Liu X, Brandt CR, Gabelt BT, et al. Herpes simplex virus mediated gene transfer to primate ocular tissues. Exp Eye Res. 1999;69:385-95
184. Spencer B, Agarwala S, Miskulin M, et al. Herpes simplex virus-mediated gene delivery to the rodent visual system. Invest Ophthalmol Vis Sci. 2000;41:1392-401
185. Loewen N, Fautsch MP, Teo WL, et al. Long-term, targeted genetic modification of the aqueous humor outflow tract coupled with noninvasive imaging of gene expression in vivo. Invest Ophthalmol Vis Sci. 2004;45:3091-8
186. Challa P, Luna C, Liton PB, et al. Lentiviral mediated gene delivery to the anterior chamber of rodent eyes. Mol Vis. 2005;11:425-30
187. Barraza RA, Rasmussen CA, Loewen N, et al. Prolonged transgene expression with lentiviral vectors in the aqueous humor outflow pathway of nonhuman primates. Hum Gene Ther. 2009;20:191-200
188. Budenz DL, Bennett J, Alonso L, et al. In vivo gene transfer into murine corneal endothelial and trabecular meshwork cells. Invest Ophthalmol Vis Sci. 1995;36:2211-5
189. Borras T, Tamm ER, Zigler JS, Jr. Ocular adenovirus gene transfer varies in efficiency and inflammatory response. Invest Ophthalmol Vis Sci. 1996;37:1282-93
190. Borras T, Gabelt BT, Klintworth GK, et al. Non-invasive observation of repeated adenoviral GFP gene delivery to the anterior segment of the monkey eye in vivo. J Gene Med. 2001;3:437-49
191. Kee C, Sohn S, Hwang JM. Stromelysin gene transfer into cultured human trabecular cells and rat trabecular meshwork in vivo. Invest Ophthalmol Vis Sci. 2001;42:2856-60
192. Spiga MG, Borras T. Development of a gene therapy virus with a glucocorticoid-inducible MMP1 for the treatment of steroid glaucoma. Invest Ophthalmol Vis Sci. 2010;51:3029-41
193. Gerometta R, Spiga MG, Borras T, et al. Treatment of sheep steroid-induced ocular hypertension with a glucocorticoid-inducible MMP1 gene therapy virus. Invest Ophthalmol Vis Sci. 2010;51:3042-8
194. Borras T, Buie LK, Spiga MG. Inducible scAAV2.GRE.MMP1 lowers IOP long-term in a large animal model for steroid-induced glaucoma gene therapy. Gene Ther. 2016;23:438-49
** This article was the first to show that an inducible virus expressing MMP in the anterior chamber could reduce IOP in an animal model.
195. Manno CS, Pierce GF, Arruda VR, et al. Successful transduction of liver in hemophilia by AAV-Factor IX and limitations imposed by the host immune response. Nat Med. 2006;12:342-7
196. Murphy SL, High KA. Gene therapy for haemophilia. Br J Haematol. 2008;140:479-87
197. McCarty DM, Monahan PE, Samulski RJ. Self-complementary recombinant adeno-associated virus (scAAV) vectors promote efficient transduction independently of DNA synthesis. Gene Ther. 2001;8:1248-54
198. Buie LK, Rasmussen CA, Porterfield EC, et al. Self-complementary AAV virus (scAAV) safe and long-term gene transfer in the trabecular meshwork of living rats and monkeys. Invest Ophthalmol Vis Sci. 2010;51:236-48
199. Bennett J. Taking Stock of Retinal Gene Therapy: Looking Back and Moving Forward. Mol Ther. 2017;25:1076-94
200. Spark Therapeutics 2017 [19/05/17]. Available from: http://sparktx.com/

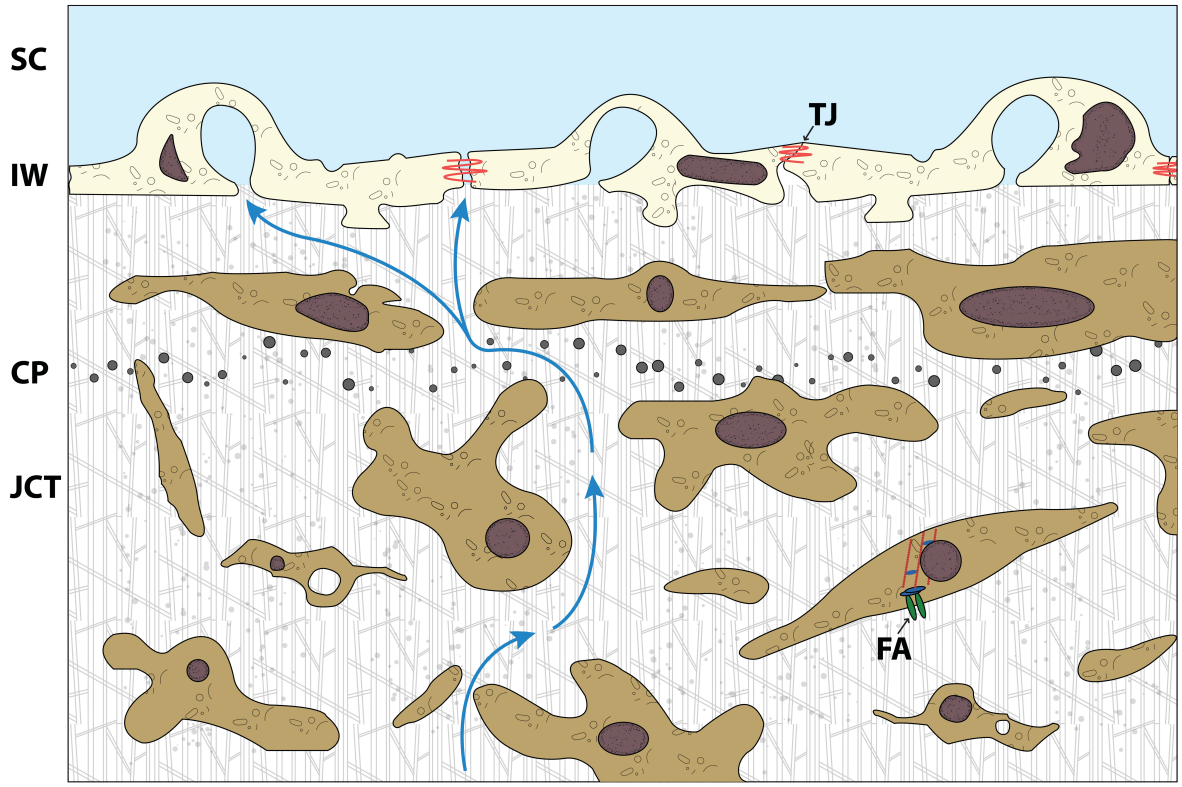

Figure 1: An expanded view of the JCT region.

Diagram depicting a cross section of the conventional outflow tissues including various ECM elements. AH traverses the TM, exiting the juxtacanalicular region (JCT) through the inner wall (IW) into the lumen of the Schlemm's canal (SC), via either the transcellular route through giant vacuoles, or the paracellular route through tight junctions (TJ). Cells are embedded in a structured ECM and adhesion to the matrix is facilitated by the focal

adhesion (FA) site where integrins bind both extracellular material and the intracellular actin cytoskeleton (red). The cribriform plexus (CP) comprising elastin sheaths is predominantly found underlying the first sub-endothelial layer.

Table 1. Comparison of traditional vs emerging formulations in glaucoma treatment

Class of Medication	Clinical Prevalence Today	Primary Mode of Action	Mechanism	References
Traditional				
Prostaglandin F2α Analogue	1st line- Common	Increases unconventional and conventional outflow	Ciliary muscle relaxation, ECM remodelling by MMPs	124 - 127
B-blockers	2nd line - Uncommon	Reduces AH production	Block β1/β2 adrenoceptors, vasoconstriction at ciliary body	131, 132
Carbonic Anhydrase inhibitors	2nd line - Uncommon	Reduces AH production	Inhibit bicarbonate formation	135
Cholinergics	3rd line - Uncommon	Increases conventional outflow	Ciliary muscle contraction	136 - 138
A2-adrenergic receptor agonists	Rarely used due to side effects	Reduces AH production, increases unconventional outflow	Block α2-adrenergic receptors, elevate prostaglandin expression	133, 134
Emerging				
ROCK inhibitor	Approved in Japan, phase III trials in US	Increases conventional outflow	Cytoskeletal disorganisation, promotes cell migration	143, 144
Macrolides	Phase I trials	Increases conventional outflow	Disruption of actin cytoskeleton	155-164
Adenosine receptor agonists (A_1)	Phase III trials	Increases conventional outflow	ECM remodelling by MMPs	165-170
siRNA	Phase II trials	Reduces AH production	Inhibit β2-adrenergic receptors at ciliary body	178, 179
AAV	Preclinical development	Increases conventional outflow	ECM remodelling by MMPs	194, 98